

# **For Reference**

---

**NOT TO BE TAKEN FROM THIS ROOM**



Ex LIBRIS  
UNIVERSITATIS  
ALBERTAENSIS









THE UNIVERSITY OF ALBERTA

EPR AND NMR STUDIES OF LIGAND COORDINATION AND  
EXCHANGE FOR VANADYL COMPLEXES

by



GERALD ALBERT MILLER

A THESIS

SUBMITTED TO THE FACULTY OF GRADUATE STUDIES AND RESEARCH  
IN PARTIAL FULFILMENT OF THE REQUIREMENTS FOR THE DEGREE  
OF

DOCTOR OF PHILOSOPHY

DEPARTMENT OF CHEMISTRY

EDMONTON, ALBERTA

FALL, 1973





## A B S T R A C T

Vanadyl dithiophosphinates and vanadyl perchlorates were investigated by EPR and NMR techniques to study the properties of the two different coordination sites of the vanadyl ion; namely, the four equivalent equatorial sites and the one axial site. The results are discussed within the context of previous studies.

Chapter III gives the results of an EPR study of the five coordinate vanadyl complexes, bis-(dimethyldithiophosphinato)-oxo-vanadium(IV), bis-(diphenyldithiophosphinato)-oxo-vanadium(IV), and bis-(O,O'-diethyldithiophosphato)-oxo-vanadium(IV) in the non-coordinating solvents toluene and  $\text{CS}_2$ . The EPR spectra correspond to the interaction of the unpaired electron with the  $^{51}\text{V}$  nucleus and two equivalent  $^{31}\text{P}$  nuclei. Addition of 1-5% by volume of the strongly coordinating ligands pyridine, dimethylformamide, or hexamethylphosphoramide results in EPR spectra indicative of hyperfine interactions with the  $^{51}\text{V}$  nucleus and a single  $^{31}\text{P}$  nucleus. It is shown that, in this vanadyl species, the added ligand coordinates at an equatorial site, resulting in a five coordinate species in which one of the dithiophosphate groups is monodentate and a six coordinate species in which one of the chelating dithiophosphinates is rearranged so that one sulfur atom occupies an equatorial position and the other the axial position. The equilibrium constants and heats of adduct formation for the equatorial ligand





addition were determined from the EPR spectra. At higher ligand concentrations, the EPR spectra show no  $^{31}\text{P}$  hyperfine interactions which indicates that both chelating dithiophosphinate groups become monodentate. Infrared and conductivity measurements indicated that the vanadyl dithiophosphinate dissociates completely in solutions with still higher ligand concentrations, but that several vanadyl species containing one or two dithiophosphinate moieties coordinated to the vanadium atom are present in these solutions.

Chapter IV presents the results of NMR line broadening studies of solvent resonances in solutions of  $\text{VO}^{2+}$  in dimethylformamide (DMF) and dimethylacetamide (DMA). These results indicate that chemical exchange from axial and equatorial coordination sites can control the formyl proton relaxation in DMF, but axial exchange does not produce broadening of the methyl resonances in either DMF or DMA which could be distinguished from outer sphere broadening. The results also showed an inner-sphere broadening region which was attributed to relaxation by a dipole-dipole interaction for the formyl proton resonance in DMF and the C-methyl resonance in DMA and to hyperfine interactions for the N-methyl resonances. These assertions were substantiated by the values of the tumbling times of the complexes in solution which were determined from analyses of the EPR spectra of the complexes in the particular solvents. Similar studies of bis-(diphenyldithiophosphinato)-oxo-vanadium(IV)

Digitized by the Internet Archive  
in 2023 with funding from  
University of Alberta Library

<https://archive.org/details/Miller1973>



in DMF and DMA are also presented in Chapter IV and indicate that DMA completely displaces the dithiophosphinate chelate from the first coordination sphere of  $\text{VO}^{2+}$  but that in DMF at least one monodentate dithiophosphinate remains coordinated to the vanadyl ion.





## A C K N O W L E D G E M E N T

I wish to thank Dr. R. E. D. McClung for his assistance, direction and encouragement throughout the course of this work.

I would also like to thank Dr. R. B. Jordan for numerous helpful suggestions concerning the line broadening studies.

A special thanks is also extended to Mrs. Mary Waters for the excellent preparation of this manuscript.

Financial assistance from the University of Alberta and the National Research Council of Canada is gratefully acknowledged.



# T A B L E   O F   C O N T E N T S

<u>CHAPTER</u>		<u>Page</u>
I	INTRODUCTION . . . . .	1
	A. General Considerations . . . . .	1
	B. EPR Spectra. . . . .	3
	C. Electronic Spectra . . . . .	7
	D. Infrared Spectra . . . . .	10
	E. Kinetic Studies . . . . .	12
II	EXPERIMENTAL TECHNIQUES . . . . .	16
	A. Purification of Solvents . . . . .	16
	B. Preparation and Characterization of Complexes. . . . .	16
	1. Vanadyl Dithiophosphinates . . . . .	16
	2. Vanadyl Perchlorates . . . . .	17
	3. Bis-(o-phenanthroline)-oxo-vanadium(IV) Perchlorate. . . . .	18
	4. Other Complexes . . . . .	18
	C. Sample Preparation . . . . .	19
	D. Instrumentation and Measurement Techniques .	21
III	STUDY OF THE COORDINATION OF LEWIS BASES TO VANADYL DITHIOPHOSPHINATES . . . . .	23
	A. Introduction . . . . .	23
	B. Theory . . . . .	24
	C. Experimental Measurements . . . . .	33
	D. Results . . . . .	35





<u>CHAPTER</u>		<u>Page</u>
III		
	1. Analysis of EPR Spectra in Toluene and CS <sub>2</sub> . . . . .	35
	2. Analysis of EPR Spectra in Mixed Solvents. . . . .	45
	3. Analysis of Optical Spectra . . . . .	66
	4. Analysis of Infrared Spectra. . . . .	71
	5. Conductance Results . . . . .	76
E.	Discussion . . . . .	77
	1. Discussion of Equilibria Between Different Vanadyl Species . . . . .	77
	2. Interpretation of g-values and Hyperfine Splitting Constants . . . . .	101
	3. Hyperfine Interactions . . . . .	107
F.	Comparisons with Other Systems . . . . .	109
IV	EQUATORIAL AND AXIAL SOLVENT EXCHANGE RATES OF VANADYL COMPLEXES . . . . .	114
A.	Introduction . . . . .	114
B.	Theory of NMR Line Broadening by Paramagnetic Complexes . . . . .	116
	1. General Theory . . . . .	116
	2. Temperature Dependence of Exchange Rates, Nuclear Relaxation Times and Chemical Shifts . . . . .	124
C.	Experimental . . . . .	128
D.	Results . . . . .	130
	1. Analysis of Infrared, Visible and EPR Spectra . . . . .	130
	2. VO(DMA) <sub>5</sub> (ClO <sub>4</sub> ) <sub>2</sub> in DMA . . . . .	139





<u>CHAPTER</u>	<u>Page</u>
3. VO(DMF) <sub>5</sub> (ClO <sub>4</sub> ) <sub>2</sub> in DMF . . . . .	150
4. Bis-(o-phenanthroline)-oxo-vanadium(IV) Perchlorate in DMF . . . . .	160
5. VO(acac) <sub>2</sub> in DMF . . . . .	164
6. Bis-(diphenyldithiophosphinato)-oxo-vanadium(IV) in DMF, DMA and DEF . . . . .	164
E. Discussion . . . . .	177
1. Vanadyl Perchlorates . . . . .	177
2. Vanadyl Dithiophosphinates . . . . .	183
V CONCLUSION . . . . .	186
A. Vanadyl Coordination . . . . .	186
B. Vanadyl Exchange Kinetics . . . . .	188
REFERENCES . . . . .	192
APPENDIX A . . . . .	199
APPENDIX B . . . . .	219
APPENDIX C . . . . .	222



# L I S T   O F   T A B L E S

<u>TABLE</u>		<u>Page</u>
III-1	Isotropic Magnetic Parameters for Vanadyl Dithiophosphinates in CS <sub>2</sub> and Toluene Solutions	39
III-2	EPR Linewidths of Hyperfine Components of Vanadyl Dithiophosphinates in Toluene and CS <sub>2</sub>	41
III-3	Anisotropic Magnetic Parameters for Vanadyl Dithiophosphinates in Different Solvents at -150°C	46
III-4	Isotropic Magnetic Parameters for Vanadyl Dithiophosphinates in 5% HMP/Toluene and 5% Pyridine/CS <sub>2</sub> at 30°C	51
III-5	Isotropic Magnetic Parameters for Vanadyl Dithiophosphinates in Coordinating Solvents	63
III-6	Electronic Spectra of Vanadyl Dithiophosphinates in Various Solvents	70
III-7	Frequencies of Symmetric P-S Stretching Vibrations in Diphenyldithiophosphate Compounds	74
III-8	Dependence of Conductance on Concentration of Bis-(diphenyldithiophosphinato)-oxo-vanadium(IV) in Several Solvents	77
III-9	Calculated Values of Equilibrium Constant K <sub>T-D</sub>	84
III-10	Equilibrium Constants at 298K and Enthalpies of Adduct Formation	86
III-11	Molecular Orbital Coefficients	106





# L I S T   O F   T A B L E S

<u>Table</u>		<u>Page</u>
IV-1	EPR Linewidth Parameters for Vanadyl Complexes	135
IV-2	Magnetic Parameters of Vanadyl Perchlorate in DMF and DMA	137
IV-3	Least Squares Parameters and Calculated Nuclear Relaxation and Exchange Rates of DMA Protons in Solutions Containing $\text{VO}(\text{DMA})_5(\text{ClO}_4)_2$	146
IV-4	Least Squares Parameters and Calculated Nuclear Relaxation and Exchange Rates of DMF Protons in Solutions Containing $\text{VO}(\text{DMF})_5(\text{ClO}_4)_2$	157
IV-5	Least Squares Parameters and Calculated Nuclear Relaxation and Exchange Rates of DMA Protons in Solutions Containing Bis-(diphenyldithiophosphinato)-oxo-vanadium(IV)	168
IV-6	Least Squares Parameters and Calculated Nuclear Relaxation and Exchange Rates of DMF Protons in Solutions Containing Bis-(diphenyldithiophosphinato)-oxo-vanadium(IV)	174
V-1	Kinetic Parameters for Solvent Exchange from the Solvated Vanadyl Ion	190
A-1	Proton Line Broadening of DMA Solutions Containing $\text{VO}(\text{DMA})_5(\text{ClO}_4)_2$	200
A-2	Proton Line Broadening of DMF Solutions Containing $\text{VO}(\text{DMF})_5(\text{ClO}_4)_2$	204
A-3	Proton Line Broadening of DMF Solutions Containing Bis-(o-phenanthroline)-oxo-vanadium(IV) Perchlorate	208





L I S T   O F   T A B L E S

<u>Table</u>		<u>Page</u>
A-4	Formyl Proton Line Broadening of DMF Solutions Containing VO(acac) <sub>2</sub>	210
A-5	Proton Line Broadening of DMA Solutions Containing Bis-(diphenyldithiophosphinato)-oxo-vanadium(IV)	211
A-6	Proton Line Broadening of DMF Solutions Containing Bis-(diphenyldithiophosphinato)-oxo-vanadium(IV)	215
A-7	Formyl Proton Line Broadening of DEF Solutions Containing Bis-(diphenyldithiophosphinato)-oxo-vanadium(IV)	217
B-1	Conductance of Several Solvents Containing Various Concentrations of Bis-(diphenyldithiophosphinato)-oxo-vanadium(IV)	220



# L I S T   O F   F I G U R E S

<u>FIGURE</u>		<u>PAGE</u>
III-7	EPR spectra of $10^{-3}$ <u>M</u> liquid solutions of bis-(diphenyldithiophosphinato)-oxo-vanadium(IV) in HMP at 116°C and DMF at 30°C	59
III-8	EPR spectra of $10^{-3}$ <u>M</u> liquid solutions of bis-(diphenyldithiophosphinato)-oxo-vanadium(IV) in pyridine at 30°C and 90°C	60
III-9	EPR spectra of $10^{-3}$ <u>M</u> liquid solutions of bis-(dimethyldithiophosphinato)-oxo-vanadium(IV) in pyridine/CS <sub>2</sub> mixtures of various compositions at -45°C	62
III-10	EPR spectra of $10^{-3}$ <u>M</u> liquid solutions of bis-(dimethyldithiophosphinato)-oxo-vanadium(IV) in 10% dimethyl sulfoxide/chloroform at 60°C and bis-(O,O'-diethyldithiophosphato)-oxo-vanadium(IV) in 10% trimethyl phosphate/toluene at 40°C	65
III-11	EPR spectra of $10^{-3}$ <u>M</u> liquid solutions of bis-(O,O'-diethyldithiophosphato)-oxo-vanadium(IV) in ethanol at 25°C and at 60°C	67
III-12	Electronic absorption spectra of bis-(diphenyldithiophosphinato)-oxo-vanadium(IV) in various solvents	68
III-13	Energy level schemes for oxo-vanadium(IV) complexes	72





# L I S T   O F   F I G U R E S

<u>FIGURE</u>		<u>PAGE</u>
III-14	Infrared spectra of bis-(diphenyldithio-phosphinato)-oxo-vanadium(IV) in pyridine/ CS <sub>2</sub> solutions of various compositions	75
III-15	Temperature dependence of the equilibrium constants for the formation of adducts of the vanadyl dithiophosphinates in pyridine, HMP and DMF	88
III-16	Computer synthesized EPR solution spectra of bis-(dimethyldithiophosphinato)-oxo-vanadium(IV) in 5% HMP/toluene at 60°C for a 1:1 ratio of doublet:triplet pattern at various linewidths of the doublet pattern relative to the triplet pattern	91
III-17	EPR spectra of 10 <sup>-3</sup> <u>M</u> liquid solutions of bis-(dimethyldithiophosphinato)-oxo-vanadium(IV) in DMF at various temperatures	98
III-19	EPR spectra of 10 <sup>-3</sup> <u>M</u> liquid solutions of bis-(O,O'-diethyldithiophosphato)-oxo-vanadium(IV) in DMF at various temperatures	99
III-19	EPR spectra of 10 <sup>-3</sup> <u>M</u> liquid solutions of VO(acac) <sub>2</sub> in HMP at various temperatures	111
IV-1	Electronic absorption spectra of VO(DMA) <sub>5</sub> (ClO <sub>4</sub> ) <sub>2</sub> in DMA, and VO(DMF) <sub>5</sub> (ClO <sub>4</sub> ) <sub>2</sub> in DMF	131
IV-2	EPR spectra of 5 x 10 <sup>-3</sup> <u>M</u> liquid solutions of VO(DMF) <sub>5</sub> (ClO <sub>4</sub> ) <sub>2</sub> in DMF at various temperatures	133



# L I S T O F F I G U R E S

<u>FIGURE</u>		<u>PAGE</u>
IV-3	Temperature dependence of isotropic $^{51}\text{V}$ hyperfine interactions and g-values of $\text{VO}(\text{DMA})_5(\text{ClO}_4)_2$ in DMA and $\text{VO}(\text{DMF})_5(\text{ClO}_4)_2$ in DMF	134
IV-4	Temperature dependence of rotational tumbling time of $\text{VO}(\text{DMA})_5(\text{ClO}_4)_2$ in DMA and $\text{VO}(\text{DMF})_5(\text{ClO}_4)_2$ in DMF	138
IV-5	EPR spectrum of $5 \times 10^{-3}$ M liquid solutions of $\text{VO}(\text{DMA})_5(\text{ClO}_4)_2$ in DMA at $120^\circ\text{C}$	140
IV-6	60 MHz NMR spectrum at $25^\circ\text{C}$ of DMA	141
IV-7	Temperature dependence of the methyl proton linewidths of DMA	142
IV-8	Temperature dependence of $1/T_{2P}$ for the methyl protons in DMA solutions of $\text{VO}(\text{DMA})_5(\text{ClO}_4)_2$	144
IV-9	60 MHz NMR spectrum at $25^\circ\text{C}$ of DMF	152
IV-10	Temperature dependence of the proton linewidths of DMF	153
IV-11	Temperature dependence of $1/T_{2P}$ for the formyl and methyl protons in DMF solutions of $\text{VO}(\text{DMF})_5(\text{ClO}_4)_2$	154
IV-12	Temperature dependence of $1/T_{2P}$ for the formyl and methyl protons in DMF solutions of bis-(o-phenanthroline)-oxo-vanadium(IV) perchlorate	162





## L I S T   O F   F I G U R E S

<u>FIGURE</u>	<u>PAGE</u>
IV-13      EPR spectra of $10^{-2}$ <u>M</u> liquid solutions of bis-(o-phenanthroline)-oxo-vanadium(IV) perchlorate    in DMF	163
IV-14      Temperature dependence of $1/T_{2P}$ for the formyl protons in DMF solutions of $VO(acac)_2$	165
IV-15      Temperature dependence of $1/T_{2P}$ for the methyl protons in DMA solutions of bis- (diphenyldithiophosphinato)-oxo-vanadium (IV)	167
IV-16      Temperature dependence of $1/T_{2P}$ for the formyl and methyl protons in DMF solutions of bis-(diphenyldithiophosphinato)-oxo- vanadium(IV)	171
IV-17      Temperature dependence of $1/T_{2P}$ for the formyl proton in DEF solutions of bis- (diphenyldithiophosphinato)-oxo-vanadium (IV)	175
IV-18      Temperature dependence of the formyl proton linewidths of DEF	176
IV-19      Stereochemistry of DMF coordinated to the vanadyl ion	182



CHAPTER II N T R O D U C T I O NA. General Considerations

The chemistry of vanadium(IV) is dominated by the oxo-vanadium(IV) species, more commonly referred to as the vanadyl species. The vanadyl unit,  $\text{VO}^{2+}$ , remains intact in most environments used for chemical reactions and hence vanadyl coordination complexes with a large variety of ligands including multidentate ligands have been prepared. These vanadyl complexes which may be anions, cations or neutral complexes are often unstable in air. Surveys of the known vanadyl complexes have been compiled in review articles by Selbin.<sup>1,2</sup>

A special aspect of the vanadyl ion is its facility to form both five and six coordinate complexes. For example, in bis-(acetylacetonato)-oxo-vanadium(IV),  $[\text{VO}(\text{acac})_2]$ , the vanadium atom lies at approximately the center of gravity of the five oxygen atoms arranged in a rectangular pyramid.<sup>3</sup> The axial position, trans to the vanadyl oxygen, is vacant in this complex but has been shown to readily accept a sixth ligand which has strong electron donor properties.<sup>4-7</sup> Adducts of  $\text{VO}(\text{acac})_2$  have also been isolated in which one oxygen atom of the one acetylacetonate chelate occupies the axial position and the second coordinating oxygen occupies an equatorial position (cis to vanadyl





oxygen).<sup>7,8</sup> The remaining equatorial coordination site is occupied by a Lewis base type ligand. Whether the Lewis base occupies an axial or equatorial coordination site in the  $\text{VO}(\text{acac})_2$  adduct is probably a function of its base strength and its steric characteristics but no general correlations have been proposed.

Differences in the coordination properties of the axial and equatorial sites of the vanadyl ion should also be reflected in the differences in ligand exchange rates from the two types of sites. Since one expects Lewis base coordination at the axial site, trans to the vanadyl oxygen, to be weaker than at the equatorial sites, the rate of exchange from the axial site should be faster. In Chapter IV the results of ligand exchange studies by the nuclear magnetic resonance (NMR) solvent line broadening technique show that this is indeed the case for the vanadyl ion in the Lewis base solvents N,N-dimethylformamide and N,N-dimethylacetamide.

The recent interest in sulphur chemistry has resulted in the preparation of a variety of vanadyl complexes containing the bidentate monothio-acetylacetonate<sup>9</sup>, dithiocarbamate<sup>10,11</sup>, 1,2-dithiolene<sup>12</sup>, or dithiophosphate<sup>13-15</sup> ligands. The results of a spectroscopic investigation of three vanadyl dithiophosphate complexes are presented in this thesis. In particular, the complexes studied were bis-(dimethyldithiophosphinato)-oxo-vanadium(IV)<sup>13</sup>,



bis-(diphenyldithiophosphinato)-oxo-vanadium(IV)<sup>13,16</sup> and bis-(O,O'-diethyldithiophosphato)-oxo-vanadium(IV)<sup>13,17,18</sup> and will be referred to individually as the methyl, phenyl and ethoxy complexes respectively. An X-ray<sup>19</sup> crystal structure of the methyl complex indicated that it is structurally similar to  $\text{VO}(\text{acac})_2$  with the four sulphur atoms forming the base of a rectangular pyramid and the coordination site trans to the vanadyl oxygen being vacant. (See Fig. I-1). These complexes were conveniently studied by electron paramagnetic resonance (EPR) spectroscopy. The changes in the EPR spectra upon addition of Lewis bases to solutions of the vanadyl complexes are sensitive to changes in the coordination of the vanadyl ion. The results indicate that several distinct species can be formed when a Lewis base coordinates to a vanadyl dithiophosphinate complex.

#### B. EPR Spectra

EPR spectroscopy<sup>20</sup> is a useful technique for studying the environment of the single unpaired electron in the vanadyl systems. The application of a magnetic field removes the spin state degeneracy and transitions between the spin states can be induced by the introduction of energy in the microwave region. The EPR spectrum is essentially a recording of energy absorptions as a function of the applied magnetic field strength. The spectrum of a vanadyl



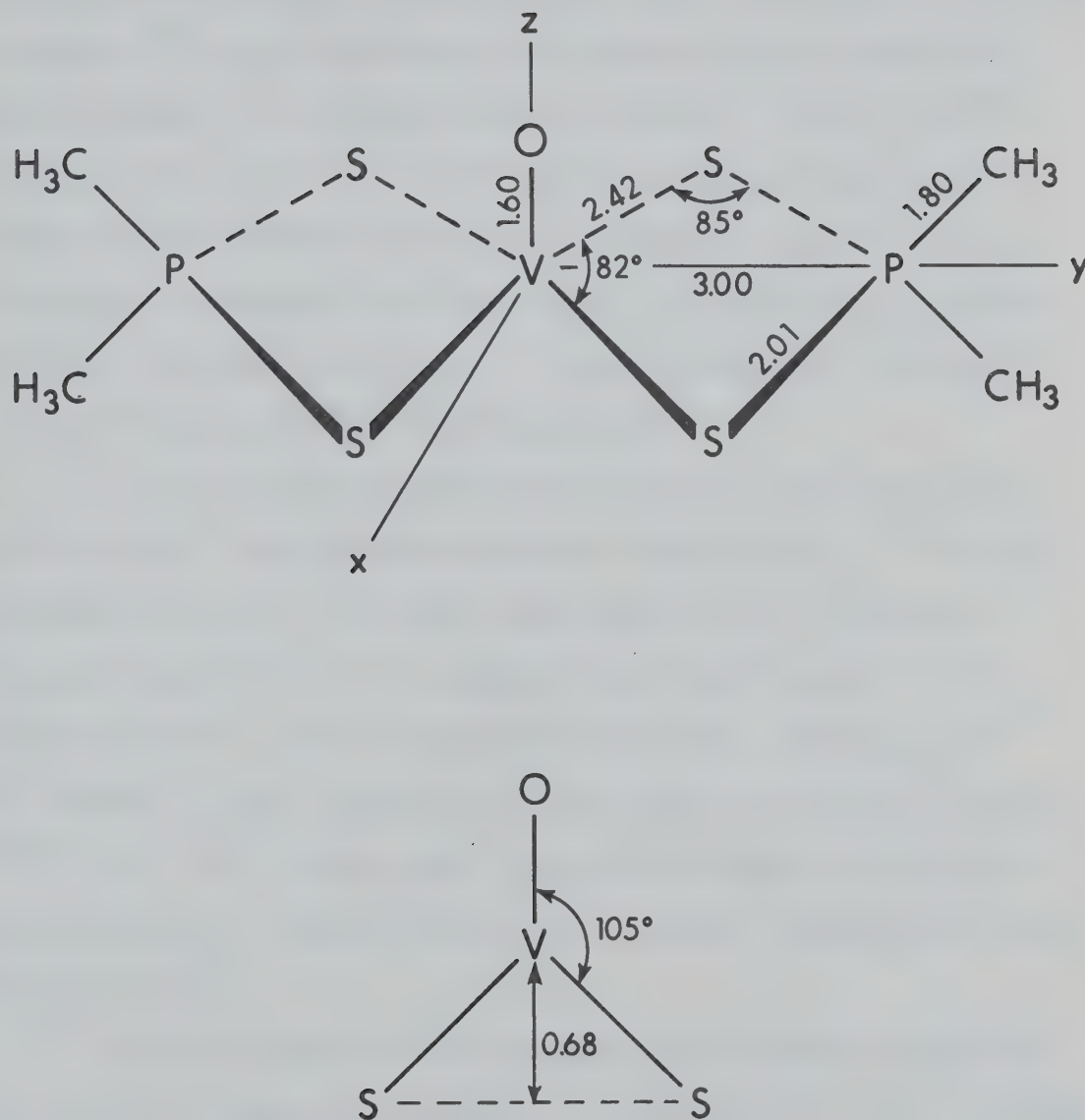


FIGURE I-1 Structure of bis-(dimethyldithiophosphinato)-oxo-  
vanadium(IV).<sup>19</sup>





complex in liquid solutions is characterized by an isotropic g-value  $g_0$ , which is a measure of the magnitude of the electronic Zeeman interaction, and a hyperfine splitting constant  $a_0^V$  which describes the interaction between the electron and  $^{51}\text{V}$  nuclear magnetic moment. Since the  $^{51}\text{V}$  nucleus has a spin of  $7/2$ , the EPR spectrum consists of eight lines with the spacing approximately equal to  $a_0^V$ , centered at magnetic flux  $B = \hbar\omega_0/g_0\beta_0$  where  $\hbar$  is Planck's constant divided by  $2\pi$ ,  $\omega_0$  is the spectrometer frequency in  $\text{sec}^{-1}$  and  $\beta_0$  is the Bohr magneton.

The vanadium hyperfine splitting constant is proportional to the unpaired electron spin density<sup>20</sup> at the vanadium nucleus. In turn, one expects this unpaired electron spin density to depend upon coordination at the vacant site of a five coordinate complex. Coordination of ligands to the vanadyl ion has been extensively studied,<sup>21-23</sup> but the results give limited information because it is difficult to assess the site of ligand coordination from changes in  $a_0^V$ .

EPR results for the vanadyl dithiophosphinates are much more enlightening because, in addition to the  $^{51}\text{V}$  hyperfine splitting, the spectra show a second hyperfine splitting,  $a^P$ , due to the two equivalent  $^{31}\text{P}$  nuclei of spin  $1/2$ .  $a^P$  depends on the amount of overlap of the phosphorus s-type orbitals and the orbital of vanadium in which the unpaired electron resides. On this basis, changes in  $a^P$  observed



when a ligand coordinates to vanadyl dithiophosphinates can be directly related to the position of the phosphorus atoms relative to the orbital containing the unpaired electron.

The EPR spectra of solid solutions of vanadyl complexes indicate that the Zeeman interaction and the  $^{51}\text{V}$  hyperfine interaction are both anisotropic, i.e. the magnitude of the g-value and the  $^{51}\text{V}$  hyperfine splitting constant depend on the orientation of the vanadyl species relative to the applied magnetic field. These anisotropies contain information about the highest occupied and some of the lower unoccupied molecular orbitals of the complex.<sup>24-27</sup>

The anisotropic magnetic interactions are not completely averaged by the rotational motion of the complexes in liquid solutions, and produce variations in the linewidths of the hyperfine components of the EPR spectra.<sup>28</sup> An analysis of the solution EPR linewidths, combined with the anisotropic magnetic parameters determined from the spectra of the solid solutions, permits the calculation of the reorientational correlation time,  $\tau_r$ , of the complex. This correlation time, which can qualitatively be viewed as the time required for the complex to reorient by 1 radian, controls the rate of numerous magnetic relaxation mechanisms and is intimately involved in the interpretation of the relaxation times of the nuclei on ligands attached to the paramagnetic vanadyl ions. These relaxation times are considered in detail in Chapter IV in connection with solvent NMR line broadening by vanadyl ions.





### C. Electronic Spectra

In general, the room temperature spectra of vanadyl complexes display three bands in the 7.5 to 30 kilokaeyer (kK) region which are designated Band I (11 - 16 kK), Band II (14.5 - 19 kK) and Band III (20 - 30 kK).<sup>1,2</sup> Band III is often concealed under an intense band attributed to a charge transfer transition. The three bands are assigned to the transitions from the non-bonding  $d_{x^2-y^2}$  orbital to the anti-bonding levels on the basis of the following discussion.

Considerable controversy still surrounds the interpretation of the electronic spectra of vanadyl complexes. All bonding schemes proposed for vanadyl complexes agree that the unpaired electron resides in a molecular orbital which is essentially the non-bonding  $3d_{x^2-y^2}$  atomic orbital of vanadium. However, the ordering of the antibonding levels to which the electron is promoted in the optical excitations is not firmly established. Early crystal field models<sup>29</sup> employing crystal fields of  $C_{4v}$  symmetry appropriate to  $VO(H_2O)_5^{2+}$ , suggested the order  $d_{x^2-y^2} < d_{xz}, d_{yz} < d_{xy} < d_z^2$ , but did not account for the known multiple bond character of the vanadyl unit.<sup>30</sup> Ballhausen and Gray<sup>31</sup> presented a molecular orbital treatment of  $VO(H_2O)_5^{2+}$  in which the molecular orbitals were constructed from appropriate linear combinations of metal 3d, 4s and 4p orbitals, the 2s, 2p<sub>z</sub>, 2p<sub>x</sub> and 2p<sub>y</sub> orbitals of the vanadyl oxygen and



the  $sp_O$  hybrid orbitals for the water oxygens. The resulting bonding scheme, shown in Fig. I-2, assigns  $\pi$  bonding to the vanadyl unit and has served as a model for a host of vanadyl systems. The unpaired electron is localized mainly in the non-bonding  $d_{x^2-y^2}$  orbital and the antibonding orbitals have the same relative order as predicted by the crystal field model.

Vanquickenborne and McGlynn<sup>32</sup> performed extended-Hückel type molecular orbital calculations for  $VO(H_2O)_5^{2+}$  and showed that the relative energies of the antibonding orbitals were particularly sensitive to the  $\overset{O}{\parallel}V-O$  angle. A change of  $15^\circ$  caused shifts of 5-10 kK and could result in a crossover of the  $d_{xy}(b_2)$  and the  $d_{xz}, d_{yz}(e)$  levels. Since the  $\overset{O}{\parallel}V-O$  angle is undoubtedly changed by the coordination of a Lewis base at the axial position of a five coordinate complex, caution is necessary when comparing the electronic spectra of the same complex in different solvents<sup>22,23</sup> or different complexes in the same coordinating solvent.<sup>10</sup> Selbin<sup>1,2</sup> has also pointed out that equatorial bonding may invert the order of the  $d_{xy}(b_2)$  and the  $d_{xz}, d_{yz}(e)$  levels. This inverted order is supported by McCormick<sup>10</sup> from studies of the vanadyl dithiocarbamates.

Hitchman and Belford<sup>27</sup> have assigned the bands of cis-bis-(benzoylacetonato)-oxo-vanadium(IV). Their criteria for assignment was the scheme which gave the most reasonable values for the molecular orbital coefficients which were



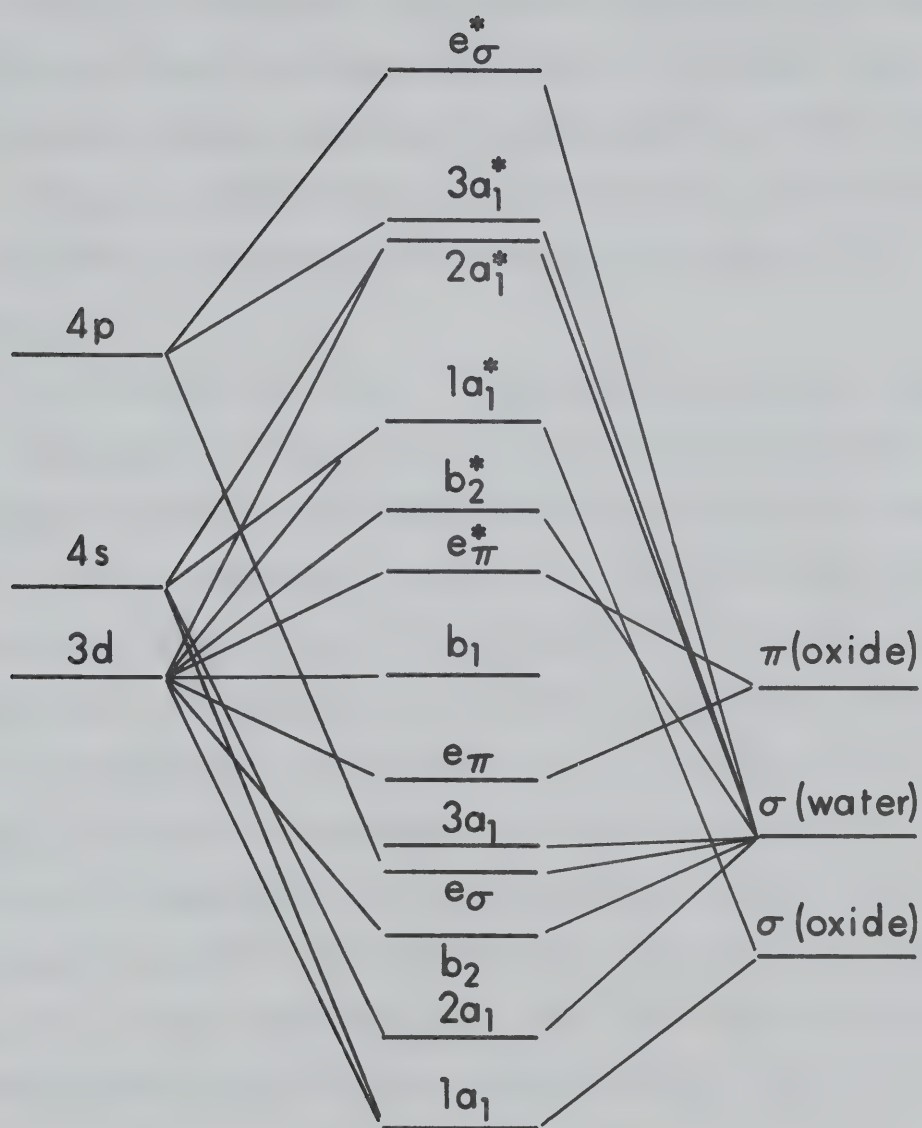


FIGURE I-2 Ballhausen and Gray molecular orbital scheme <sup>31</sup> for  $\text{VO}(\text{H}_2\text{O})_5^{2+}$ .





calculated from measured anisotropic EPR parameters and electronic transition energies. Their assignment required the relative energy ordering proposed by Ballhausen and Gray. This conclusion also agrees with the results of a low-temperature polarized single crystal spectrum of  $\text{VO}(\text{H}_2\text{O})_5^{2+}$ .<sup>33,34</sup>

Ballhausen and Gray<sup>31</sup> have also pointed out that their assignment of electronic transitions agrees with an assignment based on the relative intensities of the observed bands. In  $C_{4v}$  symmetry, the electric dipole vector components transform as the  $A_1$  and E representations and thus only transitions from the  $b_1$  ground state to excited states of  $b_1$  or e symmetries are allowed, i.e. the transition to the  $d_{xz}, d_{yz}(e)$  level is expected to be more intense than the other two transitions. The assignments proposed for the complexes studied in this work also agree with the expected intensity of the bands and show that the relative energies depend on the type of ligand coordinated to the  $\text{VO}^{2+}$  unit.

#### D. Infrared Spectra

Infrared spectroscopy is another technique commonly applied in the study of vanadyl complexes. The infrared spectrum is characterized by a sharp intense band at approximately  $1000\text{ cm}^{-1}$  which is attributed to the vanadium-oxygen stretch.<sup>1,2</sup> Since the multiple bond character of



the VO unit is believed to arise from electron donation from filled  $p_x$  and  $p_y$  orbitals of oxygen to empty  $d_{xz}$  and  $d_{yz}$  vanadium orbitals, coordination of a Lewis base in the axial position of a five coordinate complex should reduce the vanadium acceptor properties and lower the  $VO^{2+}$  stretching frequency. For example, addition of a pyridine molecule to  $VO(acac)_2$  lowers the vanadyl V-O stretching frequency<sup>35</sup> from 996 to 964  $cm^{-1}$ . The V-O stretching frequencies of a number of  $VO(acac)_2$  adducts with substituted pyridines have been studied, and the observed shifts in the V-O stretch upon adduct formation fall into either of two ranges, namely  $42 \pm 4 \text{ cm}^{-1}$  or  $29 \pm 4 \text{ cm}^{-1}$ .<sup>8,36</sup> It has also been shown that the complexes producing the small shift had the substituted pyridine coordinated in the axial position, and that the large shift corresponded to complexes having the substituted pyridine coordinated at an equatorial site.<sup>7,8</sup>

Infrared spectroscopy is also useful for studying the nature of the ligands coordinated to the vanadyl unit. The P-S stretches in dithiophosphinates are sensitive to the type of coordination in which the dithiophosphinate is involved.<sup>13</sup> This coordination may be bidentate, monodentate or ionic. The characteristic feature of the infrared spectra of vanadyl complexes containing the amides N,N-dimethylformamide and N,N-dimethylacetamide as ligands is the carbonyl absorption in the region 1600-1700  $cm^{-1}$ . The changes in the absorption frequencies observed upon





coordination to the vanadyl ion suggest that the amides coordinate via the carbonyl oxygen.<sup>37,38</sup>

#### E. Kinetic Studies

The host of experimental results already quoted and the theoretical descriptions of the bonding in vanadyl complexes definitely support the hypothesis that the chemical properties of the axial and equatorial coordination sites of vanadyl are quite different. It is well known that the axial vanadium-ligand bond is weaker than the equatorial bonds, since many six-coordinate vanadyl complexes release the ligand from the axial position when heated or dissolved in inert solvents.<sup>5,39</sup> One would expect therefore, that the rates of chemical exchange of the two types of coordinated ligands with uncoordinated ligands in solution would be rather different.

The effect of the coordination site on the exchange rate can be delineated by investigating complexes where all five of the ligands coordinated to the vanadyl ion are the same. The exchange of ligands from bulk solvent to the inner coordination spheres of two such complexes, penta-(N,N-dimethylformamido)-oxo-vanadium(IV) perchlorate ( $\text{VO}(\text{DMF})_5(\text{ClO}_4)_2$ ) and penta-(N,N-dimethylacetamido)-oxo-vanadium(IV) perchlorate ( $\text{VO}(\text{DMA})_5(\text{ClO}_4)_2$ ), have been studied and the results are discussed in detail in Chapter IV. When  $\text{VO}(\text{DMF})_5(\text{ClO}_4)_2$  is dissolved in DMF, an exchange



reaction may occur in which a coordinated DMF ligand is replaced by a DMF molecule from the bulk solvent. Such a reaction involves no net chemical change but can be studied by NMR because it has been well established that NMR lineshapes are influenced by dynamic processes such as an exchange of nuclei between nonequivalent magnetic sites.<sup>40,41</sup> The width of an NMR line depends on the transverse relaxation rate of the nuclei which in turn may be controlled by chemical exchange processes. Furthermore, the nuclear relaxation rate depends on its magnetic interactions with the paramagnetic species and the overall effect, as shown in mathematical detail in Chapter IV, is to broaden the NMR line of the bulk solvent.

In  $^{17}\text{O}$  NMR studies of the solvent line broadening by vanadyl ions in  $^{17}\text{O}$ -enriched water<sup>42,43</sup> the existence of two distinct types of coordinated water molecules was invoked in order to explain the observed line broadenings. The equatorially coordinated water molecules exchanged with those in the bulk solvent at a rate which could be determined from the line broadening data. The broadening due to the second type of coordinated water molecules indicated that their exchange rate was considerably faster than that for the equatorially coordinated water molecules. This second type of coordinated water could be either an axially coordinated molecule in the first coordination sphere, or



water molecules in outer solvation spheres, since both would be expected to exhibit rapid exchange with the bulk solvent. NMR studies of vanadyl perchlorate in other solvents<sup>44-46</sup>, and studies of vanadyl complexes in water<sup>47</sup> have not resolved this ambiguity. In all cases, the rates of the axial exchange process and second coordination sphere exchange were too rapid to permit quantitative study by the line broadening method.

EPR studies of vanadyl acetylacetonate and its amine adducts in benzene solution<sup>39</sup> have shown that the rate of elimination of an axially coordinated amine ligand is in the range  $10^6 - 10^8 \text{ sec}^{-1}$  at room temperature. The rate of exchange of equatorially coordinated water molecules in vanadyl perchlorate solutions<sup>42,43</sup> is in the range  $10^2$  to  $10^3 \text{ sec}^{-1}$ , several orders of magnitude slower than that observed for axial ligand elimination from the vanadyl acetylacetonate adducts. The rate of this latter reaction is too large to measure by NMR line broadening techniques, but was obtained from the EPR measurements.<sup>39</sup>

The NMR line broadening of the formyl proton in dimethylformamide (DMF) solutions of vanadyl perchlorate has been reported by Angerman and Jordan.<sup>44,45</sup> They obtained an activation energy of 7.25 kcal/mole for the exchange of DMF molecules between the first coordination sphere of the vanadyl ion and the bulk solvent. This activation energy is considerably lower than the 13.7





kcal/mole found for the exchange of equatorial water ligands in aqueous solutions of vanadyl perchlorate<sup>42,43</sup>, and similar values for other solvent ligands.<sup>48</sup> This observation indicated that further investigation of the vanadyl perchlorate - DMF system was warranted.



## CHAPTER II

### EXPERIMENTAL TECHNIQUES

#### A. Purification of Solvents

The solvents toluene (Allied Chemical Reagent), carbon disulfide (Mallinckrodt Analytical Reagent), pyridine (Raylo Reagent), hexamethylphosphoramide (Aldrich), N,N-dimethylformamide (Baker Reagent), N,N-dimethylacetamide (Fisher Certified) and N,N-diethylformamide (Eastman Organic Chemicals) were all purified by double vacuum distillation from phosphorus pentoxide or from molecular sieves (BDH type 3A) and stored under vacuum over molecular sieves. All solvents were subsequently transferred by distillation under vacuum except for hexamethylphosphoramide (B.P. = 100°C at 6 torr) <sup>49</sup> which was transferred with a syringe under a dry nitrogen atmosphere.

#### B. Preparation and Characterization of Complexes

##### 1. Vanadyl Dithiophosphinates <sup>13,14</sup>

The vanadyl complexes bis-(dimethyldithiophosphinato)-oxo-vanadium(IV), bis-(diphenyldithiophosphinato)-oxo-vanadium(IV) and bis-(O,O'-diethyldithiophosphato)-oxo-vanadium(IV), to be referred to as the methyl, phenyl and ethoxy complexes respectively, were prepared by adding the sodium salt of the corresponding dithiophosphinic or dithiophosphoric acid obtained from Dr. R. G. Cavell, University of Alberta,



to an aqueous solution saturated with vanadyl sulfate (Fisher). The resulting blue paste was extracted with chloroform. The vanadyl dithiophosphinate was left behind when the chloroform was removed under vacuum. The ethoxy complex was sensitive to air, but the phenyl and methyl complexes were washed in air with ether and then dried under vacuum. The methyl and phenyl complexes were stored under nitrogen with no decomposition, whereas the ethoxy complex showed black deposits within 15 minutes of exposure to air.

The complexes were characterized by their EPR spectra.<sup>13</sup> In addition the phenyl complex was subjected to microanalysis.

#### Analysis:

$\text{VO}(\text{S}_2\text{P}\phi_2)_2$ : Calc: C: 50.97 H: 3.56 S: 22.68

Found: C: 49.08 H: 3.72 S: 22.22

## 2. Vanadyl Perchlorates

$\text{VO}(\text{DMF})_5(\text{ClO}_4)_2$  was prepared by dissolving hydrated vanadyl perchlorate<sup>44,45</sup> in DMF and distilling off the water as a benzene-water azeotrope. Upon cooling the solution to  $-10^\circ\text{C}$ , blue crystals appeared which were collected by filtration. Drying under vacuum removed the excess solvent from the crystals.  $\text{VO}(\text{DMA})_5(\text{ClO}_4)_2$  was prepared by the same method with DMF being replaced by DMA. Characterization consisted of microanalysis.





## Analysis:

VO(DMF)<sub>5</sub>(ClO<sub>4</sub>)<sub>2</sub>:    Calc:    C: 29.59    H: 5.59    N: 11.08  
                                  Found:    C: 28.48    H: 5.76    N: 10.93

VO(DMA)<sub>5</sub>(ClO<sub>4</sub>)<sub>2</sub>    Calc:    C: 34.25    H: 6.47    N: 9.98  
                                  Found:    C: 33.50    H: 6.45    N: 9.86

3.    Bis-(o-phenanthroline)-oxo-vanadium(IV) perchlorate<sup>50</sup>

VO(C<sub>12</sub>H<sub>8</sub>N<sub>2</sub>)<sub>2</sub>(ClO<sub>4</sub>)<sub>2</sub> was prepared by adding an acetone solution of o-phenanthroline to an acetone solution of VO(H<sub>2</sub>O)<sub>5</sub>(ClO<sub>4</sub>)<sub>2</sub> which was acidified with dilute perchloric acid. Within several minutes of stirring, a fine green precipitate appeared. After cooling to -10°, the green powder was filtered, washed with acetone, washed with ether and dried under vacuum. The complex was characterized by microanalytical results.

## Analysis:

                                 Calc:    C: 46.03    H: 2.58    N: 8.95  
                                  Found:    C: 45.87    H: 3.46    N: 8.33

4.    Other Complexes

Numerous attempts were made to prepare HMP and pyridine adducts of the vanadyl dithiophosphinates in crystalline form by adding an excess of ligand and then removing this under vacuum. In all cases only an oil resulted. However, when VO(acac)<sub>2</sub> was dissolved in HMP and



the excess HMP pumped off there remained a green powder which was shown to be  $\text{VO}(\text{acac})_2 \cdot \text{HMP}$ .

Analysis:

Calc: C: 43.26 H: 7.26

Found: C: 43.01 H: 7.14

Thermogravimetric analysis showed the loss of one HMP group per  $\text{VO}(\text{acac})_2 \cdot \text{HMP}$  at a temperature of  $90^\circ\text{C}$ .

C. Sample Preparation

Solutions of the vanadyl dithiophosphinate complexes were prepared under vacuum by distilling a calibrated volume of solvent ( $\text{CS}_2$  or toluene) into a vessel containing a weighed amount of the vanadyl complex. Required amounts of coordinating ligand were either distilled in (DMF and pyridine), or added with a syringe under dry  $\text{N}_2$  atmosphere in a glove bag. The solution was then thoroughly degassed by several freeze-pump-thaw cycles and transferred under vacuum to an attached 1 cm quartz spectrophotometer cell for optical measurements and/or a 4 mm pyrex tube suitable for EPR measurements. For NMR studies, an NMR tube was attached to the vessel and 5% by volume of hexamethyldisilane or cyclopentane were distilled in to serve as internal references to facilitate chemical shift measurements. All EPR and NMR tubes were sealed and stored at liquid  $\text{N}_2$  temperature until used.



The vessel was constructed such that after the EPR and NMR tubes had been sealed, the vessel could be placed into a modified cell compartment of the Cary 14 spectrophotometer. Samples of vanadyl perchlorates were prepared in an analogous manner.

Toluene solutions of the complexes containing pyridine consistently showed black deposits in the sample tube when prepared at room temperature. At lower temperatures, no decomposition was observed, but the EPR lines were so broad at these temperatures that the hyperfine splitting details of the spectra were not resolved. In order to study the pyridine-vanadyl dithiophosphinate complexes,  $\text{CS}_2$  was used as a solvent. The much lower viscosity of  $\text{CS}_2$  produced spectra showing well-resolved hyperfine structures over the temperature range  $-45^\circ\text{C}$  to  $+45^\circ\text{C}$ . The disadvantage of using  $\text{CS}_2$  as a solvent is that the complexes do not remain in solution as the frozen state is approached and glass spectra could not be obtained.

Solutions for conductance and infrared measurements were prepared under bench conditions using only the most stable of the dithiophosphinate complexes, the phenyl complex. These solutions showed color changes after approximately a thirty minute exposure to air. Experiments quoted were completed within this time. Nujol mulls of the vanadyl perchlorates were prepared under dry  $\text{N}_2$  in a glove bag and the spectra recorded immediately





after preparation.

D. Instrumentation and Measurement Techniques

Electronic and near infrared spectra were recorded on a Cary 14 spectrophotometer equipped with a vertically extended cell compartment to accommodate sample vessel and spectrophotometer cell. Infrared spectra were recorded on both a Perkin-Elmer 457 using cesium iodide plates and a Beckman IR-11 using 0.5 mm cesium bromide cells.

The EPR spectra were obtained with a Varian V-4502 EPR spectrometer equipped with an Alpha model 3093 Digital NMR Gaussmeter for magnetic field calibration. Normal precautions were taken to prevent lineshape distortion by excessive 100 Kc field modulation. The g-values were measured relative to Fremy's salt ( $g = 2.00550$ )<sup>51</sup> using a Varian V-4532 dual cavity accessory or calculated from the ratio of the magnetic field to the klystron frequency. Klystron frequencies were measured using a Hewlett Packard model X532B frequency meter. Both methods gave g-values which were equal within the experimental error. The sample was maintained at constant temperature ( $\pm 1^\circ\text{C}$ ) with a Varian V-4557 temperature controller and the temperature was measured with a copper constantan thermocouple combined with a Hewlett-Packard 3420A DC Differential Voltmeter.

Proton NMR spectra were recorded on Varian A60-D and HA-100 NMR spectrometers equipped with variable



temperature accessories. Sample temperatures on the A60-D were determined by comparison of the peak to peak separation of methanol or ethylene glycol samples with calibration charts published by Varian Associates.<sup>52</sup> Temperatures on the HA-100 were determined with a copper constantan thermocouple. In both cases temperatures were accurate to  $\pm 1^\circ\text{C}$ . Linewidths were measured on expanded sweeps and were reproducible to  $\pm 1$  Hz. The normal precautions were taken to prevent signal saturation and ensure correct phasing. Chemical shifts relative to the internal standards cyclopentane or hexamethyldisilane were measured directly on a 500 Hz sweep spectrum for the A60-D spectra whereas a Hewlett-Packard model 5326C frequency counter was used to obtain shifts on the HA-100. The accuracy of the shift measurements were limited by the error involved in determining the centers of the solvent resonance lines.

Conductance results were obtained by measuring the resistance of a YSI 3400 series conductance cell from Yellow Springs Instrument Co. with an Impedance Bridge Type 1650-A from the General Radio Company, Concord, Massachusetts. Thermogravimetric analyses were carried out under vacuum using the Dupont Model 950 Thermogravimetric Analyzer combined with the Dupont 900 Differential Thermal Analyzer.

Chemical analysis for C, H, N and S were performed by the microanalytical service at the University of Alberta, Department of Chemistry.



## CHAPTER III

### STUDY OF THE COORDINATION OF LEWIS BASES TO VANADYL DITHIO- PHOSPHINATES

#### A. Introduction

The formation of six-coordinate vanadyl complexes from five-coordinate complexes may be investigated by monitoring the changes in the spectroscopic properties of the vanadyl system caused by the addition of a Lewis base. The vanadyl dithiophosphinates are suitable complexes for these studies since the position trans to the vanadyl oxygen is vacant in non-coordinating solvents and this position is expected to accept a good electron donor group.

In vanadyl dithiophosphinates, the single unpaired electron couples to the  $^{51}\text{V}$  and the two  $^{31}\text{P}$  nuclei and exhibits a 24 line EPR spectrum in non-coordinating solvents. (See Fig. III-1). Additions of small amounts of Lewis base produce dramatic changes in the  $^{31}\text{P}$  hyperfine structure of the EPR spectra. The changes were found to be reversible and to vary with temperature and ligand concentration. The results could not be accommodated by the simple model proposed in studies of adducts of vanadylacetylacetonate with Lewis bases <sup>39</sup>, in which the Lewis base coordinates to the vacant trans position of the vanadyl complex. Instead, changes in the arrangement of the chelating dithiophosphate groups about the vanadyl ion must occur if the measurements





of the dithiophosphinate complexes are to be explained.

The EPR studies of the dithiophosphinates and their reactions with Lewis bases in solution are described in this chapter. The magnetic parameters which characterize the various vanadyl species and the determination of these parameters from the EPR spectra are discussed in the context of the relevant theory of EPR in section III-B. The experimental measurements are described in section III-C, the results obtained from these measurements are given in section III-D and the interpretation of the results and their implications in the chemistry of vanadyl dithiophosphinates is given in section III-E.

The visible spectra of the vanadyl dithiophosphinates show changes when the coordination about the vanadyl ion is modified. In the following sections, the electronic spectra of the various vanadyl species are given, the major transitions assigned and the transition energies are used in conjugation with the measured magnetic parameters to gain some insight into the MO occupied by the unpaired electron.

## B. Theory

A general spin Hamiltonian for vanadyl dithiophosphinate complexes is

$$\hat{\mathcal{H}} = \beta_0 \hat{\underline{S}} \cdot \underline{\underline{g}} \cdot \underline{\underline{B}} + \hbar \hat{\underline{I}}_V \cdot \underline{\underline{A}}^V \cdot \hat{\underline{S}} + \hbar \hat{\underline{I}}_{P1} \cdot \underline{\underline{A}}^{P1} \cdot \hat{\underline{S}} + \hbar \hat{\underline{I}}_{P2} \cdot \underline{\underline{A}}^{P2} \cdot \hat{\underline{S}} ,$$

(III-1)



where  $\beta_0$  is the Bohr magneton,  $\hat{S}$  is the electron spin operator,  $\underline{g}$  is the Zeeman interaction tensor,  $\vec{B}$  is the flux of the applied magnetic field and  $\hbar$  is Planck's constant divided by  $2\pi$ .  $\hat{I}_V$ ,  $\hat{I}_{P1}$  and  $\hat{I}_{P2}$  are respectively the nuclear spin operators for the  $^{51}\text{V}$  nucleus (spin 7/2) and the two  $^{31}\text{P}$  nuclei (spin 1/2).  $\underline{A}^V$ ,  $\underline{A}^{P1}$  and  $\underline{A}^{P2}$  are the nuclear-electronic hyperfine interaction tensors for the  $^{51}\text{V}$  and the two  $^{31}\text{P}$  nuclei respectively.

The observed EPR spectra of the vanadyl dithiophosphinates in solid solutions indicate that both the Zeeman and  $^{51}\text{V}$  hyperfine interactions have axial symmetry and that the  $^{31}\text{P}$  hyperfine interactions are isotropic. It is then convenient to expand the tensor interactions into individual terms and write the spin Hamiltonian as

$$\hat{\mathcal{H}} = \beta_0 g_{||} B \cos\theta \hat{S}_z - \beta_0 g_{\perp} B \sin\theta \hat{S}_x + \hbar A_{||}^V \hat{I}_{Vz} \hat{S}_z + \hbar A_{\perp}^V (\hat{I}_{Vx} \hat{S}_x + \hat{I}_{Vy} \hat{S}_y) + \hbar A^{P1} (\hat{I}_{P1} \cdot \hat{S}) + \hbar A^{P2} (\hat{I}_{P2} \cdot \hat{S}) \quad , \quad (\text{III-2})$$

where  $\theta$  is the angle between the molecular symmetry axis and the laboratory z-axis,  $g_{||}$  and  $g_{\perp}$  are the g-values parallel to and perpendicular to the symmetry axis respectively, and  $A_{||}^V$  and  $A_{\perp}^V$  are the  $^{51}\text{V}$  parallel and perpendicular hyperfine splitting constants (in  $\text{sec}^{-1}$ ).  $A^{P1}$  and  $A^{P2}$  are the isotropic hyperfine splitting constants for the two  $^{31}\text{P}$  nuclei (in  $\text{sec}^{-1}$ ). The solution of the Schrödinger equation



for the spin system represented by the Hamiltonian (III-2) in an appropriate set of basis functions, gives the allowed energy levels of the spin system. The electron spin transition probabilities between the states can be calculated by using time dependent perturbation theory<sup>41</sup> to describe the effects of the oscillating microwave field which is applied in a direction perpendicular to the static field B in an EPR experiment. The result is an EPR spectrum described by the resonance condition<sup>28,53,54</sup>

$$\omega_0 = \frac{g\beta_0 B}{\hbar} + A_V^V M_V + \frac{\hbar A_{\perp}^V (A_{\parallel}^V + A_V^V)}{4g\beta_0 B A_V^2} \cdot [I(I+1) - M_V^2] \\ + A^{P1} M_{P1} + A^{P2} M_{P2} \quad , \quad (\text{III-3})$$

$$\text{where} \quad g^2 = g_{\perp}^2 \sin^2 \theta + g_{\parallel}^2 \cos^2 \theta \quad , \quad (\text{III-4})$$

$$\text{and} \quad g^2 A_V^2 = g_{\perp}^2 A_{\perp}^2 \sin^2 \theta + g_{\parallel}^2 A_{\parallel}^2 \cos^2 \theta \quad . \quad (\text{III-5})$$

In equation (III-3),  $\omega_0$  is the spectrometer operating frequency in  $\text{sec}^{-1}$ , B is the applied magnetic flux in Gauss,  $M_V$  is the vanadium nuclear spin quantum number, I has the value 7/2 and  $M_{P1}$  and  $M_{P2}$  are the phosphorus nuclear spin quantum numbers. The  $^{51}\text{V}$  hyperfine interaction is considered to second order<sup>55</sup> while the  $^{31}\text{P}$  hyperfine interactions appear





only to first order since the corresponding second order contributions are very small.

Since the  $^{31}\text{P}$  interactions are isotropic, the anisotropic information is all described by the first three terms of equation (III-3). It is therefore convenient to consider the field positions  $B_{M_V}$  at the centres of each of the  $^{31}\text{P}$  superhyperfine multiplets. The spectrum arising from molecules whose molecular axes are parallel to the applied magnetic field is described by the resonance condition

$$\omega_0 = \frac{g_{\parallel} \beta_0 B_{M_V}}{\hbar} + A_{\parallel}^V M_V + \frac{\hbar}{g_{\parallel} \beta_0 B_{M_V}} \cdot \frac{A_{\perp}^V{}^2}{2} \cdot [I(I+1) - M_V^2], \quad (\text{III-6})$$

which is obtained from equation (III-3) with  $\theta = 0$ . Setting  $\theta = \pi/2$ , one obtains the resonance condition for the perpendicular spectrum

$$\omega_0 = \frac{g_{\perp} \beta_0 B_{M_V}}{\hbar} + A_{\perp}^V M_V + \frac{\hbar}{g_{\perp} \beta_0 B_{M_V}} \cdot \frac{A_{\perp}^V{}^2 + A_{\parallel}^V{}^2}{4} \cdot [I(I+1) - M_V^2]. \quad (\text{III-7})$$

Usually, the values of the magnetic field,  $B_{M_V}$ , for a resonance of given  $M_V$  value can be measured experimentally. The hyperfine constant for the parallel lines in the spectrum is expressed to a good approximation by



$$\frac{\hbar A_{||}^V}{g_{||} \beta_0} = a_{||}^V = \frac{1}{2} (B_{M_V} - B_{M_V-1} + B_{-M_V+1} - B_{-M_V}) \quad (\text{III-8})$$

where  $A_{||}^V$  is the hyperfine splitting in  $\text{sec}^{-1}$  and  $a_{||}^V$  is the splitting in units of Gauss. Units of Gauss are usually used when comparing splitting constants of various systems while units of  $\text{sec}^{-1}$  are convenient in expressions describing relaxation interactions as will be shown in Chapter IV. An expression similar to equation (III-8) can be given for  $A_{\perp}^V$  and  $a_{\perp}^V$  which characterize the resonance lines in the perpendicular spectrum. Since the vanadium hyperfine splitting constant is negative<sup>56</sup>, the lowest field multiplet corresponds to  $M_V = -7/2$ .

The g-values are determined from spectra recorded using a dual sample cavity, in which the sample of interest experiences the same magnetic flux and microwave frequency as a reference sample. The magnetic field at resonance for the standard,  $B_s$ , is different from that of the sample,  $B_{M_V}$ , if the standard g-value,  $g_s$ , is different from the sample g-value. The resonance condition for the sample is given by equation (III-3) and that for the reference by

$$\omega_0 = g_s \frac{\beta_0}{\hbar} B_s \quad (\text{III-9})$$

Combining equation (III-9) with (III-6) and (III-7), one



obtains the following expressions for the anisotropic g-values.

$$g_{||} = g_S B_S / (B_{M_V} + a_{||}^V M_V) - \frac{g_{\perp}^2 a_{\perp}^2 V^2}{2g_{||} B_{M_V}} \cdot \frac{[I(I+1) - M_V^2]}{(B_{M_V} + a_{||}^V M_V)} \quad (III-10)$$

$$g_{\perp} = g_S B_S / (B_{M_V} + a_{\perp}^V M_V) - \frac{g_{||}^2 a_{||}^2 V^2 + g_{\perp}^2 a_{\perp}^2 V^2}{4g_{\perp} B_{M_V}} \cdot \frac{[I(I+1) - M_V^2]}{(B_{M_V} + a_{\perp}^V M_V)} \quad (III-11)$$

In equation (III-10) the field values  $B_{M_V}$  correspond to the parallel spectrum and in equation (III-11) they refer to the perpendicular spectrum. After determining  $a_{||}^V$  and  $a_{\perp}^V$  from equation (III-8), the anisotropic g-values are calculated by an iterative procedure using equations (III-10) and (III-11).

In liquid solutions, rapid molecular reorientations average out the anisotropic Zeeman and hyperfine interactions and the effective spin Hamiltonian is

$$\hat{\mathcal{H}} = \beta_0 g_0 \hat{\vec{S}} \cdot \hat{\vec{B}} + \hbar A_0^V \hat{\vec{I}}_V \cdot \hat{\vec{S}} + \hbar A^{P1} \hat{\vec{I}}_{P1} \cdot \hat{\vec{S}} + \hbar A^{P2} \hat{\vec{I}}_{P2} \cdot \hat{\vec{S}} \quad (III-12)$$

where  $g_0$  is the isotropic g-value and  $A_0^V$  is the  $^{51}\text{V}$  isotropic hyperfine splitting constant. Again the solution of the Schrödinger equation in an appropriate basis set yields the





energy levels of the spin system and the allowed spin transitions are determined by considering the oscillating microwave field as a time dependent perturbation. The results show that the EPR spectrum in solution is described by the resonance condition <sup>28</sup>

$$\omega_0 = \frac{g_0 \beta_0 B}{\hbar} + A_0^V M_V + \frac{A_0^{V2} \hbar}{2} \cdot \frac{[I(I+1) - M_V^2]}{g_0 \beta_0 B} + A^{P1} M_{P1} + A^{P2} M_{P2} \quad (\text{III-13})$$

Since the <sup>31</sup>P interactions are adequately described by a first order interaction, the separation between the resonance lines arising from molecules with different <sup>31</sup>P nuclear spin quantum numbers, but the same value of  $M_V$ , will be equal. These separations in Gauss give the values of  $a^{P1}$  and  $a^{P2}$ , the <sup>31</sup>P hyperfine splitting constants in units of Gauss. The values can be converted to units of  $\text{sec}^{-1}$  by multiplication by the factor  $g_0 \beta_0 / \hbar$ . As in the analysis of the anisotropic spectra, it is convenient to consider the field positions  $B_{M_V}$  at the centres of the <sup>31</sup>P superhyperfine multiplets in order to determine  $g_0$  and  $A_0^V$  from spectra recorded with a dual-sample cavity. By considering the resonance conditions at  $B_{M_V}$  and  $B_{-M_V}$ , one derives the result

$$\frac{\hbar A_0^V}{g_0 \beta_0} = a_0^V = -(B_{M_V} - B_{-M_V}) / M_V, \quad (\text{III-14})$$



where  $a_o^V$  is the  $^{51}\text{V}$  hyperfine splitting in units of Gauss. Combining equation (III-13) with equation (III-9), one obtains the following expression for  $g_o$ .

$$g_o = g_s + g_s \left\{ \frac{2B_s - (B_{M_V} - B_{-M_V})}{B_{M_V} + B_{-M_V}} \right\} - \frac{2A_o^V{}^2 \hbar^2}{g_s \beta_o^2} \frac{[I(I+1) - M_V^2]}{(B_{M_V} + B_{-M_V})^2}.$$

(III-15)

$A_o^V$  and  $g_o$  are calculated by an iterative procedure using equations (III-14) and (III-15) for each pair of  $M_V$  and  $-M_V$  resonance lines. The average of the four results is the value reported. The isotropic  $^{51}\text{V}$  hyperfine splitting which is determined from the spectrum in liquid solution is related to the anisotropic splittings determined from the glass spectrum by

$$A_o^V = (A_{||}^V + 2A_{\perp}^V)/3.$$

(III-16)

Similarly the isotropic and anisotropic  $g$ -values are related by

$$g_o = (g_{||} + 2g_{\perp})/3.$$

(III-17)

Another feature of EPR spectra of vanadyl complexes in liquid solutions is the variation of linewidths with the vanadium nuclear spin quantum number  $M_V$ . The general linewidth theory developed by Kivelson and coworkers<sup>28,57</sup> indicates that electron spin relaxation in dilute ( $10^{-3}$  M) oxygen free solutions is caused primarily by the modulation of the



anisotropic Zeeman and  $^{51}\text{V}$  hyperfine interactions by the rotational motion of the molecules<sup>28</sup> and by collisional modulation of spin-rotational interactions.<sup>57</sup> Incomplete averaging of the anisotropic interactions results in lines whose widths vary with  $M_V$ . The peak-to-peak derivative linewidths of the hyperfine lines,  $\Delta B_{M_V}$ , can be fitted to the equation

$$\Delta B_{M_V} = \alpha + \beta M_V + \gamma M_V^2 + \delta M_V^3, \quad (\text{III-18})$$

using a least squares procedure to determine  $\alpha$ ,  $\beta$ ,  $\gamma$ , and  $\delta$ . These linewidth parameters are functions of the anisotropic magnetic parameters and the rotational tumbling time  $\tau_r$ .<sup>28</sup> The transverse relaxation time for the electron  $T_{2e}$  is related to the peak-to-peak width  $\Delta B$  by

$$\frac{1}{T_{2e}} = \frac{\sqrt{3}}{2} g_o \frac{\beta_o}{\hbar} \Delta B. \quad (\text{III-19})$$

$\tau_r$  may be calculated from the  $\alpha$ ,  $\beta$ ,  $\gamma$  or  $\delta$  values combined with the measured anisotropic parameters. An expression for  $\tau_r$  is also given by the Debye theory of rotational relaxation<sup>58</sup> as

$$\tau_r = \frac{4\pi\eta r^3}{3kT} \quad (\text{III-20})$$

where  $\eta$  is the coefficient of viscosity,  $r$  is the hydrodynamic radius of the molecule,  $k$  is the Boltzman constant and  $T$  is the absolute temperature. Equation (III-20) indicates that the linewidth depends on the molecular dimensions of



the vanadyl complex.

The basic relationships given above will be used in subsequent sections to analyze the experimental EPR spectra of the vanadyl dithiophosphinates, and in Chapter IV to analyze the spectra of the vanadyl perchlorates.

### C. Experimental Measurements

The majority of the experimental work involved the recording of the EPR spectra of the vanadyl dithiophosphinates in solid and liquid solutions. All solutions were prepared as described in Chapter 2. First, the EPR spectra of the complexes in the non-coordinating solvents toluene and  $\text{CS}_2$  at several temperatures were recorded in order to characterize the five coordinate complexes on the basis of their magnetic parameters. Next were recorded at several temperatures the EPR spectra of the vanadyl dithiophosphinate complexes in toluene which contained a small amount (5% by volume) of HMP and DMF. Since the spectra in small amounts of pyridine in toluene at room temperature indicated decomposition of the vanadyl complexes, the complexes were investigated in pyridine- $\text{CS}_2$  mixtures in the liquid range of  $\text{CS}_2$  ( $-45^\circ\text{C}$  to  $45^\circ\text{C}$ ). Under these conditions, no indication of decomposition was observed. The cases of the methyl and phenyl complexes in pyridine/ $\text{CS}_2$  were also studied at constant temperature as a function of pyridine





concentration (0.1% - 5.0% by volume). The complicated spectra in the mixed solvents were analyzed with the support of computer synthesized spectra. Finally, the EPR spectra of the complexes in the pure Lewis bases HMP, DMF and pyridine were recorded. Portions of the solutions prepared for the EPR samples were simultaneously transferred to a spectrophotometer cell for the recording of the electronic spectra. Additional solutions were prepared if larger complex concentrations were required to give adequate electronic absorption spectra.

The results of the EPR investigation were complemented by infrared studies. Infrared spectral investigations were limited to the pyridine-CS<sub>2</sub> solvent system which is relatively free of absorptions in the regions of interest. The vanadyl V-O stretching frequencies for the phenyl and methyl complexes in CS<sub>2</sub> and 5% pyridine/CS<sub>2</sub> were recorded. In addition, the symmetric P-S stretching frequency of the phenyl complex in CS<sub>2</sub> was recorded as a function of added pyridine. This P-S stretch is sensitive to the type of coordination of the dithiophosphinate group.

Solutions of the complexes in mixed solvents and pure Lewis bases were tested for the presence of ionic species by conductance measurements at room temperature.



#### D. Results

##### 1. Analysis of EPR Spectra in Toluene and CS<sub>2</sub>

Changes in the coordination in vanadyl complexes generally affect the magnitudes of the magnetic parameters which are manifest in the EPR spectra. To isolate the changes that occur when a Lewis base coordinates to the five coordinate vanadyl dithiophosphinates, it is necessary to characterize the free complexes by their magnetic parameters in non-coordinating solvents such as toluene and CS<sub>2</sub>.

The EPR spectra of  $10^{-3}$  M solutions of the three vanadyl complexes in toluene at 30°C are shown in Fig. III-1 and are similar to those reported previously by other workers.<sup>14,16-18</sup> These liquid solution spectra consist of eight lines due to the interaction of the unpaired electron with the <sup>51</sup>V nuclear spin ( $I = 7/2$ ); each of these eight lines is further split into a 1:2:1 triplet of lines by the interaction of the electron with two equivalent <sup>31</sup>P nuclei ( $I = 1/2$ ). Some of the 24 possible lines are not resolved in the spectra of the ethoxy complex because the phosphorus hyperfine splitting is approximately half as large as the vanadium splitting so that there is considerable overlapping of lines. The spectra in CS<sub>2</sub> are similar to those in toluene, but the lines were narrower because the CS<sub>2</sub> solutions are less viscous.

The isotropic magnetic parameters are readily determined from the spectra in Fig. III-1 using the methods



1. The first part of the paper is devoted to the study of the properties of the function  $f(x)$  defined by the equation  $f(x) = \int_0^x f(t) dt$ . It is shown that  $f(x)$  is a constant function.

2. In the second part, we consider the function  $g(x)$  defined by the equation  $g(x) = \int_0^x g(t) dt$ . It is shown that  $g(x)$  is a constant function.

3. The third part of the paper is devoted to the study of the properties of the function  $h(x)$  defined by the equation  $h(x) = \int_0^x h(t) dt$ . It is shown that  $h(x)$  is a constant function.

FIGURE III-1 EPR spectra of  $10^{-3}$  M liquid solutions of the vanadyl dithiophosphinate complexes in toluene at 30°C.

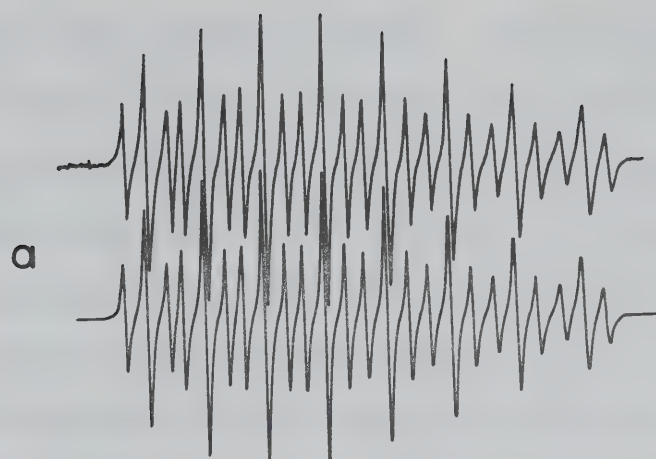
(a) bis-(dimethyldithiophosphinato)-oxo-vanadium(IV) ;

(b) bis-(diphenyldithiophosphinato)-oxo-vanadium(IV) ;

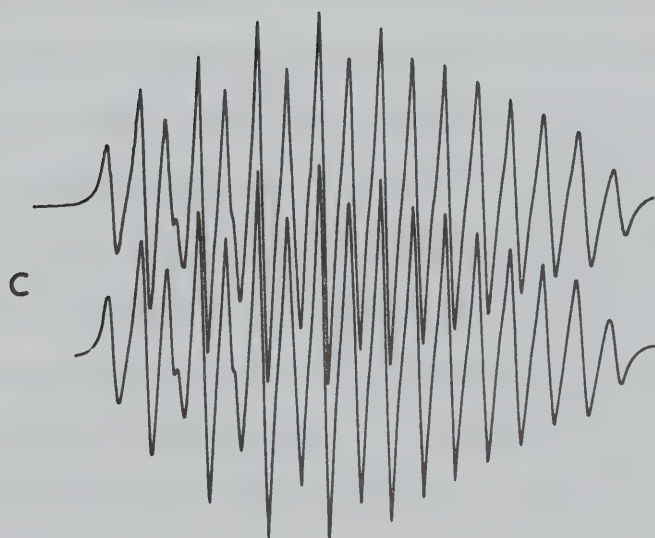
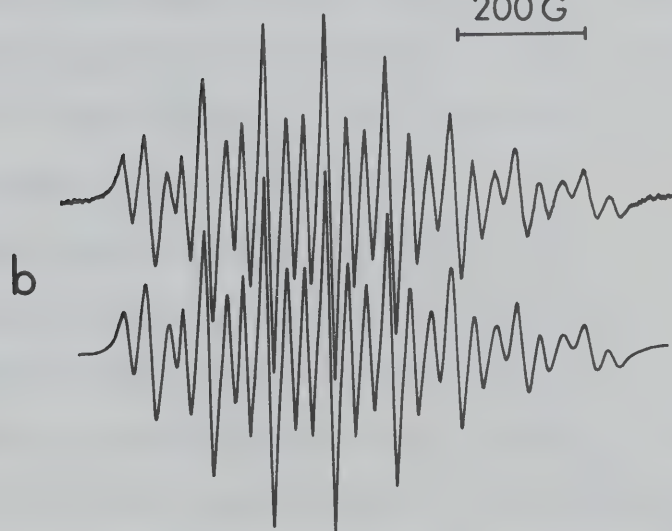
(c) bis-(O,O'-diethyldithiophosphato)-oxo-vanadium(IV) .

The experimental spectra are shown above the computer simulations in each case.





200 G





described in the previous section. The phosphorus hyperfine splitting  $a^P$  (Gauss) is simply the spacing between the components of the triplet.  $a_o^V$  and  $g_o$  are calculated from spectra recorded using a dual-cavity by an iterative procedure using equations (III-14) and (III-15). The values of the isotropic magnetic parameters for the toluene and  $CS_2$  solutions of the three complexes are given in Table III-1. The magnitudes of the variations in these parameters with temperature is similar to that observed for  $VO(acac)_2$ <sup>28</sup> and indicates that the molecular structure does not change with temperature.

The relative widths of the various lines in the spectrum were estimated from the peak-to-peak intensities of the lines. Measurement of the width of one of the lines which is relatively free of overlap on an expanded field sweep gave an absolute width from which estimates of the absolute widths of the various hyperfine lines were obtained. This procedure assumes the lineshapes are Lorentzian, in which case the product of the height and the square of the width is a constant. This method is inaccurate at low temperatures where the intensities are affected by overlapping of adjacent lines and for spectra of the ethoxy complex where overlapping of lines is severe.

Since the overlapping of lines in the spectra of the ethoxy complex and the variation of the linewidth of the hyperfine components introduces significant error in the calculation of  $a_o^V$  and  $a^P$ , the observed spectra were



TABLE III-1

Isotropic Magnetic Parameters<sup>†</sup> for Vanadyl Dithiophosphinates in CS<sub>2</sub> and Toluene Solutions

Substituent of Dithiophos- phinate	CS <sub>2</sub> at -30°			CS <sub>2</sub> at 30°			Toluene at 30°			Toluene at 116°		
	g <sub>o</sub>	V a <sub>o</sub>	a <sup>P</sup> a	g <sub>o</sub>	V a <sub>o</sub>	a <sup>P</sup> a	g <sub>o</sub>	V a <sub>o</sub>	a <sup>P</sup> a	g <sub>o</sub>	V a <sub>o</sub>	a <sup>P</sup> a
Methyl	1.9777	94.8	34.0	1.9766	95.4	33.4	1.9773	94.8	32.8	1.9728	95.7	32.4
Phenyl	1.9787	95.0	34.2	1.9781	95.5	33.3	1.9784	95.5	33.0	1.9765	95.9	32.6
Ethoxy	1.9819	94.8	50.7	1.9811	95.2	50.2	1.9814	95.0	49.7	1.9798	95.6	49.2

<sup>†</sup> Hyperfine splittings are in Gauss. Estimated errors are  $\pm .3$  Gauss for hyperfine splittings and  $\pm .0003$  for g-values.



compared with those synthesized by a digital computer. The computer program (see Appendix C) sets up a stick spectrum from input hyperfine splitting constants and assigns to each line a Lorentzian lineshape with a width characterized by an input parameter. Adjustments are made in the hyperfine splitting constants and linewidths on successive simulations until the agreement between the observed and calculated spectra is satisfactory. The calculated spectra which agree best with the observed ones are shown below the experimental spectra in Fig. III-1. The excellent fit for the spectrum of the ethoxy complex shows that this method allows the determination of splitting constants and linewidths under conditions of significant overlap. For cases where there is a minimum of overlap, the hyperfine splitting constants determined from the computer synthesized spectra agree with the values determined by direct calculation. The linewidths determined from the computer synthesized spectra are given for the three complexes in Table III-2. The much smaller linewidths of the methyl complex can be attributed to its small molecular radius compared to the radii of the phenyl and ethoxy complexes. The linewidth decrease with increasing temperature results from the decrease in solvent viscosity and the consequently smaller  $\tau_r$  values at higher temperatures.

The EPR spectrum of the phenyl complex in toluene at  $-150^\circ\text{C}$  is shown in Fig. III-2a.  $a^P$  is measured directly





TABLE III-2

EPR Linewidths in Gauss of Hyperfine Components of Vanadyl Dithiophosphinates at Various Temperatures in Toluene and CS<sub>2</sub>.

Methyl Complex in Toluene

Temp °C	-7/2	-5/2	-3/2	-1/2	1/2	3/2	5/2	7/2
0	7.50	6.29	5.78	5.80	6.41	7.47	9.19	11.3
30	6.03	5.36	5.18	5.20	5.57	6.25	7.17	8.40
60	5.08	4.69	4.61	4.67	4.96	5.41	6.04	6.76
90	5.14	4.83	4.77	4.82	5.06	5.37	5.88	6.45
116	5.40	5.09	5.09	5.14	5.29	5.54	5.87	6.28

Methyl Complex in CS<sub>2</sub>

Temp °C	-7/2	-5/2	-3/2	-1/2	1/2	3/2	5/2	7/2
-45	7.65	6.42	5.87	5.87	6.45	7.51	9.10	11.2
-30	6.80	5.88	5.47	5.54	5.99	6.88	8.15	9.59
-15	6.29	5.53	5.26	5.33	5.69	6.45	7.51	8.80
0	5.78	5.19	4.94	5.00	5.33	5.98	6.86	7.84
15	5.42	4.96	4.80	4.86	5.15	5.69	6.39	7.33
30	5.11	4.82	4.69	4.82	5.11	5.58	6.23	7.09
45	4.71	4.45	4.41	4.54	4.78	5.20	5.93	6.69

(continued.....)



TABLE III-2 (continued)

## Phenyl Complex in Toluene

Temp °C	-7/2	-5/2	-3/2	-1/2	1/2	3/2	5/2	7/2
0	21.2	15.4	12.6	12.1	14.0	18.0	24.2	32.6
30	13.7	10.4	8.82	8.68	9.91	12.6	16.3	21.1
60	10.1	7.87	7.02	7.04	8.04	10.0	12.3	15.2
90	8.22	6.79	6.17	6.25	6.97	8.40	10.4	13.1
116	6.96	5.97	5.58	5.65	6.25	7.28	8.81	10.5

Phenyl Complex in CS<sub>2</sub>

Temp °C	-7/2	-5/2	-3/2	-1/2	1/2	3/2	5/2	7/2
-30	19.5	13.6	11.0	10.7	12.3	16.4	23.4	32.9
-15	15.7	11.5	9.52	9.29	10.7	13.7	18.7	26.3
0	13.2	10.0	8.43	8.28	9.42	11.9	15.8	21.7
15	11.5	8.89	7.65	7.60	8.57	10.7	13.9	18.4
30	10.1	7.99	7.00	6.98	7.85	9.58	12.3	15.9
45	9.20	7.41	6.65	6.68	7.48	9.06	11.4	14.4

## Ethoxy Complex in Toluene

Temp °C	-7/2	-5/2	-3/2	-1/2	1/2	3/2	5/2	7/2
0	17.5	14.3	12.5	12.1	12.9	15.0	18.1	22.3
30	13.8	11.9	10.7	10.6	11.1	12.5	14.5	17.3

(continued.....)



TABLE III-2 (continued)

Ethoxy Complex in Toluene (continued)

Temp °C	-7/2	-5/2	-3/2	-1/2	1/2	3/2	5/2	7/2
60	10.7	9.64	9.06	9.01	9.40	10.3	11.6	13.3
75	10.2	9.25	8.74	8.67	9.05	9.83	11.0	12.5
90	9.02	8.29	7.93	7.89	8.19	8.87	9.82	11.0
105	8.42	7.77	7.46	7.46	7.75	8.34	9.19	10.3





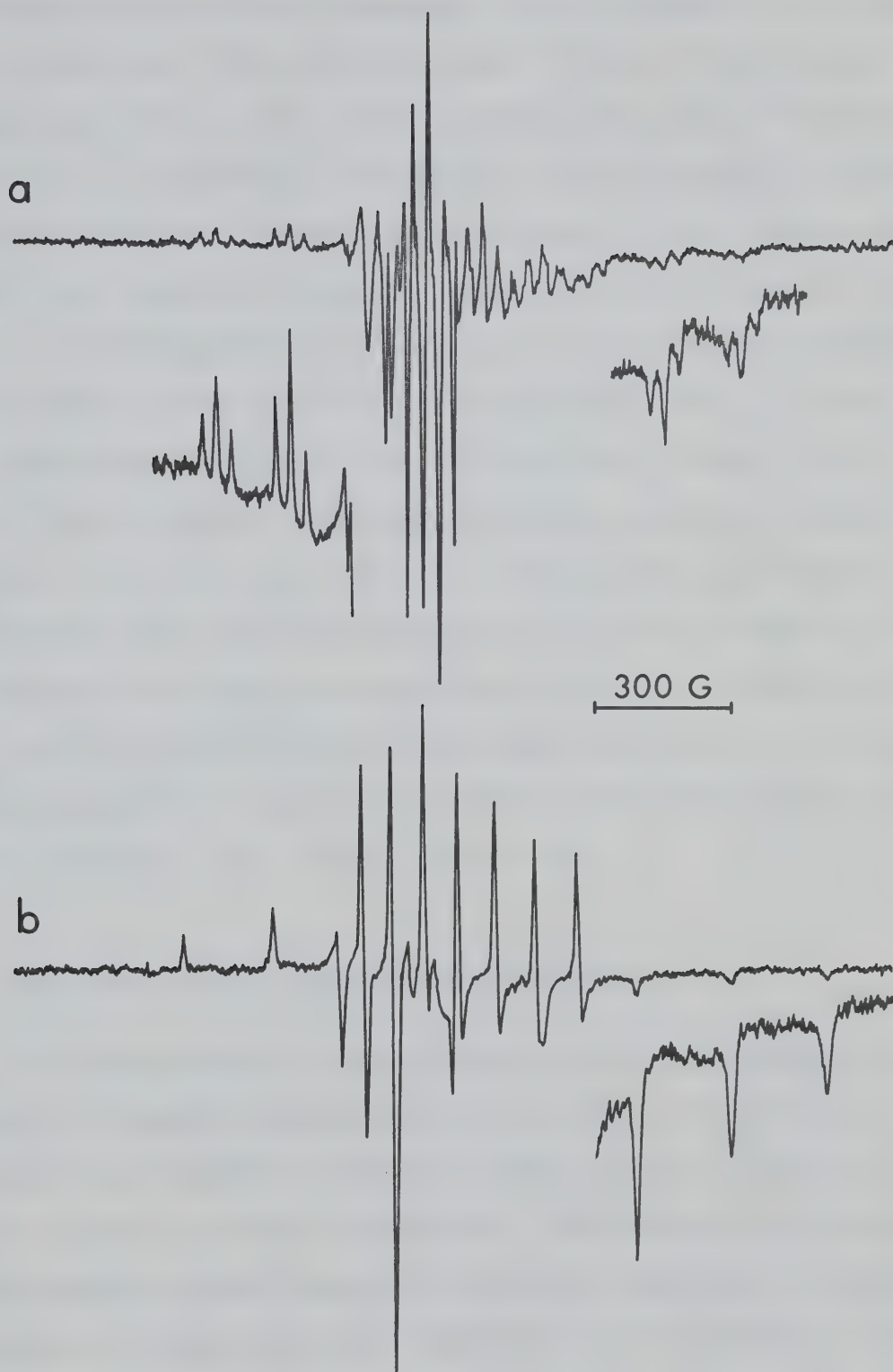


FIGURE III-2. EPR spectra of  $10^{-3}$  M solid solutions of bis-(diphenyldithiophosphinato)-oxo-vanadium(IV) at  $-150^{\circ}\text{C}$  in (a) toluene and (b) 5% HMP/toluene.



as the spacing of the components of the triplet of the parallel spectrum. The value is equal to that found in the liquid spectrum. Some of the previous EPR work <sup>18</sup> indicated that the  $^{31}\text{P}$  hyperfine interaction was anisotropic, but the observed isotropic phosphorus splittings do not agree well with those predicted from the anisotropic splittings. Since there is considerable overlapping of lines in the perpendicular part of the solid solution spectrum, only  $g_{||}$  and  $A_{||}^V$  are determined directly from the spectra. Values for  $g_{\perp}$  and  $A_{\perp}^V$  were computed from the isotropic parameters using equation (III-16) and (III-17). The magnetic parameters determined from the glass spectra are given in Table III-3. Values for solid  $\text{CS}_2$  solutions could not be obtained because the vanadyl dithiophosphinates became insoluble as the  $\text{CS}_2$  freezing point was approached and the EPR spectrum of the solid consisted of a single broad line.

## 2. Analysis of EPR Spectra in Mixed Solvents

The appearance of the EPR spectra of the vanadyl complexes is changed dramatically when a small amount of a strongly coordinating ligand is added to the solution in an inert solvent at room temperature. The triplet structure superimposed on the vanadium hyperfine components is replaced by a doublet pattern indicative of a species in which the unpaired electron is interacting with only one phosphorus nucleus. See Fig. III-3a. Furthermore, the phosphorus



TABLE III-3

Anisotropic Magnetic Parameters<sup>†</sup> of the Vanadyl Dithiophosphate Complexes in Different Solvents at -150°C

Solvent	Methyl Complex			Phenyl Complex			Ethoxy Complex		
	$g_{  }$	$g_{\perp}$	$\frac{V}{a_{  }} \frac{V}{a_{\perp}}$	$g_{  }$	$g_{\perp}$	$\frac{V}{a_{  }} \frac{V}{a_{\perp}}$	$g_{  }$	$g_{\perp}$	$\frac{V}{a_{  }} \frac{V}{a_{\perp}}$
Toluene <sup>††</sup>	1.959	1.986	168 58	1.957	1.989	167 60	1.968	1.988	167 59
5% HMP/toluene	†††	†††	†††	1.923	1.974	203 77	1.949 <sup>*</sup>	1.980 <sup>*</sup>	180 <sup>*</sup> 62
HMP	1.922	1.975	206 77	1.923	1.974	201 76	1.922	1.974	206 78
5% DMF/toluene	†††	†††	†††	1.936	1.977	195 71	1.933	1.975	196 72
DMF	1.935	1.977	198 72	1.932	1.977	197 73	1.935	1.976	196 72
5% pyridine/toluene	†††	†††	†††	1.956	1.982	169 58	1.959 <sup>**</sup>	1.982 <sup>**</sup>	168 <sup>**</sup> 60
Pyridine	1.956	1.977	174 58	1.954	1.979	171 57	1.954	1.980	173 60

<sup>†</sup> Hyperfine splitting constants are in Gauss. Estimated errors are  $\pm 0.02$  in  $g$ -values and  $\pm 1$  Gauss in splittings.

<sup>††</sup> The spectra in toluene show isotropic hyperfine interaction with two equivalent  $^{31}\text{P}$  nuclei.  $^{31}\text{P}$  splittings are 33.1, 33.5, and 51.5 Gauss, respectively, for the methyl, phenyl and ethoxy complexes.  $g_{||}$  and  $A_{||}^V$  could not be measured directly and were determined from the relations  $g_{\perp} = (3g_0 - g_{||})/2$  and  $a_{\perp}^V = (3a^V - a_{||}^V)/2$ .

<sup>†††</sup> The spectrum is a complicated mixture of several species and the parameters could not be measured accurately.

<sup>\*</sup> The spectrum of the ethoxy complex in 5% HMP/toluene is a superposition of a spectrum showing no  $^{31}\text{P}$  interaction, and a spectrum indicating hyperfine interaction with a single  $^{31}\text{P}$  nucleus. The parameters in the Table are those of the singlet. The parameters for the singlet species are essentially the same as those for the ethoxy complex in HMP.

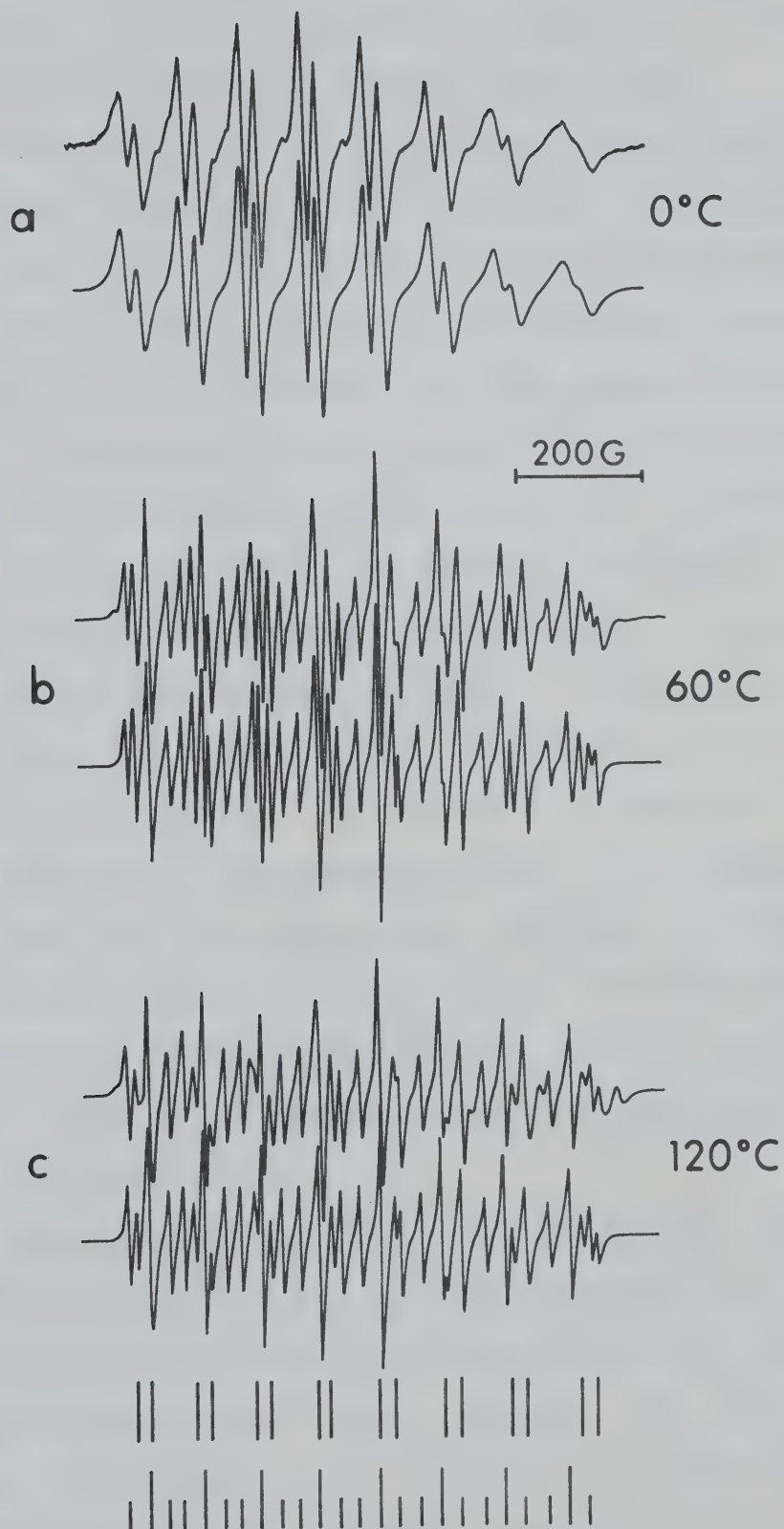
<sup>\*\*</sup> The spectrum of the ethoxy complex in 5% pyridine/toluene is predominantly a spectrum indicating hyperfine interaction with a single  $^{31}\text{P}$  nucleus. The parameters in the Table are those of the doublet spectrum with  $a^{PI} = 36.4$ . The parameters for the singlet species are essentially the same as those for the ethoxy complex in pyridine.







FIGURE III-3 EPR spectra of  $10^{-3}$  M liquid solutions of bis-(dimethyldithiophosphinato)-oxo-vanadium(IV) in 5% HMP/toluene at various temperatures. The experimental spectra are shown above the computer simulations in each case. Stick spectra for the two dominant vanadyl species are shown at the bottom of the figure.





splitting has decreased substantially compared to the splittings observed in solutions without added ligand.

The EPR spectra of  $10^{-3}$  M solutions of the methyl complex in 5% HMP/toluene solution at various temperatures are shown in Fig. III-3. The doublet patterns are observed in the range 0°C to 30°C. Below 0°C, the spectral lines become broad and poorly resolved. As the temperature of the solution is increased a triplet hyperfine pattern begins to appear and the doublet pattern decreases in intensity. See Fig. III-3b. At 120°C, the doublet structure is very weak and the spectrum consists predominantly of triplets, indicating that the unpaired electron is interacting with two equivalent  $^{31}\text{P}$  nuclei. Since the magnetic parameters describing this spectrum are identical to those for the vanadyl complexes in the absence of HMP, it is logical to conclude that this high temperature spectrum in 5% HMP/toluene solution arises from the vanadyl dithiophosphinate complex which is uncoordinated by HMP. Cooling the sample back to 0°C gave an EPR spectrum which was identical to the original spectrum at 0°C.

The appearance of the spectra of the vanadyl complexes in 5% HMP/toluene at 0°C and at 120°C suggests that the spectra obtained at intermediate temperatures are superpositions of doublet and triplet patterns. The doublet phosphorus splittings in the low temperature spectra were determined by fitting the observed spectrum at 0°C with



computer synthesized spectra. With these phosphorus splittings, the triplet phosphorus splittings and the linewidths of the various hyperfine components from the corresponding triplet spectra in toluene, computed spectra for a mixture of the two species with one and two phosphorus splittings were generated. Since the g-values of the doublet and triplet spectra are different (see Table III-4), a field shift between the centers of the two spectra to be superimposed was incorporated in the spectral computation. The relative proportions of doublet and triplet spectra were adjusted until the agreement between calculated and observed was satisfactory. The individual synthesized doublet and triplet spectra and the weighted sum of the two spectra that constitute the calculated spectrum in Fig. III-3b are shown in Fig. III-4.

The linewidths of the doublet species obtained in pyridine/ $\text{CS}_2$  solutions of the methyl complex were studied from  $-45^\circ\text{C}$  to  $+45^\circ\text{C}$ . In all cases, the linewidths of the doublet species were larger than the linewidths of the triplet species in  $\text{CS}_2$  solutions of the methyl complex at the same temperature. Since the amounts of pyridine required for predominance of the doublet species were small (1-5%), these differences could not be attributed to solution viscosity differences.<sup>59</sup> Detailed studies of the linewidths of the doublet species obtained in the HMP/toluene and DMF/toluene systems were not carried out because





TABLE III-4

Isotropic Magnetic Parameters<sup>†</sup> for Vanadyl Dithiophosphinates in 5% HMP/Toluene and 5% Pyridine/CS<sub>2</sub> at 30°C<sup>††</sup>

Substituent of Dithiophosphate	5% Pyridine/CS <sub>2</sub>			5% HMP/Toluene		
	g <sub>o</sub>	a <sub>o</sub> <sup>V</sup>	a <sup>P</sup>	g <sub>o</sub>	a <sub>o</sub> <sup>V</sup>	a <sup>P</sup>
Methyl	1.974	95.0	24.9	1.970	100.1	24.0
Phenyl	1.975	95.0	25.5	1.968	100.2	24.5
Ethoxy	1.976	94.8	36.0	1.972	99.4	31.2

<sup>†</sup> Hyperfine splittings are in Gauss. Estimated errors are  $\pm .5$  Gauss for splittings and  $\pm .001$  for g-values

<sup>††</sup> Only the ethoxy dithiophosphate in 5% DMF/toluene at 30°C gives a predominantly doublet spectrum with  $g_o = 1.975$   $a_o^V = 97.5$  Gauss and  $a^P = 35.0$  Gauss. Other dithiophosphate complexes give only triplets in 5% DMF/toluene.



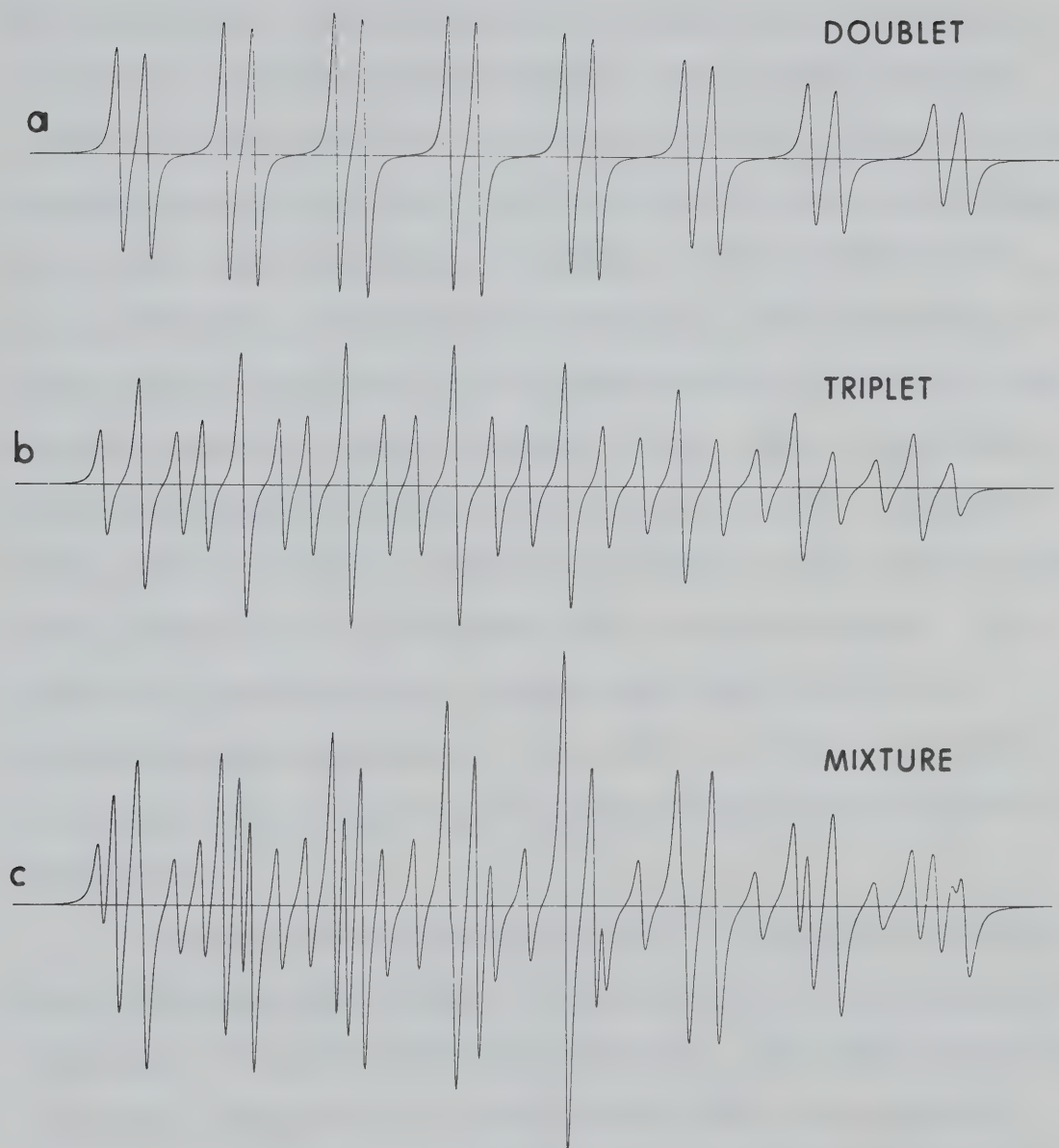


**FIGURE 111-4** Computer simulated EPR spectra of bis-(dimethyldithiophosphinato)-oxo-vanadium(IV) in 5% HMP/toluene at 60°C. (a) Doublet spectrum; (b) triplet spectrum; (c) sum of doublet and triplet spectrum.



the addition of large amounts of these ligands to the solutions would be required in order for the doublet species to predominate. The estimation of doublet linewidths, in solutions containing considerably less ligand, from the linewidths obtained from solutions where the doublet species predominates is difficult because the solution viscosities are often very different. Instead, it was assumed that the linewidths of the doublet species in HMP/toluene and DMF/toluene solutions can be approximated by those of the triplet species in pure toluene at the same temperature. This approximation leads to small errors in the determinations of the relative amounts of doublet and triplet species from comparison of calculated and observed spectra. The calculated spectra which agreed most closely with the observed ones are shown in Fig. III-3, and the magnetic parameters characterizing the doublet species are given in Table III-4.

Further changes occur in the  $^{31}\text{P}$  hyperfine structure when solutions containing a small amount of Lewis base are frozen and the glass spectra recorded. The EPR spectrum of the phenyl complex in 5% HMP/toluene (see Fig. III-2b) shows no phosphorus splitting at all. However, the spectrum of the methyl complex in the same solvent showed a mixture of several species whose individual magnetic parameters could not be measured. The spectra of the ethoxy complex in 1% HMP/toluene indicated the presence of two species -



one without phosphorus hyperfine splitting, and another with splitting due to one phosphorus nucleus. See Fig. III-5. The relative intensities of the singlet and doublet patterns were altered by changes in the HMP concentration, with a 1% HMP/toluene solution yielding a spectrum composed of predominantly doublets. See Fig. III-5. The  $a^P$  value determined from the glass spectrum and the average of the anisotropic  $^{51}\text{V}$  hyperfine splittings computed using equation (III-16) are equal to the respective isotropic values determined from the doublet spectrum of the liquid. The glass spectrum of the phenyl complex shows a singlet pattern in both 5% DMF/toluene and 5% pyridine/toluene solutions, although the spectrum of the methyl complex shows a complicated mixture in both solvent systems. The ethoxy complex in 5% DMF/toluene has a singlet glass spectrum, while in 5% pyridine/toluene the spectrum shows two patterns - a singlet and a doublet.  $a^P$  is again equal to the  $a^P$  value determined for the doublet species in the liquid spectrum of the same sample. These results point out that vanadyl complexes in solid solutions in 5% Lewis base/toluene produce two species - one giving rise to a doublet spectral pattern and a second giving rise to a singlet pattern. The magnetic parameters of the observed species in the various solvents are compiled in Table III-3.

The EPR spectra of the vanadyl dithiophosphinates in pyridine, DMF and HMP glasses all show the absence of any





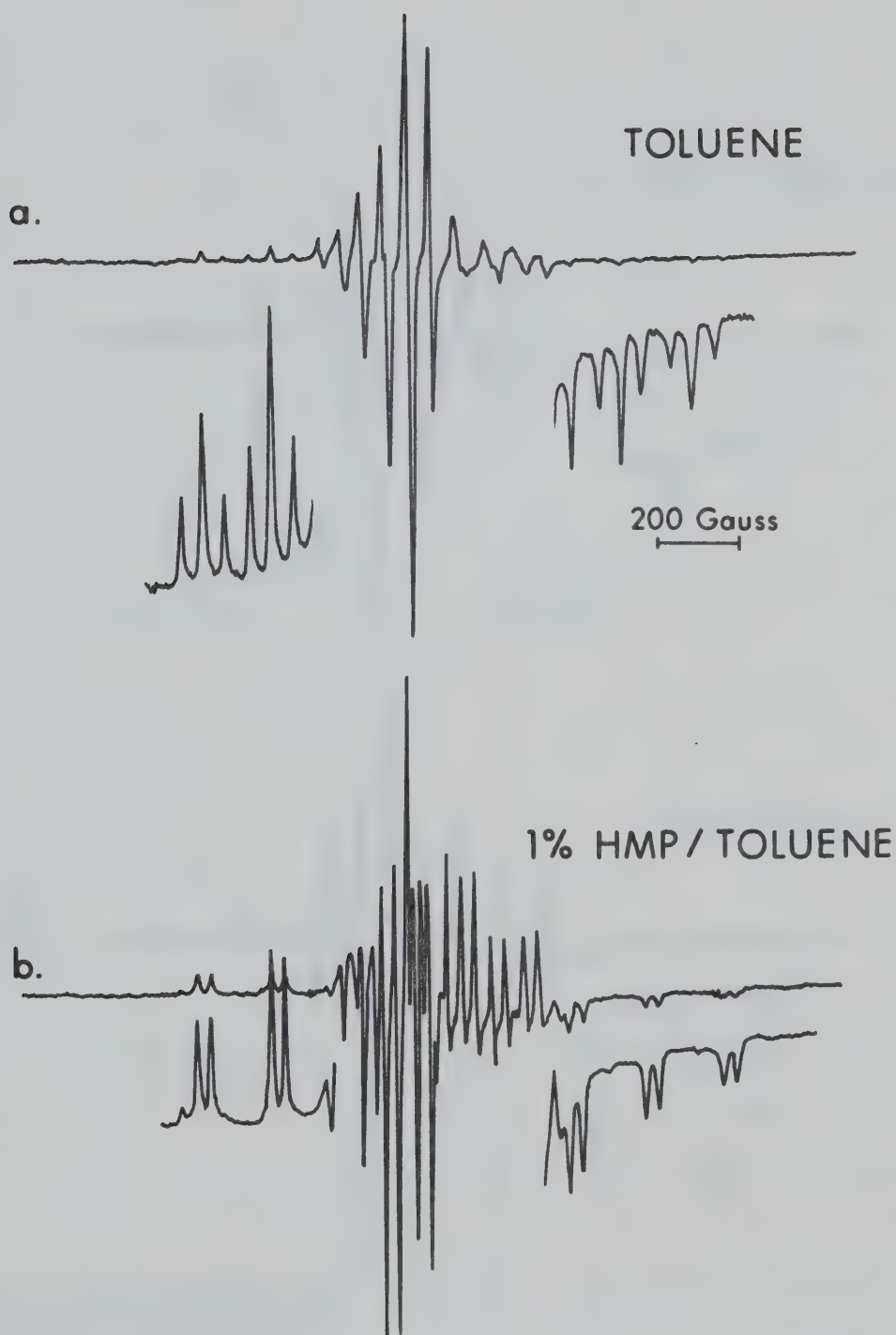


FIGURE III-5 EPR spectra of  $10^{-3}$  M solid solutions of bis-(O,O'-diethyldithiophosphinato)-oxovanadium(IV) at  $-150^{\circ}\text{C}$  in (a) toluene; (b) 1% HMP/toluene;

(continued....)



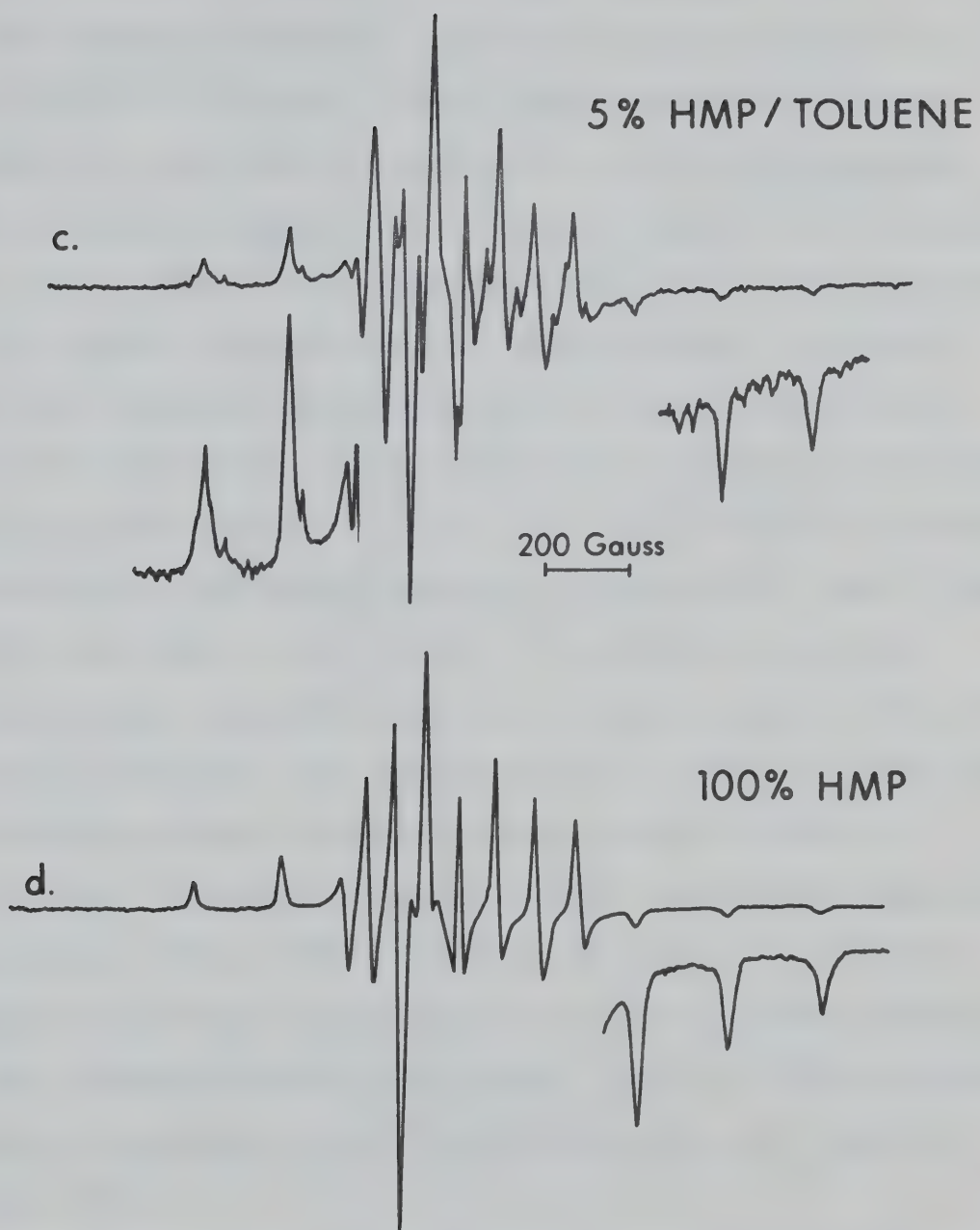


FIGURE III-5 (continued)

(c) 5% HMP/toluene; (d) HMP.



phosphorus hyperfine interaction. The spectra of the phenyl complex in the three solid solutions are shown in Fig. III-6. The magnetic parameters for these singlet spectra for a given complex are equal, within experimental uncertainty, to those for the singlet spectra in 5% Lewis base/toluene solid solutions (compare the values in Table III-3). Furthermore, the spectra of the complexes in pyridine, DMF and HMP at 30°C consist predominantly of eight singlet hyperfine lines with magnetic parameters equal, within experimental error, to the average of the anisotropic parameters obtained from the glass spectrum for the same complex-solvent system. The spectra of the phenyl complex in HMP at 116°C and in DMF at 30°C are shown in Fig. III-7. The singlet hyperfine patterns remain singlets within the liquid range of HMP and DMF, but in pyridine the spectrum shows a mixture of doublet and singlet patterns at higher temperatures as shown in Fig. III-8. The behavior of the methyl and ethoxy complexes in pyridine, HMP and DMF is similar to that of the phenyl complex in pyridine except that the doublet pattern appears at lower temperatures for the methyl complex. The isotropic magnetic parameters for the singlet patterns are compiled in Table III-5.

The EPR spectra of the methyl complex in pyridine/CS<sub>2</sub> mixed solvents at -45°C and in neat pyridine at 30°C are shown in Fig. III-9. It is clear that the doublet spectrum observed at low concentrations of pyridine decreases in





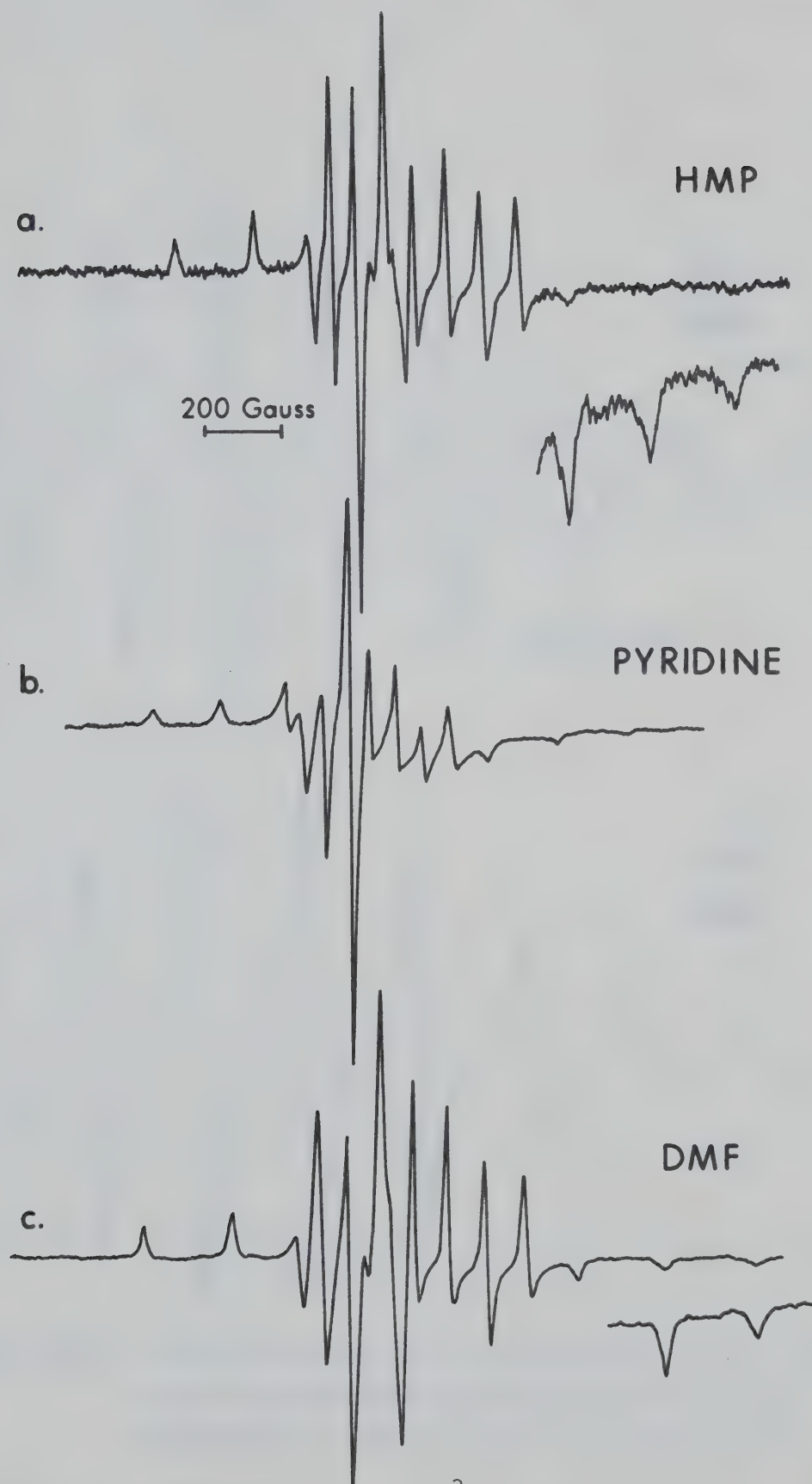


FIGURE III-6 EPR spectra of  $10^{-3}$  M solid solutions of bis-(diphenyldithiophosphinato)-oxo-vanadium(IV) at  $-150^{\circ}\text{C}$  in (a) HMP; (b) pyridine; (c) DMF.



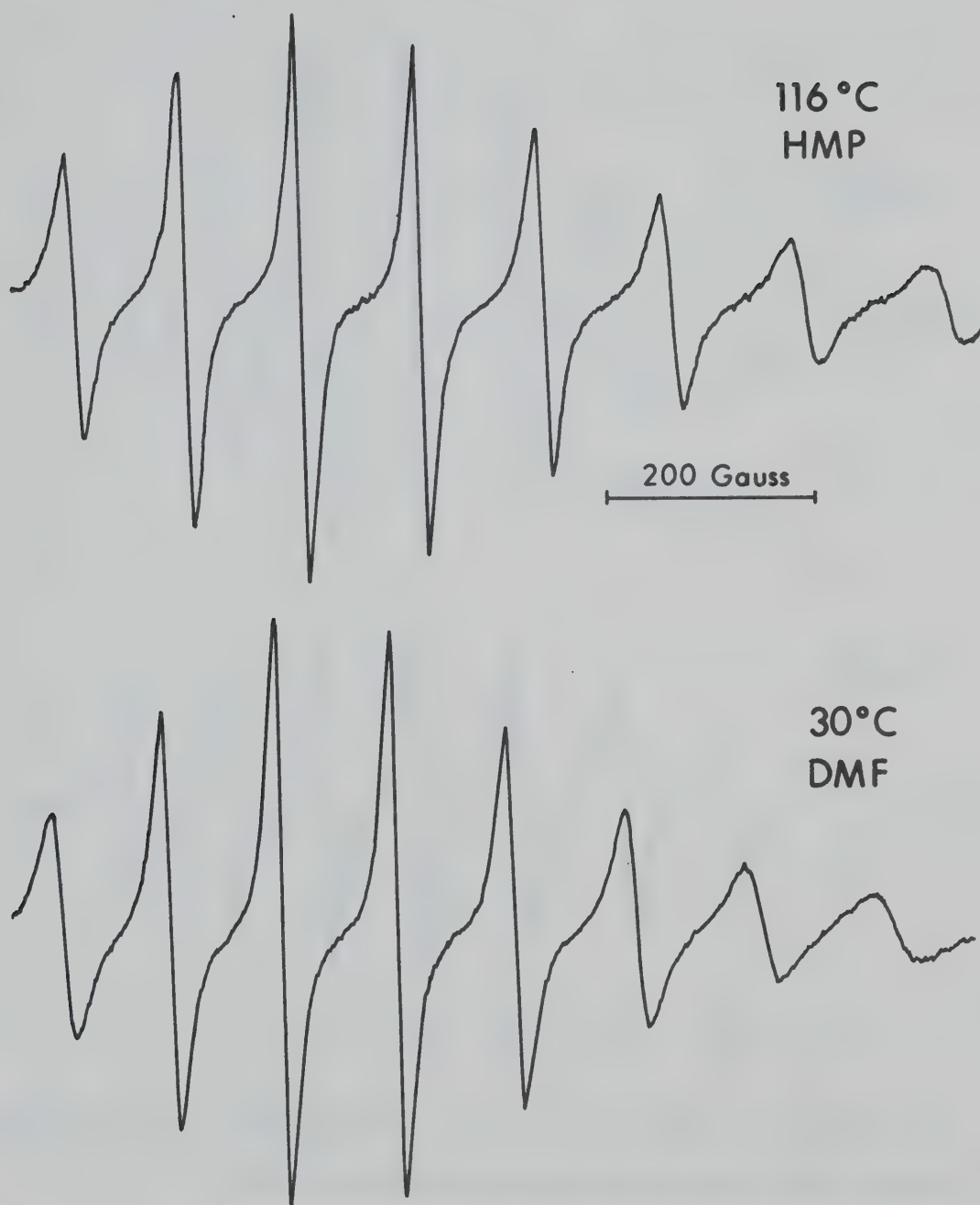


FIGURE III-7 EPR spectra of  $10^{-3}$  M liquid solutions of bis-(diphenyldithiophosphinato)-oxo-vanadium(IV) in HMP at 116°C and DMF at 30°C.



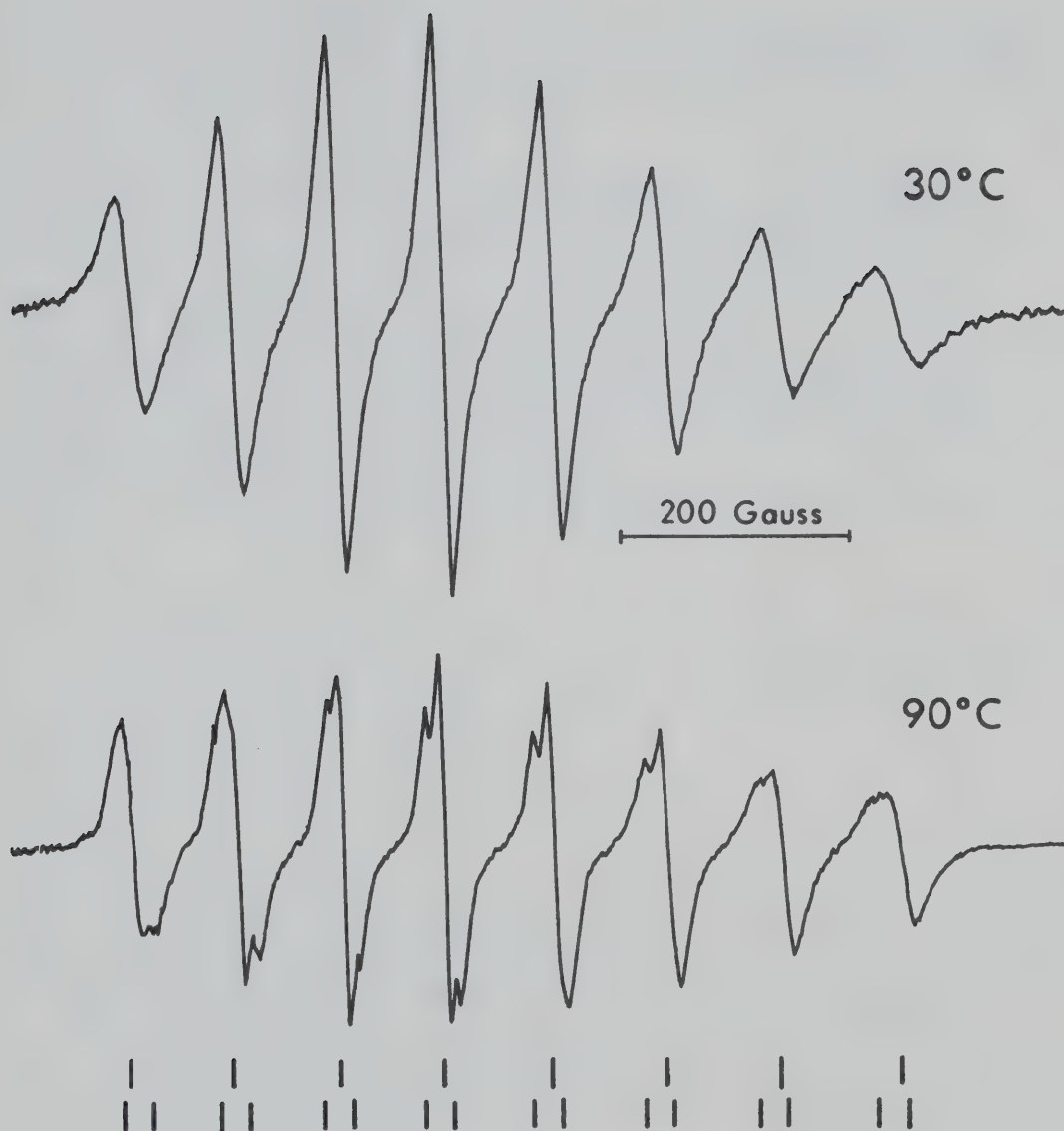


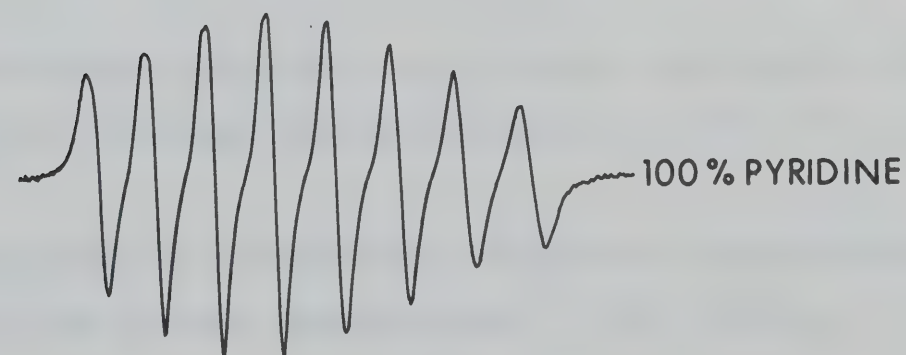
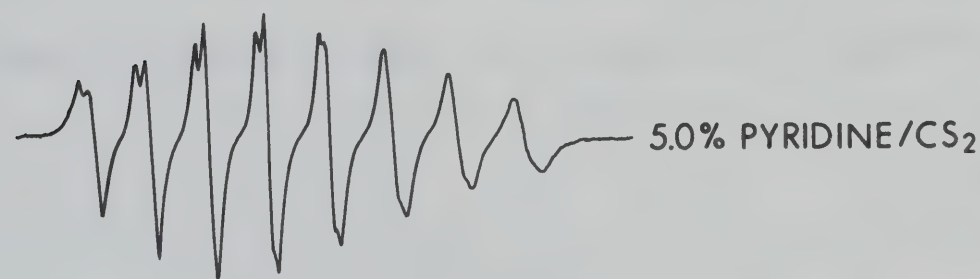
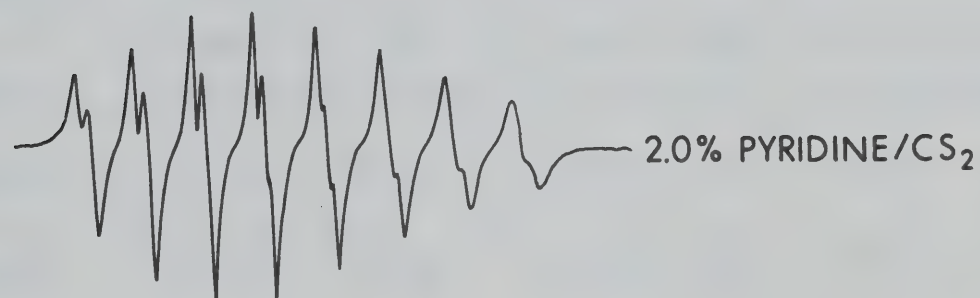
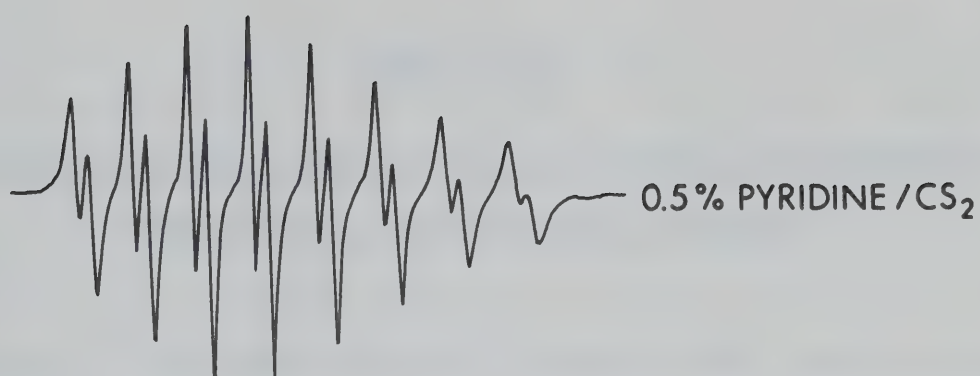
FIGURE III-8 EPR spectra of  $10^{-3}$  M liquid solutions of bis-(diphenyldithiophosphinato)-oxo-vanadium(IV) in pyridine at 30°C and 90°C. The stick spectra for the two dominant vanadyl species are given at the bottom of the figure.







FIGURE III-9 EPR spectra of  $10^{-3}$  M liquid solutions of bis-(dimethyldithiophosphinato)-oxo-vanadium(IV) in pyridine/ $\text{CS}_2$  mixtures of various compositions at  $-45^\circ\text{C}$ . The spectrum in 100% pyridine was recorded at  $30^\circ\text{C}$ . The stick spectra for the two dominant vanadyl species are given at the bottom of the figure.



200 G



TABLE III-5

Isotropic Magnetic Parameters<sup>†</sup> of Vanadyl Dithiophosphate  
Complexes in Coordinating Solvents

Complex	Pyridine at 30°C		DMF at 30°C		HMP at 116°C	
	$g_0$	$a_0^V$	$g_0$	$a_0^V$	$g_0$	$a_0^V$
Methyl	1.9740	93.5	1.9666	111.0	1.9657	113.9
Phenyl	1.9741	95.8	1.9649	112.9	1.9605	118.8
Ethoxy	1.9738	95.6	1.9652	113.0	1.9675 <sup>††</sup>	109.8 <sup>††</sup>

---

<sup>†</sup> Hyperfine splittings are in Gauss. Estimated errors are  $\pm 0.5$  for hyperfine splittings and  $\pm .0005$  for g-values.

<sup>††</sup> Spectrum is predominantly doublets. Parameters are those of the doublet species with  $a^P = 30.0$  Gauss.



intensity as the pyridine concentration is increased and a new spectrum appears which has no  $^{31}\text{P}$  hyperfine structure. The magnetic parameters of the singlet are equal, within the experimental error, to the magnetic parameters of the methyl complex in pure pyridine. A close examination of the spectra of the vanadyl dithiophosphinates in liquid toluene solutions with low HMP concentrations indicates the presence of peaks of low intensity which are not accounted for by the dominant doublet and triplet spectra. See Fig. III-3c. These weak lines occur at positions which are very close to those found in the singlet spectra of the complexes in solutions with high HMP concentrations. It appears that in all cases, when a Lewis base with strong electron donor properties is added to the toluene solutions of the vanadyl dithiophosphinates, three species, each with a dramatically different EPR spectrum, are present.

The preceding description of the experimental results has concentrated on the effects of the ligands HMP, DMF and pyridine on the EPR spectra of the vanadyl dithiophosphate complexes. Experiments have also been performed with other ligands which are less strongly coordinating. In toluene solutions containing various concentrations of dimethyl sulfoxide, phosphoryl chloride, triphenylphosphine oxide or trimethyl phosphate, the EPR spectra indicated the presence of more than one species and most of the lines could be ascribed to singlet, doublet or triplet  $^{31}\text{P}$  hyperfine patterns. See Fig. III-10. Detailed





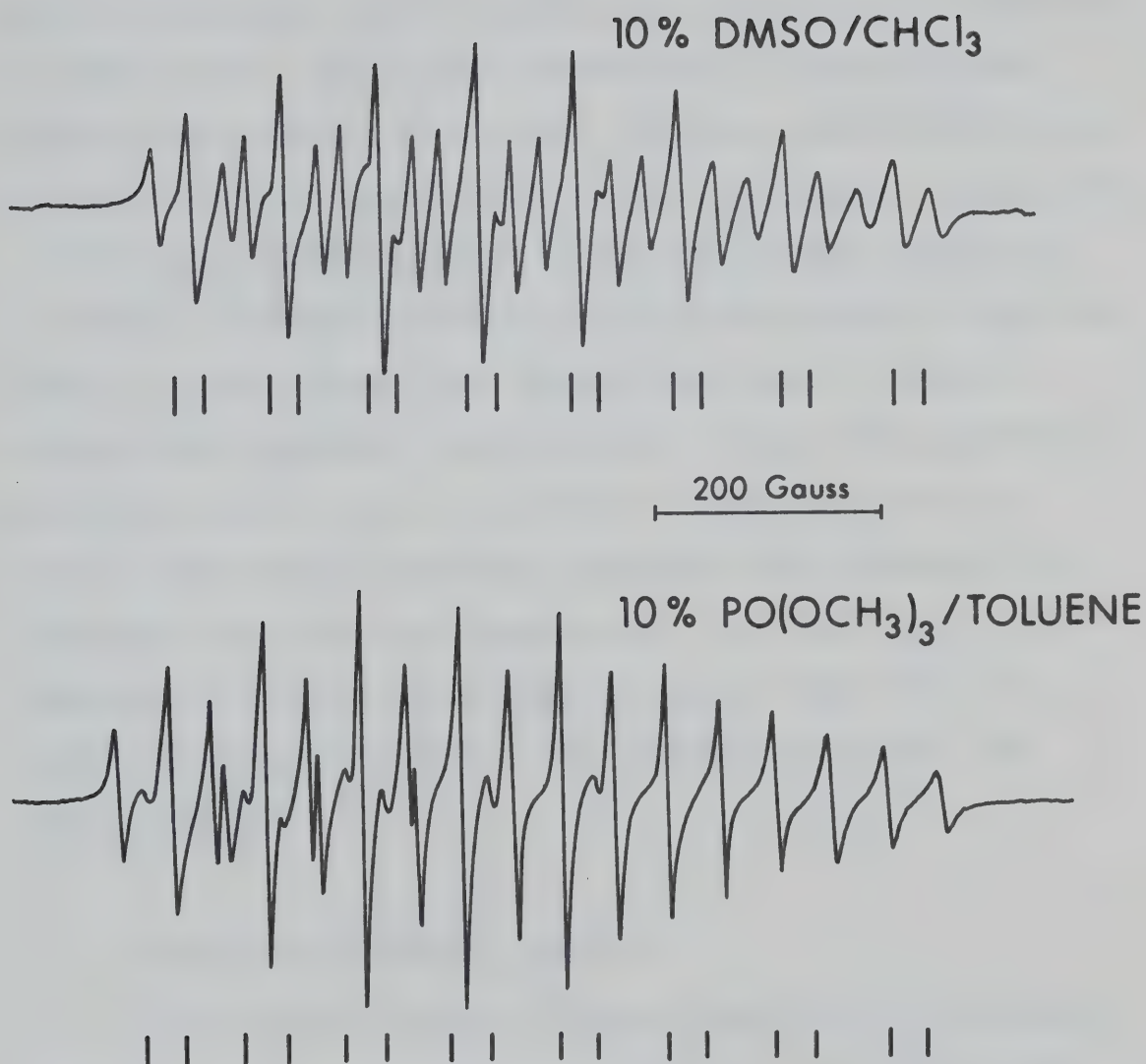


FIGURE III-10 EPR spectra of  $10^{-3}$  M liquid solutions of bis-(dimethyldithiophosphinato)-oxo-vanadium(IV) in 10% dimethyl sulfoxide/chloroform at 60°C and bis-(O,O'-diethyldithiophosphinato)-oxo-vanadium(IV) in 10% trimethyl phosphate/toluene at 40°C. The stick spectrum of the doublet pattern is shown below the experimental spectrum in each case.



analyses of the behaviour of the dithiophosphinate complexes in these solvent systems were not carried out since the HMP, DMF, and pyridine systems typify the results to be expected in other cases, and a clear separation of the different species was possible in the HMP, DMF, and pyridine solutions by variations in ligand concentration and sample temperature.

It has been reported <sup>17</sup> that the ethoxy complex is unstable in ethanol solutions. An investigation of the EPR spectra of both phenyl and ethoxy complexes in ethanol showed that the phenyl complex gives triplet <sup>31</sup>P hyperfine splitting, while the ethoxy complex shows a mixture of doublet and triplet hyperfine patterns whose relative intensities vary with the temperature. See Fig. III-11. The behavior of ethanol is similar to that of DMF which produced a mixture of doublets and triplets only with the ethoxy complex.

### 3. Analysis of Optical Spectra

The visible and near infrared spectra of the phenyl complex in several solvents are shown in Fig. III-12. The spectrum in toluene displays bands at 14.3, 17.1 and 24.4 kK which are characteristic of vanadyl complexes. In contrast to the spectra of  $\text{VO}(\text{H}_2\text{O})_5^{2+}$  <sup>31</sup> and  $\text{VO}(\text{acac})_2$  <sup>60</sup>, the spectrum of the phenyl complex in toluene has a low intensity shoulder on the low energy side rather than on the high energy side of the intense band at 17.1 kK. However,



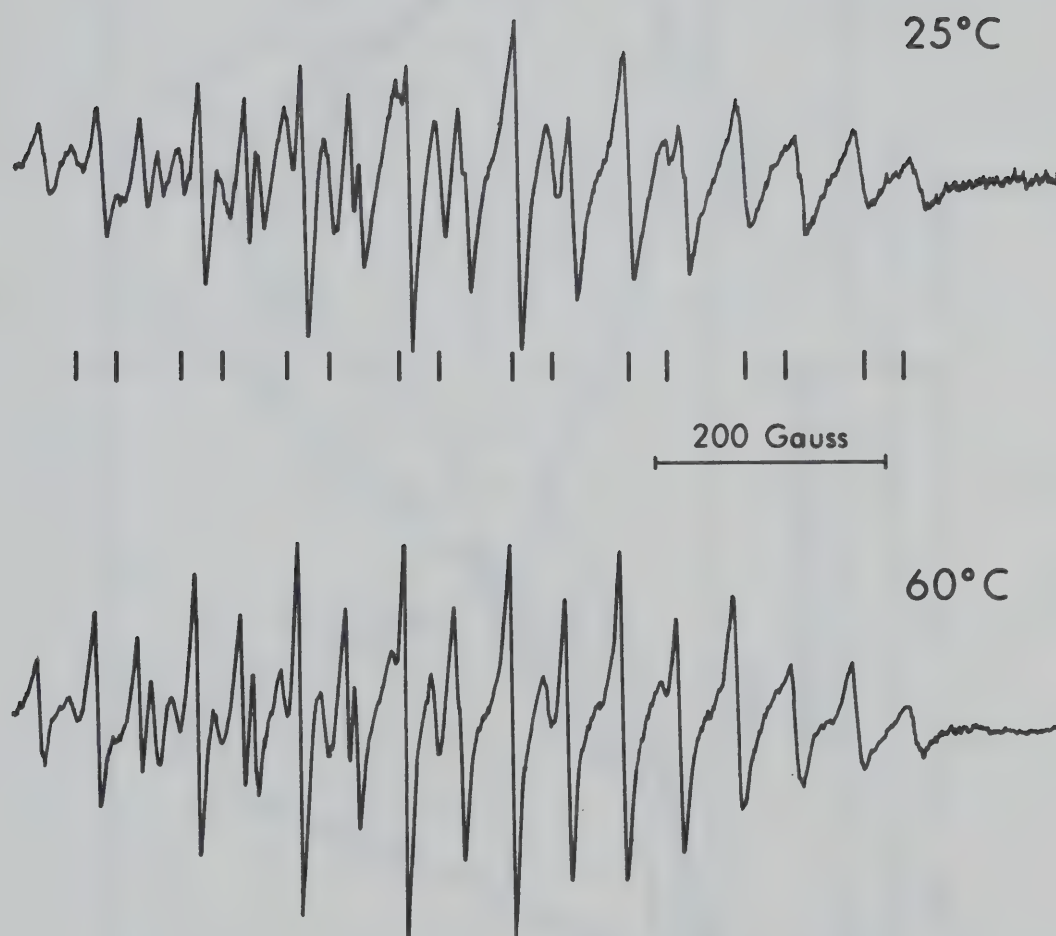


FIGURE III-11. EPR spectra of  $10^{-3}$  M liquid solutions of bis-(O,O'-diethyldithiophosphinato)-oxovanadium(IV) in ethanol at 25°C and at 60°C. The stick spectrum of the doublet pattern is shown below the experimental spectrum at 25°C.



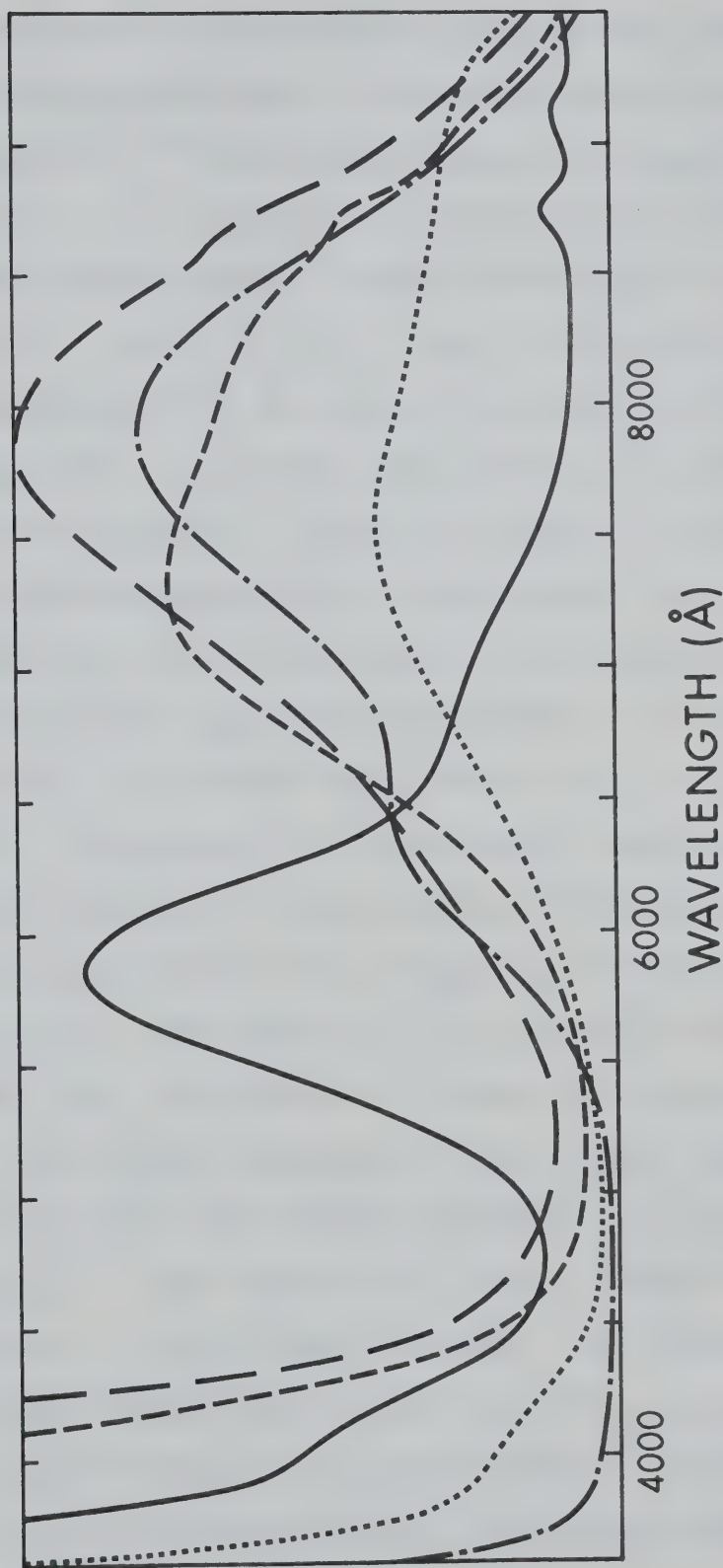


FIGURE III-12 Electronic absorption spectra of bis-(diphenyldithiophosphinato)-oxovanadium(IV) in various solvents. —, toluene; ----, 5% HMP/toluene, ...., HMP; —•—, DMF; — — —, pyridine.





the spectrum in toluene does parallel the spectra of vanadyl dithiocarbamates in non-coordinating solvents reported by McCormick.<sup>10</sup> McCormick assigned the most intense band to the  $b_1 \rightarrow e^*$  transition since this band experienced significant shifts when a ligand coordinated to the sixth position. The  $e^*(d_{zx}, d_{zy})$  level is expected to be changed by coordination at the axial site while the  $b_2^*(d_{xy})$  level is expected to be nearly independent of coordination at the sixth position. Since the ligand field produced by the dithiocarbamates should approximate that of the dithiophosphinates, it is reasonable to assign the electronic transitions as proposed by McCormick.<sup>10</sup> Then, with increasing energy, the three transitions are  $b_1 \rightarrow b_2^*$ ,  $b_1 \rightarrow e^*$  and  $b_1 \rightarrow a_1^*$ . The spectra for the methyl and ethoxy complexes are very similar to the spectrum of the phenyl complex and the transitions are assigned equivalently as shown in Table III-6. The spectra in the other non-coordinating solvent,  $CS_2$ , are similar to those in toluene.

The visible spectrum of the phenyl complex in the Lewis bases DMF and pyridine resembles the spectrum of  $VO(H_2O)_5^{2+}$ .<sup>31</sup> One expects the phenyl complex to be six-coordinate in Lewis base solvents. The presence of an additional ligand could shift the  $e^*(d_{zx}, d_{zy})$  level to lower energy while the  $b_2^*$  level remains relatively constant. With this inversion of levels, the transitions in order of increasing energy would be  $b_1 \rightarrow e^*$ ,  $b_1 \rightarrow b_2^*$  and  $b_1 \rightarrow a_1^*$ ,



TABLE III-6

Electronic Spectra of Dithiophosphinate Complexes <sup>†</sup>

Complex	Solvent <sup>††</sup>	Assignment		
		$a_2^*$	$b_1^*, b_2^*$	$a_1^*$
Methyl	A	14.3	16.7	24.7 sh
	B	12.2	13.5	26.0 sh
	C	11.9	13.2	†††
	D	15.4	12.6	†††
	E	14.7	12.0	†††
Phenyl	A	14.3	17.1	24.4 sh
	B	12.0	13.7	25.6 sh
	C	11.2	13.2	24.4 sh
	D	15.4	12.7	†††
	E	15.9	12.7	†††
Ethoxy	A	14.9	17.5	24.4 sh
	B	12.8	13.7	25.3 sh
	C	11.1	13.3	25.0 sh
	D	15.4	12.7	†††
	E	16.4	12.7	22.2 sh

<sup>†</sup> Absorption maxima in kK.

†† A, toluene; B, 5% HMP/toluene; C, HMP; D, DMF:

E, pyridine. CS<sub>2</sub> and toluene spectra are equivalent.

††† No shoulder is observed.



which is the assignment Ballhausen and Gray<sup>31</sup> have proposed for the pentaquo vanadyl cation. The two energy level schemes are shown in Fig. III-13.

In both pure HMP and 5% HMP/toluene solutions, it appears that both the  $e^*$  and  $b_2^*$  levels are shifted to lower energy by the addition of an HMP ligand to the vanadyl complex. The energy levels are assumed to have the same relative order as in toluene. However, the species in 5% HMP/toluene is different from the species in pure HMP because vanadyl complexes in 5% HMP/toluene give rise to a doublet pattern in the EPR spectrum and in pure HMP they give rise to a singlet pattern. Shifts of the optical bands of vanadyl complexes resulting from addition of Lewis bases have also been observed by other workers.<sup>10,22,60</sup>

The shifts observed for the vanadyl dithiophosphinates support the EPR results in that new species are formed in the presence of a Lewis base and one anticipates the new species are a result of differences in the coordination to the vanadyl ion.

The spectral results discussed above for the phenyl complex are also observed for the methyl and ethoxy complexes. The absorption maxima and band assignments are given explicitly in Table III-6.

#### 4. Analysis of Infrared Spectra

The frequency of the vanadyl vanadium-oxygen stretch





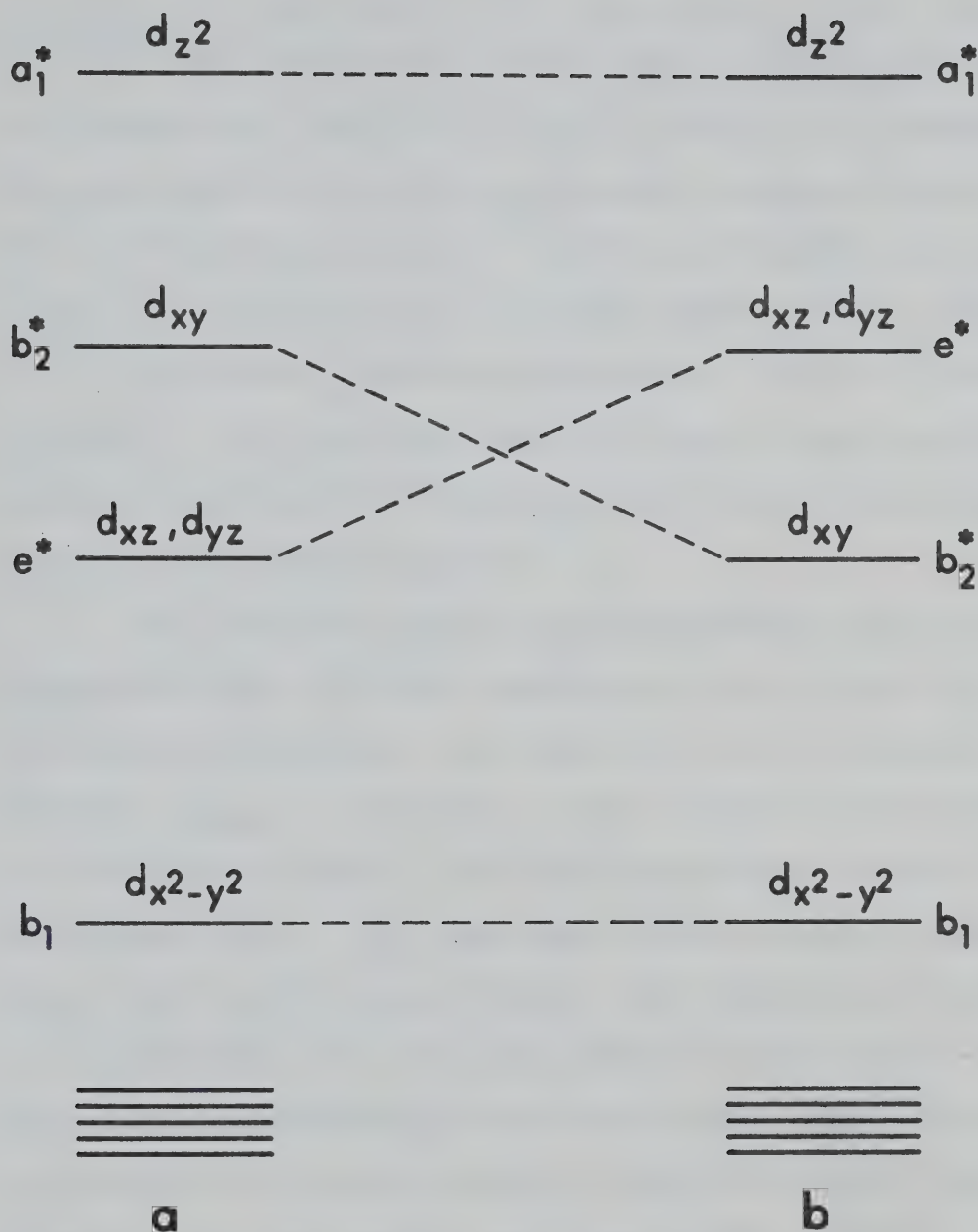


FIGURE III-13

Energy level schemes for oxo-vanadium(IV) complexes. (a), Ballhausen-Gray scheme<sup>31</sup>; (b), inverted level scheme.<sup>2</sup> The closely spaced lines represent filled bonding levels. The splittings are not drawn to scale.



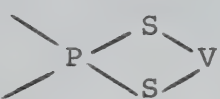
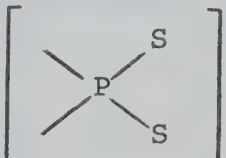
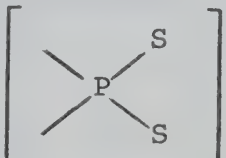
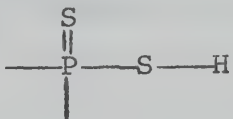
is often used to infer information about the coordination at the axial position of five coordinate vanadyl compounds.<sup>8,36,61</sup> The V-O stretch in the phenyl complex was observed to change from  $1000\text{ cm}^{-1}$  in  $\text{CS}_2$  to  $976\text{ cm}^{-1}$  in 5% pyridine/ $\text{CS}_2$  and the V-O stretch in the methyl complex changed from  $996\text{ cm}^{-1}$  in  $\text{CS}_2$  to  $972\text{ cm}^{-1}$  in 5% pyridine/ $\text{CS}_2$ . In both cases the shift is  $24\text{ cm}^{-1}$  and EPR spectra of the samples in 5% pyridine/ $\text{CS}_2$  showed predominantly doublet hyperfine patterns. This evidence suggests that the species giving rise to the doublet EPR spectrum has the position trans to the vanadyl oxygen occupied.

The infrared spectra of dithiophosphinates in the region  $500\text{--}700\text{ cm}^{-1}$  show absorptions due to the P-S stretching vibrations. The position of the symmetric P-S stretch,  $\nu_{\text{sym}}$ , is sensitive to the nature of the bonding of the sulfur atoms in the dithiophosphate moiety.<sup>13,15</sup> See Table III-7.  $\nu_{\text{sym}}$  decreases progressively as the bonding at the sulfur atoms changes from bidentate to ionic to monodentate. The infrared absorption of the bis-(diphenyldithiophosphinato)-oxo-vanadium(IV) complex in  $\text{CS}_2$  solutions with various amounts of pyridine added has been studied, and the results are shown in Fig. III-14. In the absence of pyridine, a single  $\nu_{\text{sym}}$  absorption is observed at  $570\text{ cm}^{-1}$ . Upon the addition of pyridine, additional absorptions at  $560\text{ cm}^{-1}$  and  $538\text{ cm}^{-1}$  appear. As the concentration of pyridine is increased, the intensity of the



TABLE III-7

Frequencies of Symmetric P-S Stretching Vibrations in Diphenyl-  
dithiophosphate Compounds<sup>†</sup>

<u>Compound</u>	<u>Bonding at Sulfur</u>	<u><math>\nu_{\text{sym}}(\text{cm}^{-1})</math></u>	<u>Medium</u>
Bis-(diphenyldithio- phosphinato)-oxo- vanadium(IV)		570	CS <sub>2</sub>
Sodium diphenyldithio- phosphate		565	Nujol mull
Ammonium diphenyldi- thiophosphate		561	Nujol mull
Diphenyldithiophosphinic acid		530	Nujol mull

<sup>†</sup> Infrared frequencies from ref. 13 and 15.



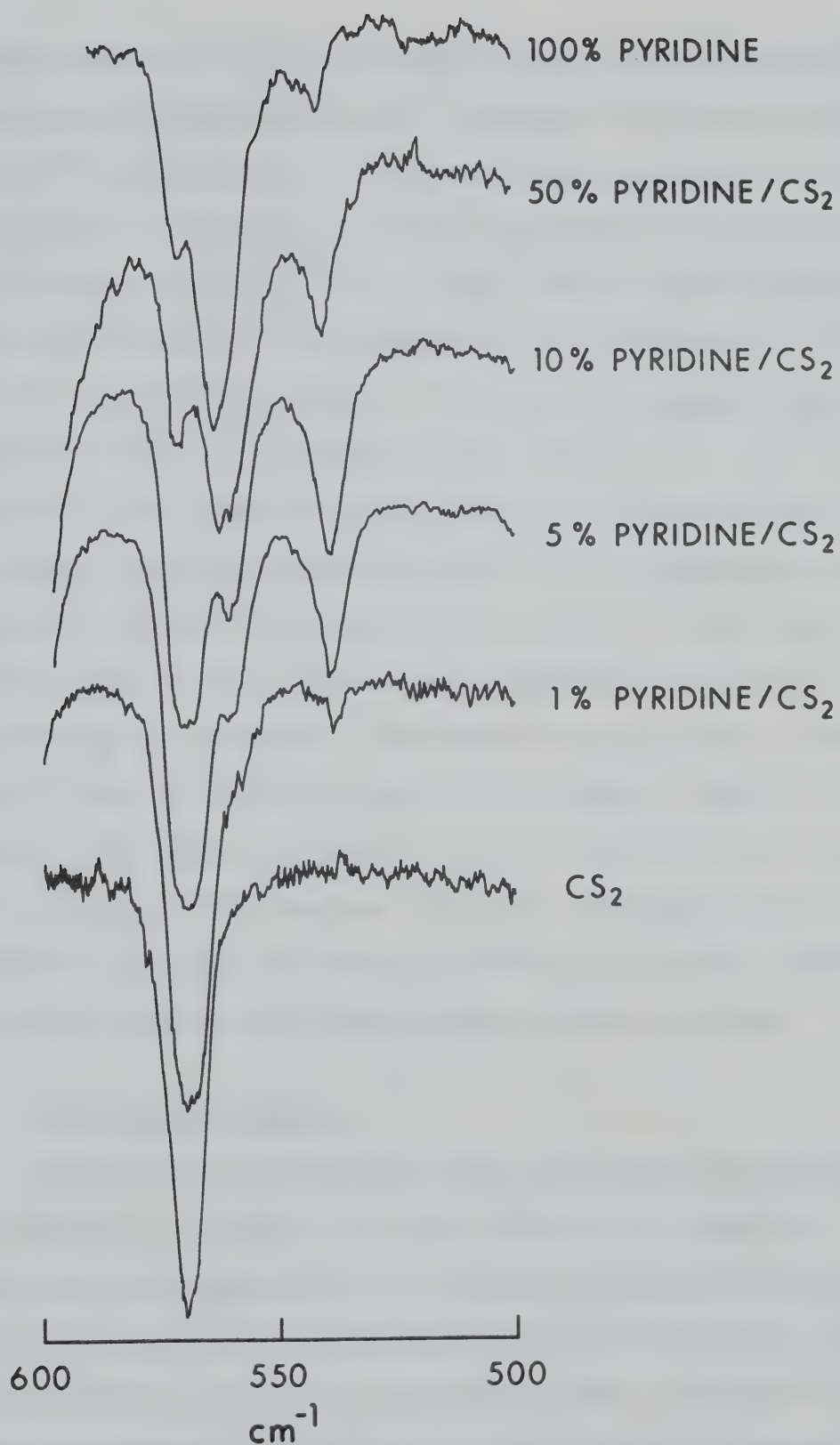


FIGURE III-14 Infrared spectra of bis-(diphenyldithiophosphinato)-oxo-vanadium(IV) in pyridine/CS<sub>2</sub> solutions of various compositions.





absorption at  $570\text{ cm}^{-1}$  decreases, while the intensities of the peaks at  $538$  and  $560\text{ cm}^{-1}$  increase. The absorption at  $538\text{ cm}^{-1}$  is maximum at a pyridine concentration of 10%, and decreases in intensity at higher pyridine concentrations. It is clear from Fig. III-14, that three distinct absorptions are present in the symmetrical P-S stretching region in 100% pyridine solutions of the phenyl complex. Spectral studies of the methyl complex were hampered by the low solubility of the complex in  $\text{CS}_2$ , and the air sensitivity of the ethoxy complex prevented study of its infrared spectrum. Infrared studies with other mixed solvent systems were not feasible due to the presence of interfering absorptions in the regions of interest. The conclusions formed on the basis of the infrared spectra of the phenyl complex in the pyridine- $\text{CS}_2$  mixed solvent should be applicable to the other mixed solvent systems since the EPR results in the pyridine- $\text{CS}_2$  mixed solvent are similar to the EPR results in the HMP-toluene and DMF-toluene solvent systems.

## 5. Conductance Results

Conductance measurements were performed to establish the presence or absence of ionic species in solutions. The conductance was measured as a function of the concentration of bis-(diphenyldithiophosphinato)-oxo-vanadium(IV) in several solvents. Since the experiments were carried out under bench conditions, only the most stable phenyl complex was



investigated. The numerical results are given in Appendix B and the summary of those results is shown in Table III-8.

TABLE III-8

Dependence of Conductance on Concentration of Bis-(diphenyl-dithiophosphinato)-oxo-vanadium(IV) in Several Solvents.

<u>Solvent</u>	<u>Concentration Dependence</u>
1% HMP/toluene	independent
5% pyridine/CS <sub>2</sub>	independent
10% HMP/toluene	linear
HMP	linear
Pyridine	linear
DMF	linear

#### E. Discussion

##### 1. Discussion of Equilibria Between Different Vanadyl Species.

The EPR, infrared and electronic spectral results presented in the previous section indicate the presence of at least three distinct vanadyl species in solutions containing a low concentration of a vanadyl dithiophosphate



complex and varying concentrations of a strongly coordinating ligand. The species which dominates at the highest temperatures with low concentrations of coordinating ligand, and gives rise to a triplet  $^{31}\text{P}$  hyperfine pattern in the EPR spectrum, indicating the presence of two equivalent phosphorus atoms, has been identified as the 5-coordinate vanadyl dithiophosphinate itself and will be referred to as species T.

A second vanadyl species, to be referred to as species D, is characterized by a doublet hyperfine structure in the EPR spectrum, which indicates that the unpaired electron is interacting with only one  $^{31}\text{P}$  nucleus. This vanadyl species may contain a single phosphorus atom or it may contain two non-equivalent phosphorus atoms, only one of which gives rise to an observable hyperfine splitting. The former possibility would require dissociation of the vanadyl dithiophosphinate to form a species with a single dithiophosphinato chelating moiety. Since the only possible ligands which can replace the chelating ligand are the uncharged Lewis bases in relatively low concentration in the solution, any vanadyl species containing a single dithiophosphinate chelate would be charged - a most unlikely species in non-polar solvents such as toluene and  $\text{CS}_2$ .

A simple procedure for detecting the presence of charged species in solution is to measure the conductance of the solution. For a solute that ionizes completely, the





conductance of the solution increases linearly with increasing solute concentration up to approximately  $10^{-1}$  M.<sup>62</sup> The conductivities of solutions containing the phenyl complex in concentrations ranging from zero to  $7 \times 10^{-3}$  M in the solvents 1% HMP/toluene and 5% pyridine/CS<sub>2</sub> were determined. In both solvent systems, the conductance was unaffected by the presence of the phenyl complex. The EPR spectra of the same solutions exhibited a predominantly doublet hyperfine pattern. One concludes that species D is not charged. However, the conductance experiments do not rule out the possibility that species D is a solvent separated ion pair in which the solvent (in this case the Lewis base present in the solution) occupies the first coordination sphere and the dithiophosphate counterion resides in the second coordination sphere. The formation of such ion pairs is favorable when there is a strong interaction between the ion and the solvent and the counterion is relatively large.<sup>63</sup> These conditions are certainly the case for the phenyl complex in 1% HMP/toluene or in 5% pyridine/CS<sub>2</sub>.

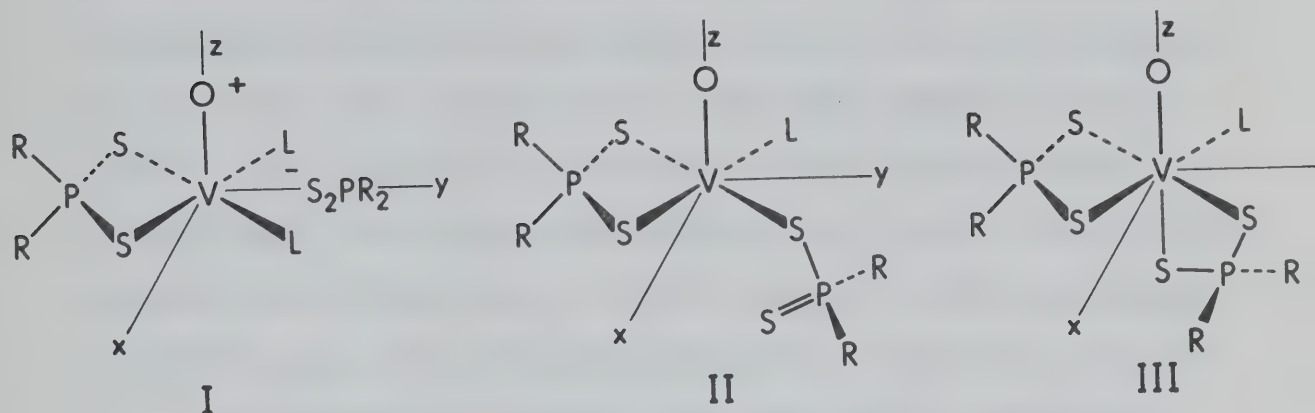
The infrared spectrum of the phenyl complex in 5% pyridine/CS<sub>2</sub> solution indicates the presence of three dithiophosphate species in addition to species T, the five-coordinate vanadyl complex (see Fig. III-14). A small shoulder at  $560\text{ cm}^{-1}$  suggests that the solution contains an ionic diphenyldithiophosphate species (see Table III-7), which, on the basis of the conductance measurements,



could be either an ion pair (see structure I) or a free dithiophosphinate ion at a concentration below the detection level of the conductance apparatus ( $<10^{-4}$  M). The infrared absorption at  $538\text{ cm}^{-1}$  indicates the presence of a species containing a monodentate dithiophosphinate moiety<sup>15</sup>, for which structure II is suggested. In this structure, one phosphorous nucleus is sufficiently far removed from the vanadium atom that it will not experience significant hyperfine interaction with the unpaired electron. The presence of a third species, for which is suggested a possible structure III, is indicated by a broadening of the band at  $570\text{ cm}^{-1}$  due to overlapping with a new absorption at lower frequency. (See Fig. III-14). This second band could arise from a structure with one of the diphenyldithiophosphinate ligands arranged so that one of its sulfur atoms occupies the axial coordination site, and a pyridine ligand is coordinated at the equatorial site (structure III). Similar arrangements are known for adducts of  $\text{VO}(\text{acac})_2$ .<sup>8,36</sup> The axial sulfur-vanadium bonding is expected to be weaker than the equatorial sulfur-vanadium bonding, and the non-equivalence of the sulfur atoms should cause the P-S stretching frequency to shift towards that of monodentate dithiophosphinates. In structure III, the two phosphorus nuclei are non-equivalent and it is conceivable that the hyperfine interaction of the phosphorus nucleus in the cross-coordinated chelate would be too small to be



observed in the EPR spectrum.



On the basis of the intensities of the infrared absorptions, the concentration of the species which gives rise to the absorption at  $560\text{ cm}^{-1}$  (structure I) is small in solutions containing 5% pyridine or less, and need not be considered further in the discussion of species D. The EPR spectra of solutions where the doublet hyperfine pattern predominates provide no evidence for the existence of two distinct species, structures II and III, as suggested by the infrared spectra. The magnetic parameters, particularly the  $^{31}\text{P}$  hyperfine interactions, of structure II and III are likely to be similar since the axial sulfur-vanadium bonding is expected to be very weak. It is shown above that the coordination of a pyridine molecule at the axial position either does not occur, or that the effect of such coordination on the magnetic parameters of the complex is insignificant, because the EPR spectra of the





vanadyl species T in 1% pyridine/CS<sub>2</sub> and in pure CS<sub>2</sub> solutions are identical. Furthermore, the rate of exchange between structures II and III is probably fast on the EPR time scale so that any small differences in the EPR spectra of structures II and III would be averaged out and undetectable. It is therefore concluded that species D is in fact two distinct species with structures II and III, but that EPR measurements can detect only the composite spectrum of these structures.

The number  $x$  of Lewis base molecules L involved in the equilibrium



was determined for the vanadyl dithiophosphinates by analyzing the EPR spectra of solutions containing different Lewis base and complex concentrations. The appropriate equilibrium constant is written as

$$K_{T-D} = \frac{[D]}{[T][L]^x} \quad (\text{III-21})$$

The relative concentrations of species D and species T were obtained from computer-synthesized EPR spectra which resembled most closely the observed EPR spectra. Knowing the ratio of the concentration of these species,  $R = [D]/[T]$ , one can express  $K_{T-D}$  in terms of the known quantities  $R$ ,  $[L]^0$ , the total Lewis base concentration, and  $[T]^0$ , the total vanadyl concentration.





$$K_{T-D} = \frac{R(R + 1)^x}{([L]^{\circ} + R[L]^{\circ} - xR[T]^{\circ})^x} \quad (\text{III-22})$$

Examples of the calculated values of  $K_{T-D}$  for integral values of  $x$  are shown in Table III-9. Consistent values of  $K_{T-D}$  were obtained only for the case  $x = 1$ , which is compatible with structures II and III for species D. The equilibrium constant  $K_{T-D}$  was determined at several temperatures, for the three complexes in various solvent systems and the results are shown in Fig. III-15. The values of  $K_{T-D}$  at 298K, and the enthalpies of adduct formation  $\Delta H_{T-D}^{\circ}$  calculated from the slopes of the lines in Fig. III-15 are given in Table III-10. These heats of adduct formation are similar in magnitude to those for the vanadyl acetylacetonate adducts with HMP, DMF and various amines.<sup>4,5</sup> The  $\text{VO}(\text{acac})_2$  adducts were assumed to arise from Lewis base coordination at the axial position whereas the adducts of the vanadyl dithiophosphinates have been shown to arise from ligand coordination at an equatorial site.

The room temperature equilibrium constants obtained from spectrophotometric measurements of the vanadyl dithiophosphate complexes in toluene solutions containing different amounts of HMP and DMF are also shown in Fig. III-15. The equilibrium constants obtained from the spectrophotometric measurements were consistently higher than expected from an extrapolation of the equilibrium constants obtained from the EPR studies. This discrepancy can be attributed



TABLE III-9

Calculated  $K_{T-D}$  Values for Integral Values of  $x$ , the Number of  
Lewis Base Molecules in Triplet-Doublet Equilibrium

a. Bis-(diphenyldithiophosphinato)-oxo-vanadium(IV) in HMP-  
 Toluene Mixed Solvents

x	1% HMP/Toluene			5% HMP/Toluene		
	75°	90°C	105°C	75°C	90°C	105°C
1	11	6.6	4.5	11	6.6	5.1
2	210	120	82	39	24	18
3	4,400	2,500	1,600	160	89	68
4	99,000	52,000	31,000	560	340	230

b. Bis-(diphenyldithiophosphinato)-oxo-vanadium(IV) in Pyri-  
 dine-CS<sub>2</sub> Mixed Solvents at 45°C

x	0.5% Pyridine/CS <sub>2</sub>	1.0% Pyridine/CS <sub>2</sub>	2.0% Pyridine/CS <sub>2</sub>
1	13	16	14
2	240	140	59
3	4,600	1,300	260
4	97,000	14,000	1,200

c. Bis-(dimethyldithiophosphinato)-oxo-vanadium(IV) in Pyridine-  
 CS<sub>2</sub> Mixed Solvents at 45°C

x	1.0% Pyridine/CS <sub>2</sub>	2.0% Pyridine/CS <sub>2</sub>
1	9.3	8.0
2	77	33

(continued...)



TABLE III-9 (continued)

x	1.0% Pyridine/CS <sub>2</sub>	2.0% Pyridine/CS <sub>2</sub>
3	670	140
4	6,200	630

d. Bis-(dimethyldithiophosphinato)-oxo-vanadium(IV) in Pyridine-CS<sub>2</sub> Mixed Solvents at 0°C

x	0.10% Pyridine/CS <sub>2</sub>	0.20% Pyridine/CS <sub>2</sub>
1	110	84 <sup>v</sup>
2	23,000	5,200
3	23 x 10 <sup>6</sup>	47,000
4	27 x 10 <sup>12</sup>	71 x 10 <sup>6</sup>





TABLE III-10

Equilibrium Constants at 298K and Enthalpies of Adduct  
Formation<sup>†</sup>

<u>Complex</u>	<u>Ligand</u>	<u>K<sub>T-D</sub> (l/mole)</u>	<u>-ΔH<sub>T-D</sub><sup>O</sup> (kcal/mole)</u>
Methyl	HMP	42	5.7 ± .9
	Pyridine	23	9.3 ± .2
Phenyl	HMP	63	7.7 ± 1.2
	Pyridine	31	7.7 ± .4
Ethoxy	HMP	160	7.5 ± 1.1
	DMF	1	7.2 ± 1.1

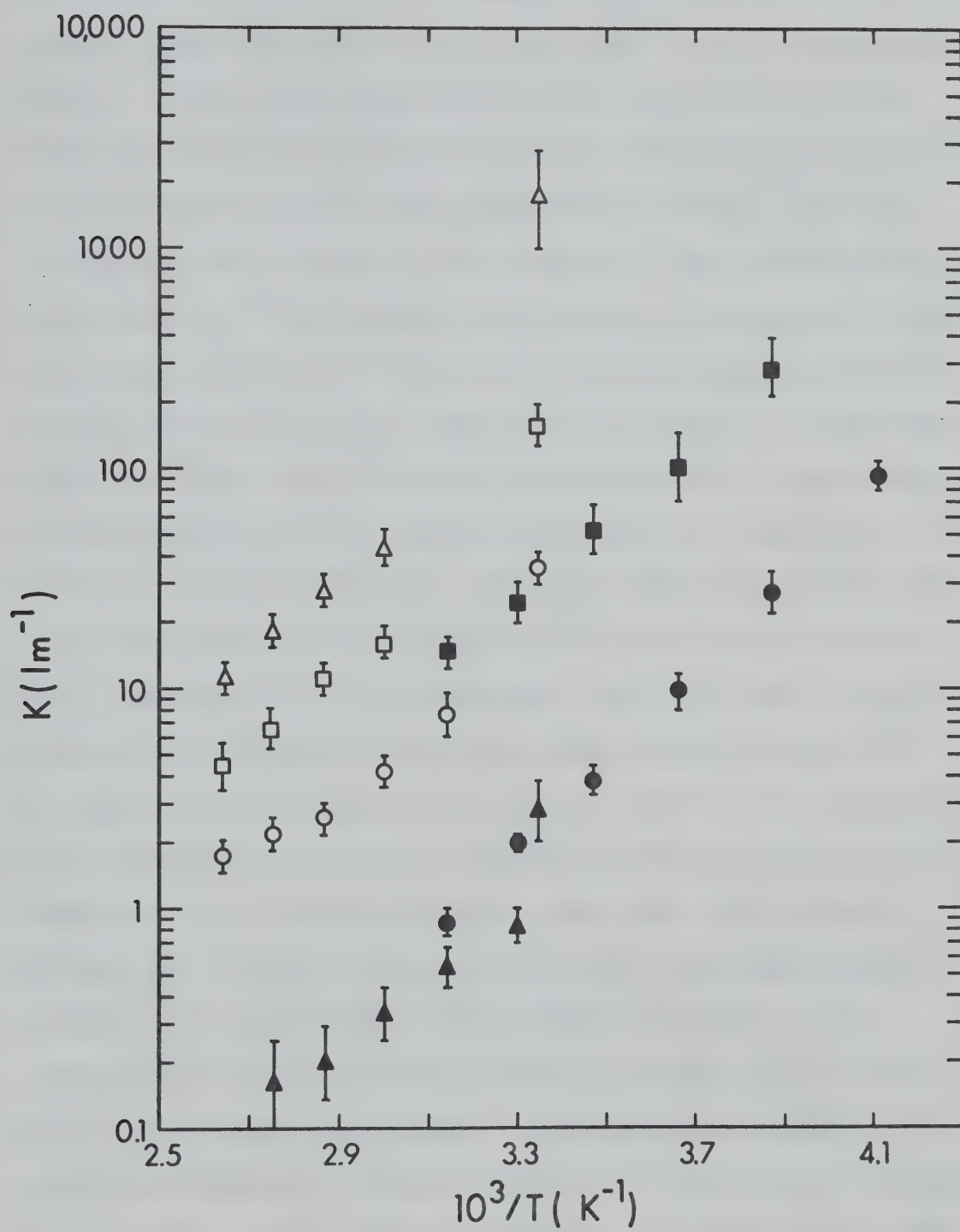
---

<sup>†</sup> Experimental K<sub>T-D</sub> values were least squares fitted to  $K_{T-D} = Ae^{-\Delta H_{T-D}^O/RT}$  and errors given are the standard errors from the least squares routine. K<sub>T-D</sub> at 298K is calculated using the least squares parameters.



Date	Description	Particulars	Amount	Balance	Total
1890					
Jan 1	Balance forward				
Jan 2	Jan 1				
Jan 3	Jan 2				
Jan 4	Jan 3				
Jan 5	Jan 4				
Jan 6	Jan 5				
Jan 7	Jan 6				
Jan 8	Jan 7				
Jan 9	Jan 8				
Jan 10	Jan 9				
Jan 11	Jan 10				
Jan 12	Jan 11				
Jan 13	Jan 12				
Jan 14	Jan 13				
Jan 15	Jan 14				
Jan 16	Jan 15				
Jan 17	Jan 16				
Jan 18	Jan 17				
Jan 19	Jan 18				
Jan 20	Jan 19				
Jan 21	Jan 20				
Jan 22	Jan 21				
Jan 23	Jan 22				
Jan 24	Jan 23				
Jan 25	Jan 24				
Jan 26	Jan 25				
Jan 27	Jan 26				
Jan 28	Jan 27				
Jan 29	Jan 28				
Jan 30	Jan 29				
Jan 31	Jan 30				
Feb 1	Jan 31				
Feb 2	Feb 1				
Feb 3	Feb 2				
Feb 4	Feb 3				
Feb 5	Feb 4				
Feb 6	Feb 5				
Feb 7	Feb 6				
Feb 8	Feb 7				
Feb 9	Feb 8				
Feb 10	Feb 9				
Feb 11	Feb 10				
Feb 12	Feb 11				
Feb 13	Feb 12				
Feb 14	Feb 13				
Feb 15	Feb 14				
Feb 16	Feb 15				
Feb 17	Feb 16				
Feb 18	Feb 17				
Feb 19	Feb 18				
Feb 20	Feb 19				
Feb 21	Feb 20				
Feb 22	Feb 21				
Feb 23	Feb 22				
Feb 24	Feb 23				
Feb 25	Feb 24				
Feb 26	Feb 25				
Feb 27	Feb 26				
Feb 28	Feb 27				
Feb 29	Feb 28				
Feb 30	Feb 29				
Feb 31	Feb 30				
Mar 1	Feb 31				
Mar 2	Mar 1				
Mar 3	Mar 2				
Mar 4	Mar 3				
Mar 5	Mar 4				
Mar 6	Mar 5				
Mar 7	Mar 6				
Mar 8	Mar 7				
Mar 9	Mar 8				
Mar 10	Mar 9				
Mar 11	Mar 10				
Mar 12	Mar 11				
Mar 13	Mar 12				
Mar 14	Mar 13				
Mar 15	Mar 14				
Mar 16	Mar 15				
Mar 17	Mar 16				
Mar 18	Mar 17				
Mar 19	Mar 18				
Mar 20	Mar 19				
Mar 21	Mar 20				
Mar 22	Mar 21				
Mar 23	Mar 22				
Mar 24	Mar 23				
Mar 25	Mar 24				
Mar 26	Mar 25				
Mar 27	Mar 26				
Mar 28	Mar 27				
Mar 29	Mar 28				
Mar 30	Mar 29				
Mar 31	Mar 30				
Apr 1	Mar 31				
Apr 2	Apr 1				
Apr 3	Apr 2				
Apr 4	Apr 3				
Apr 5	Apr 4				
Apr 6	Apr 5				
Apr 7	Apr 6				
Apr 8	Apr 7				
Apr 9	Apr 8				
Apr 10	Apr 9				
Apr 11	Apr 10				
Apr 12	Apr 11				
Apr 13	Apr 12				
Apr 14	Apr 13				
Apr 15	Apr 14				
Apr 16	Apr 15				
Apr 17	Apr 16				
Apr 18	Apr 17				
Apr 19	Apr 18				
Apr 20	Apr 19				
Apr 21	Apr 20				
Apr 22	Apr 21				
Apr 23	Apr 22				
Apr 24	Apr 23				
Apr 25	Apr 24				
Apr 26	Apr 25				
Apr 27	Apr 26				
Apr 28	Apr 27				
Apr 29	Apr 28				
Apr 30	Apr 29				
Apr 31	Apr 30				
May 1	Apr 31				
May 2	May 1				
May 3	May 2				
May 4	May 3				
May 5	May 4				
May 6	May 5				
May 7	May 6				
May 8	May 7				
May 9	May 8				
May 10	May 9				
May 11	May 10				
May 12	May 11				
May 13	May 12				
May 14	May 13				
May 15	May 14				
May 16	May 15				
May 17	May 16				
May 18	May 17				
May 19	May 18				
May 20	May 19				
May 21	May 20				
May 22	May 21				
May 23	May 22				
May 24	May 23				
May 25	May 24				
May 26	May 25				
May 27	May 26				
May 28	May 27				
May 29	May 28				
May 30	May 29				
May 31	May 30				
Jun 1	May 31				
Jun 2	Jun 1				
Jun 3	Jun 2				
Jun 4	Jun 3				
Jun 5	Jun 4				
Jun 6	Jun 5				
Jun 7	Jun 6				
Jun 8	Jun 7				
Jun 9	Jun 8				
Jun 10	Jun 9				
Jun 11	Jun 10				
Jun 12	Jun 11				
Jun 13	Jun 12				
Jun 14	Jun 13				
Jun 15	Jun 14				
Jun 16	Jun 15				
Jun 17	Jun 16				
Jun 18	Jun 17				
Jun 19	Jun 18				
Jun 20	Jun 19				
Jun 21	Jun 20				
Jun 22	Jun 21				
Jun 23	Jun 22				
Jun 24	Jun 23				
Jun 25	Jun 24				
Jun 26	Jun 25				
Jun 27	Jun 26				
Jun 28	Jun 27				
Jun 29	Jun 28				
Jun 30	Jun 29				
Jun 31	Jun 30				
Jul 1	Jun 31				
Jul 2	Jul 1				
Jul 3	Jul 2				
Jul 4	Jul 3				
Jul 5	Jul 4				
Jul 6	Jul 5				
Jul 7	Jul 6				
Jul 8	Jul 7				
Jul 9	Jul 8				
Jul 10	Jul 9				
Jul 11	Jul 10				
Jul 12	Jul 11				
Jul 13	Jul 12				
Jul 14	Jul 13				
Jul 15	Jul 14				
Jul 16	Jul 15				
Jul 17	Jul 16				
Jul 18	Jul 17				
Jul 19	Jul 18				
Jul 20	Jul 19				
Jul 21	Jul 20				
Jul 22	Jul 21				
Jul 23	Jul 22				
Jul 24	Jul 23				
Jul 25	Jul 24				
Jul 26	Jul 25				
Jul 27	Jul 26				
Jul 28	Jul 27				
Jul 29	Jul 28				
Jul 30	Jul 29				
Jul 31	Jul 30				
Aug 1	Jul 31				
Aug 2	Aug 1				
Aug 3	Aug 2				
Aug 4	Aug 3				
Aug 5	Aug 4				
Aug 6	Aug 5				
Aug 7	Aug 6				
Aug 8	Aug 7				
Aug 9	Aug 8				
Aug 10	Aug 9				
Aug 11	Aug 10				
Aug 12	Aug 11				
Aug 13	Aug 12				
Aug 14	Aug 13				
Aug 15	Aug 14				
Aug 16	Aug 15				
Aug 17	Aug 16				
Aug 18	Aug 17				
Aug 19	Aug 18				
Aug 20	Aug 19				
Aug 21	Aug 20				
Aug 22	Aug 21				
Aug 23	Aug 22				
Aug 24	Aug 23				
Aug 25	Aug 24				
Aug 26	Aug 25				
Aug 27	Aug 26				
Aug 28	Aug 27				
Aug 29	Aug 28				
Aug 30	Aug 29				
Aug 31	Aug 30				
Sep 1	Aug 31				
Sep 2	Sep 1				
Sep 3	Sep 2				
Sep 4	Sep 3				
Sep 5	Sep 4				
Sep 6	Sep 5				
Sep 7	Sep 6				
Sep 8	Sep 7				
Sep 9	Sep 8				
Sep 10	Sep 9				
Sep 11	Sep 10				
Sep 12	Sep 11				
Sep 13	Sep 12				
Sep 14	Sep 13				
Sep 15	Sep 14				
Sep 16	Sep 15				
Sep 17	Sep 16				
Sep 18	Sep 17				
Sep 19	Sep 18				
Sep 20	Sep 19				
Sep 21	Sep 20				
Sep 22	Sep 21				
Sep 23	Sep 22				
Sep 24	Sep 23				
Sep 25	Sep 24				
Sep 26	Sep 25				
Sep 27	Sep 26				
Sep 28	Sep 27				
Sep 29	Sep 28				
Sep 30	Sep 29				
Sep 31	Sep 30				
Oct 1	Sep 31				
Oct 2	Oct 1				
Oct 3	Oct 2				
Oct 4	Oct 3				
Oct 5	Oct 4				
Oct 6	Oct 5				
Oct 7	Oct 6				
Oct 8	Oct 7				
Oct 9	Oct 8				
Oct 10	Oct 9				
Oct 11	Oct 10				
Oct 12	Oct 11				
Oct 13	Oct 12				
Oct 14	Oct 13				
Oct 15	Oct 14				
Oct 16	Oct 15				
Oct 17	Oct 16				
Oct 18	Oct 17				
Oct 19	Oct 18				
Oct 20	Oct 19				
Oct 21	Oct 20				
Oct 22	Oct 21				
Oct 23	Oct 22				
Oct 24	Oct 23				
Oct 25	Oct 24				
Oct 26	Oct 25				
Oct 27	Oct 26				
Oct 28	Oct 27				

FIGURE III-15    Temperature dependence of the equilibrium constants,  $K_{T-D}$  for the formation of adducts of the vanadyl dithiophosphinates with pyridine, HMP and DMF.  $K_{T-D}$  values are calculated from EPR results except for values at  $10^3/T = 3.35 \text{ K}^{-1}$  which are calculated from visible spectrum results.  $\Delta$ , bis-(O,O'-diethyldithiophosphato)-oxo-vanadium (IV) in HMP/toluene;  $\blacktriangle$ , bis-(O,O'-diethyldithiophosphato)-oxo-vanadium(IV) in DMF/toluene;  $\square$ , bis-(diphenyldithiophosphinato)-oxo-vanadium(IV) in HMP/toluene;  $\blacksquare$ , bis-(diphenyldithiophosphinato)-oxo-vanadium(IV) in pyridine/CS<sub>2</sub>;  $\circ$ , bis-(dimethyldithiophosphinato)-oxo-vanadium(IV) in HMP/toluene;  $\bullet$ , bis-(dimethyldithiophosphinato)-oxo-vanadium(IV) in pyridine/CS<sub>2</sub>. For clarity, the values of  $K_{T-D}$  shown on the Figure for bis-(dimethyldithiophosphinato)-oxo-vanadium(IV) in pyridine/CS<sub>2</sub> are the observed values divided by 10. The bars indicate estimated uncertainties in the values of  $K_{T-D}$ .





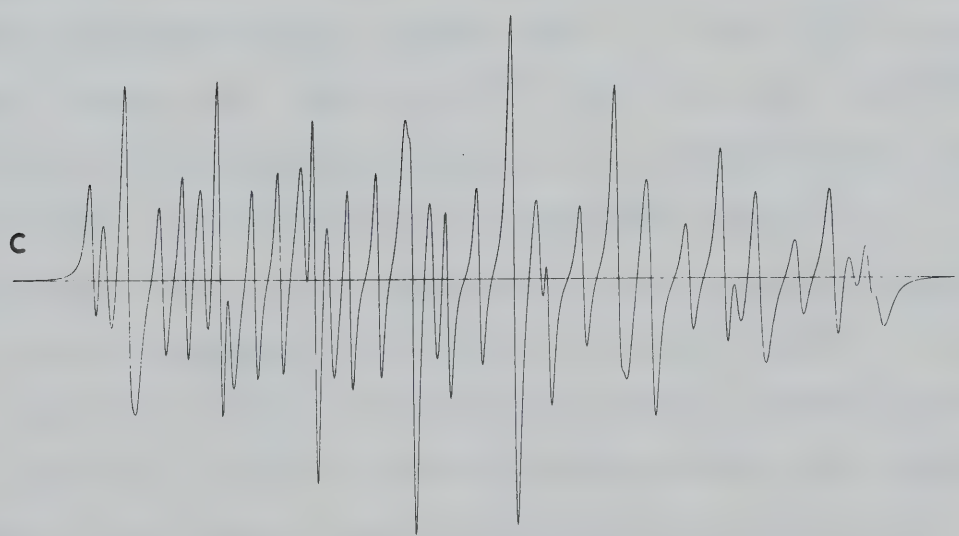
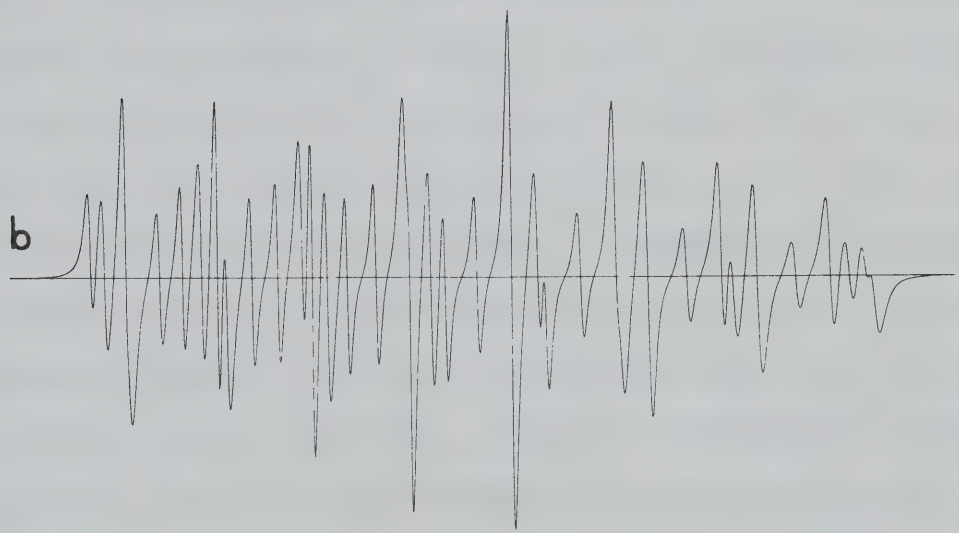
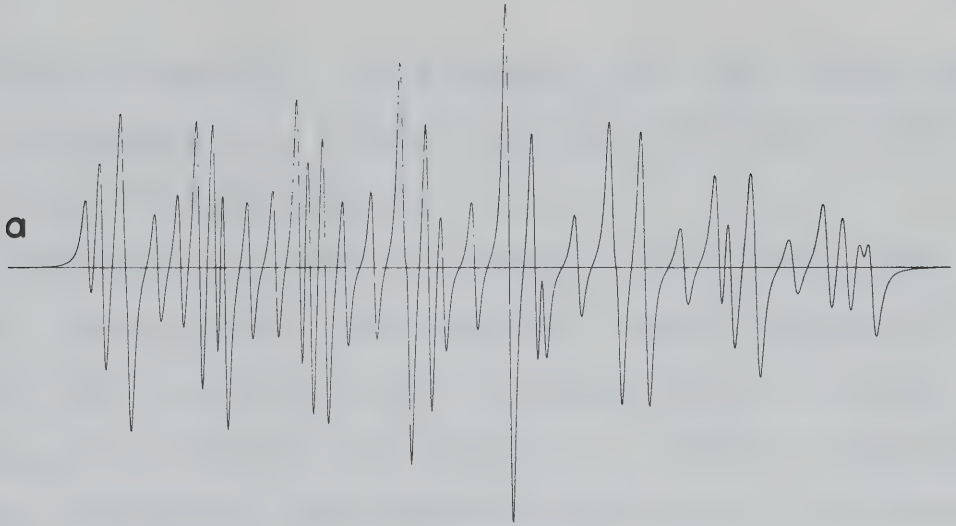
to the presence of a third vanadyl species (which gives the singlet hyperfine structure in the EPR) in low concentrations. In the EPR measurements, the ratio  $[D]/[T]$  was determined from the observed spectra, but this ratio could not be measured spectrophotometrically since a solution containing only D could not be prepared and the extinction coefficients of this adduct could not be determined. Instead, the concentration of T was measured spectrophotometrically and the concentration of species D obtained by difference from the known total vanadyl concentration in the solution. The spectrophotometric equilibrium data is, therefore, less reliable than the EPR data, but does substantiate the conclusions based on the analysis of the EPR data. Furthermore, the ratio  $[D]/[T]$  calculated from the best fit EPR spectra for the HMP/toluene and DMF/toluene systems will be lower than the true value because the D and T linewidths were assumed to be equal. The EPR spectra of the methyl complex in .1 - 5% pyridine/ $CS_2$  show that the doublet pattern has slightly larger linewidths than the triplet pattern. If one broadens the doublet spectrum in the computer synthesis of the spectra, a larger  $[D]/[T]$  ratio would be required to produce a spectrum with relative intensities similar to those obtained if triplets and doublets are assumed to have the same widths. See Fig III-16. Thus the  $K_{T-D}$  values calculated from EPR spectra in the HMP/toluene and DMF/toluene systems are lower limits for the





The first of these is the fact that the  
 system is not a simple one. It is a  
 complex one, and it is not possible to  
 describe it in a simple way. It is a  
 system of many parts, and it is not  
 possible to describe it in a simple way.  
 It is a system of many parts, and it is  
 not possible to describe it in a simple  
 way. It is a system of many parts, and  
 it is not possible to describe it in a  
 simple way. It is a system of many  
 parts, and it is not possible to describe  
 it in a simple way. It is a system of  
 many parts, and it is not possible to  
 describe it in a simple way. It is a  
 system of many parts, and it is not  
 possible to describe it in a simple way.

FIGURE III-16 Computer synthesized EPR solution spectra of bis-(dimethyldithiophosphinato)-oxo-vanadium(IV) in 5% HMP/toluene at 60°C for a 1:1 ratio of doublet:triplet pattern at various linewidths of the doublet pattern relative to the triplet pattern. (a), equal linewidths for doublet and triplet pattern; (b), doublet linewidths 25% broader than corresponding triplet linewidths; (c), doublet linewidths 50% broader than triplet linewidths.





equilibrium constants. This accounts for some of the discrepancy between  $K_{T-D}$  values determined from spectrophotometric and EPR measurements.

The two structures postulated to give rise to the doublet pattern in the EPR spectrum, namely structures II and III, are expected to have slightly larger molecular dimensions in solution than species T. Since the reorientational correlation time depends on the cube of the molecular radius (see equation III-20), a small increase in  $r$  will result in a larger  $\tau_r$  and hence broader EPR lines. However, the lines of the doublet spectrum could also be effectively broadened by a second  $^{31}\text{P}$  hyperfine interaction. This coupling could be large enough to split each line of the observed doublet into an unresolved doublet and thus effectively broaden the line. Computer synthesized spectra for species D of the methyl complex in the pyridine/ $\text{CS}_2$  solvent, incorporating a second small  $^{31}\text{P}$  hyperfine interaction, showed that the second  $^{31}\text{P}$  splitting was resolved before the lines became as broad as the experimental lines. Furthermore, the lineshape on an expanded sweep was Lorentzian, which is not expected if the broadening results from the overlapping of two lines. On this basis, it is concluded the broader lines for the doublet pattern result from species D having a slightly larger radius than species T rather than from an unresolved hyperfine interaction.

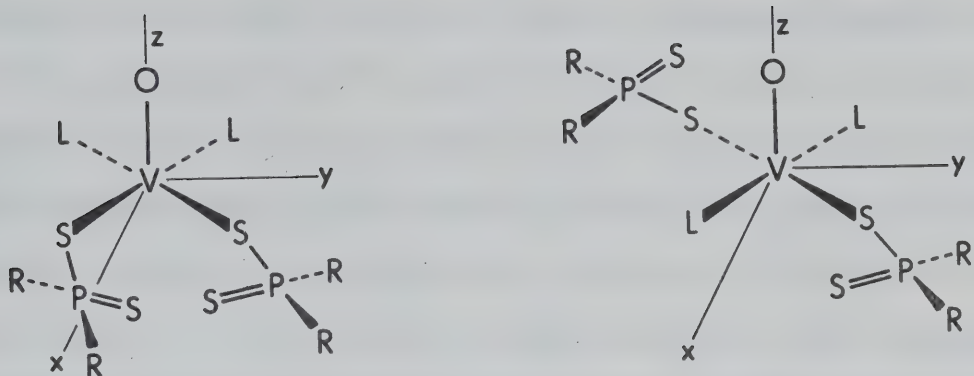
A third vanadyl species, henceforth referred to as





species S, gives rise to an EPR spectrum which shows no hyperfine interactions between the unpaired electron and the phosphorus nuclei. The absence of  $^{31}\text{P}$  hyperfine interactions indicates that species S has no chelating dithiophosphinate moieties. This species predominates under conditions of low temperature and high Lewis base concentration. The conductance of a solution of the phenyl complex in 10% HMP/toluene varies approximately linearly with the concentration of the vanadyl complex. This implies that the vanadyl dithiophosphinate complex dissociates under these conditions. The infrared spectrum of the phenyl complex in 10% pyridine/ $\text{CS}_2$  solution (Fig. III-14) indicates that dithiophosphinate species with bidentate and monodentate coordination are present in addition to the ionic species. The structures IV are suggested as possible molecular arrangements which are consistent with the EPR spectrum and with monodentate dithiophosphinate coordination. The cis and trans isomers of IV are possible and could give rise to different EPR spectra if the magnetic parameters of the two isomers were sufficiently different. It is expected however that the differences in the magnetic parameters of the cis and trans isomers of IV would be very small.





IV

The relative concentrations of the D and S species involved in the equilibrium



in 1-5% pyridine/ $\text{CS}_2$  solutions were determined by comparing the observed EPR spectra with computed spectra. The equilibrium constant

$$K_{D-S} = \frac{[S]}{[D][L]^{x'}} \quad (\text{III-23})$$

was calculated for integral values of  $x'$ , and the values obtained were consistent with  $x' = 1$  only. At  $-45^\circ\text{C}$ ,  $K_{D-S}$  has the value 3.1 l/mole for the methyl complex. This result indicates that the formation of species S from species D involves displacement of one of the sulfur atoms from vanadyl coordination by a ligand molecule. The species S involved in this equilibrium is assumed to have structure IV since the species must result from the addition of a single



ligand to structure II or III which represent species D, and the simplest way for this to occur is for a second ligand to displace one of the sulfur atoms of the bidentate dithiophosphinate of structure II or III to make it a monodentate ligand in structure IV. However, to explain the conductance of the 10% HMP/toluene solution, the structure IV species must be in equilibrium with ionized species in which one or both dithiophosphinates are displaced from the first coordination sphere of the vanadyl ion and ionized. All species giving rise to a singlet EPR spectrum apparently have very similar magnetic parameters since only one singlet species was resolved in the EPR spectrum.

The temperature dependence of the equilibrium between species S and D warrants some comments since the EPR spectra of the vanadyl dithiophosphinate complexes in pyridine, HMP or DMF solution exhibit a temperature dependence. At +30°C, the spectrum of the phenyl complex in pyridine (see Fig. III-8) consists of eight well resolved lines with no evidence of phosphorus hyperfine splittings. At higher temperatures, doublets appear in the EPR spectrum. This result is consistent with the decrease in the dielectric constant <sup>64</sup> of pyridine as the temperature increases. The lower dielectric constant destabilizes the dissociated form and drives the equilibrium to the D side. Similar EPR results were obtained for the ethoxy and methyl complexes with the doublets appearing at lower temperatures in the



methyl and ethoxy complexes than in the phenyl complexes. This may result from the greater stabilization of the diphenyldithiophosphinate anion due to charge delocalization to the phenyl groups. Obviously there are numerous structures possible for the vanadyl species containing two or more ligand molecules and yielding singlet hyperfine EPR patterns. However, their magnetic parameters would be similar and separate EPR lines for each would not be resolved.

In DMF, the methyl complex shows EPR spectra above 40°C which are mixtures of triplets and singlets and a relatively small amount of doublet. The spectra, shown in Fig. III-17, indicate that the species giving rise to a doublet pattern (structures I, II and III) are not predominant in pure DMF. This is in contrast to the results of the methyl complex in 5% HMP/toluene and 5% pyridine/CS<sub>2</sub> where there was clearly a doublet-triplet equilibrium. The phenyl and ethoxy complexes show singlet EPR spectra over the complete temperature range of the liquid DMF. The ethoxy spectra are shown in Fig. III-18. Attempts to gain further insight into the coordination of DMF in the vanadyl species that gives a singlet EPR spectrum were made by studying the paramagnetic broadening of the NMR lines of the DMF solvent. The temperature dependence of the line broadening results for the phenyl complex in DMF was similar to that for VO(DMF)<sub>5</sub>(ClO<sub>4</sub>)<sub>2</sub> in DMF but the magni-

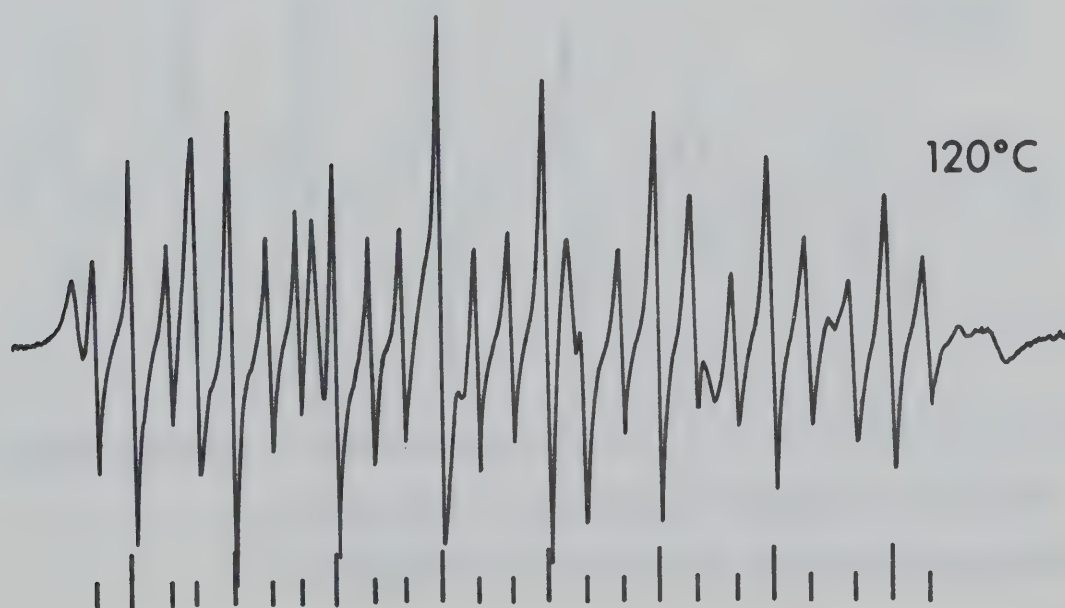
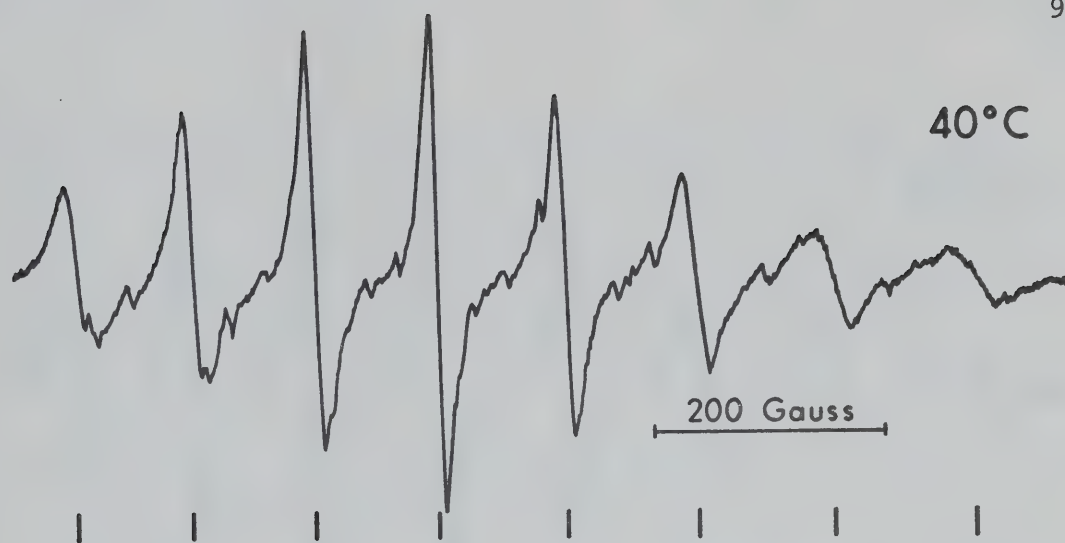








FIGURE III-17. EPR spectra of  $10^{-3}$  M liquid solutions of bis-(dimethyldithiophosphinato)-oxo-vanadium(IV) in DMF at various temperatures. The stick spectra for the predominant vanadyl species at 40°C and 120°C are given below the corresponding experimental spectra.





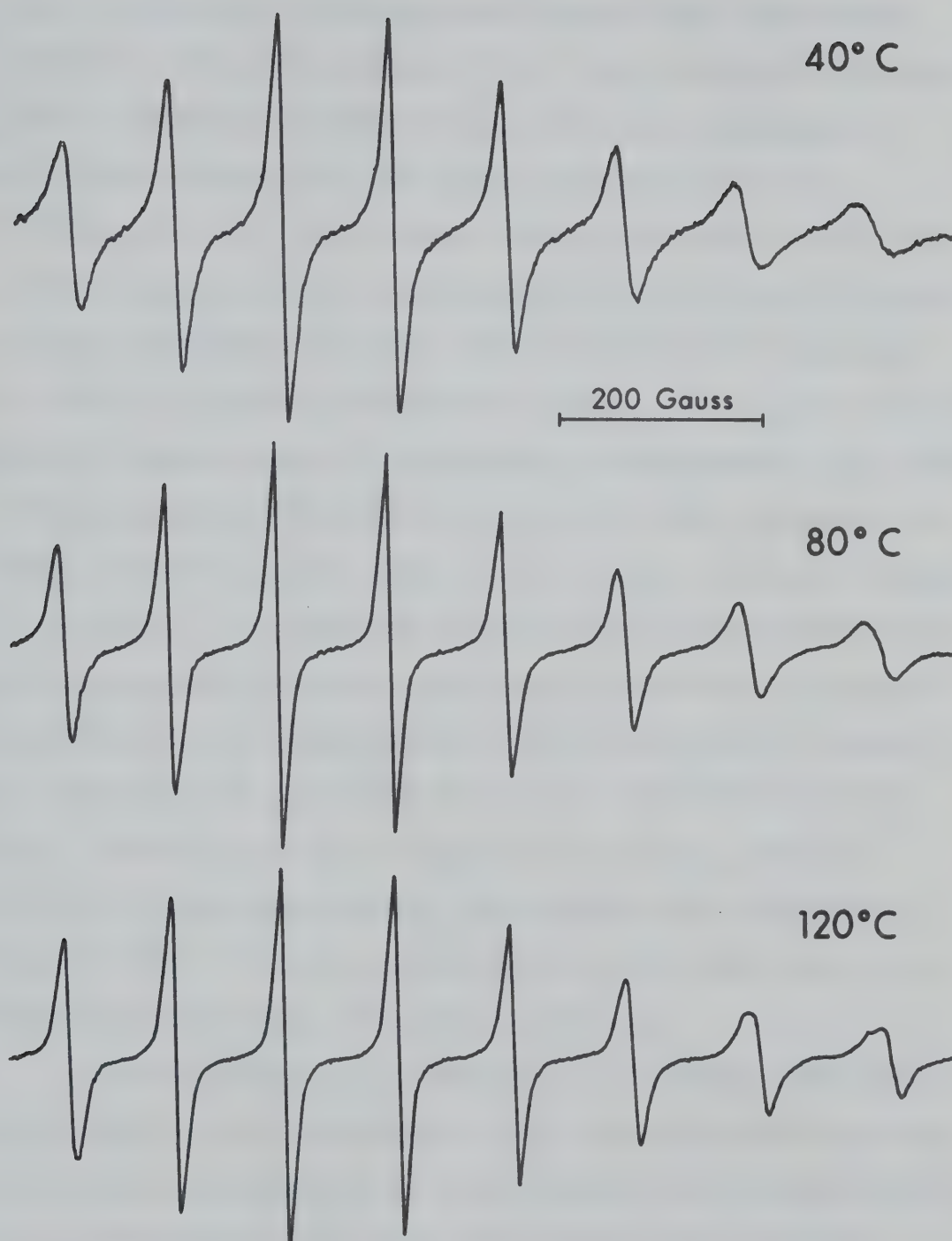


FIGURE III-18. EPR spectra of  $10^{-3}$  M liquid solutions of bis-(O,O'-diethyldithiophosphinato)-oxovanadium(IV) in DMF at various temperatures.



tude of the line broadening was greater for the phenyl complex in DMF. (See Chapter IV). This indicated that the rate of exchange of DMF from the vanadyl coordination sphere was faster for the phenyl complex than for  $\text{VO}(\text{DMF})_5(\text{ClO}_4)_2$ . Furthermore, the conductance of the DMF solution was linear in the concentration of phenyl complex. It was therefore concluded that the predominant species in a DMF solution of the phenyl complex is a singly charged vanadyl complex with a monodentate dithiophosphinate ligand occupying one coordination position and DMF occupying the other positions. The lower charge of this species compared to  $\text{VO}(\text{DMF})_5^{2+}$  is expected to weaken the vanadium-DMF bond and consequently increase the rate of exchange. The persistence of this dissociated form for the phenyl complex is attributed to the high dielectric constant <sup>64</sup> of DMF (36.1) relative to that of pyridine (12.3). The EPR spectra of the complexes in HMP solution are similar to those in DMF. This is expected since the dielectric constants of HMP (30.0) and DMF are similar.

The EPR spectra of the phenyl and methyl complexes in 5% DMF/toluene solution at 25°C are predominantly triplets, while the spectra of the complexes in 5% pyridine/ $\text{CS}_2$  or 5% HMP/toluene solutions are predominantly doublets. This difference in the solvent systems is due primarily to the differences in the electron donor properties of the ligands.<sup>65</sup> The observation of adduct formation of the





ethoxy complex at lower ligand concentrations than those required for formation of analogous adducts with the methyl or phenyl complex indicates that the ethoxy complex is a stronger Lewis acid than the methyl or phenyl complexes.

## 2. Interpretation of g-values and Hyperfine Splitting Constants.

The g-values and hyperfine splittings combined with the energies of the electronic transitions form a basis for the discussion of the molecular orbitals describing the bonding in the vanadyl dithiophosphinates. Before the magnetic parameters can be related to molecular orbital coefficients, it is necessary to ascertain the ground electronic state of the complexes. Kivelson and Lee<sup>25</sup> have concluded that the unpaired electron resides in a  $b_1(d_{x^2-y^2})$  orbital in  $VO(acac)_2$  and vanadyl tetraphenylporphyrin. If the electron were in a  $b_2(d_{xy})$  orbital, the coupling to the nitrogen nuclei in vanadyl tetraphenylporphyrin would be larger than the observed value of 2.8 Gauss. Furthermore, residence in an  $e(d_{xz}, d_{yz})$  orbital would result in a short spin-lattice relaxation time due to a slight splitting of the degeneracy by ligand field distortions away from  $C_{4v}$  symmetry and would lead to much broader EPR lines than are observed.

The unpaired electron in vanadyl dithiophosphinates and their Lewis base adducts is also believed to occupy a



molecular orbital of  $b_1$  symmetry which is primarily the  $d_{x^2-y^2}$  atomic orbital on the vanadium atom. If the electron were in the  $b_2(d_{xy})$  orbital, then hyperfine interactions with the phosphorus atoms would occur via the sulphur linkage; and the  $^{31}\text{P}$  coupling would be expected to decrease by approximately one-half if the dithiophosphinate chelate became monodentate. On the other hand, if the unpaired electron resides in a  $b_1(d_{x^2-y^2})$  orbital, coupling to  $^{31}\text{P}$  nuclei can occur via direct overlap of the vanadium  $d_{x^2-y^2}$  orbital and the P 3s orbital. Then removing the phosphorus atom from the region of high probability of the  $d_{x^2-y^2}$  orbital, as is the case for the species giving rise to the doublet spectrum, destroys the coupling to one P atom. The other  $^{31}\text{P}$  atom is still in a region of high  $d_{x^2-y^2}$  probability and of course interaction with this phosphorus atom is still observed. Residence in an  $e(d_{xz}, d_{yz})$  level is unacceptable for the reasons given above for vanadyl tetraphenylporphyrin. Furthermore, the assignment of the unpaired electron to the  $b_1(d_{x^2-y^2})$  orbital agrees with McCormick's<sup>10</sup> assignment for the vanadyl dithiocarbomates and their pyridine and dimethyl sulfoxide adducts.

The methods by which the magnetic parameters can be related to the molecular orbital coefficients and the energies of the excited electronic states in metal ions are described in detail by McGarvey.<sup>66</sup> In the LCAO



approximation, the molecular orbital occupied by the unpaired electron in the ground electronic state of the vanadyl complex having  $C_{2v}$  symmetry is assumed to be

$$\psi_1 = \alpha\{a |x^2-y^2\rangle + b |3z^2-r^2\rangle\} - \alpha' |L_1\rangle \quad (\text{Symmetry } A_1) ,$$

and the lowest lying unoccupied molecular orbitals to be

$$\psi_2 = \beta |xy\rangle - \beta' |L_2\rangle \quad (\text{Symmetry } A_2) ,$$

$$\psi_3 = \gamma |zx\rangle - \gamma' |L_3\rangle \quad (\text{Symmetry } B_1) ,$$

$$\psi_4 = \delta |yz\rangle - \delta' |L_4\rangle \quad (\text{Symmetry } B_2) ,$$

and 
$$\psi_5 = \eta\{a |3z^2-r^2\rangle - b |x^2-y^2\rangle\} - \eta' |L_5\rangle \quad (\text{Symmetry } A_1) .$$

where  $|x^2-y^2\rangle$ ,  $|3z^2-r^2\rangle$ ,  $|zx\rangle$ ,  $|yz\rangle$  and  $|xy\rangle$  are the vanadium atomic orbitals,  $|L_1\rangle$ ,  $|L_2\rangle$ , ...,  $|L_5\rangle$  are linear combinations of ligand orbitals of appropriate symmetry, and  $\alpha$ ,  $\alpha'$ ,  $\beta$ ,  $\beta'$ , ...,  $\eta$ ,  $\eta'$ , are the normalized MO coefficients. The mixing coefficients  $\underline{a}$  and  $\underline{b}$  describe the mixing of the vanadium  $|x^2-y^2\rangle$  and  $|3z^2-r^2\rangle$  orbitals in forming the MO's. It is expected that  $b \ll a$  since the mixing is brought about by the  $C_{2v}$  perturbation upon a strong  $C_{4v}$  ligand field. The spin orbit coupling,  $\xi \hat{\vec{L}} \cdot \hat{\vec{S}}$ , where  $\xi$  is the spin orbit coupling constant and  $\vec{L}$  is the orbital angular momentum operator, mixes some excited state



character into the ground state wavefunction  $\psi_1$ . The first order perturbed wavefunction,  $\psi_1'$ , for the ground state MO is then given by

$$\psi_1' = \psi_1 - i\alpha\gamma^2 \frac{(a-\sqrt{3}b)\xi|zx\rangle}{E_3} - i\alpha\delta^2 \frac{(a+\sqrt{3}b)\xi|yz\rangle}{E_3} + \frac{2i\alpha\beta^2 a\xi|xy\rangle}{E_2}.$$

Combining  $\psi_1'$  with the two possible spin functions for a single electron, one obtains a pair of molecular spin orbitals. The representation of the spin Hamiltonian in this basis set requires the following relationships between the elements of the  $g$  and  $A^V$  tensors and the MO coefficients and the energies of the electronic transitions.

$$g_{||} - 2.0023 = -8a^2\alpha^2\beta^2\xi/E_2 \quad (\text{III-24})$$

$$g_{\perp} - 2.0023 = -2a^2\alpha^2\gamma^2\xi/E_3 \quad (\text{III-25})$$

$$a_{||}^V = P \left\{ -K - \frac{4}{7} a^2\alpha^2 + (g_{||} - 2.0023) + \frac{3}{7}(g_{\perp} - 2.0023) \right\} \quad (\text{III-26})$$

$$a_{\perp}^V = P \left\{ -K + \frac{2}{7} a^2\alpha^2 + \frac{11}{14}(g_{\perp} - 2.0023) \right\} \quad (\text{III-27})$$

where  $K$  is the isotropic hyperfine contribution and  $P = 2.0023 \beta_N g_N \beta_N \langle r^{-3} \rangle$  where  $g_N$  is the  $g$ -value of the nucleus and  $\beta_N$  is the nuclear magneton. The excitation energies of the states described by  $\psi_2$  and  $\psi_3$  relative to the





state  $\psi_1$ , are designated  $E_2$  and  $E_3$ .

In the equations (III-24) to (III-27) orbital overlap corrections have not been included, and the effects of the admixture of some  $|3z^2-r^2\rangle$  into the orbital  $\psi_1$ , have been ignored because the observed EPR spectra are adequately described in terms of axial symmetry. The assumption of approximate axial symmetry implies the near degeneracy of the states  $\psi_3$  and  $\psi_4$ . The neglect of contributions from the spin-orbit interactions of the sulfur nuclei is justified since the unpaired electron is highly localized on the vanadium atom.

In order to interpret the observed magnetic parameters in terms of MO coefficients and thereby obtain information about the bonding in the vanadyl complexes, an assignment of the electronic spectrum must be made. The basis for this assignment has been discussed in the previous section for the various solvent systems and the assignments given in Table III-6.

The MO coefficients  $\alpha$ ,  $\beta$  and  $\gamma$  were determined from the observed g-values and vanadium hyperfine splitting components using equations (III-24 to III-27) and <sup>27</sup>P = 133 Gauss and  $\xi = 168 \text{ cm}^{-1}$ . The MO coefficients are tabulated in Table III-11. The magnitudes of the coefficients cannot be considered accurate because of the uncertainties in the spin-orbit coupling  $\xi$  and the dipolar hyperfine factor P.



TABLE III-11Molecular Orbital Coefficients

<u>Complex</u>	<u>Solvent</u>	<u>Species</u>	<u><math>\alpha^2</math></u>	<u><math>\beta^2</math></u>	<u><math>\gamma^2</math></u>	<u>K</u>	<u><math>K/\alpha^2</math></u>
Phenyl	Toluene	T	.892	.642	.742	.696	.780
Ethoxy	Toluene	T	.914	.412	.798	.694	.759
Ethoxy	5% HMP/Toluene	D	.866	.538	1.04	.730	.843
Ethoxy	HMP	S	1.04	.635	1.06	.862	.829
Ethoxy	DMF	S	1.02	.752	.962	.812	.796
Ethoxy	Pyridine	S	.928	.631	.896	.703	.758

---



As Hitchman and Belford <sup>27</sup> have indicated,  $\alpha$  is close to 1 in all cases, indicating that the electron is essentially localized on the vanadium atom.  $\alpha$  is lower for species T than for the S species which suggests the  $d_{zx}$  and  $d_{zy}$  orbitals contribute more to  $\pi$  bonding with sulfur than with oxygen or nitrogen ligands. In all cases,  $\beta$  is smaller than unity due to the strong  $\sigma$ -interactions between the vanadium  $d_{xy}$  orbital and ligand p orbitals.<sup>67</sup> The relative  $\beta$  values suggest that  $\sigma$  bonding with S is more covalent than with N or O.

The variations in the  $^{51}\text{V}$  isotropic hyperfine parameter,  $a_o^V$  indicate that one of the factors which affects the isotropic splitting is the amount of delocalization of the  $b_1(3d_{x^2-y^2})$  orbital onto the ligands. The largest  $\alpha$  values correspond to species which also have the largest observed  $a_o^V$ . As Kivelson and Lee <sup>25</sup> have indicated, the variations in  $K/\alpha^2$  are probably due to changes in coordination at the vanadium atom. The amount of s-character in the  $b_1$  orbital, containing the unpaired electron, and the effectiveness of spin polarization contributions to the isotropic  $^{51}\text{V}$  interaction will certainly differ in species with different coordination.

### 3. Hyperfine Interactions

The mechanism of the hyperfine interaction between the  $^{31}\text{P}$  nuclei in the dithiophosphate chelates with the unpaired electron on the vanadium atom is believed to be



through a  $\sigma$ -interaction between the vanadium  $d_{x^2-y^2}$  orbital and an appropriate linear combination of the two P-S  $\sigma$ -bonding orbitals.<sup>16</sup> The hyperfine splittings will be influenced by the amount of phosphorus 3s character in the P-S  $\sigma$ -bonds. The coefficient  $C_{3s}^P$ , of the phosphorus 3s atomic orbital in the molecular orbital containing the unpaired electron, is related to the phosphorus hyperfine splitting by<sup>68</sup>

$$a^P = 3636 |C_{3s}^P|^2 .$$

The values of  $C_{3s}^P$  calculated from the observed  $^{31}\text{P}$  hyperfine splittings in the phenyl and ethoxy complexes in toluene solutions are 0.095 and 0.117 respectively. The large difference in the coefficients and phosphorus splittings in these two complexes can be attributed to the difference in the amount of phosphorus s-character in the P-S bonds of the dithiophosphinate and dithiophosphate moieties. In the dithiophosphate complex, the P-S bonds are shorter and have more s-character than in the dithiophosphinate complexes. Infrared<sup>69</sup> and X-ray<sup>70</sup> evidence for differences in P-S bonding in these complexes have been reported.

When a Lewis base displaces one of the sulfur atoms of the dithiophosphinate or dithiophosphate from its coordination to the vanadium atom, the  $^{31}\text{P}$  nucleus of this chelate no longer experiences significant hyperfine interactions because the spatial arrangement leads to a sub-





stantial decrease in the interaction between the vanadium  $d_{x^2-y^2}$  orbital and the P-S  $\sigma$ -orbitals. The hyperfine splitting of the  $^{31}\text{P}$  nucleus of the dithiophosphate chelate which has not been displaced is altered because the bonding in the  $\text{V} \begin{smallmatrix} \text{S} \\ \diagup \quad \diagdown \\ \text{S} \end{smallmatrix} \text{P}$  grouping will be modified by the asymmetry of the coordination at the other equatorial sites. In the species D which result from the phenyl and ethoxy complexes in solutions containing low concentrations of pyridine,  $C_{3\text{S}}^{\text{P}}$  has the values 0.084 and 0.100 respectively. It would appear that the destruction of the symmetry of the coordination trans to the dithiophosphate chelate leads to lengthening of one or both of the P-S bonds and a decrease in the amount of phosphorus s-character in the P-S  $\sigma$ -bonds. The HMP adducts of the phenyl and ethoxy complexes show smaller  $^{31}\text{P}$  hyperfine splittings than the pyridine adducts. This may be attributable to the difference in the effects of oxygen and nitrogen ligands coordination on the V-S and hence P-S bonding.

#### E. Comparisons With Other Systems

Since the vanadyl dithiophosphinates are structurally similar to  $\text{VO}(\text{acac})_2$ , both having the vanadium atom within a square pyramidal arrangement of other atoms, a comparison of the effect of Lewis base addition in the two systems should be useful. The EPR results in both systems show



that  $a_o^V$  is changed by adduct formation.  $a_o^V$  for  $VO(acac)_2$  in toluene is 108 Gauss but decreases to 105 Gauss in the pyridine adduct and 103 Gauss in the HMP adduct.<sup>39</sup>  $a_o^V$  for the vanadyl dithiophosphinates is 95 Gauss in toluene, remains unchanged in the pyridine adduct and increases to 100 Gauss in the HMP adduct. The adducts of the vanadyl dithiophosphinates being discussed here are those giving rise to a doublet pattern in the EPR spectrum (species D), a species which has been shown to contain one Lewis base molecule per vanadyl complex molecule. The decrease in  $a_o^V$  observed upon adduct formation in  $VO(acac)_2$  is in contrast to the unchanged or increased  $a_o^V$  values observed for adduct formation of the vanadyl dithiophosphinates. The difference may be a result of the coordination by the Lewis base at different sites in the two vanadyl systems. Studies of  $VO(acac)_2$  in 10% pyridine/benzene<sup>39</sup> assumed the pyridine coordinated at the axial site. Subsequent infrared studies have shown this to be the case for pyridine.<sup>8</sup> In contrast, previous sections of this Chapter showed that pyridine and HMP coordinated at the equatorial site of the vanadyl dithiophosphinates. It has also been pointed out that the EPR spectrum of  $VO(acac)_2$  in 10% HMP/benzene at room temperature is composed of two species<sup>39</sup>, one species having  $a_o^V$  equal to 103 Gauss and one species having  $a_o^V$  equal to 112 Gauss. Fig. III-19 shows that the relative amounts of the two species are nearly independent of temperature.



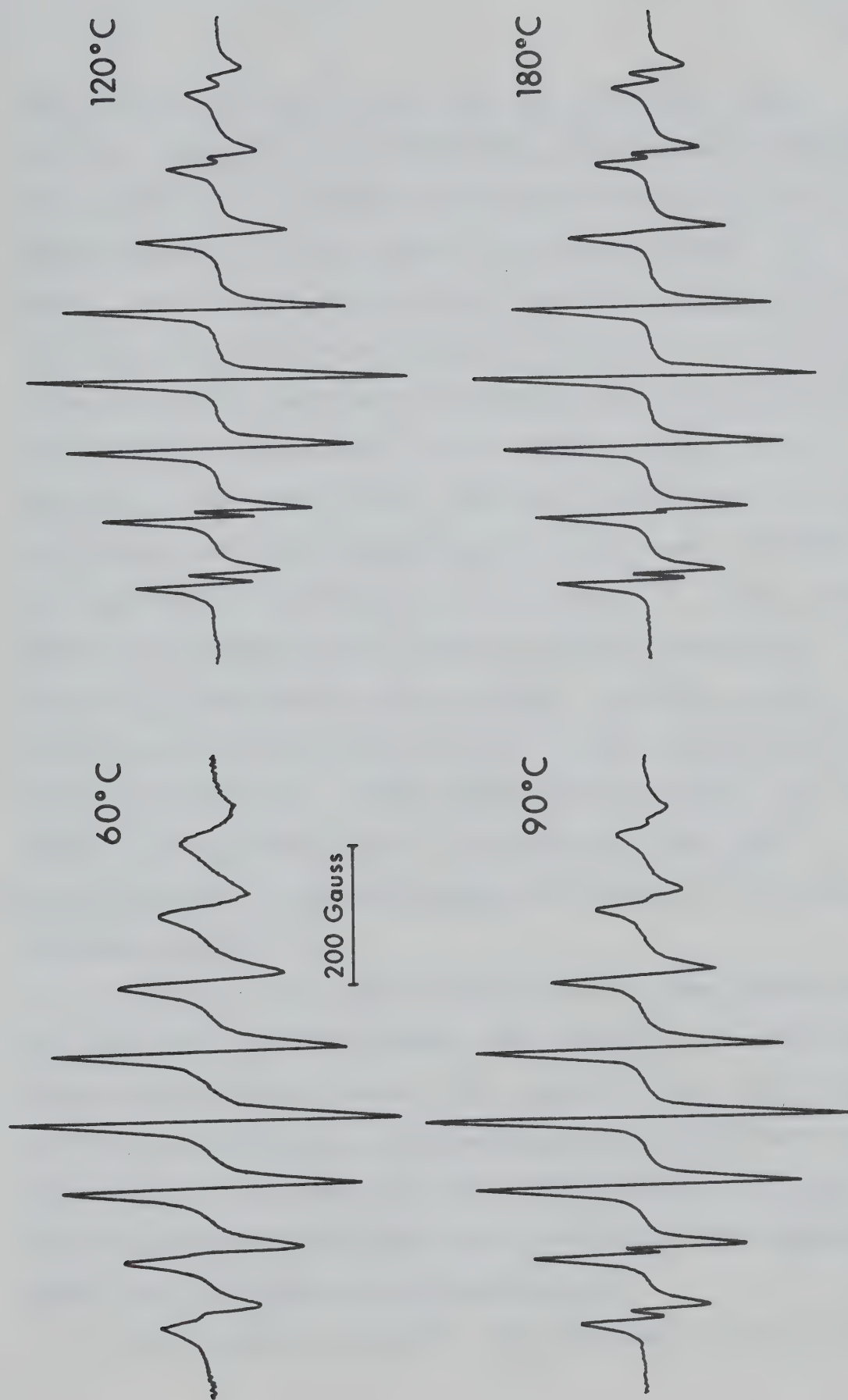


FIGURE III-19 EPR spectra of  $10^{-3}$  M liquid solutions of  $\text{VO}(\text{acac})_2$  in HMP at various temperatures.



The increase in the  $a_o^V$  value for one of the HMP adduct species, compared to  $a_o^V$  of  $VO(acac)_2$  in benzene, parallels the increase in  $a_o^V$  observed when HMP coordinates at an equatorial site in the vanadyl dithiophosphinates. On this basis, the  $VO(acac)_2 \cdot HMP$  species with the larger  $a_o^V$  value might be attributed to a complex in which HMP is coordinated at an equatorial site and the species with the smaller  $a_o^V$  value might be attributed to a complex in which HMP is attached to the axial site. Infrared studies of solutions of 2-methyl pyridine containing  $VO(acac)_2$  have indicated the simultaneous existence of two isomers.<sup>36</sup> These isomers were also assigned as the 2-methyl pyridine adducts of  $VO(acac)_2$ ; one isomer having 2-methyl pyridine axially coordinated and one isomer having 2-methyl pyridine equatorially coordinated. Other substituted pyridines have been shown to coordinate only at the equatorial position<sup>8</sup>, which parallels the results presented here for the vanadyl dithiophosphinates.

Removal of the excess mixed solvent under vacuum from the EPR sample used to produce the spectra in Fig. III-19 left behind a green solid. This compound gave a microanalysis and a thermograph corresponding to a compound with the molecular formula  $VO(acac)_2 \cdot HMP$ . The isolation of this compound suggests that HMP does not displace the acetylacetonate from the first coordination sphere.

The conclusions reached from the study of Lewis base





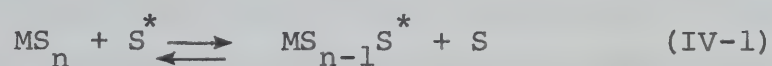


coordination to vanadyl dithiophosphinates suggest that the results of studies with vanadyl dithiocarbamates should be re-examined. One expects the V-S bonds of dithiophosphinates and dithiocarbamates to have similar properties. Adduct formation of vanadyl dithiocarbamates was assumed to involve coordination of Lewis bases such as pyridine and dimethylsulfoxide at the axial position.<sup>9,10</sup> This was concluded on the basis of changes in the vanadyl V-O stretching frequency and the  $^{51}\text{V}$  hyperfine couplings, but the work reported in this thesis indicates that these probes are not sensitive enough to determine the changes in coordination about the vanadium atom that occur in the presence of Lewis base ligands. On the basis of the vanadyl dithiophosphate results, one might expect coordination at the equatorial site at low Lewis base concentrations and displacement of the sulphur atoms from the first coordination sphere at higher concentrations.



CHAPTER IVEQUATORIAL AND AXIAL SOLVENT EXCHANGE RATES OF VANADYL  
COMPLEXESA. Introduction

The rates of solvent exchange from the first coordination sphere of a metal ion are an important aspect of inorganic solution kinetics. The general exchange reaction can be represented by



where S and S\* are chemically identical and n is the number of solvent molecules coordinated to the metal. On the left hand side in equation (IV-1), S\* is a bulk solvent molecule, while on the right hand side S\* is in the first coordination sphere of the metal ion. The kinetic parameters for these types of reactions can often be determined by the nuclear magnetic resonance line broadening technique. In the following section the relevant magnetic relaxation theory is presented and it is shown that under certain conditions <sup>71</sup>, the line broadening of the solvent resonance by a paramagnetic ion is related to the solvent exchange rate, and the temperature dependence of the line broadening can give the activation parameters of the exchange process. The magnitude of the line broadening can also be used to calculate the nuclear relaxation times of nuclei on solvent molecules coordinated to the metal ion. These relaxation times are



interpreted in terms of the mechanisms causing the relaxation. Ultimately the relaxation times are controlled by the rotational correlation time of the metal complex which can be determined from the EPR linewidths of the metal complex.

The complexes  $\text{VO}(\text{DMF})_5(\text{ClO}_4)_2$  and  $\text{VO}(\text{DMA})_5(\text{ClO}_4)_2$  dissolved in DMF and DMA respectively can undergo the reaction represented by equation (IV-1). Since the vanadium atomic orbitals in these complexes which participate in the bonding of the axial ligand to the metal ion are different from those involved in the bonding of the equatorial ligands<sup>31,32</sup>, the chemical properties of the two coordination sites should be quite different. Previous studies were not able to distinguish the exchange from the axial site to bulk solvent from the exchange of solvent molecules from the second coordination sphere into the bulk solvent. The results in section D show that the axial exchange has a special effect on the line broadening of DMF by vanadyl ion from which the kinetic parameters for both equatorial and axial exchange can be determined. Section D also contains line broadening studies of DMF solutions of  $\text{VO}(\text{acac})_2$  and bis-(o-phenanthroline)-oxo-vanadium(IV) perchlorate, both of which are expected to accept a DMF ligand at the vacant site.

The EPR and infrared data presented in Chapter III showed that Lewis bases in low concentrations coordinated



at the equatorial site of the vanadyl dithiophosphinates. At higher Lewis base concentrations, several coordination positions are occupied by the base molecules, but it was not firmly established that the dithiophosphate ligands had been completely displaced from the first coordination sphere of the vanadyl ion. To define the species in a solution of Lewis base, the DMF and DMA line broadening data of the phenyl complex was collected and compared to the data for the vanadyl perchlorates where the five inner sphere coordination positions are known to be occupied by solvent molecules. These results are given in section D-6.

A discussion of the solvent line broadening data is presented in section E as well as some comparisons with kinetic data from previous studies of vanadyl systems.

## B. Theory of NMR Line Broadening by Paramagnetic Complexes

### 1. General Theory

The time dependence of the magnetization  $\vec{M}$  for an ensemble of free spins in a homogeneous magnetic field of flux  $\vec{B}$  is given by

$$\frac{d\vec{M}}{dt} = \gamma \vec{M} \times \vec{B}, \quad (\text{IV-2})$$

where  $\gamma$  is the gyromagnetic ratio of the spins. Upon the application of a static magnetic field  $\vec{B} = (0, 0, B_0)$ , Bloch<sup>72</sup> assumed that the magnetization relaxed to its equilibrium value  $M^0$  with exponential time-dependence characterized by a time constant  $T_1$ , the longitudinal or spin-







lattice relaxation time. If the magnetization receives a component in the plane perpendicular to  $B_0$ , this magnetization is assumed to decay with a time constant  $T_2$ , the transverse or spin-spin relaxation time. In a conventional NMR experiment, the nuclear spins experience both a large static field  $B_0$  and a small field  $B_1$  perpendicular to  $B_0$  oscillating with a frequency  $\omega$ ; i.e.  $\vec{B} = (B_1 \cos \omega t, -B_1 \sin \omega t, B_0)$ . Under these conditions the motion of the magnetization is a superposition of the relaxation processes on the motion of the free spins as indicated by the equation

$$\frac{d\vec{M}}{dt} = \gamma(\vec{M} \times \vec{B}) - \frac{(\vec{x}M_x + \vec{y}M_y)}{T_2} - \frac{(M_z - M_0)\vec{z}}{T_1}, \quad (\text{IV-3})$$

where  $\vec{x}$ ,  $\vec{y}$  and  $\vec{z}$  are unit vectors in a laboratory system in which  $B_0$  lies along the  $\vec{z}$  direction. The three equations, one for each component of the magnetization, represented by equation (IV-3) are the well known phenomenological Bloch equations. For mathematical convenience, the Bloch equations are usually expressed in a rotating coordinate system in which the x and y axes are rotating at frequency  $\omega$  about the z axis and the rotating component of  $\vec{B}_1$  lies along the x-axis of this rotating coordinate system. This transformation is performed by defining the components of the magnetization in the rotating coordinate system as



$$u = M_x \cos \omega t - M_y \sin \omega t,$$

$$v = M_x \sin \omega t - M_y \cos \omega t .$$

The component  $u$  is in phase with the magnetic field  $B_1$  while  $v$  is the out-of-phase component. In the rotating coordinate system the Bloch equations take the form

$$\frac{du}{dt} = (\omega_0 - \omega)v - u/T_2 , \quad (\text{IV-4})$$

$$\frac{dv}{dt} = -(\omega_0 - \omega)u + \gamma B_1 M_z - v/T_2 , \quad (\text{IV-5})$$

$$\frac{dM_z}{dt} = -\gamma B_1 v - (M_z - M_0)/T_1 , \quad (\text{IV-6})$$

where  $\omega_0 = \gamma B_0$ . By defining a complex magnetization,  $G$ , as the complex sum of the in-phase and out-of-phase components of the magnetization,

$$G = u + iv, \quad (\text{IV-7})$$

equations (IV-4) and (IV-5) may be combined into the single equation

$$\frac{dG}{dt} = -i\gamma B_1 M_z - \left( \frac{1}{T_2} - i\Delta\omega \right) G , \quad (\text{IV-8})$$

where  $\Delta\omega = \omega_0 - \omega$ .

McConnell <sup>73</sup> has modified the Bloch equations to include the transfer of magnetization between different sites



by the chemical exchange of nuclei. For the simple case of two sites, a solvent site S and a metal site M, the Bloch equations for the nuclei in site S are written as

$$\frac{dG_S}{dt} = -i\gamma B_1 M_z^S - \left( \frac{1}{T_{2S}} + \frac{1}{\tau_S} - i\Delta\omega_S \right) G_S + \frac{G_M}{\tau_M}, \quad (\text{IV-9})$$

where  $\Delta\omega_S = \omega_S - \omega$ ,  $\omega_S = \gamma_S B_0$ ,  $T_{2S}$  is the relaxation time for nuclei in site S,  $\tau_S$  is the lifetime of the spins in site S and  $\tau_M$  is the lifetime of the spins in site M. The corresponding expression for the magnetization in site M is

$$\frac{dG_M}{dt} = -i\gamma B_1 M_z^M - \left( \frac{1}{T_{2M}} + \frac{1}{\tau_M} - i\Delta\omega_M \right) G_M + \frac{G_S}{\tau_S}, \quad (\text{IV-10})$$

where  $\Delta\omega_M = \omega_M - \omega$ ,  $\omega_M = \gamma_M B_0$  and  $T_{2M}$  is the relaxation time for nuclei in site M. In NMR experiments, the out-of-phase component  $v$  is monitored as the field  $B_0$  or the frequency  $\omega$  is swept through the resonance at a rate which is generally long compared to the intrinsic relaxation times so that the spin system is always in equilibrium. This

condition is equivalent to setting  $\frac{dM_z^S}{dt} = \frac{dM_z^M}{dt} = dG_S/dt =$

$dG_M/dt = 0$ . Furthermore  $M_z^S = M_0^S$  and  $M_z^M = M_0^M$  since the field  $B_1$  is kept small enough to avoid saturation effects. With these considerations, equations (IV-9) and (IV-10) can be solved for the complex magnetization in the solvent site,  $G_S$ . The resulting complicated expression can be



simplified by considering the special conditions used in studies of solvent linebroadening by paramagnetic species. First of all, the concentration of the solvent (site S) is much larger than that of the paramagnetic species (site M) and one is justified in dropping terms involving  $M_o^M$  compared to  $M_o^S$  terms. Also, the total magnetization,  $G = G_S + G_M$ , to a good approximation is equal to  $G_S$  since the signal being observed is that of nuclei in S sites. With these approximations,  $G$  can be written

$$G = \frac{-i\gamma B_1 M_o^S}{\left( \frac{1}{T_{2S}} + \frac{1}{\tau_S} - i\Delta\omega_S \right) - \frac{1}{\tau_S \tau_M} \left( \frac{1}{\frac{1}{T_{2M}} + \frac{1}{\tau_M} - i\Delta\omega_M} \right)} \quad (\text{IV-11})$$

with imaginary part

$$v = \gamma B_1 M_o^S T_2 / [1 + \Delta\omega^2 T_2^2] , \quad (\text{IV-12})$$

where

$$\frac{1}{T_2} = \frac{1}{T_{2S}} + \frac{1}{\tau_S} \left\{ \frac{\frac{1}{T_{2M}^2} + \frac{1}{T_{2M}\tau_M} + \Delta\omega_M^2}{\left( \frac{1}{T_{2M}} + \frac{1}{\tau_M} \right)^2 + \Delta\omega_M^2} \right\} , \quad (\text{IV-13})$$

and

$$\Delta\omega = \Delta\omega_S - \frac{\Delta\omega_M}{\tau_S \tau_M \left[ \left( \frac{1}{T_{2M}} + \frac{1}{\tau_M} \right)^2 + \Delta\omega_M^2 \right]} . \quad (\text{IV-14})$$





This implies that the solvent NMR will be a Lorentzian line of width  $\Delta\nu_{\text{obs}}$  (Hz) at half-height

$$\Delta\nu_{\text{obs}} = 1/\pi T_2, \quad (\text{IV-15})$$

centred at

$$\omega_{\text{obs}} = \omega_S - \Delta\omega_M / \tau_M \tau_S \left[ \left( \frac{1}{T_{2M}} + \frac{1}{\tau_M} \right)^2 + \Delta\omega_M^2 \right], \quad (\text{IV-16})$$

where  $\Delta\omega_M$  in this last equation is the difference between the resonance frequencies of the nuclei in sites M and S. Furthermore,

$$\frac{1}{\tau_S} = n \frac{[M]}{[S]} \frac{1}{\tau_M}, \quad (\text{IV-17})$$

where  $n$  is the number of equivalent sites per paramagnetic species whose molal concentration,  $[M]$ , is low compared to the solvent molality,  $[S]$ .<sup>74</sup>

The paramagnetic line broadening

$$\begin{aligned} \Delta\nu_P &= \pi^{-1} \left( \frac{1}{T_2} - \frac{1}{T_{2S}} \right) \\ &= \pi^{-1} \frac{n[M]}{[S]\tau_M} \left\{ \frac{\frac{1}{T_{2M}^2} + \frac{1}{T_{2M}\tau_M} + \Delta\omega_M^2}{\left( \frac{1}{T_{2M}} + \frac{1}{\tau_M} \right)^2 + \Delta\omega_M^2} \right\}, \end{aligned} \quad (\text{IV-18})$$



and resonance shift

$$\begin{aligned}\Delta\omega_{\text{obs}} &= \omega_{\text{obs}} - \omega_S \\ &= \frac{-n[M]\Delta\omega_M}{[S]\{(1 + \tau_M/T_{2M})^2 + \tau_M^2\Delta\omega_M^2\}}, \quad (\text{IV-19})\end{aligned}$$

therefore vary linearly with concentration of paramagnetic ion.

Swift and Connick <sup>71</sup> have presented the analogous derivation for the three site problem and their result can be generalized to describe the situation for any number of sites. The resulting expressions for the line broadening and resonance shift are

$$\Delta\nu_P = \pi^{-1} \frac{[M]}{[S]} \sum_j \frac{n_j}{\tau_{M_j}} \cdot \frac{\frac{1}{T_{2M_j}^2} + \frac{1}{T_{2M_j}} \tau_{M_j} + \Delta\omega_j^2}{\left(\frac{1}{T_{2M_j}} + \frac{1}{\tau_{M_j}}\right)^2 + \Delta\omega_j^2}, \quad (\text{IV-20})$$

$$\Delta\omega_{\text{obs}} = - \frac{[M]}{[S]} \sum_j \frac{n_j \Delta\omega_j}{(1 + \tau_{M_j}/T_{2M_j})^2 + (\tau_{M_j} \Delta\omega_j)^2}, \quad (\text{IV-21})$$

where  $n_j$  is the number of solvent molecules coordinated at sites of type  $j$ ,  $\tau_{M_j}$  is the average lifetime of a molecule coordinated at the  $j$ -th site,  $1/T_{2M_j}$  is the nuclear relaxation time in the  $j$ -th site and  $\Delta\omega_j$  is the difference between the resonance frequency for a nucleus in site  $j$



and the observing frequency. The derivation of equations (IV-20) and (IV-21) neglects any exchanges among the different coordination sites since only bulk solvent to coordinated site exchange is included.

In the experimental NMR measurements of solutions containing vanadyl complexes, no paramagnetic shifts of the resonance frequencies were observed nor did the linewidths exhibit a frequency dependence. Therefore it was assumed that the  $\Delta\omega_j^2$  terms in equation (IV-20) and (IV-21) were small compared to the other terms in the sum and could be neglected. This simplifies the expressions for  $\Delta\nu_P$  and  $\Delta\omega_{\text{obs}}$  to

$$\Delta\nu_P = \pi^{-1} \frac{[M]}{[S]} \sum_j n_j / (\tau_{M_j} + T_{2M_j}) \quad , \quad (\text{IV-22})$$

$$\Delta\omega_{\text{obs}} = \frac{[M]}{[S]} \sum_j n_j \Delta\omega_j / (1 + \tau_{M_j} / T_{2M_j})^2 \quad . \quad (\text{IV-23})$$

The analysis of the linewidth data was performed using the reduced paramagnetic contribution,  $1/T_{2P}$ , defined by

$$\frac{1}{T_{2P}} = \pi \Delta\nu_P [S]/[M] \quad , \quad (\text{IV-24})$$

which, from equation (IV-22), is given by

$$\frac{1}{T_{2P}} = \sum_j n_j / (\tau_{M_j} + T_{2M_j}) \quad . \quad (\text{IV-25})$$



$1/T_{2P}$  values are then independent of the properties of a particular sample and depend only on the relaxation times,  $T_{2M_j}$ , and the exchange rates,  $1/\tau_{M_j}$ , of the chemical system.

The paramagnetic line broadening produced by exchange between a coordinated site  $j$  and the bulk solvent exhibits two limiting conditions which are of interest in the present study. When  $\tau_{M_j} \gg T_{2M_j}$ , the contribution to  $1/T_{2P}$  from exchange at the  $j$ -th site is  $n_j/\tau_{M_j}$ . In this limit, often referred to as the exchange controlled region, the nuclei are coordinated at site  $j$  for times which are long compared to the nuclear relaxation time at this site so that the rate of relaxation of molecules in the bulk solvent due to exchange with coordinated molecules is controlled by  $\tau_{M_j}$ . When  $\tau_{M_j} \ll T_{2M_j}$ , the nuclei spend only a short time in coordination site  $j$  before reentering the bulk solvent and they may exchange many times before being relaxed at the coordinated site. In this limit, therefore, the contribution to  $1/T_{2P}$  from exchange between bulk solvent and coordination site  $j$  is  $n_j/T_{2M_j}$ . This limiting condition is referred to as the  $T_{2M}$  region.

## 2. Temperature Dependence of Exchange Rates, Nuclear Relaxation Times and Chemical Shifts.

The temperature dependence of  $1/T_{2P}$  is determined by the temperature dependence of the individual terms  $\tau_{M_j}$





and  $T_{2M_j}$ . The solvent exchange rates,  $\tau_{M_j}^{-1}$ , are of the form

$$\tau_{M_j}^{-1} = \frac{kT}{h} \exp \left( -\frac{\Delta H_j^\ddagger}{RT} + \frac{\Delta S_j^\ddagger}{R} \right) \quad (\text{IV-26})$$

on the basis of the transition state theory.<sup>75</sup> In equation (IV-26),  $k$  is Boltzmann's constant,  $h$  is Planck's constant,  $R$  the gas constant,  $T$  the absolute temperature and  $\Delta H_j^\ddagger$  and  $\Delta S_j^\ddagger$  are the enthalpy and entropy of activation for the exchange of molecules from the  $j$ -th coordination site into the bulk solvent.  $T_{2M_j}$  is determined by intimate details of the interaction of the nuclear spin with the unpaired electrons in the paramagnetic ion and the electron relaxation time. Ultimately, the nuclear relaxation rates for all coordination sites are related to the tumbling time  $\tau_r$  for the complex ion. One therefore assumes that the temperature dependence of all  $T_{2M_j}$  is determined by the temperature dependence of  $\tau_r$  and one writes

$$T_{2M_j}^{-1} = C_{M_j} \exp E_M/RT, \quad (\text{IV-27})$$

where  $E_M$  is the activation energy for molecular tumbling and  $C_{M_j}$  are constants to be determined from the NMR line broadening data.

The rate of nuclear relaxation of a nucleus near a paramagnetic ion is dominated by the fluctuations of the dipolar and hyperfine interactions of the nuclear and



electron spins. A detailed analysis of the time-dependence of these interactions predicts that <sup>76,77</sup>

$$\frac{1}{T_{2M}} = \frac{7\gamma_I^2 g_o^2 \beta_o^2 S(S+1) \tau_r}{15r_i^6} + \frac{S(S+1)}{3} A_o^2 T_{1e} \quad (\text{IV-28})$$

where  $r_i$  is the average electron-nuclear separation,  $\gamma_I$  is the nuclear gyromagnetic ratio,  $S$  the electron spin angular momentum ( $S = 1/2$  in the present studies),  $A_o$  is the nuclear-electronic hyperfine interaction and  $T_{1e}$  is the longitudinal electron relaxation time. The first term in equation (IV-28) represents the dipolar relaxation and the second is the relaxation rate due to modulation of hyperfine interactions.  $\tau_r$  may be calculated from the EPR linewidth parameters  $\alpha$ ,  $\beta$ ,  $\gamma$  and  $\delta$  defined in equation (III-18) and measured values of the anisotropic magnetic parameters. The dependence of  $\tau_r$  on these parameters is given explicitly by Wilson and Kivelson.<sup>28</sup> Angerman and Jordan<sup>78</sup> have indicated that the linewidth parameter  $\gamma$  is less sensitive to experimental errors than the other parameters and the values of  $\gamma$  obtained from an analysis of the EPR spectra can be used to calculate reliable values for the tumbling times  $\tau_r$  of the vanadyl complexes.  $\gamma$  and  $\tau_r$  are related by the equation <sup>28</sup>



$$\gamma = \tau_r \left\{ \frac{b^2}{8} - \frac{7b(g_{||} - g_{\perp})A_o^V}{30g_o} + \frac{1}{1+\omega_o^2\tau_r^2} \left[ -\frac{b^2}{40} - \frac{b(g_{||} - g_o)A_o^V}{6g_o} - \frac{2b(g_{||} - g_{\perp})A_o^V\omega_o^2\tau_r^2}{5(1+\omega_o^2\tau_r^2)g_o} + \frac{b^2A_o^V\omega_o\tau_r^2}{8(1+\omega_o^2\tau_r^2)} \right] \right\}, \quad (\text{IV-29})$$

where

$$b = \frac{2}{3}(A_{||}^V - A_{\perp}^V), \quad (\text{IV-30})$$

$\omega_o$  is here the resonance frequency of the electron and other symbols are as defined earlier. Since equation (IV-29) results in a cubic equation for  $\tau_r$ ,  $\tau_r$  was determined by an iterative procedure.

Another quantity which must be determined is the longitudinal electron relaxation time  $T_{1e}$ . The dominant contributions to  $T_{1e}^{-1}$  are the rotational modulation of anisotropic magnetic interactions<sup>28</sup> and collisional modulation of spin-rotational interactions.<sup>57</sup> The theory of relaxation by these mechanisms leads to the expression

$$\frac{1}{T_{1e}} \simeq \frac{2\tau_r}{1+\omega_o^2\tau_r^2} \left[ \left( \frac{g_{||} - g_{\perp}}{g_o} \right)^2 \frac{\omega_o^2}{15} + \frac{7b^2I(I+1)}{40} + \frac{b(g_{||} - g_{\perp})\omega_o M_V}{5g_o} - \frac{b^2 M_V^2}{40} \right] + \frac{(g_{||} - g_{e1})^2 + 2(g_{\perp} - g_{e1})^2}{9\tau_r}, \quad (\text{IV-31})$$



where  $g_{e1} = 2.0023$  is the  $g$ -value of a free electron.

The temperature dependence of the contact shift of the NMR resonance  $\Delta\omega_M$  and its dependence on the hyperfine coupling has been given by Bloembergen<sup>79</sup> as

$$\Delta\omega_M/\omega_I = \frac{S(S+1)g_o\beta_oA_o}{3\gamma_I kT} \quad (\text{IV-32})$$

where  $\omega_I$  is the frequency of the NMR resonance of the solvent. Then if  $1/T_{2M}$  results predominantly from a hyperfine interaction, one can calculate the expected contact shift and compare it with the experimental values.

The following analyses of the line broadening in DMA and DMF are concerned with three types of coordination sites: equatorial, axial and outer sphere. The exchange between outer solvation sphere and bulk solvent is fast compared to the relaxation of nuclei in the outer coordination sphere in the temperature regions investigated. Thus no outer sphere-bulk solvent exchange-controlled region for  $1/T_{2P}$  is observed and the outer sphere contribution to  $1/T_{2P}$  is described only by the relaxation time  $n/T_{2Mos}$  for the nuclei in the outer coordination sphere.

### C. Experimental

The investigation of the solvent exchange kinetics of the vanadyl complexes required measurement of the NMR spectra of the solvent alone and of solutions containing the para-





magnetic ion over the liquid range of the solvent. The concentration of the paramagnetic species was adjusted to maximize  $\Delta\nu_p$  while maintaining a resonance narrow enough to produce adequate intensities. From the recorded spectra were measured the widths at half height and the chemical shift relative to an internal reference. The raw line-width data were converted to  $1/T_{2p}$  as defined by equation (IV-24) and plotted versus reciprocal temperature for subsequent analysis. These experiments were carried out for  $\text{VO}(\text{DMF})_5(\text{ClO}_4)_2$  in DMF,  $\text{VO}(\text{DMA})_5(\text{ClO}_4)_2$  in DMA, and bis-(diphenyldithiophosphinato)-oxo-vanadium(IV) in DMF, DMA and in N,N-diethylformamide (DEF).

The EPR spectra of these systems were also studied as a function of temperature and the linewidths of the individual lines determined. In addition, the spectra of the solid solutions were recorded and the anisotropic magnetic parameters for the complexes were determined.

Infrared spectra in the  $1600 - 1700 \text{ cm}^{-1}$  containing the carbonyl stretch absorption<sup>80</sup> were recorded for mulls of the vanadyl perchlorates and liquid films of the amides. Changes in the carbonyl absorption band upon coordination are related to the type of coordination of the amides to the vanadyl ion. The visible spectra of the vanadyl perchlorates in DMF and DMA were also recorded and compared with the optical absorption spectra of other vanadyl systems.



## D. Results

### 1. Analysis of Infrared, Visible and EPR Spectra

The characteristic feature of the infrared spectra of DMA, DMF and coordination compounds containing these molecules as ligands, is the carbonyl absorption in the region  $1600 - 1700 \text{ cm}^{-1}$ . The carbonyl band of  $\text{VO}(\text{DMF})_5(\text{ClO}_4)_2$  is shifted  $30 \text{ cm}^{-1}$  to lower frequency compared to uncoordinated DMF.<sup>81</sup> In addition, the carbonyl absorption for the complex is considerably broader than that in the free solvent. This indicates that there may be a number of non-equivalent coordinated DMF molecules. A similar broadening and a shift of  $40 \text{ cm}^{-1}$ , relative to liquid DMA, occurs in  $\text{VO}(\text{DMA})_5(\text{ClO}_4)_2$ .

The visible spectrum of  $\text{VO}(\text{DMF})_5(\text{ClO}_4)_2$  in DMF solution has an absorption maximum at  $12,600 \text{ cm}^{-1}$ , and that of  $\text{VO}(\text{DMA})_5(\text{ClO}_4)_2$  in DMA occurs at  $12,300 \text{ cm}^{-1}$ . See Fig. IV-1. The absorption spectra of both complexes show distinct shoulders on the high energy side of the absorption maximum just as the absorption spectrum of  $\text{VOSO}_4 \cdot 5\text{H}_2\text{O}$  does.<sup>31</sup> The similarity between the visible spectra of the vanadyl amide complex ions and the spectrum of the aquo vanadyl ion indicates that the molecular orbital description of the bonding in  $\text{VO}(\text{H}_2\text{O})_5^{2+}$  given by Ballhausen and Gray<sup>31</sup> should be valid for the amide complexes. The unpaired electron in the  $\text{VO}(\text{DMA})_5^{2+}$  and  $\text{VO}(\text{DMF})_5^{2+}$  ions is



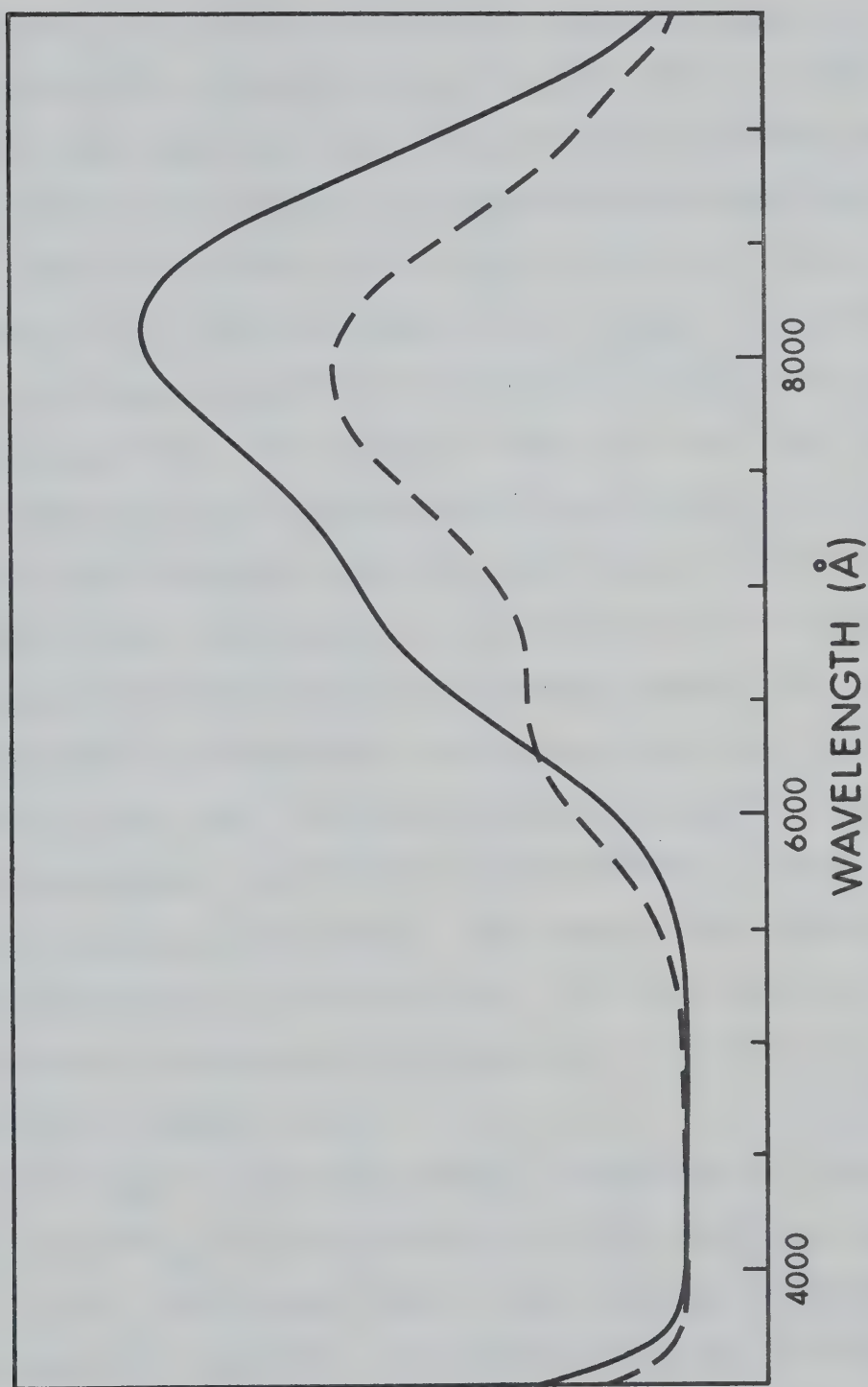


FIGURE IV-1. Electronic absorption spectra of  $\text{VO(DMA)}_5(\text{ClO}_4)_2$  in DMA, —; and  $\text{VO(DMF)}_5(\text{ClO}_4)_2$  in DMF, ----.



expected to be in an orbital of  $b_1$  symmetry which is essentially the vanadium  $d_{x^2-y^2}$  atomic orbital. This orbital has regions of high electron density along axes which bisect the equatorial ligand-vanadium bond axes.

The EPR spectra of solutions of  $\text{VO}(\text{DMF})_5(\text{ClO}_4)_2$  and  $\text{VO}(\text{DMA})_5(\text{ClO}_4)_2$  show the eight line pattern characteristic of an isotropic hyperfine interaction between the unpaired electron and the  $^{51}\text{V}$  nucleus of spin  $7/2$ . See Fig. IV-2. Each spectrum can be described by the isotropic  $g$ -value,  $g_0$ , and the isotropic hyperfine splitting constant  $A_0^V$ .  $A_0^V$  and  $g_0$  were determined from the positions of the pairs of lines with  $^{51}\text{V}$  nuclear spin quantum numbers  $+M_V$  and  $-M_V$  as described by equations (III-14) and (III-15), and the results of the four calculations were averaged. The magnetic parameters for  $\text{VO}(\text{DMF})_5^{2+}$  and  $\text{VO}(\text{DMA})_5^{2+}$  were found to be temperature dependent. The temperature dependence of these parameters is shown in Fig. IV-3 and indicates that no changes in molecular structure are occurring as a function of temperature.

The peak to peak derivative linewidths of the hyperfine lines  $\Delta B_{M_V}$  follow equation (III-18) and the values of  $\alpha$ ,  $\beta$ ,  $\gamma$  and  $\delta$  determined from a least squares analysis of the measured linewidths to equation (III-18) are given in Table IV-1. In order to extract  $\tau_r$ , the rotational tumbling time from the linewidth parameters, the anisotropic magnetic parameters were determined by studying the EPR





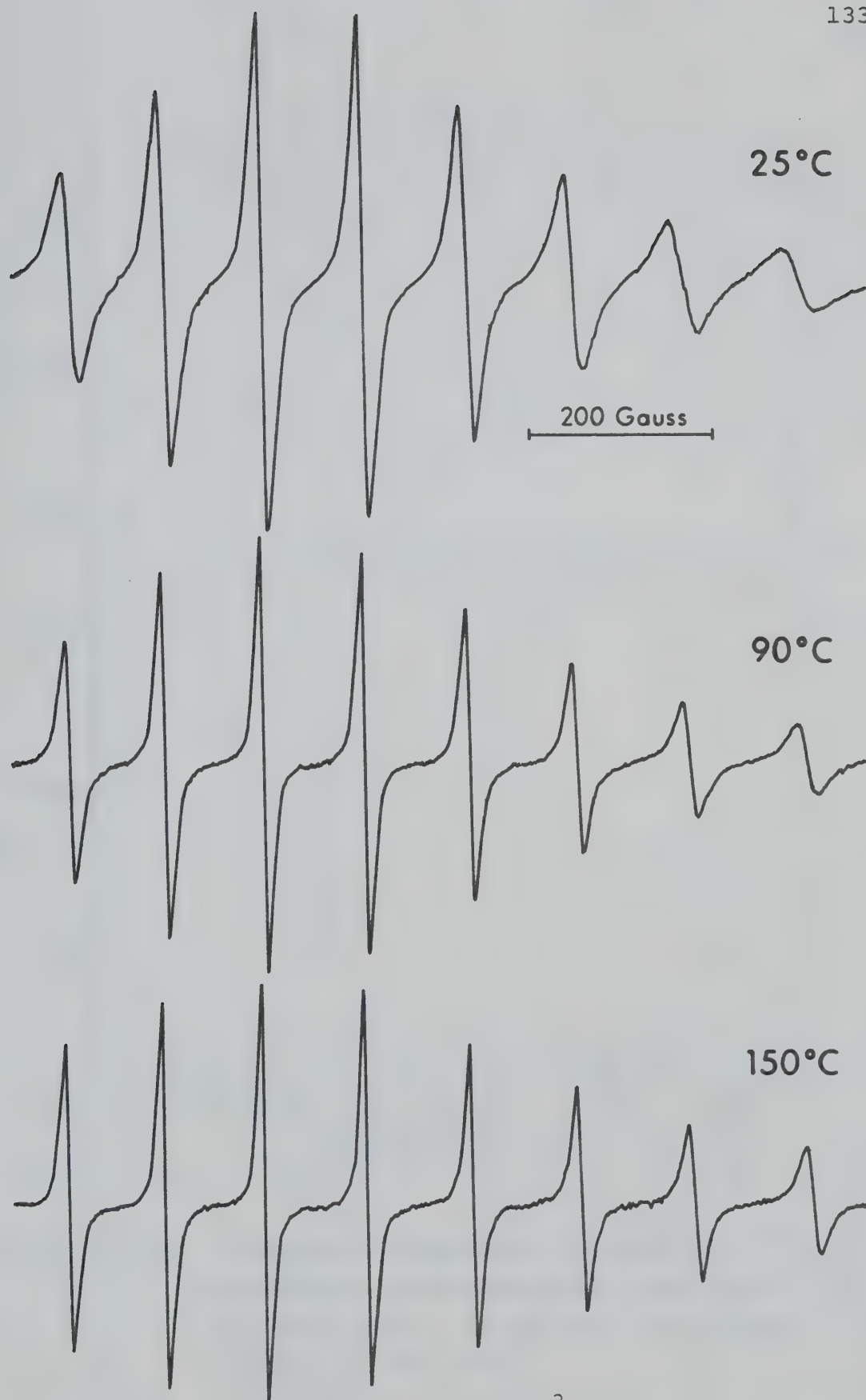


FIGURE IV-2. EPR spectra of  $5 \times 10^{-3}$  M liquid solutions of  $\text{VO}(\text{DMF})_5(\text{ClO}_4)_2$  in DMF at various temperatures.



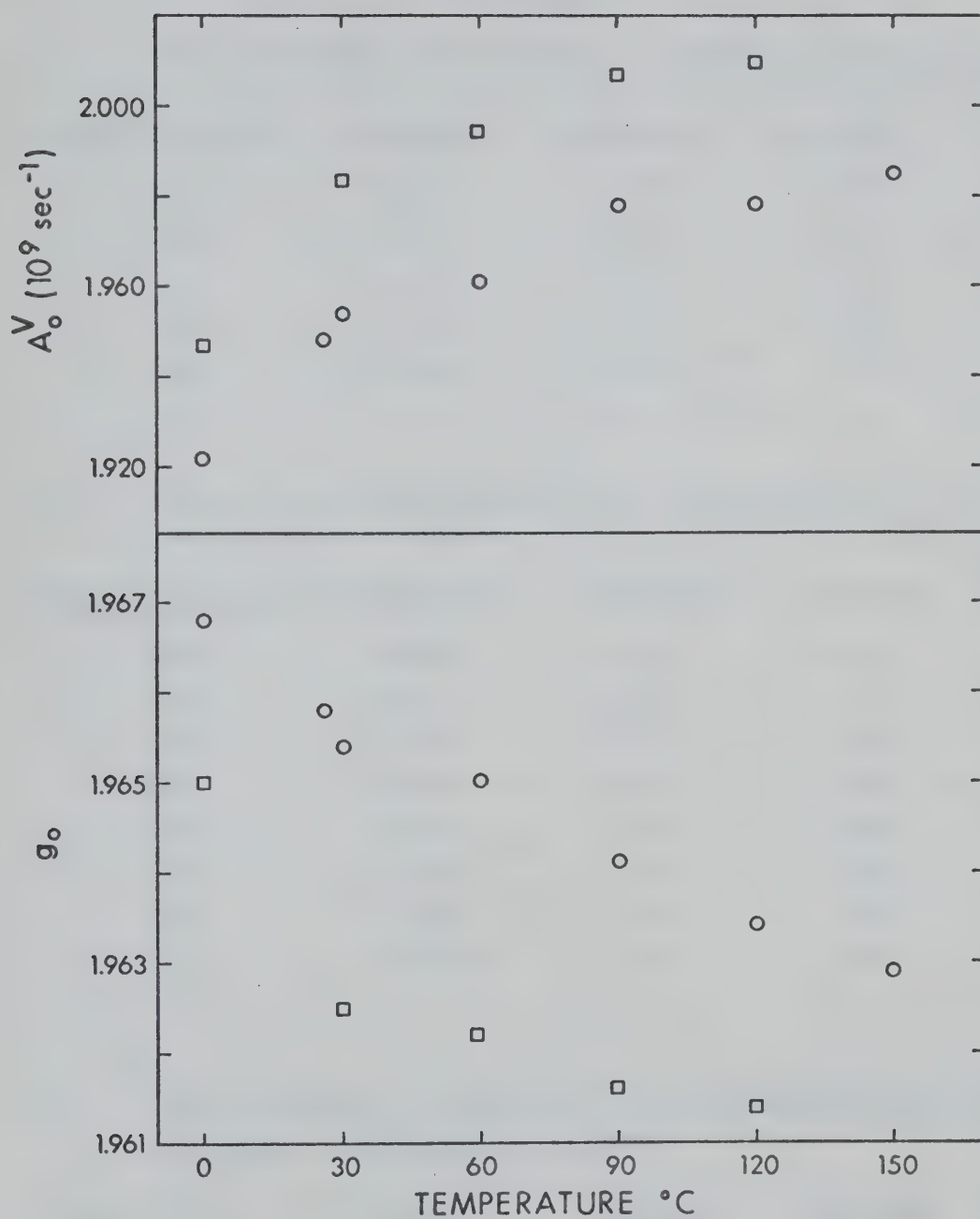


FIGURE IV-3. Temperature dependence of isotropic  $^{51}\text{V}$  hyperfine interactions and  $g$ -values of  $\text{VO}(\text{DMA})_5(\text{ClO}_4)_2$  in DMA ( $\square$ ) and  $\text{VO}(\text{DMF})_5(\text{ClO}_4)_2$  in DMF ( $\circ$ ).



TABLE IV-1

a. EPR Linewidth Parameters of  $\text{VO}(\text{DMA})_5(\text{ClO}_4)_2$  in DMA

<u>Temperature (K)</u>	<u><math>\alpha</math> (Gauss)</u>	<u><math>\beta</math> (Gauss)</u>	<u><math>\gamma</math> (Gauss)</u>	<u><math>\delta</math> (Gauss)</u>
275	23.02	5.47	2.29	-.054
293	16.54	3.56	1.57	-.002
313	13.76	3.10	1.07	-.060
333	11.78	2.50	.869	-.039
353	10.80	2.24	.750	-.033

b. EPR Linewidth Parameters of  $\text{VO}(\text{DMF})_5(\text{ClO}_4)_2$  in DMF

<u>Temperature (K)</u>	<u><math>\alpha</math> (Gauss)</u>	<u><math>\beta</math> (Gauss)</u>	<u><math>\gamma</math> (Gauss)</u>	<u><math>\delta</math> (Gauss)</u>
275	20.89	4.41	2.15	.003
293	16.31	3.39	1.45	-.030
313	13.30	2.51	1.08	-.025
333	11.29	1.94	.798	-.018
353	10.31	1.73	.642	-.027
373	9.469	1.47	.542	-.016
393	9.217	1.23	.436	-.011
413	9.197	1.11	.410	-.004

c. EPR Linewidth Parameters of Bis-(diphenyldithiophosphinato)-oxo-vanadium(IV) in DMF

<u>Temperature (K)</u>	<u><math>\alpha</math> (Gauss)</u>	<u><math>\beta</math> (Gauss)</u>	<u><math>\gamma</math> (Gauss)</u>	<u><math>\delta</math> (Gauss)</u>
273	26.22	6.22	2.85	-.040
293	18.81	3.76	1.51	-.067
313	14.78	2.80	1.05	-.053
333	12.73	2.33	.799	-.048
353	11.42	1.97	.649	-.034
373	10.61	1.64	.534	-.021



spectra of the vanadyl complexes in solid solutions at low temperature. The glass spectra indicated that the complexes were of axial symmetry and allowed direct determination of the components of the  $g$ -value and hyperfine tensors along the symmetry axis of the molecule;  $g_{||}$  and  $A_{||}^V$  respectively. The components of the tensors along axes perpendicular to the axis of symmetry were determined from the isotropic and parallel components using equations (III-16) and (III-17). In these calculations, the values of  $g_o$  and  $A_o^V$  at 25°C were used. The values of  $g_{\perp}$  and  $A_{\perp}^V$  obtained in this way are subject to some error since  $g_o$  and  $A_o^V$  are temperature dependent, but this error is not larger than the estimated errors in the values of  $g_{\perp}$  and  $A_{\perp}^V$  measured directly from the glass spectrum. The magnetic parameters for the vanadyl perchlorates are given in Table IV-2.

The experimental values of  $\gamma$  and the magnetic parameters allow one to solve equation (IV-29) for  $\tau_r$  by an iterative procedure. The values of  $\tau_r$  for solutions of  $\text{VO}(\text{DMF})_5(\text{ClO}_4)_2$  and  $\text{VO}(\text{DMA})_5(\text{ClO}_4)_2$  are shown as a function of temperature in Fig. IV-4. The activation energies for molecular tumbling in liquid DMF and DMA obtained from the data in Fig. IV-4 are  $2.7 \pm 0.1$  and  $2.8 \pm 0.2$  kcal/mole respectively. The activation energy for DMF is in excellent agreement with the value 2.8 kcal/mole predicted from the viscosity of the liquid.<sup>82</sup> The correlation times  $\tau_r$  were required for detailed interpretation of the NMR line broad-





TABLE IV-2

Magnetic Parameters of Vanadyl Perchlorate in DMF and DMA<sup>†</sup>

<u>Parameter</u>	<u>DMF</u>	<u>DMA</u>
$g_o$	1.966	1.963
$g_{  }$	1.934	1.931
$g_{\perp}$	1.982	1.979
$A_o^{\perp} (10^9 \text{ sec}^{-1})$	1.945	1.977
$A_{  }^{\perp} (10^9 \text{ sec}^{-1})$	3.343	3.405
$A_{\perp}^{\perp} (10^9 \text{ sec}^{-1})$	1.229	1.245

†

Estimated error  $\pm 0.5\%$



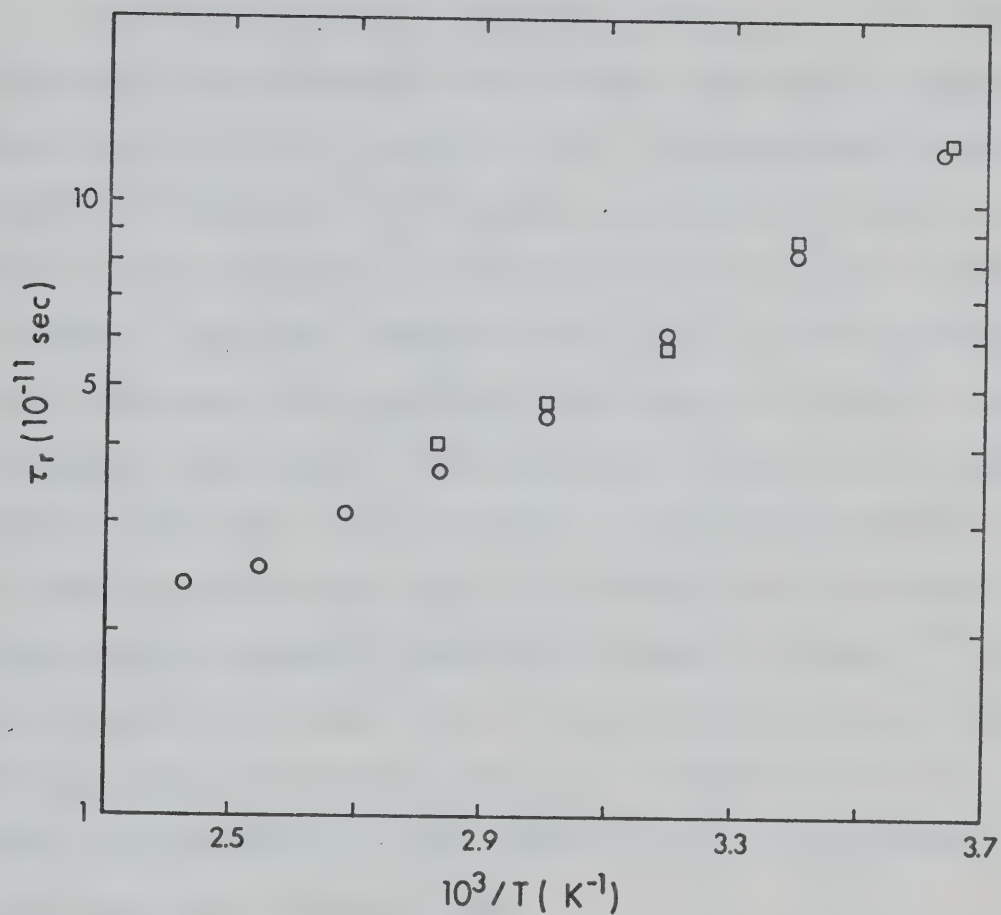


FIGURE IV-4. Temperature dependence of rotational tumbling time of  $VO(DMA)_5(ClO_4)_2$  in DMA ( $\square$ ) and  $VO(DMF)_5(ClO_4)_2$  in DMF ( $\circ$ ).



ening results as shown in a later section.

The EPR spectrum of  $\text{VO}(\text{DMA})_5(\text{ClO}_4)_2$  in liquid DMA indicates the presence of two vanadyl species at temperatures above  $120^\circ\text{C}$ . See Fig. IV-5. This species may be  $\text{VO}(\text{DMA})_4^{2+}$  although the vanadium hyperfine splitting in this second species is smaller than that for the  $\text{VO}(\text{DMA})_5^{2+}$  ion and it has been observed that loss of axial coordination increases the hyperfine splitting in vanadyl acetylacetonate complexes.<sup>39</sup> The presence of this second vanadyl species will have little effect on the interpretation of the NMR linebroadening results because the abundance of this species is small compared to that of  $\text{VO}(\text{DMA})_5^{2+}$  in the temperature range used in the NMR experiments. The EPR spectrum of  $\text{VO}(\text{DMF})_5(\text{ClO}_4)_2$  in liquid DMF did not reveal the presence of any species other than  $\text{VO}(\text{DMF})_5^{2+}$  over the liquid range of DMF.

## 2. $\text{VO}(\text{DMA})_5(\text{ClO}_4)_2$ in DMA

The 60 MHz NMR spectrum of DMA<sup>83</sup> at  $25^\circ\text{C}$  is shown in Fig. IV-6 and the temperature dependence of the linewidths of the solvent resonances is shown in Fig. IV-7. In the  $40$ - $90^\circ\text{C}$  temperature range the resonances corresponding to the N-methyl protons change dramatically. At  $40^\circ\text{C}$  the rotation about the C-N bond in DMA is rapid enough to broaden the individual N-methyl peaks while at  $90^\circ\text{C}$  the two resonances have completely coalesced to a sharp singlet.



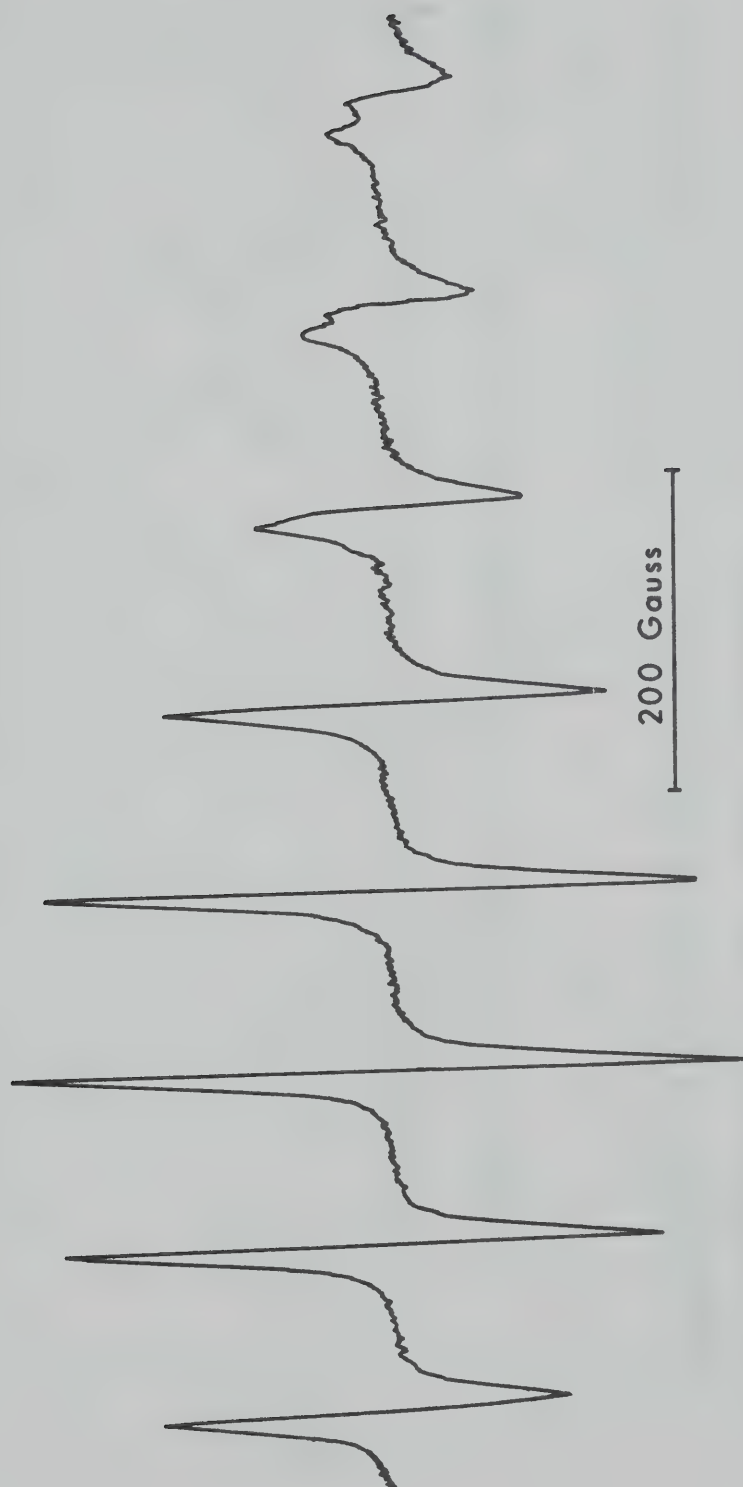


FIGURE IV-5. EPR spectrum of  $5 \times 10^{-3}$  M liquid solution of  $\text{VO}(\text{DMA})_5(\text{ClO}_4)_2$  in DMA at  $120^\circ\text{C}$ .





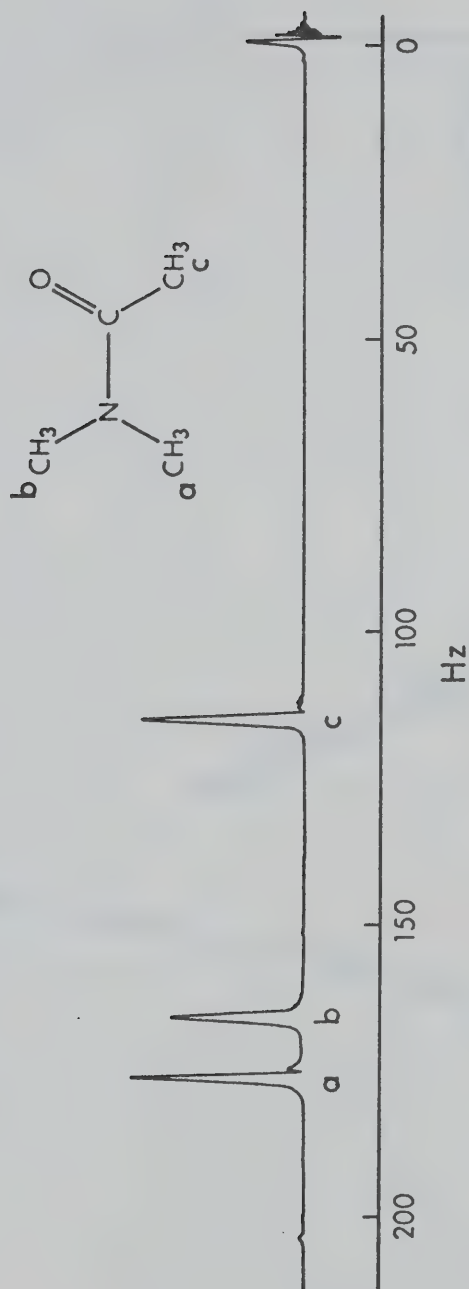


FIGURE III-6. 60 MHz NMR spectrum at 25°C of DMA containing 5% by volume hexamethyldisilane as the internal reference.



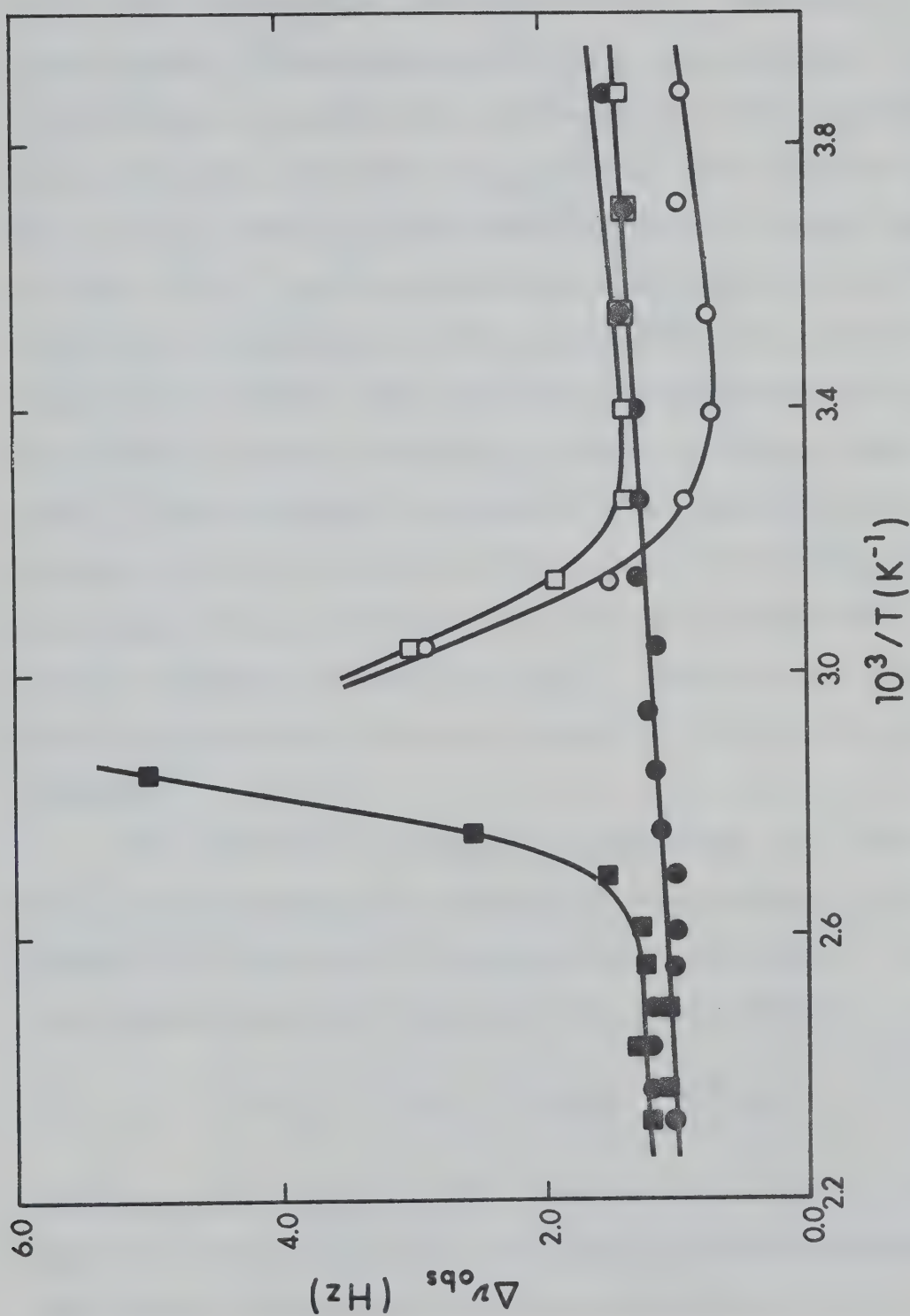


FIGURE IV-7. Temperature dependence of the methyl proton linewidths of DMA. ●, C-CH<sub>3</sub> protons; □, cis-N-methyl protons; ○, trans-N-methyl protons; ■, N-methyl protons for the temperature range in which the two N-methyl proton groups show a single resonance.



This large temperature dependence of  $\Delta\nu_{\text{obs}}$  results in large errors in measurements of  $1/T_{2P}$  and thus data for the N-methyl resonance line broadening in this temperature range were not used for analysis. The observed values of  $1/T_{2P}$  for the three methyl groups of DMA are shown in Fig. IV-8. The curves indicate that two definite limiting cases of equation (IV-25) are realized in different temperature regions: the exchanged controlled region with its negative slope, and the  $T_{2M}$  region at higher temperatures. The activation energies of the exchange controlled regions are similar for all three types of protons, but the values of  $T_{2M}$  for each group are quite different. The slight curvature of the  $1/T_{2P}$  vs  $T^{-1}$  curve at low temperatures is indicative of outer sphere and/or axial ligand exchange.

The exchange reaction which dominates the line broadening is undoubtedly the equatorial ligand-bulk solvent exchange as observed in  $\text{VO}(\text{H}_2\text{O})_5(\text{ClO}_4)_2$  in water. The line broadenings were analyzed using the equation

$$1/T_{2P} = 4/(\tau_{\text{Meq}} + T_{2\text{Meq}}) + n/T_{2\text{Mos}} \quad (\text{IV-33})$$

where  $\tau_{\text{Meq}}$  and  $T_{2\text{Meq}}$  are the lifetime and nuclear relaxation time of a group of protons on a DMA molecule coordinated to the vanadyl ion at one of the four equatorial sites, and  $n/T_{2\text{Mos}}$  represents the contributions due to outer sphere



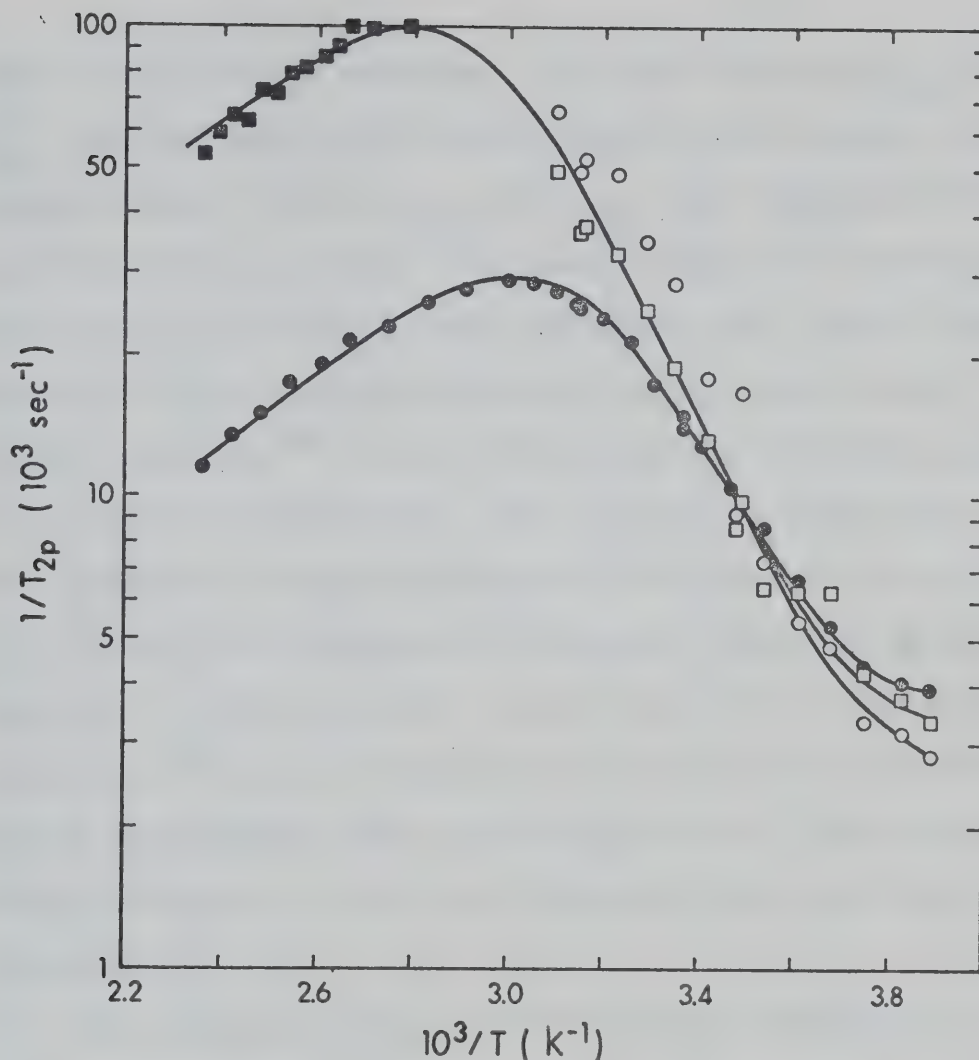


FIGURE IV-8. Temperature dependence of  $1/T_{2p}$  for the methyl protons in DMA solutions of  $\text{VO}(\text{DMA})_5(\text{ClO}_4)_2$ . ●, C- $\text{CH}_3$  protons; □, cis-N-methyl protons; ○, trans-N-methyl protons; ■, N-methyl protons for the temperature range in which the pure solvent spectrum shows a single resonance for the two N-methyl proton groups. The solid lines represent the least squares fits to the experimental points.





and/or axial ligand exchange. In this analysis  $E_{\text{Meq}}$  and  $E_{\text{Mos}}$  (see equation (IV-27)) were taken to be equal, and the preexponential factors  $C_{\text{Meq}}$  and  $C_{\text{Mos}}$  were determined for all three methyl groups. The determination of these parameters and the exchange rate parameters  $\Delta H^\ddagger$  and  $\Delta S^\ddagger$  (see equation (IV-26)) was performed by a non-linear least squares analysis<sup>84</sup> of the  $1/T_{2p}$  data for all three types of protons simultaneously. The parameters which give the best agreement between calculated and observed values of  $1/T_{2p}$  as well as calculated relaxation rates are given in Table IV-3. The criterion for the best fit is the minimization of the sum of squares of the relative residuals between experimental and predicted values. The calculated curves are shown in Fig. IV-8 together with the experimental points.

The chemical exchange rate and the enthalpy and entropy of activation are similar to those observed in the solvent exchange of the vanadyl ion in water<sup>42,43</sup> and in alcohols<sup>48</sup> which supports the assignment to equatorial-bulk solvent exchange. It should be noted that the values of  $T_{2\text{Meq}}^{-1}$  for the N-methyl protons are about four times as large as  $T_{2\text{Meq}}^{-1}$  for the C-methyl protons. The nuclear relaxation rates  $T_{2\text{Meq}}^{-1}$  are due to a dipolar and/or a hyperfine mechanism as detailed in equation (IV-28). If one assumes that the values of  $T_{2\text{Meq}}^{-1}$  for all types of methyl protons in DMA are determined completely by the



TABLE IV-3

Least Square Parameters<sup>†</sup> and Calculated Nuclear Relaxation and Exchange Rates<sup>††</sup> of

DMA Protons in Solutions Containing VO(DMA) <sub>5</sub> (ClO <sub>4</sub> ) <sub>2</sub>					
Protons	E <sub>M</sub> (kcal/mole)	C <sub>Meq</sub> (sec <sup>-1</sup> )	C <sub>Mos</sub> (sec <sup>-1</sup> )	1/T <sub>2Meq</sub> (sec <sup>-1</sup> )	n/T <sub>2Mos</sub> (sec <sup>-1</sup> )
C-CH <sub>3</sub>	3.6 ± .3	3.8 ± 1.6 x 10 <sup>1</sup>	2.3 ± 1.5	1.8 x 10 <sup>4</sup>	1.1 x 10 <sup>3</sup>
cis-N-CH <sub>3</sub>	3.6 ± .3	1.9 ± .7 x 10 <sup>2</sup>	1.9 ± 1.2	8.9 x 10 <sup>4</sup>	9.0 x 10 <sup>2</sup>
trans-N-CH <sub>3</sub>	3.6 ± .3	2.0 ± .7 x 10 <sup>2</sup>	1.5 ± 1.0	9.1 x 10 <sup>4</sup>	6.9 x 10 <sup>2</sup>

Equatorial exchange parameters:

$$\Delta H_{eq}^{\ddagger} = 10.1 \pm .5 \text{ kcal/mole} \quad \Delta S_{eq}^{\ddagger} = -7.9 \pm 1.6 \text{ e.u.} \quad 1/\tau_{Meq} = 4.73 \times 10^3 \text{ sec}^{-1}$$

† Errors quoted are the standard errors obtained from the least squares analysis.

†† Relaxation rates and exchange rates are calculated at 25°C from least squares parameters.



dipolar mechanism, the values of  $r_i$  calculated from  $1/T_{2P}$  and  $\tau_r$  determined from the EPR measurements are  $2.7 \text{ \AA}$  for the C-methyl protons and  $2.0 \text{ \AA}$  for the N-methyl protons.  $r_i$  represents an average distance between nuclear and electronic magnetic dipoles. The value of  $r_i$  for the C-methyl protons is reasonable since DMA is bonded to the vanadium ion by the oxygen. The small values of  $r_i$  calculated for the N-methyl protons are inconsistent with oxygen coordination to the vanadyl ion and the origin of  $T_{2Meq}^{-1}$  for the N-methyl protons cannot be ascribed to dipolar interactions.

The alternative interpretation, that the N-methyl protons are relaxed only by hyperfine interactions, requires some justification since one might expect to observe significant contact shifts<sup>79</sup> and frequency-dependent linewidths<sup>71</sup> in this case. It must be ascertained if the magnitude of the hyperfine interaction is large enough to produce the observed line broadening, but too small to give observable contact shifts and frequency dependent widths. In order to determine the magnitudes of  $A_o^V$  required to give the observed values of  $1/T_{2P}$ , one must estimate  $T_{1e}$  using equation (IV-31). In this expression  $1/T_{1e}$  is a function of  $M_V$  and one calculates  $1/T_{1e}$  for the average of the possible  $M_V$  values. At  $25^\circ\text{C}$ , the average value of  $T_{1e}$  is  $6.5 \times 10^{-8} \text{ sec}$  in a 14.1 kG field. With this value for  $T_{1e}$ , and the observed  $1/T_{2P}$





values for the N-methyl protons, one obtains a value of  $2.4 \times 10^6 \text{ sec}^{-1}$  for the hyperfine splitting constant  $A_o^V$ . The corresponding contact shift of the NMR resonance  $\Delta\omega_M$  can be calculated from equation (IV-32) with the result 590 Hz at 25°C in a 60 MHz NMR experiment. Comparison of this  $\Delta\omega_M$  value with the magnitudes of  $T_{2\text{Meq}}$  and  $\tau_{\text{Meq}}$  under these conditions confirms the insignificance of the  $\Delta\omega_M^2$  terms in equation (IV-20).

The most favorable conditions for the observation of a shift in the NMR resonance will occur at high temperature where  $T_{2\text{Meq}}$  dominates the relaxation. Under these conditions, the observed shift,  $\Delta\omega_{\text{obs}}$ , will be given by

$$\Delta\omega_{\text{obs}} = \frac{4[M]}{[S]} \Delta\omega_M \quad . \quad (\text{IV-34})$$

For a sample containing 0.020 molal  $\text{VO}(\text{DMA})_5(\text{ClO}_4)_2$  in DMA at 130°C, the width of the N-methyl resonance is  $41 \pm 4$  Hz, while  $\Delta\omega_{\text{obs}}$  would be 3.0 Hz since  $\Delta\omega_M = 439$  Hz at 130°C. This shift in the resonance frequency is clearly within the experimental error in determining the centre of a peak 40 Hz wide.

In order to pursue the search for an observable shift, 100 MHz measurements were performed. One would expect a shift of 5.0 Hz for the N-methyl resonances in a 0.020 molal  $\text{VO}(\text{DMA})_5(\text{ClO}_4)_2$  solution at 130°C. The observed shifts were  $4 \pm 2$  Hz for the N-methyl resonance and  $2 \pm 2$  Hz for the C-methyl resonance. These observations





are consistent with the hypothesis that the relaxation of the N-methyl protons is governed by a hyperfine mechanism while the C-methyl protons relax via the dipolar mechanism. They do not preclude the possibility that both mechanisms contribute to the relaxation of all protons, with the major contribution for C-methyl protons being dipolar, and the major contribution for N-methyl protons being hyperfine interactions.

A further point which must be considered, is the frequency dependence of the N-methyl proton resonance line-widths. Since  $1/T_{1e}$  contains terms which depend on the electronic Larmor frequency,  $\omega_0$ , (see equation (IV-31)), a difference in the widths of the N-methyl proton resonances at 60 MHz and 100 MHz is expected if the hyperfine contribution to  $1/T_{2Meq}$  is dominant. At 130°C, the values of  $T_{1e}$ , for  $VO(DMA)_5^{2+}$  in DMA calculated using equation (IV-31) are  $6.5 \times 10^{-8}$  and  $7.1 \times 10^{-8}$  sec at 60 MHz and 100 MHz respectively. One would therefore expect the line-widths at 100 MHz to be 10% broader than those at 60 MHz. Since our estimated errors in the linewidth measurements are at least as large as this, the frequency dependence of the linewidths was not observed.

The least squares analysis of the  $VO(DMA)_5(ClO_4)_2$  line broadening data indicated significant outer sphere contributions at room temperature and below (see Fig. IV-8 and Table IV-3). On the basis of a simple model developed



by Luz and Meiboom<sup>85</sup>, the average distance,  $d_o$ , of closest approach of the solvent molecules, beyond the first coordination sphere, can be estimated from

$$\frac{1}{T_{2Mos}} = \frac{4\pi}{45} \cdot \frac{\rho N[M]}{1000} \cdot \frac{S(S+1) \gamma_I^2 g_o^2 \beta_o^2}{d_o^3} \cdot 7\tau_r \quad (\text{IV-35})$$

where  $\rho$  is the density of the solution,  $N$  is Avogadro's number and the other symbols have been defined earlier. The values for  $d_o$  obtained from the values of  $n/T_{2Mos}$  given in Table IV-3, are 5.4 Å for the C-methyl protons, 5.8 Å for the cis-N-methyl protons and 6.3 Å for the trans-N-methyl protons. These values seem to be smaller than one would expect on the basis of molecular models, but some of the broadening ascribed to outer sphere effects may be due to exchange of solvent molecules with DMA molecules coordinated at the axial position of the vanadyl. If the axial-solvent exchange rate were rapid, the contribution to the linewidth from axial exchange would be  $T_{2Max}^{-1}$ , and it would have a temperature dependence which would be indistinguishable from the outer sphere broadening. This problem will be discussed further after an analysis of the line broadening of DMF by  $VO(DMF)_5(ClO_4)_2$  is presented.

### 3. $VO(DMF)_5(ClO_4)_2$ in DMF

The 60 MHz NMR spectrum of DMF<sup>83,86</sup> at 25°C is shown



in Figure IV-9. The linewidths of the resonances as a function of temperature are given in Fig. IV-10. In the temperature range 100-135°C, internal rotation about the C-N bond has an appreciable affect on the widths and shape of the N-methyl resonances of the solvent. Therefore  $1/T_{2P}$  data in this region was not used in the analysis. The experimental paramagnetic broadenings of the formyl proton and methyl proton resonances are plotted against  $T^{-1}$  in Fig. IV-11. The magnitude and temperature dependence of the line broadening of the methyl resonances is similar to that observed for the N-methyl protons in DMA (see Fig. IV-8), and, at high temperatures, the methyl resonances are broader than the formyl resonance just as the N-methyl resonances of DMA are broader than the C-methyl resonance. The  $T_{2M}$  (high temperature) region in DMF is less well defined than the corresponding region in DMA, but the outer sphere effects in DMF are very clearly defined.

In contrast to the line broadening of the methyl resonances in DMF and those in DMA, the temperature dependence of the broadening of the formyl resonance in DMF is much less pronounced in the region where chemical exchange effects are dominant. Since all bonds in DMF are expected to remain intact when it coordinates with the vanadyl ion, the slopes of the  $\log(1/T_{2P})$  vs  $T^{-1}$  lines in the exchange controlled region should be the same



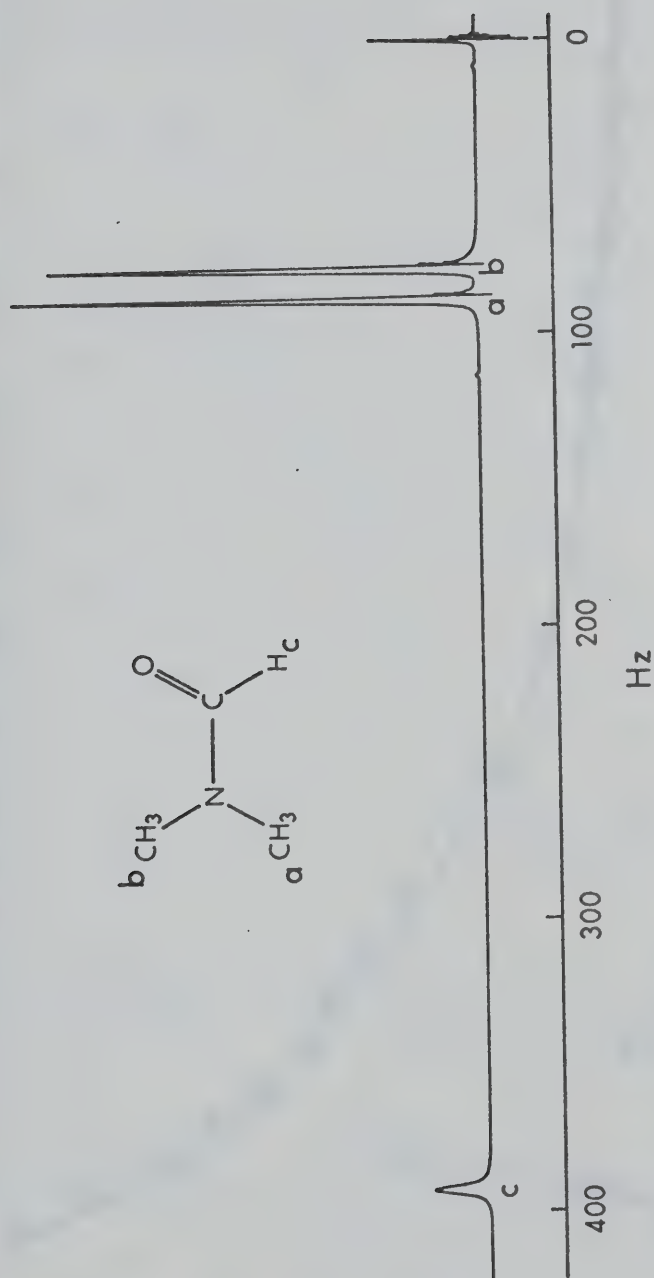


FIGURE IV-9. 60 MHz NMR spectrum at 25°C of DMF containing 5% by volume cyclopentane as the internal reference.





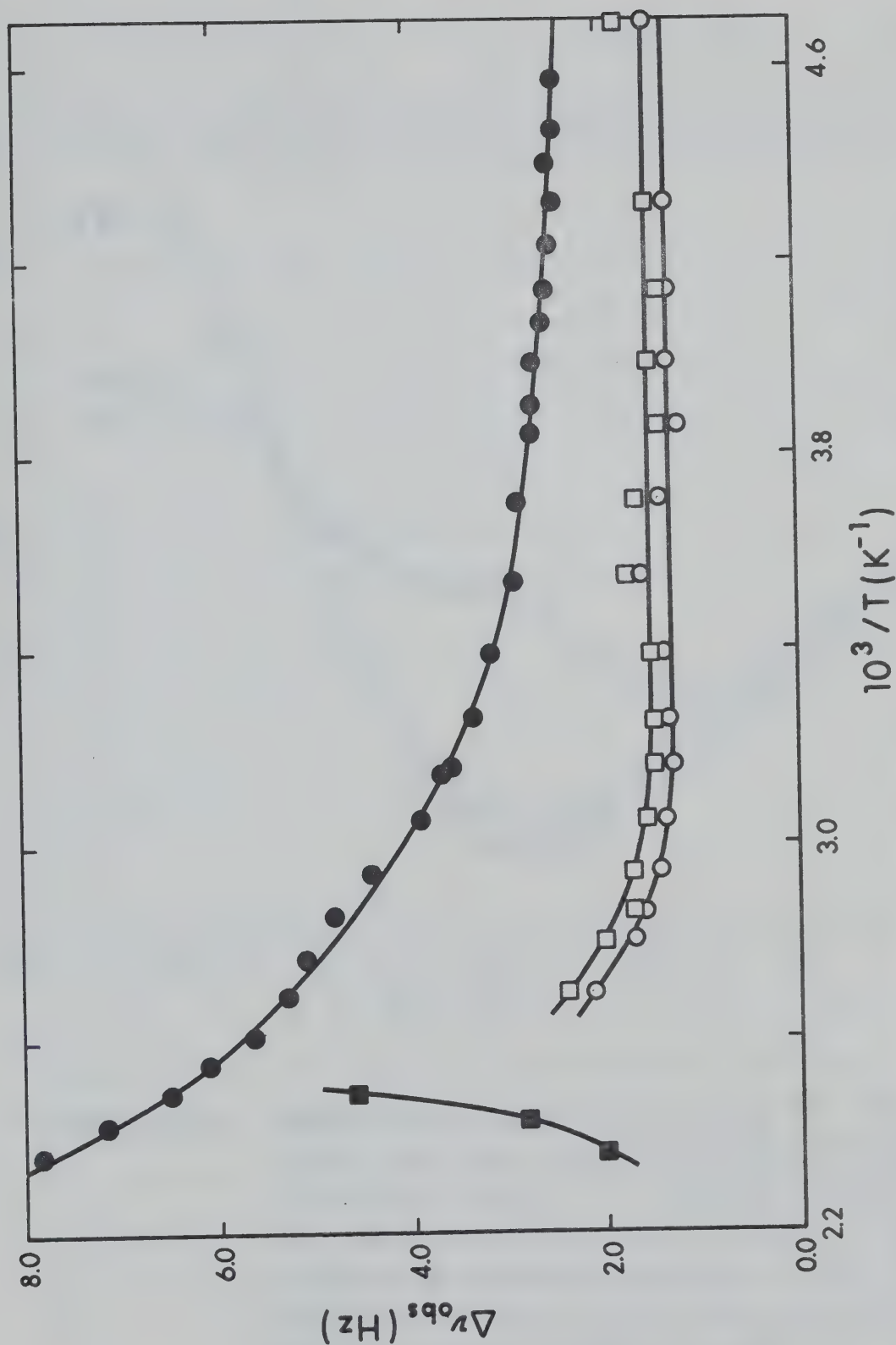


FIGURE IV-10. Temperature dependence of the proton linewidths of DMF. ●, formyl proton; □, cis-N-methyl protons; ○, trans-N-methyl protons; ■, N-methyl protons for the temperature range in which the two N-methyl proton groups show a single resonance.



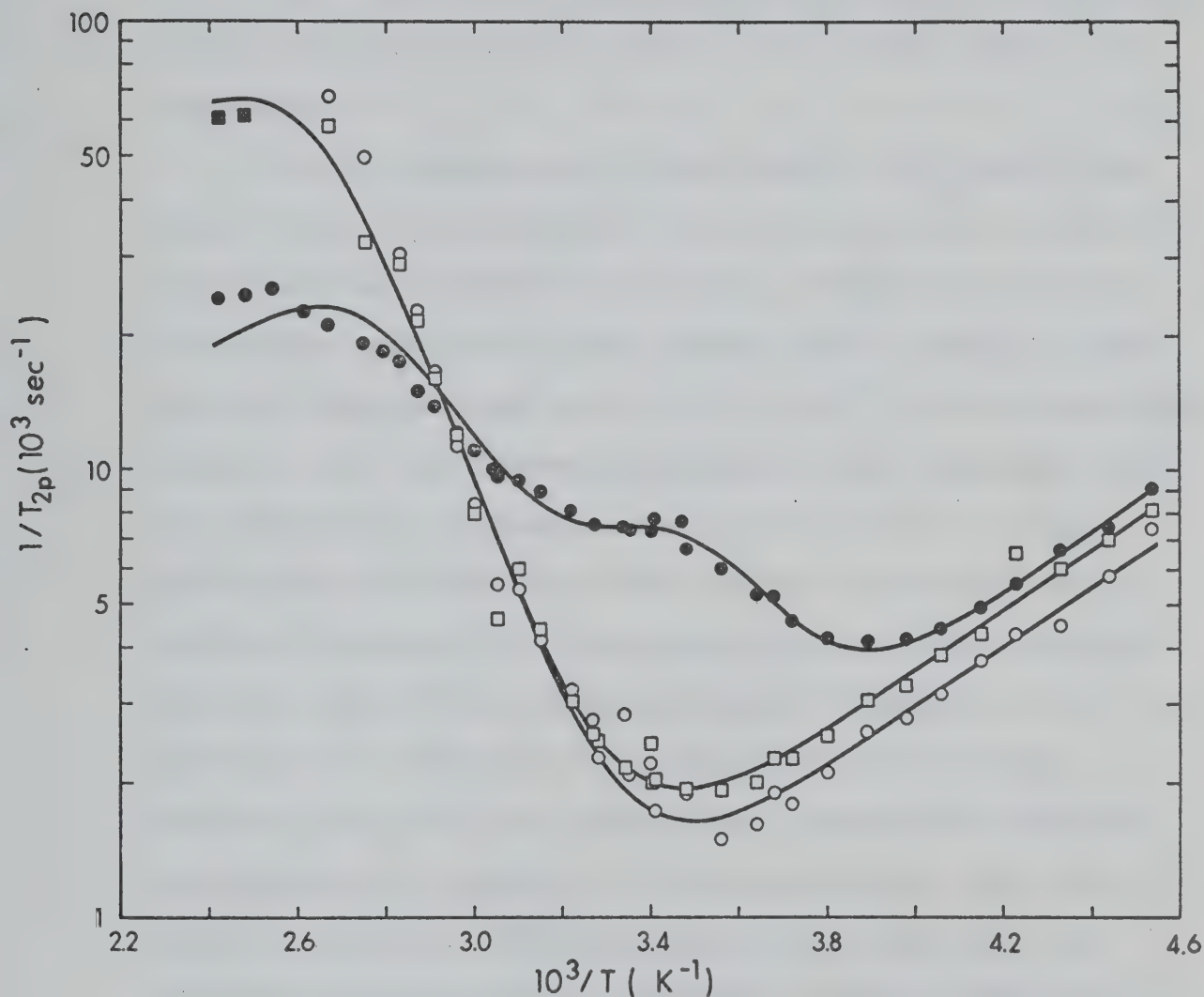


FIGURE IV-11. Temperature dependence of  $1/T_{2P}$  for the formyl and methyl protons in DMF solutions of  $\text{VO}(\text{DMF})_5(\text{ClO}_4)_2$ .  $\bullet$ , formyl proton;  $\square$ , cis-N-methyl protons;  $\circ$ , trans-N-methyl protons;  $\blacksquare$ , N-methyl protons for the temperature range in which the pure solvent spectrum shows a single resonance for the two N-methyl groups. The solid lines represent the least squares fits to the experimental points.



for the formyl resonance and both methyl resonances. Clearly the formyl broadening indicates the presence of an exchange reaction which does not appear in the methyl proton line broadening.

Careful examination of the formyl  $1/T_{2P}$  data indicates that a single straight line does not give a good fit of the exchange-controlled region. Indeed, the results are better described by two linear portions with a leveling off between them near  $10^3/T = 3.4 \text{ K}^{-1}$ . This observation suggests that two exchange processes, with different rates and temperature dependence, are controlling the formyl proton line broadening in this region. One postulates that the broadening of the formyl proton in the low temperature part of the exchange-controlled region is due to exchange of a DMF molecule coordinated at the axial position, and that the rate of this process is different from equatorial exchange and distinguishable from outer sphere broadening. This hypothesis requires that the broadening of the methyl resonances by axial exchange is insignificant, while providing an adequate explanation of the formyl proton broadening.

The unpaired electron in vanadyl complexes is localized in the vanadium  $3d_{x^2-y^2}$  atomic orbital<sup>25,31</sup>, and the unpaired electron density at the protons in an axially coordinated DMF molecule is expected to be very small. One expects, therefore, that the relaxation times,  $T_{2Max}$ ,



of the protons in the axially coordinated molecule will be determined by dipolar interactions between the electron and nuclear moments, not by hyperfine interactions. The dipolar relaxation time for the formyl proton in an axially coordinated DMF molecule is expected to be about 50 times shorter than that of the methyl protons because the interaction distance for the methyl protons is about twice as large as that for the formyl proton and the dipolar line-width varies as the sixth power of the interaction distance (see equation (IV-28)). One expects, therefore, that  $(T_{2\text{Max}})^{-1}$  for the methyl protons is small, but  $(T_{2\text{Max}})^{-1}$  for the formyl proton is comparable in magnitude to  $\tau_{\text{Meq}}^{-1}$  in the low temperature portion of the exchange-controlled region. Since the line broadenings of the methyl resonances in the exchange-controlled region show no significant deviation from a single straight line, it was assumed that  $(T_{2\text{Max}})^{-1}$  for the methyl protons is negligible compared to either  $(\tau_{\text{Meq}})^{-1}$  or  $T_{2\text{Meq}}^{-1}$ .

The line broadening data was analyzed by a least squares method in terms of the model postulated above which describes the formyl proton widths as arising from the exchange between bulk solvent and three distinct coordination sites (axial, equatorial and outer sphere), and the methyl proton broadening arising from exchange between solvent and two distinct sites (equatorial and outer sphere). The  $1/T_{2p}$  data for both methyl resonances







was analyzed first in order to determine  $\Delta H_{eq}^\ddagger$ ,  $\Delta S_{eq}^\ddagger$ ,  $E_M$  and the preexponential factors  $C_{Meq}$  and  $C_{Mos}$  for each methyl group. Next, the formyl line broadening data was fit holding  $\Delta H_{eq}^\ddagger$ ,  $\Delta S_{eq}^\ddagger$  and  $E_M$  constant at the values determined from the analysis of the methyl proton data, and the parameters  $\Delta H_{ax}^\ddagger$ ,  $\Delta S_{ax}^\ddagger$ ,  $C_{Max}$ ,  $C_{Meq}$  and  $C_{Mos}$  for the formyl protons were varied until convergence of the least squares procedure was achieved. The solid curves in Fig. IV-11 are calculated using the parameters obtained from these least squares analyses. The parameters and calculated relaxation rates are given in Table IV-4.

The relaxation rates for the methyl protons in DMF at high temperatures are considerably higher than that for the formyl proton. If one assumes that  $T_{2M}^{-1}$  for all types of protons is dominated by dipolar interactions, interaction distances of 2.6, 3.2 and 2.0 Å for equatorial formyl protons, axial formyl protons and equatorial methyl protons respectively are obtained. Arguments analogous to those given in the analysis of  $T_{2Meq}$  for the N-methyl protons in DMA lead to the conclusion that the methyl protons in DMF are relaxed predominantly by hyperfine interactions modulated by the relaxation of the unpaired electron of the Vanadyl complex, while dipolar interactions modulated by molecular tumbling account satisfactorily for the magnitudes of  $(T_{2Meq})^{-1}$  and  $(T_{2Max})^{-1}$  for the formyl protons.



TABLE IV-4

Least Squares Parameters<sup>†</sup> and Calculated Nuclear Relaxation and Exchange Rates<sup>††</sup> of DMF

Protons in Solutions Containing VO(DMF) <sub>5</sub> (ClO <sub>4</sub> ) <sub>2</sub>					
Protons	C <sub>M</sub> (sec <sup>-1</sup> )	C <sub>Mos</sub> (sec <sup>-1</sup> )	E <sub>M</sub> (kcal/mole)	1/T <sub>2M</sub> (sec <sup>-1</sup> )	n/T <sub>2Mos</sub> (sec <sup>-1</sup> )
axial C-H	3.5 ± .2 x 10 <sup>1</sup>	-	3.0 ± .2	5.8 x 10 <sup>3</sup>	-
equatorial C-H	1.1 ± .1 x 10 <sup>2</sup>	8.7 ± .3	3.0 ± .2	1.9 x 10 <sup>4</sup>	1.5 x 10 <sup>3</sup>
equatorial cis N-CH <sub>3</sub>	4.3 ± .9 x 10 <sup>2</sup>	7.9 ± 2.8	3.0 ± .2	7.2 x 10 <sup>4</sup>	1.3 x 10 <sup>3</sup>
equatorial trans N-CH <sub>3</sub>	4.6 ± 1.0 x 10 <sup>2</sup>	6.5 ± 2.3	3.0 ± .2	7.8 x 10 <sup>4</sup>	1.1 x 10 <sup>3</sup>

Equatorial and axial exchange parameters:

$$\Delta H_{eq}^{\dagger} = 13.1 \pm .6 \text{ kcal/mole} \quad \Delta S_{eq}^{\dagger} = -4.1 \pm 1.8 \text{ e.u.} \quad 1/\tau_{Meq} = 2.0 \times 10^2 \text{ sec}^{-1}$$

$$\Delta H_{ax}^{\dagger} = 15.3 \pm 2.5 \text{ kcal/mole} \quad \Delta S_{ax}^{\dagger} = 13.9 \pm 9.0 \text{ e.u.} \quad 1/\tau_{Max} = 4.6 \times 10^4 \text{ sec}^{-1}$$

<sup>†</sup> Errors quoted are the standard errors given by the least squares analysis.<sup>††</sup> Relaxation rates and exchange rates are calculated at 25°C from least squares parameters.



The interaction distance between the unpaired electron and the formyl proton in axial coordination is significantly larger than the interaction distance for the formyl proton in equatorial coordination. This is in agreement with the weaker bond between the axial ligand and the vanadium atom, and is supported by crystallographic studies of other 6-coordinate vanadyl complexes.<sup>6</sup>

The interaction distance between the unpaired electron and the methyl protons of an axially-coordinated DMF molecule will be at least  $5 \text{ \AA}$  if the interaction distance for the formyl proton in axial coordination is  $3.2 \text{ \AA}$ . The relaxation rate  $(T_{2\text{Max}})^{-1}$  for methyl protons is therefore insignificant ( $410 \text{ sec}^{-1}$  at  $25^\circ\text{C}$ ) compared with  $(T_{2\text{Meq}})^{-1}$  or  $(\tau_{\text{Meq}})^{-1}$ . As indicated above, no hyperfine contribution to the methyl  $(T_{2\text{Max}})^{-1}$  is expected since the unpaired electron density is very small at the axial methyl protons. The neglect of broadening of methyl resonance by axial exchange was therefore justified.

The hyperfine interaction for the equatorial methyl protons must be  $2.0 \times 10^6 \text{ sec}^{-1}$  if  $(T_{2\text{Meq}})^{-1}$  is determined only by hyperfine interactions. This interaction is slightly smaller than the value determined for the N-methyl protons of DMA, and arguments, analogous to those presented previously for the DMA N-methyl data, can be given to account for the unobservability of frequency shifts or frequency-dependent line broadening.





The outer sphere interaction distances for the protons in DMF were calculated using Luz and Meiboom's theory<sup>85</sup> and the values of  $n/T_{2\text{Mos}}$  given in Table IV-4. The distances are 5.2, 5.4 and 5.8 Å respectively for the formyl, cis-methyl and trans-methyl protons. These values are smaller than those determined above for DMA molecules in the second coordination sphere of  $\text{VO}(\text{DMA})_5^{2+}$ , and the effects of axial exchange have been included explicitly here. It would appear that the outer sphere interaction distances obtained from  $n/T_{2\text{Mos}}$  are smaller than one would expect on the basis of molecular models and that this is due to the naivety of the model for outer sphere interactions, not the neglect of the axial exchange process. The observation that the  $n/T_{2\text{Mos}}$  values are approximately equal for all three types of protons suggests the molecular arrangement in the second coordination sphere is not highly structured. Then orientations of the amides may be such that on the average the methyl protons are nearly as close as the formyl proton to the vanadyl ion. Another possibility is that outer sphere relaxation results from a hyperfine interaction which may be more effective for the methyl protons than the formyl protons.

#### 4. Bis-(o-phenanthroline)-oxo-vanadium(IV) Perchlorate in DMF

The results presented in the previous section indicate





that the effect of axial exchange on the solvent line broadening could be separated from the effects of equatorial exchange in certain circumstances. A simple chemical method of accomplishing this separation is to choose a system where the equatorial sites are blocked and only the axial site can accept the solvent molecules. Furthermore, the species should have a formal charge of +2 for a meaningful comparison of the results with the vanadyl ion studies in sections 2 and 3. The neutral bidentate ligand, o-phenanthroline, is believed to coordinate at the equatorial positions of the vanadyl ion and the resulting complex has a +2 charge.<sup>50</sup> Solvent line broadening studies of DMF solutions of the bis-(o-phenanthroline)-oxovanadium(IV) complex were performed and the results are shown in Fig. IV-12. The  $1/T_{2p}$  data indicate an exchange controlled region above 60°C, but the EPR spectrum at the same temperature, shown in Fig. IV-13, indicates the presence of two species in solution. Presumably, the o-phenanthroline ligand is being replaced by DMF at the equatorial position in the first coordination sphere above 60°C. The exchange of these DMF molecules can then contribute to  $1/T_{2p}$ . Calculations showed that the  $1/T_{2p}$  values given in Fig. III-12 are compatible with 10% conversion of the bis-(o-phenanthroline)-oxovanadium(IV) to  $\text{VO}(\text{DMF})_5^{2+}$ . The lower values of  $1/T_{2p}$  observed in the outer sphere  $T_{2M}$  region for bis-(o-phenanthroline)-oxo-



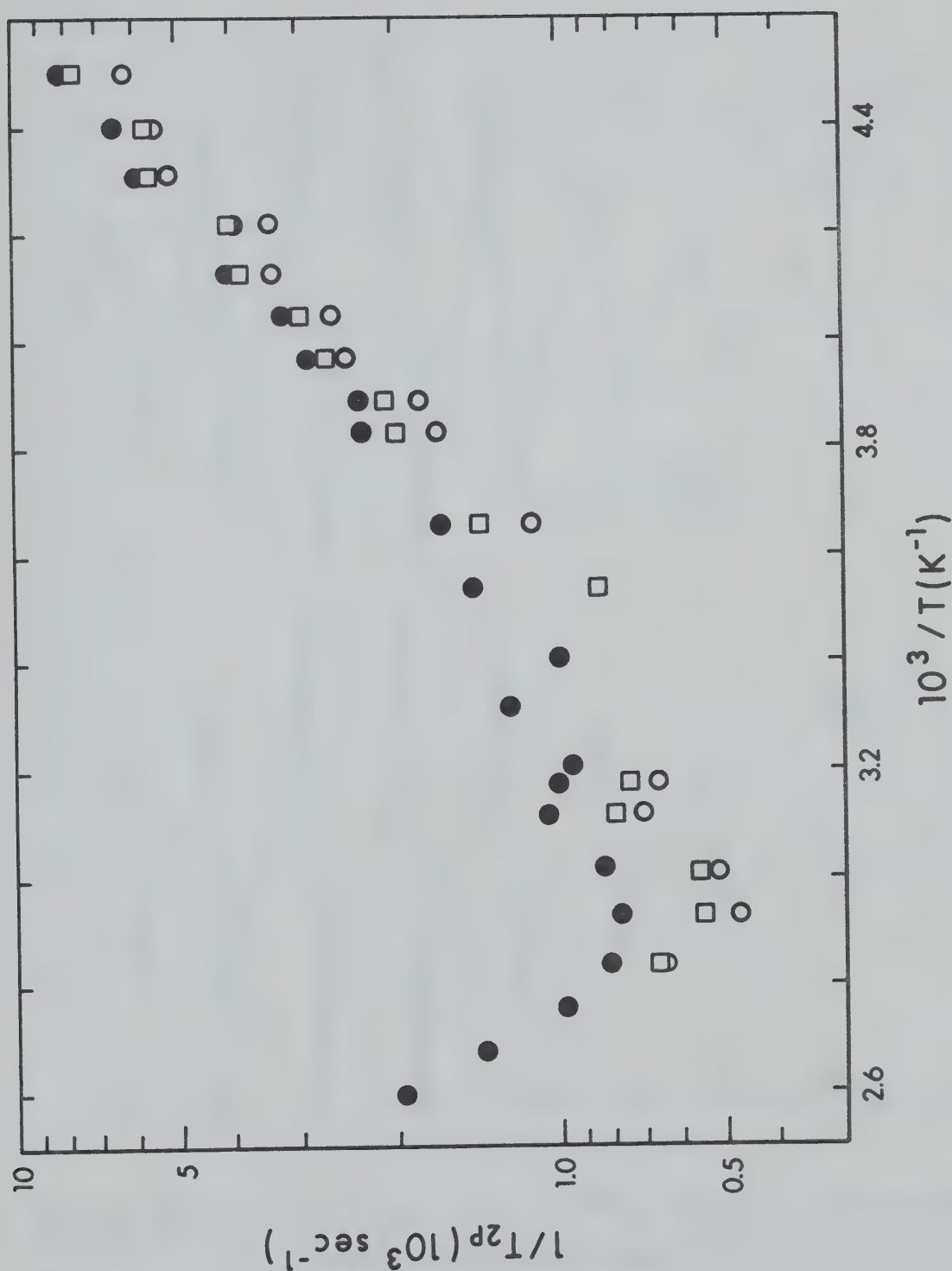


FIGURE IV-12. Temperature dependence of  $1/T_{2p}$  for the formyl and methyl protons in DMF solutions of bis-(o-phenanthroline)-oxo-vanadium(IV) perchlorate. ●, formyl proton; □, cis-N-methyl protons; ○, trans-N-methyl protons.



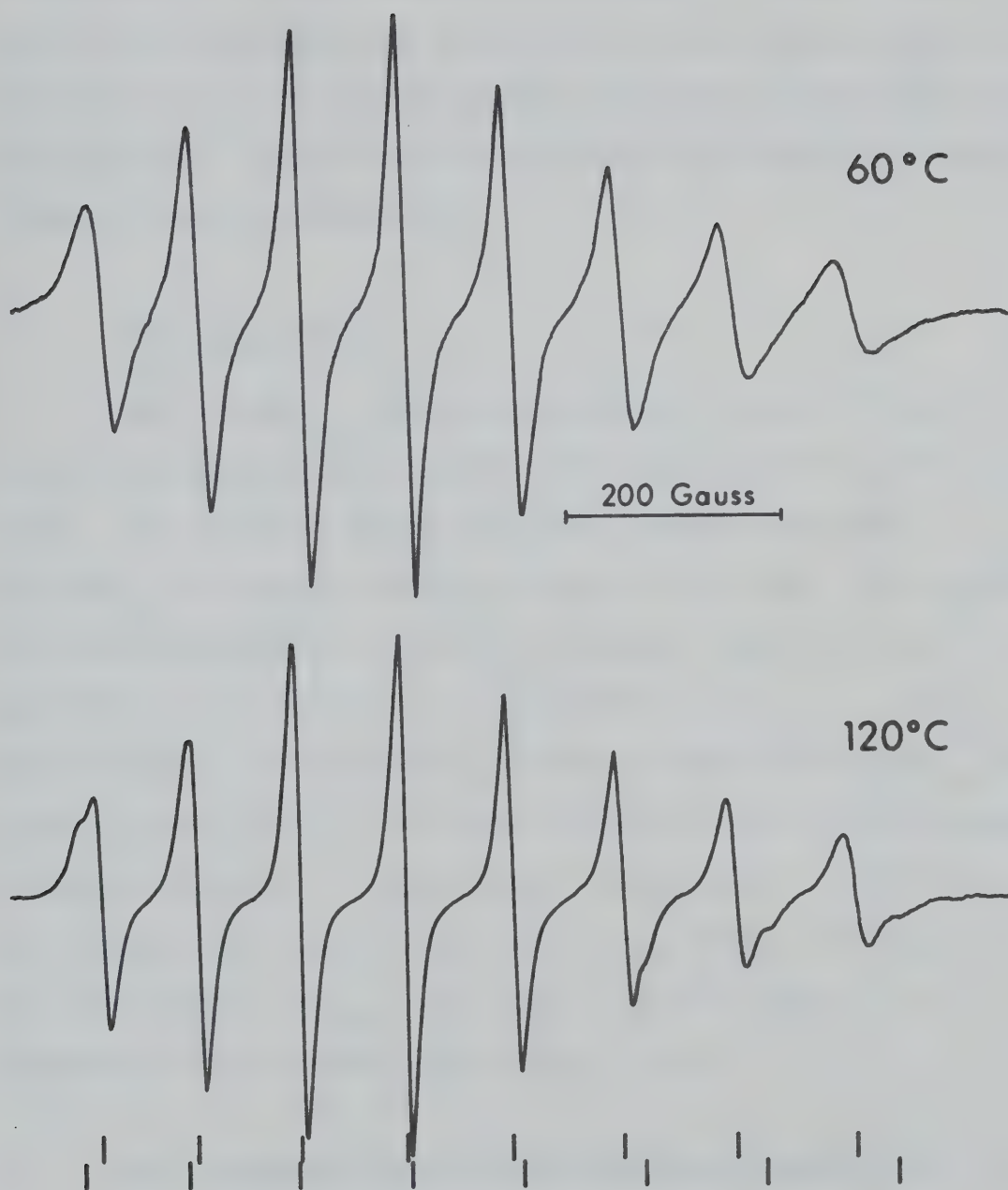


FIGURE IV-13. EPR spectra of  $10^{-2}$  M liquid solutions of bis-(o-phenanthroline)-oxo-vanadium(IV) perchlorate in DMF at 60°C and 120°C. The stick spectra for the two vanadyl species at 120°C are given at the bottom of the figure.



vanadium(IV) in DMF compared to  $\text{VO}(\text{DMF})_5^{2+}$  in DMF (see Fig. IV-11) reflect the bulkiness of the o-phenanthroline ligands; i.e., the outer sphere interaction distances are considerably larger for bis-(o-phenanthroline)-oxo-vanadium(IV) than for  $\text{VO}(\text{DMF})_5^{2+}$ .

#### 5. $\text{VO}(\text{acac})_2$ in DMF

The  $\text{VO}(\text{acac})_2$  complex is another system in which only one position is available for coordination by the solvent. In contrast to the systems already described  $\text{VO}(\text{acac})_2$  is neutral and one expects the rates of exchange of electron donating solvent molecules from the axial position to be faster than in  $\text{VO}(\text{DMF})_5(\text{ClO}_4)_2$ .<sup>47</sup> The NMR solvent line broadening of DMF caused by  $\text{VO}(\text{acac})_2$  is shown in Fig. IV-14 and shows no indication of an exchange controlled region. Apparently, the exchange is too fast to control the  $1/T_{2p}$  values. The  $1/T_{2p}$  values are described by the equation  $1/T_{2p} = 4.5 \exp (1,800/T)$  which is the equation of the solid line in Fig. IV-14.

#### 6. Bis-(diphenyldithiophosphinato)-oxo-vanadium(IV) in DMF, DMA and DEF.

The NMR line broadening of DMF, DMA and DEF by the vanadyl dithiophosphate was investigated to gain more information about the nature of the vanadyl species in solutions containing the dithiophosphinates and Lewis





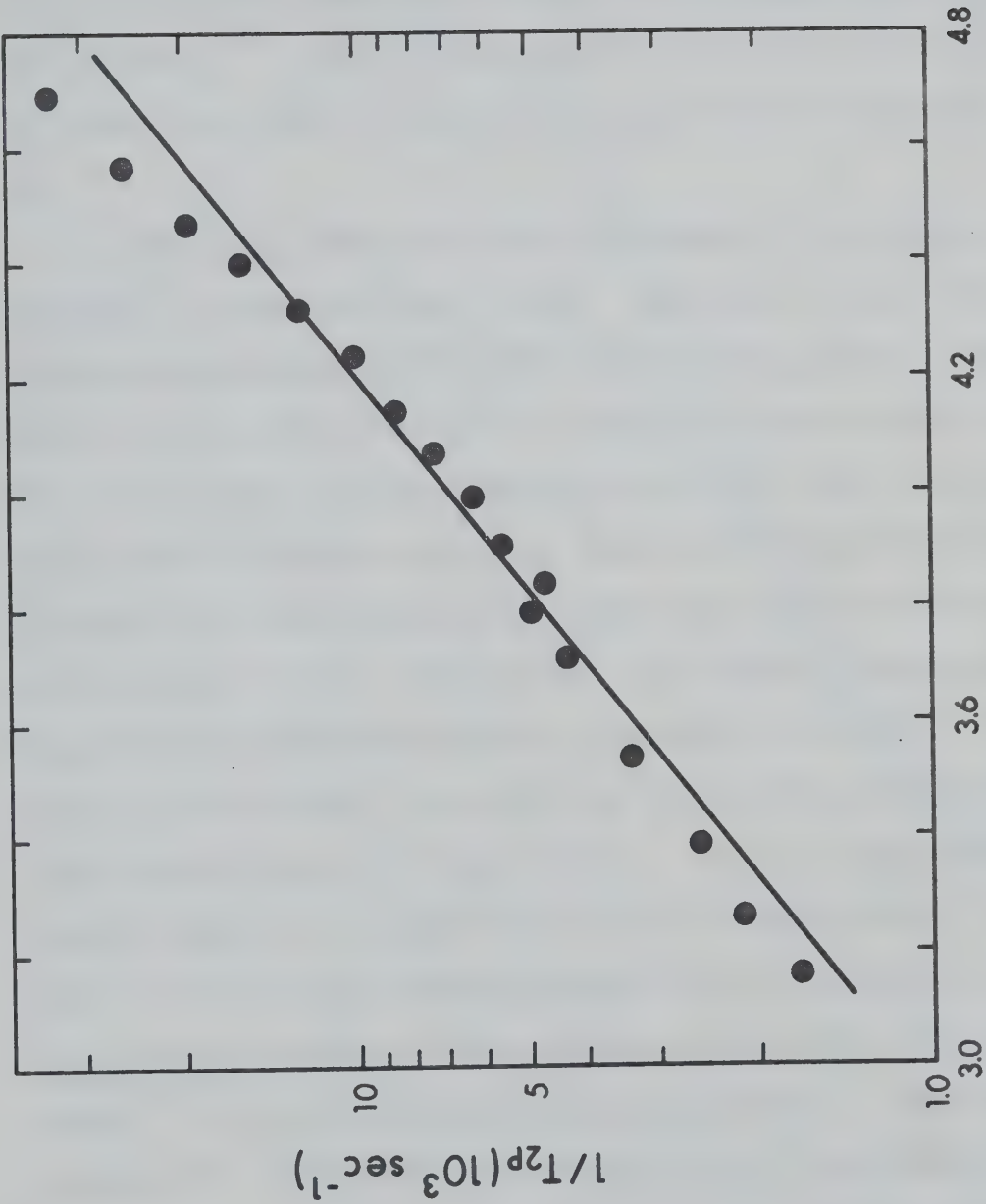


FIGURE IV-14. Temperature dependence of  $1/T_{2p}$  for the formyl protons in DMF solutions of  $\text{VO}(\text{acac})_2$ . The solid line represents the least squares fit to the experimental points.



bases. Complete replacement of the dithiophosphinate groups in the first coordination sphere by the solvent molecules DMF or DMA would result in the species  $\text{VO}(\text{DMF})_5^{2+}$  and  $\text{VO}(\text{DMA})_5^{2+}$ . The line broadening for the perchlorates of these ions have already been presented in section 2 and 3.

The  $1/T_{2P}$  data for DMA solutions of the phenyl complex is shown in Fig. IV-15. The plot of this data is almost superimposable on that for  $\text{VO}(\text{DMA})_5(\text{ClO}_4)_2$  in DMA shown in Fig. IV-8 except for the high temperature region. The equivalent line broadening results for the two systems below  $100^\circ\text{C}$  indicate that the diphenyldithiophosphinate chelates are completely displaced from the first coordination sphere of the vanadyl ion. At higher temperatures, the diphenyldithiophosphinate presumably becomes coordinated to the vanadyl ion and this effectively reduces the line broadening in the  $T_{2M}$  region. This is supported by the EPR spectrum of the DMA solution of the phenyl complex at  $145^\circ\text{C}$  which shows patterns of low intensity that arise from coupling of the electron spin with other nuclei, namely  $^{31}\text{P}$  of the diphenyldithiophosphinate. The least squares fit of the dithiophosphinate line broadening data to the model proposed in section 2 for the vanadyl perchlorates in DMA gave the parameters given in Table IV-5a. The least squares curves are shown in Fig. IV-15 together with the experimental data. A comparison of the parameters



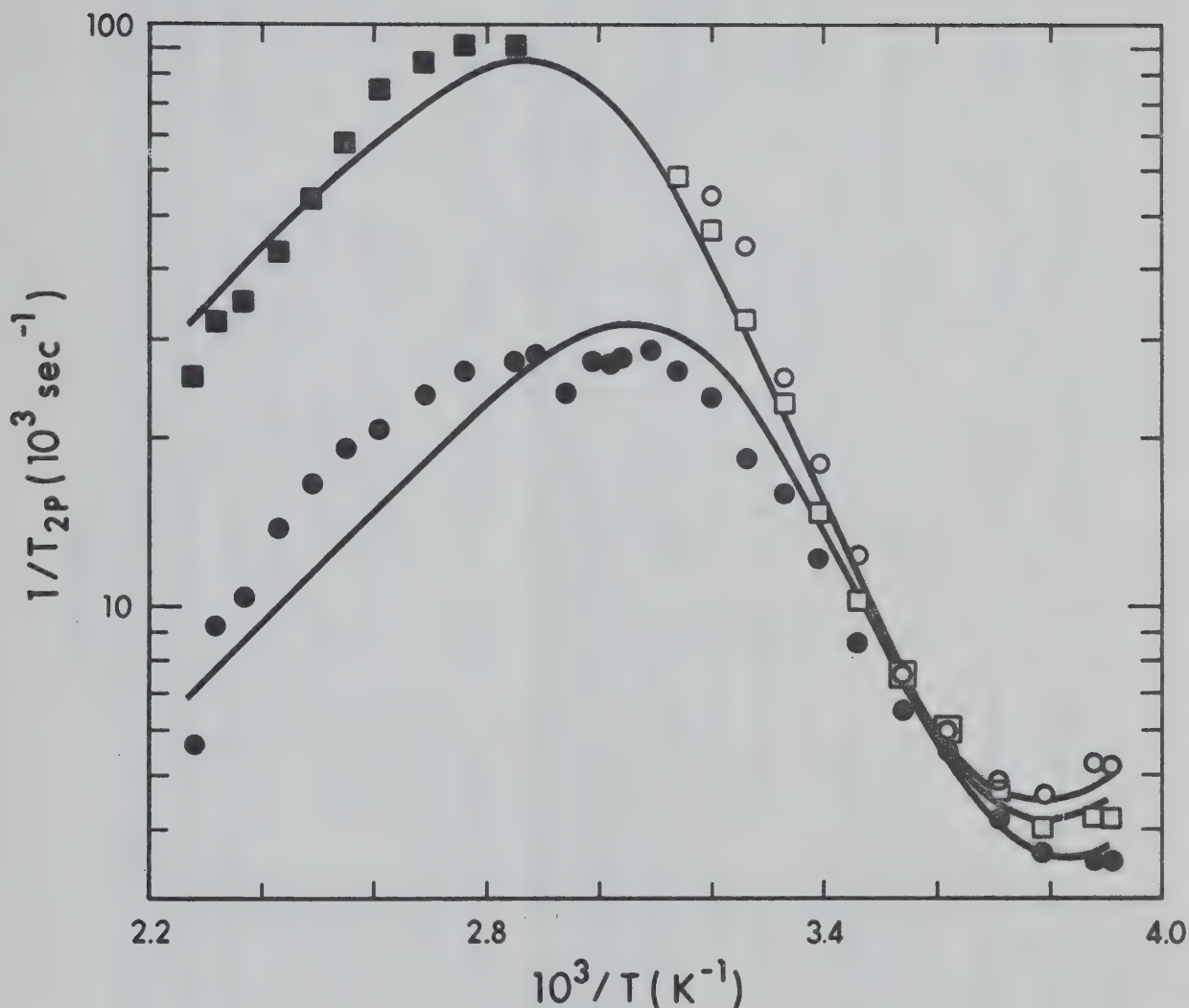


FIGURE IV-15. Temperature dependence of  $1/T_{2P}$  for the methyl protons in DMA solutions of bis-(diphenyldithio-phosphinato)-oxo-vanadium(IV). ●, C-CH<sub>3</sub> protons; □, cis-N-methyl protons; ○, trans-N-methyl protons; ■, N-methyl protons for the temperature range in which the pure solvent spectrum shows a single resonance line for the two N-methyl proton groups. The solid lines represent the least squares fits to the experimental points.



TABLE IV-5

a. Least Squares Parameters<sup>†</sup> and Calculated Nuclear Relaxation and Exchange Rates<sup>††</sup> of DMA Protons in Solutions Containing Bis-(diphenyldithiophosphinato)-oxo-vanadium(IV)

Protons	$E_M$ (kcal/mole)	$C_{Meq}$ (sec <sup>-1</sup> )	$C_{Mos}$ (sec <sup>-1</sup> )	$1/T_{2Meq}$ (sec <sup>-1</sup> )	$n/T_{2Mos}$ (sec <sup>-1</sup> )
C-CH <sub>3</sub>	4.7 ± .3	8.3 ± 3.5	4.5 ± 3.0 × 10 <sup>-1</sup>	2.2 × 10 <sup>4</sup>	1.2 × 10 <sup>3</sup>
cis-N-CH <sub>3</sub>	4.7 ± .3	3.8 ± 1.5 × 10 <sup>1</sup>	4.1 ± 2.7 × 10 <sup>-1</sup>	1.0 × 10 <sup>5</sup>	1.1 × 10 <sup>3</sup>
trans-N-CH <sub>3</sub>	4.7 ± .3	3.9 ± 1.5 × 10 <sup>1</sup>	3.3 ± 2.2 × 10 <sup>-1</sup>	1.0 × 10 <sup>5</sup>	8.6 × 10 <sup>2</sup>

Equatorial exchange parameters:

$$\Delta H_{eq}^{\dagger} = 11.7 \pm .9 \text{ kcal/mole} \quad \Delta S_{eq}^{\dagger} = -2.5 \pm 3.2 \text{ e.u.} \quad 1/\tau_{Meq} = 4.7 \times 10^3 \text{ sec}^{-1}$$

b. Least Squares Parameters<sup>†</sup> and Calculated Nuclear Relaxation and Exchange Rates<sup>††</sup> of DMA Protons in Solutions Containing Bis-(diphenyldithiophosphinato)-oxo-vanadium(IV) for Data at Temperatures Below 10<sup>3</sup>/T = 2.4 K<sup>-1</sup>

Protons	$E_M$ (kcal/mole)	$C_{Meq}$ (sec <sup>-1</sup> )	$C_{Mos}$ (sec <sup>-1</sup> )	$1/T_{2Meq}$ (sec <sup>-1</sup> )	$n/T_{2Mos}$ (sec <sup>-1</sup> )
C-CH <sub>3</sub>	3.1 ± .4	7.1 ± 3.6 × 10 <sup>1</sup>	9.6 ± 7.0	1.4 × 10 <sup>4</sup>	1.9 × 10 <sup>3</sup>
cis-N-CH <sub>3</sub>	3.1 ± .4	3.0 ± 1.4 × 10 <sup>2</sup>	8.8 ± 6.5	5.9 × 10 <sup>4</sup>	1.7 × 10 <sup>3</sup>
trans-N-CH <sub>3</sub>	3.1 ± .4	3.1 ± 1.4 × 10 <sup>2</sup>	7.4 ± 5.4	6.0 × 10 <sup>4</sup>	1.4 × 10 <sup>3</sup>

Equatorial exchange parameters

$$\Delta H_{eq}^{\dagger} = 13.5 \pm .9 \text{ kcal/mole} \quad \Delta S_{eq}^{\dagger} = 3.7 \pm 3.2 \text{ e.u.} \quad 1/\tau_{Meq} = 4.7 \times 10^3 \text{ sec}^{-1}$$

† Errors quoted are the standard errors obtained from the least squares analysis.

†† Relaxation rates and exchange rates are calculated at 25°C from least squares parameters.





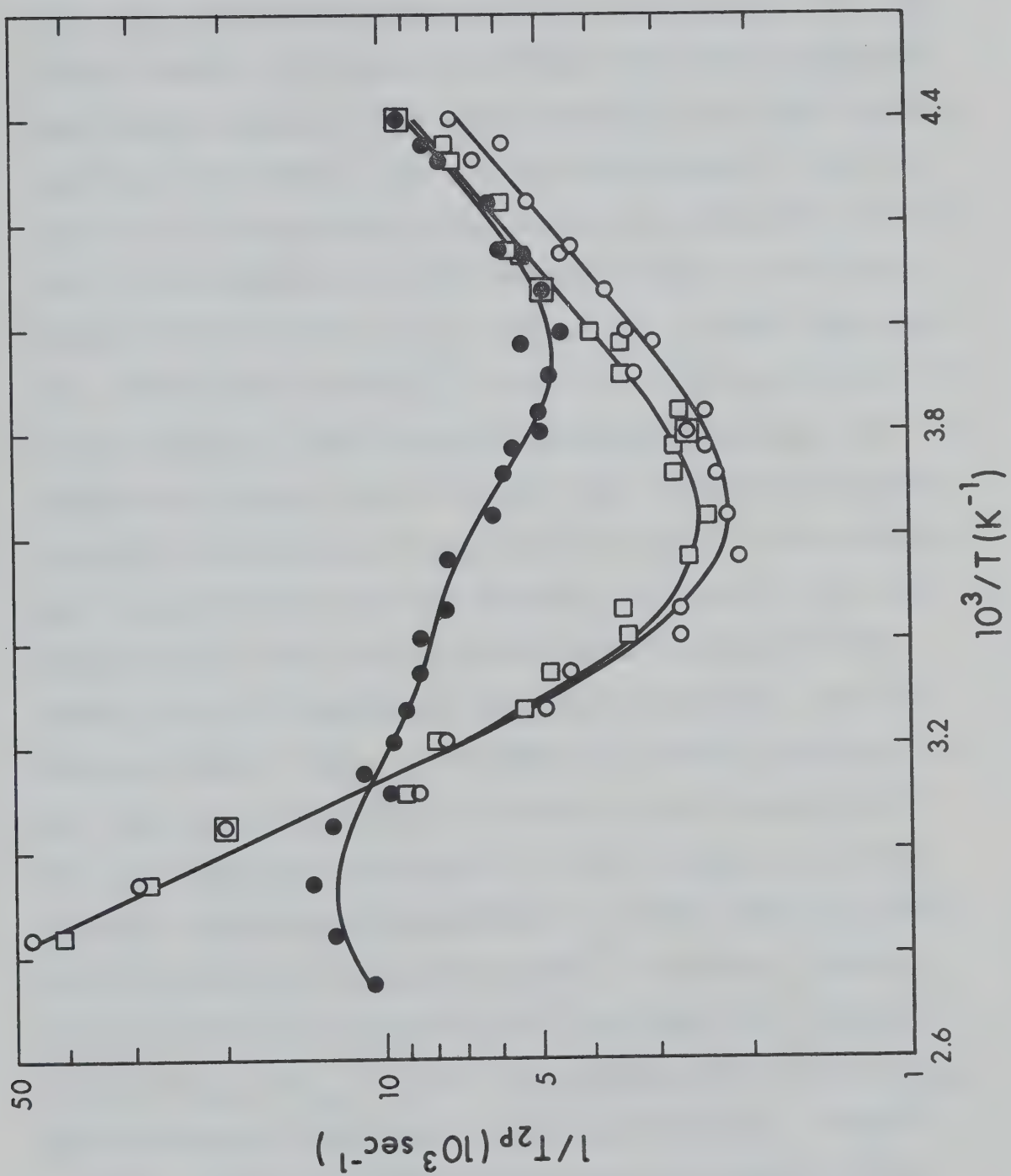
in Table IV-5a with the corresponding parameters for the  $\text{VO}(\text{DMA})_5(\text{ClO}_4)_2$  system given in Table IV-3, indicates that the parameters for the two systems are equal if one considers the error limits for the parameters to be twice the standard errors. The larger value of  $E_M$  for the dithiophosphate system compared to the perchlorate system reflects the difference between the systems in the high temperature  $T_{2M}$  region. If one considers the  $1/T_{2P}$  data in Fig. IV-15 for temperatures below  $10^3/T = 2.4 \text{ K}^{-1}$  only, then the value of  $E_M$  is decreased from 4.7 to 3.1 kcal/mole. The parameters determined from the least squares analysis for the data below  $10^3/T = 2.4 \text{ K}^{-1}$  are shown in Table IV-5b and are in good agreement with the parameters for  $\text{VO}(\text{DMA})_5(\text{ClO}_4)_2$  in Table IV-3.

Fig. IV-16 shows the  $1/T_{2P}$  data for DMF solutions containing bis-(diphenyldithiophosphinato)-oxo-vanadium (IV). The measured line broadenings above  $100^\circ\text{C}$  were found to vary with the length of time a sample remained at these elevated temperatures, and therefore are not considered in the following analysis. A comparison of the data in Fig. IV-16 with the corresponding data for  $\text{VO}(\text{DMF})_5(\text{ClO}_4)_2$  in DMF shown in Fig. IV-11 shows that the  $1/T_{2P}$  values, for both the formyl and N-methyl protons, at a given temperature in the exchange controlled region are significantly larger for the phenyl complex than for  $\text{VO}(\text{DMF})_5(\text{ClO}_4)_2$ . This result indicates that the diphenyl-



The first part of the paper is devoted to a study of the  
 properties of the function  $f(x)$  which is defined by the  
 equation  $f(x) = \int_0^x f(t) dt$ . It is shown that this  
 function is continuous and differentiable, and that its  
 derivative is equal to  $f(x)$ . The second part of the  
 paper is devoted to a study of the properties of the  
 function  $g(x)$  which is defined by the equation  
 $g(x) = \int_0^x g(t) dt$ . It is shown that this  
 function is continuous and differentiable, and that its  
 derivative is equal to  $g(x)$ .

FIGURE IV-16. Temperature dependence of  $1/T_{2p}$  for the formyl and methyl protons in DMF solutions of bis-(diphenyldithiophosphinato)-oxo-vanadium(IV). ●, formyl proton; □, cis-N-methyl protons; ○, trans-N-methyl protons. The solid lines represent the least squares fits to the experimental points.





dithiophosphate ligand is not completely displaced from the first coordination sphere of the vanadyl ion when the phenyl complex is dissolved in DMF. The EPR spectrum of the phenyl complex in DMF shows broader lines than the EPR spectrum of  $\text{VO}(\text{DMF})_5^{2+}$  at a given temperature as can be seen from a comparison of the linewidth parameters in Table IV-1. This suggests that the complex formed in DMF solutions containing the phenyl complex has a larger hydrodynamic radius than  $\text{VO}(\text{DMF})_5^{2+}$ . Also, the EPR spectrum of the phenyl complex in DMF shows no hyperfine coupling with the phosphorus nucleus which suggests the diphenyldithiophosphate coordinates as a monodentate ligand. Furthermore, the conductance of the DMF solution is linear in the concentration of the phenyl complex which indicates that there exists a dissociated species in solution. These results require that the predominant vanadyl species in a DMF solution of the phenyl complex at room temperature has one equatorial coordination site occupied by a monodentate diphenyldithiophosphate and the remaining coordination positions occupied by DMF. The methyl proton broadening data was then fit to this model and the parameters  $\Delta H_{\text{eq}}^\ddagger$ ,  $\Delta S_{\text{eq}}^\ddagger$ ,  $E_M$  and the preexponential factor  $C_{\text{Mos}}$  were determined for each of the methyl groups. Values of  $C_{\text{Meq}}$  were not determined since the  $T_{2M}$  region is not defined by the data for the methyl protons in Fig. IV-16. Next the formyl proton data was fit holding  $\Delta H_{\text{eq}}^\ddagger$ ,  $\Delta S_{\text{eq}}^\ddagger$





and  $E_M$  constant at the values obtained from the methyl data and varying the axial parameters as was done for the case of  $\text{VO}(\text{DMF})_5(\text{ClO}_4)_2$ . The parameters and calculated relaxation rates are shown in Table IV-6. A comparison of the parameters in Table IV-6 with those for  $\text{VO}(\text{DMF})_5(\text{ClO}_4)_2$  in Table IV-4 indicates that the rate of equatorial exchange is five times faster in the dithiophosphinate system.

The line broadening in DEF by the phenyl complex was investigated in order to determine whether the formyl proton broadening in DMF was typical of other formamides. Fig. IV-17 shows the  $1/T_{2P}$  results for the formyl proton of DEF solutions of bis-(diphenyldithiophosphinato)-oxovanadium(IV). The temperature dependence of the line-width of the formyl proton resonance of the pure solvent DEF is shown in Fig. IV-18. The  $1/T_{2P}$  data shown in Fig. IV-17 has a temperature dependence similar to that for the formyl proton of DMF solutions of bis-(diphenyldithiophosphinato)-oxovanadium(IV) shown in Fig. IV-11. In the exchange controlled region, the  $1/T_{2P}$  values at a given temperature are equal within experimental error for the two systems. However,  $1/T_{2P}$  values in both the inner sphere and outer sphere  $T_{2M}$  region are larger in the DEF solvent. One would expect the  $1/T_{2MOS}$  values in DEF to be smaller than in DMF since the vanadyl complex in DMF which has one monodentate diphenyldithiophosphinate ligand



TABLE IV-6

Least Squares Parameters<sup>†</sup> and Calculated Nuclear Relaxation and Exchange Rates<sup>††</sup> of  
DMF Protons in Solutions Containing Bis-(diphenyldithiophosphinato)-oxo-vanadium(IV)

Protons	$C_M(\text{sec}^{-1})$	$C_{\text{Mos}}(\text{sec}^{-1})$	$E_M(\text{kcal/mole})$	$1/T_{2M}(\text{sec}^{-1})$	$n/T_{2\text{Mos}}(\text{sec}^{-1})$
axial C-H	$6.7 \pm .6$	-	$3.9 \pm .2$	$5.4 \times 10^3$	-
equatorial C-H	$1.4 \pm .1 \times 10^1$	$1.3 \pm .1$	$3.9 \pm .2$	$1.1 \times 10^4$	$1.1 \times 10^3$
equatorial <u>cis</u> N-CH <sub>3</sub>	-	$1.3 \pm .6$	$3.9 \pm .2$	-	$1.1 \times 10^3$
equatorial <u>trans</u> N-CH <sub>3</sub>	-	$1.1 \pm .5$	$3.9 \pm .2$	-	$9.0 \times 10^2$

Equatorial and axial exchange parameters:

$$\Delta H_{\text{eq}}^{\ddagger} = 10.0 \pm .4 \text{ kcal/mole} \quad \Delta S_{\text{eq}}^{\ddagger} = -11.3 \pm 1.1 \text{ e.u.} \quad 1/\tau_{\text{Meq}} = 9.5 \times 10^2 \text{ sec}^{-1}$$

$$\Delta H_{\text{ax}}^{\ddagger} = 10.8 \pm 1.6 \text{ kcal/mole} \quad \Delta S_{\text{ax}}^{\ddagger} = -1.7 \pm 5.9 \text{ e.u.} \quad 1/\tau_{\text{Max}} = 3.4 \times 10^4 \text{ sec}^{-1}$$

<sup>†</sup> Errors quoted are the standard errors given by the least squares analysis.

<sup>††</sup> Relaxation rates and exchange rates are calculated at 25°C from least squares parameters.



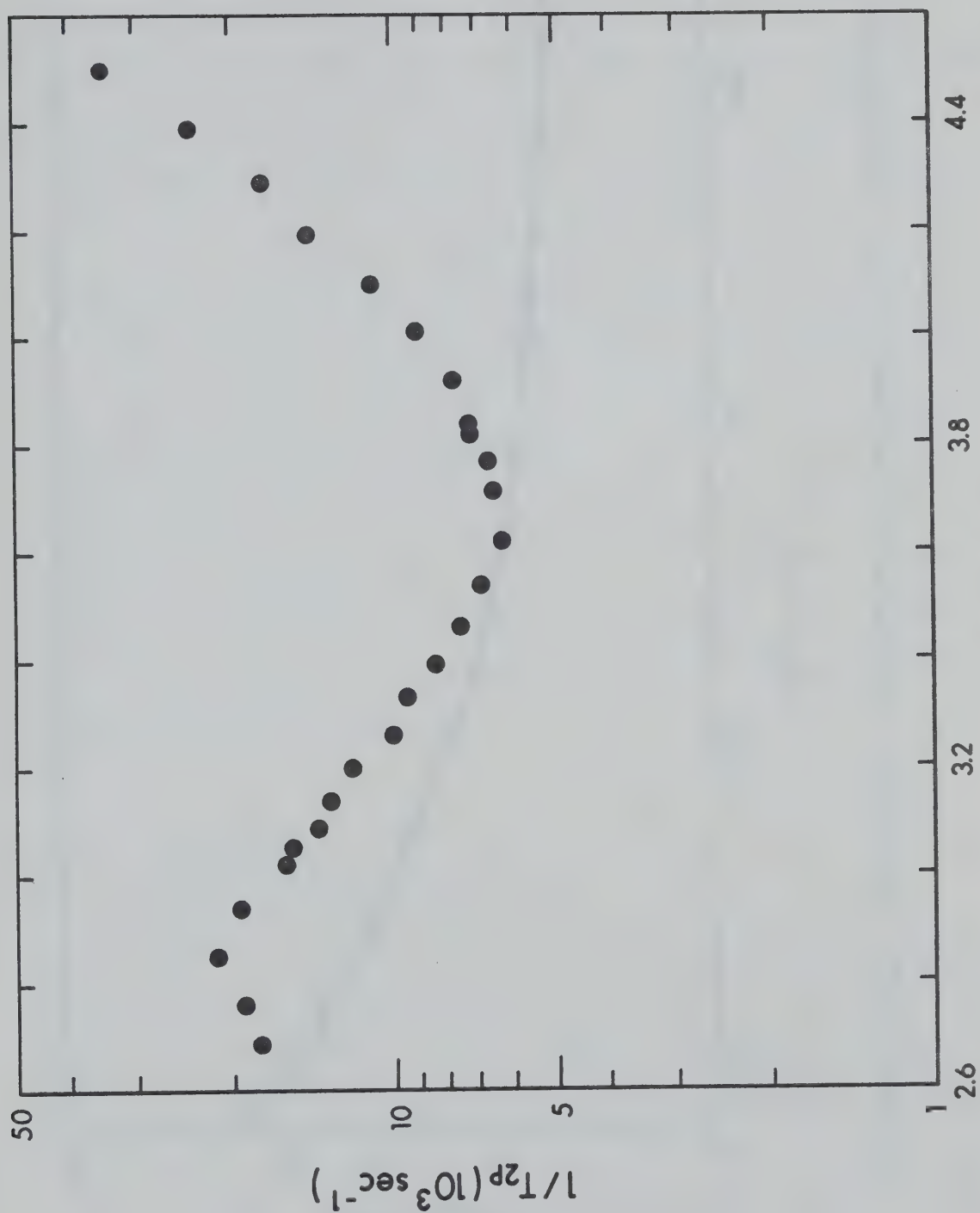


FIGURE IV-17. Temperature dependence of  $1/T_{2P}$  for the formyl proton in DEF solutions



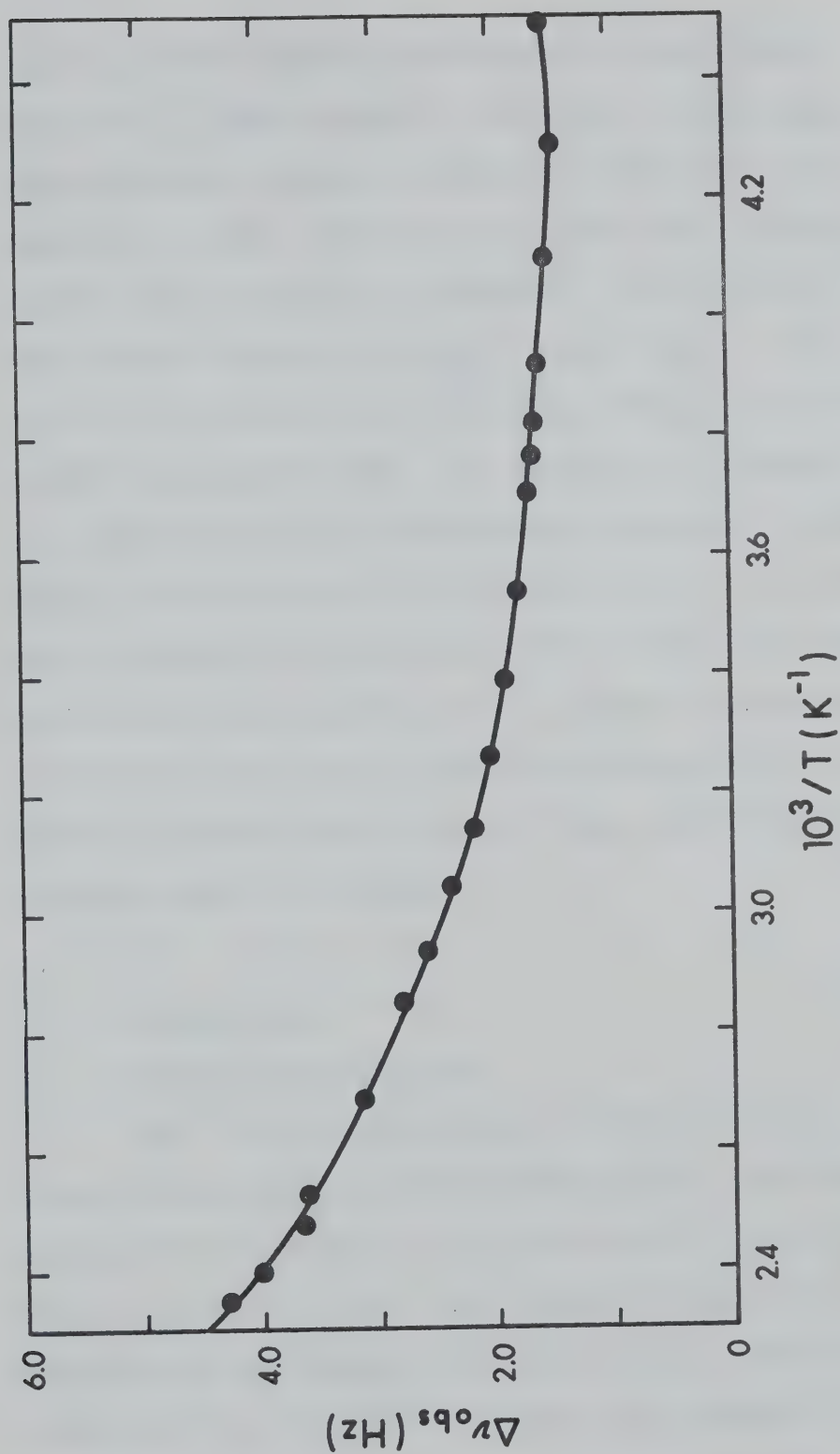


FIGURE IV-18. Temperature dependence of the formyl proton linewidths of DEF.





and four DMF ligands coordinated to the vanadyl ion is expected to have a smaller effective radius than the corresponding vanadyl complex in which the DMF ligands are replaced by DEF. On the other hand, the viscosity of DEF may be large enough to increase  $\tau_r$  sufficiently to yield the higher values of  $1/T_{2MOS}$  in DEF than in DMF. This would also account for the higher  $1/T_{2M}$  values observed in DEF compared to DMF. An analysis of the DEF system in terms of axial and equatorial exchange is not feasible since the component of the formyl proton line broadening due to equatorial exchange is not known and cannot be determined from the  $CH_3$  or  $CH_2$  proton resonances since linewidth measurements for these resonances are hampered by the spin-spin splitting of these resonances and were therefore not undertaken.

## E. Discussion

### 1. Vanadyl Perchlorates

The  $^{17}O$  line broadening by  $VO(H_2O)_5(ClO_4)_2$  at low temperatures has been attributed to the exchange of water molecules coordinated to the vanadyl ion with lifetimes which are much shorter than those of the water molecules coordinated at equatorial sites in the first coordination sphere of the ion.<sup>42,43</sup> Either the exchange of an axially-coordinated water molecule or molecules in the outer solvation sphere could account for the experimental observa-



tions. Line broadening by vanadyl complexes in other solvents<sup>44-48</sup> gives similar results with no resolution of the two processes which can conceivably explain the slow exchange region broadening. The  $\text{VO}(\text{DMF})_5(\text{ClO}_4)_2$  line broadening data presented in this thesis constitute an example where the outer sphere effects can be separated from line broadening due to axial exchange. The large difference in the dipolar relaxation times for the formyl and methyl protons in axially-coordinated DMF molecules makes the formyl proton linewidth sensitive to axial exchange while the methyl linewidths are not appreciably affected. In an attempt to substantiate the assertions in the  $\text{VO}(\text{DMF})_5(\text{ClO}_4)_2$  system, one can study the line broadening of the DMF resonances by bis-(o-phenanthroline)-oxo-vanadium(IV) perchlorate, a molecule in which the equatorial coordination sites of the vanadyl ion are occupied by the bidentate o-phenanthroline ligands.<sup>50</sup> The NMR data shown in Fig. IV-14 indicated an exchange-controlled region above 60°C, but EPR studies indicated the presence of a second vanadyl species at this temperature. See Fig. IV-15. Presumably, the o-phenanthroline ligands are not bound strongly and may be displaced by DMF solvent molecules and the equatorially-coordinated DMF molecules account for the exchange-controlled line broadening.

The uncharged vanadyl acetylacetonate complex and



its effects on the linewidths of the proton resonances of DMF were investigated also. In this case, no exchange-controlled region was observed. See Fig. IV-16. The rate of exchange between bulk solvent and axially-coordinated DMF molecules must be too fast to control the line broadening. The vanadium-DMF bond is probably weaker in the vanadyl acetonate-DMF adduct than the axial vanadium-DMF bond in  $\text{VO}(\text{DMF})_5^{2+}$  because the acetylacetonate is uncharged, and this would result in a more rapid ligand exchange. Wüthrich and Connick<sup>47</sup> have shown that the equatorial ligand exchange rate in uncharged complexes is approximately  $10^3$  times faster than the exchange in charged complexes. One might expect therefore the rate of axial exchange in the acetylacetonate to be of the order of  $10^7 \text{ sec}^{-1}$ , since the axial exchange rate in  $\text{VO}(\text{DMF})_5^{2+}$  is  $10^4 \text{ sec}^{-1}$ . EPR studies<sup>39</sup> of the axial exchange rate in amine adducts of vanadyl acetylacetonate indicate that a rate of  $10^7 \text{ sec}^{-1}$  is eminently reasonable.

The axial exchange rate in  $\text{VO}(\text{DMA})_5^{2+}$  is probably too fast, over the accessible temperature range, to contribute to the line broadening. The solvent freezes before axial exchange becomes slow enough to control the linewidth of the C-methyl resonance. The rate of equatorial exchange in  $\text{VO}(\text{DMA})_5^{2+}$  is 25 times faster than in  $\text{VO}(\text{DMF})_5^{2+}$  at  $25^\circ\text{C}$ , and has a lower enthalpy of activation. This reflects a weaker vanadium-ligand bond in the DMA



complex ion as one might expect on steric grounds. Steric factors would also increase the interaction distances between the unpaired electron and the protons of an axially coordinated DMA molecule. This would decrease  $(T_{2\text{Max}})^{-1}$  and lower the axial contribution to the linewidths as compared to the  $\text{VO}(\text{DMF})_5^{2+}$  case.

The plots of  $\log (1/T_{2\text{P}})$  vs  $T^{-1}$  for all three types of protons in DMA in Fig. IV-8 show a slight curvature at low temperature. It was assumed that this curvature was due to outer sphere effects since an axial exchange contribution, at least on the basis of the DMF results, should have produced a broadening of the C-methyl resonances while the N-methyl proton widths should have remained unaffected. The distances of closest approach by outer sphere molecules in DMF and DMA studies are comparable. However, in both cases, the N-methyl interaction distances for outer sphere molecules appear to be smaller than molecular models would predict. This may result from orientation of the molecules in the second solvation sphere in positions where the N-methyl protons are close to the paramagnetic center. Another explanation of the small outer sphere interaction distances invokes small hyperfine interactions to molecules in the second coordination sphere. Such a mechanism has been postulated for other systems <sup>47,89</sup>, but the cause of the small outer sphere distances in the present case is unclear.







The coordination of oxygen donors to metals is generally via two modes: linear coordination and angular coordination. In linear coordination the metal occupies a position between the two lone pairs of the oxygen atom, while in angular coordination the metal bonds to one of the lone pairs. Line broadening studies with  $\text{Co}(\text{DMF})_6(\text{ClO}_4)_2$ <sup>88</sup> indicate that the Co-O-C bond is bent, signifying angular coordination. The crystal structure of  $\text{Fe}(\text{DMF})_6^{3+}$  also supports the angular model.<sup>19</sup> Coordination of the planar DMF molecules in the xy plane results in steric crowding and orientations parallel to the xz and yz planes or slightly pitched from these planes is likely. Two possible coordination arrangements are illustrated in Fig. IV-19. Structure I is favored because of less steric hindrance with the axial solvent molecule. Furthermore, tilting of the DMF molecule would make the two  $\text{CH}_3$  groups more equivalent with respect to the  $d_{x^2-y^2}$  orbital. Structure I also keeps the C-H proton well removed from regions of high  $d_{x^2-y^2}$  probability which supports the observation of only dipolar coupling to the C-H proton. On the other hand, scalar coupling through space may be less favorable than scalar coupling through the  $\pi$  bonding systems of DMF and DMA. There are many sterically reasonable conformations of the complex ions in which the overlap between the vanadium  $3d_{x^2-y^2}$  atomic orbital and the amide  $\pi$ -molecular orbitals is favorable.



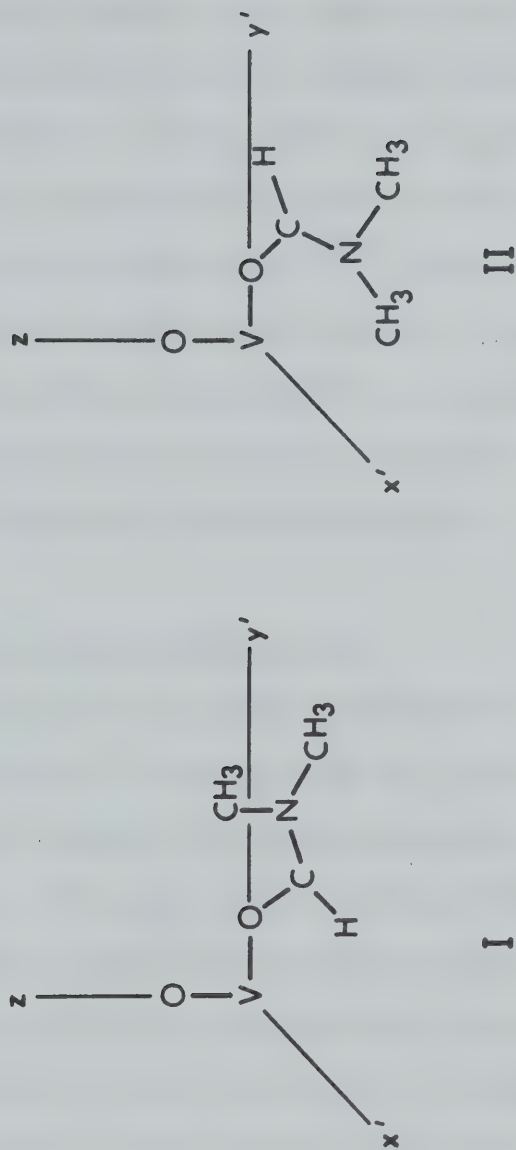


FIGURE IV-19. Stereochemistry of DMF coordinated to the vanadyl ion. The  $x'$  and  $y'$  axes are rotated  $45^\circ$  about the  $z$  axis of the  $xyz$  coordinate system defined in Fig. I-1.



Since the vanadium  $3d_{x^2-y^2}$  orbital energy<sup>31</sup> is similar to the energies of the highest occupied  $\pi$ -orbital of the amide ligand<sup>89</sup>, the molecular orbital containing the unpaired electron should have some of the character of this filled  $\pi$ -orbital of the free amide ligands. The highest occupied  $\pi$ -orbital of the amide moiety has large amplitudes at the nitrogen and oxygen atoms, but has smaller amplitude at the carbon atom.<sup>89</sup> The unpaired electron density at the nitrogen atom should be greater than that at the carbon atom, and hyperfine interactions with the N-methyl protons should therefore be more significant than those with formyl or C-methyl protons.

## 2. Vanadyl Dithiophosphinates

The EPR, infrared and conductance measurements reported in Chapter III supported the existence of ionic species when vanadyl dithiophosphinates were dissolved in Lewis bases. The same types of experiments in mixed solvents suggested equilibria between species with various numbers of coordination positions of the vanadyl ion occupied by Lewis base molecules. The NMR line broadening data presented in this Chapter confirm that DMA completely displaces the diphenyldithiophosphinate groups from the first coordination sphere of the vanadyl ion when bis-(diphenyldithiophosphinato)-oxo-vanadium(IV) is dissolved in DMA at room temperature. At higher temperatures the



diphenyldithiophosphinate again coordinates to the vanadyl ion which parallels the observations in Chapter III for the vanadyl dithiophosphinates in the mixed solvents HMP-toluene, DMF-toluene and pyridine-CS<sub>2</sub>. The prominence of uncharged species at high temperatures is presumably due to the decrease of the dielectric constant of the solvent with increasing temperature.

In contrast to the DMA line broadening results, the  $1/T_{2p}$  data for DMF solutions containing bis-(diphenyldithiophosphinato)-oxo-vanadium(IV) indicated that one equatorial coordination site of the vanadyl ion is occupied by a monodentate diphenyldithiophosphinate ligand. The exchange rate for the DMF molecules coordinated at the remaining three equatorial sites was greatly enhanced compared to equatorial exchange rates for  $VO(DMF)_5^{2+}$ . This is expected since the coordination of the diphenyldithiophosphinate anion to the vanadyl ion reduces the charge on vanadium and weakens the electrostatic V-DMF interaction. Wüthrich and Connick<sup>47</sup> have presented similar evidence which shows that the ligand exchange rate increases when the formal charge on vanadium is reduced.

Since conductivity measurements were undertaken only at room temperature, it is not known whether the species at high temperatures has one or two diphenyldithiophosphinate groups coordinated to the vanadyl ion. If coordination by the monodentate diphenyldithiophosphin-





ate occurs at two equatorial sites, then the number of equatorial sites for DMF coordination is reduced to two which could account for the small  $1/T_{2M}$  values observed for the formyl proton for the phenyl complex compared to  $VO(DMF)_5(ClO_4)_2$ . Coordination of two diphenyldithiophosphinates to the vanadyl ion produces a neutral complex which further decreases the strength of the vanadium-DMF bond. This effectively increases the vanadium-formyl proton interaction distance and consequently decreases the values of  $1/T_{2M}$ . If different species do indeed exist in DMF solutions containing the phenyl complex, they must have similar magnetic parameters because the EPR spectra of the DMF solutions showed no evidence of more than one species.



CHAPTER VC O N C L U S I O NA. Vanadyl Coordination

Several conclusions can be drawn from the results presented in this thesis which improve the understanding of the chemistry of vanadyl complexes in solution. Hopefully, these conclusions will be useful in the planning and interpretation of further studies of five and six coordinate vanadyl complexes.

A popular assumption in studies of the chemistry of vanadyl complexes has been that five coordinate vanadyl complexes take up a Lewis base type molecule at the vacant axial position. In contrast, the primary conclusion drawn from the investigation of the reactions of the five coordinate vanadyl dithiophosphinates with Lewis bases reported in this thesis is that these complexes form six coordinate complexes by coordination of Lewis bases at an equatorial position with the simultaneous rearrangement of one dithiophosphate chelate to occupy the axial and one equatorial site. No evidence for axial coordination was obtained. These observations are complemented by the recently published work of Caira, Haigh and Nassimbeni<sup>8</sup> who found that some Lewis base adducts of  $\text{VO}(\text{acac})_2$  also exhibit this stereochemistry. Other Lewis bases have been shown to coordinate preferentially at the axial position of  $\text{VO}(\text{acac})_2$ .



Unfortunately, neither  $\text{VO}(\text{acac})_2$  nor the vanadyl dithiophosphinates have been studied in a large enough variety of Lewis bases to establish any correlations from which predictions about the site of coordination could be made.

A second conclusion of the studies with the vanadyl dithiophosphinates is that the dithiophosphinate chelate can behave as a monodentate ligand coordinated to the vanadyl ion. In such a complex, the site vacated by the dithiophosphinate sulphur is occupied by a Lewis base. Monodentate coordination has also been postulated for metal complexes of the difluorodithiophosphate ligand on the basis of infrared and NMR P-F coupling constants.<sup>90</sup>

The displacement of the dithiophosphinate moiety from the first coordination sphere of the vanadyl ion by DMF molecules in contrast to the observed stability of  $\text{VO}(\text{acac})_2$  in DMF indicates that the V-S bond is considerably weaker than the V-O bond in  $\text{VO}(\text{acac})_2$ . This can probably be attributed to the stronger electrostatic interaction between the positive vanadium and electronegative oxygen.

The observation of the  $^{31}\text{P}$  hyperfine splitting in the EPR spectra of the five coordinate vanadyl dithiophosphinates and their six coordinate Lewis base adducts supports the conclusion that the unpaired electron occupies the vanadium  $d_{x^2-y^2}$  orbital. This same conclusion



was reached by Kivelson and Lee's study of vanadyl tetraphenylporphyrin.<sup>25</sup> This conclusion seems to be applicable to all vanadyl complexes since no evidence has been presented to support occupation of a different orbital by the unpaired electron.

#### B. Vanadyl Exchange Kinetics

Kinetic studies are a useful method for investigating the details of reaction mechanisms. In particular, the kinetic studies of the vanadyl perchlorates undertaken in this thesis elucidated the differences in the properties of the equatorial and axial coordination sites of vanadyl complexes.

The most interesting conclusion from the NMR line broadening studies is that the lifetime of DMF in the axial coordination position in  $\text{VO}(\text{DMF})_5(\text{ClO}_4)_2$  is as long as  $2 \times 10^{-5}$  seconds at room temperature. This is surprising since it has been believed that the coordination at this site is very weak and that lifetimes of ligands in the axial site would be of the order of  $10^{-7} - 10^{-8}$  sec as reported for the lifetime of the pyridine adduct of  $\text{VO}(\text{acac})_2$  by Walker, Carlin and Rieger.<sup>39</sup> The large difference in lifetimes in the two systems is due to the stronger axial bonding in  $\text{VO}(\text{DMF})_5(\text{ClO}_4)_2$  in which the vanadyl ion has a positive charge. Undoubtedly, the lifetimes of molecules coordinated at the axial site in other cationic vanadyl complexes have magnitudes similar







to that in  $\text{VO}(\text{DMF})_5(\text{ClO}_4)_2$  but the combination of chemical systems studied and experimental measurement methods used could not isolate the axial exchange effects. Indeed, this was found in the study of  $\text{VO}(\text{DMA})_5(\text{ClO}_4)_2$  from which no conclusions about axial exchange can be drawn.

A comparison of the exchange parameters for the vanadyl ion in a number of solvents is given in Table V-1. Although DMA and DMF have nearly identical electron donor properties on the basis of the classification proposed by Gutmann<sup>65</sup>, DMA exchanges about 25 times faster than DMF. This difference is attributed to the steric interaction caused by the  $\text{C}-\text{CH}_3$  group in the  $\text{VO}(\text{DMA})_5^{2+}$  complex. The slower exchange rate of DMF compared to  $\text{H}_2\text{O}$  is due to the significantly smaller electron donor strength of water. Similarly,  $\text{CH}_3\text{CN}$  has a weaker electron donor strength than  $\text{H}_2\text{O}$  and  $\text{CH}_3\text{CN}$  exchanges about six times as fast as  $\text{H}_2\text{O}$ . The large error limits for  $\Delta H^\ddagger$  and  $\Delta S^\ddagger$  in the earlier study of the solventline broadening of vanadyl perchlorate in DMF<sup>44</sup>, result from the attempt to fit the formyl proton line broadening data to a single exchange process. As shown in this thesis, the line broadening is determined by both axial and equatorial exchange and the data do not correlate well with a single exchange mechanism. The significantly larger value for  $\Delta H^\ddagger$  obtained in this thesis is in much better agreement with the  $\Delta H^\ddagger$  of  $\text{H}_2\text{O}$  as expected



TABLE V-1

Kinetic Parameters for Solvent Exchange from the Solvated  
Vanadyl Ion

Solvent	Donor <sup>65</sup> Number	$1/\tau_{\text{Meq}}$ ( $10^3 \text{ sec}^{-1}$ ) at 25°C	$\Delta H^\ddagger$ kcal/mole	$\Delta S^\ddagger$ cal/deg mole
DMA	27.8	4.7	$10.1 \pm .5$	$-7.9 \pm 1.6$
CH <sub>3</sub> CN <sup>44</sup>	14.1	2.97	$6.65 \pm .29$	$-20.3 \pm .9$
CH <sub>3</sub> OH <sup>44</sup>	-	.55	$9.46 \pm .68$	$-14.2 \pm .2$
H <sub>2</sub> O <sup>43</sup>	18.0	.50	13.7	- 0.6
DMF	26.6	.20	$13.1 \pm .6$	$-4.1 \pm 1.8$
DMF <sup>44</sup>	26.6	.76	$6.77 \pm 1.94$	$-22.6 \pm 5.7$



on the basis of electron donor properties. From Table V-1 one then concludes that the lifetime of the solvent molecule in an equatorial site depends on the electron donor properties of the solvent and its steric characteristics.

Another interesting feature of the vanadyl-amide studies is the assertion that the N-methyl proton relaxation times result from modulation of hyperfine interactions between the protons and the unpaired electron. Previous proton NMR studies of the vanadyl systems have consistently explained relaxation times by postulating only a dipolar interaction between the protons and the unpaired electron. Often the magnitude of the electron nuclear interactions was not considered since the  $1/T_{2M}$  limit was not observed in the line broadening data. This was the case for the study in  $\text{CH}_3\text{OH}$  and  $\text{CH}_3\text{CN}$ . However, a re-examination of the results for  $\text{CH}_3\text{CN}$  shows that a hyperfine contribution to  $1/T_{2M}$  must be postulated in order to produce the line broadenings observed and still be in the exchange controlled limit. The transfer of unpaired spin density to nuclei far removed from the site of coordination via the  $\pi$  system of the ligand is observed in DMF, DMA and  $\text{CH}_3\text{CN}$ , and can be expected in other coordinating ligands with delocalized molecular orbitals.



R E F E R E N C E S

1. J. Selbin, Chem. Rev., 65, 153 (1965).
2. J. Selbin, Coord. Chem. Rev., 1, 293 (1966).
3. R. P. Dodge, D. H. Templeton and A. Zalkin, J. Chem. Phys., 35, 55 (1961).
4. R. T. Claunch, T. W. Martin and M. M. Jones, J. Amer. Chem. Soc., 83, 1073 (1961).
5. R. L. Carlin and F. A. Walker, ibid., 87, 2128 (1965).
6. K. Dickmann, G. Hamer, S. C. Nyburg and W. F. Reynolds, Chem. Commun., 1295 (1970).
7. M. R. Caira, J. M. Haigh and L. R. Nassimbeni, Inorg. Nucl. Chem. Letters, 8, 109 (1972).
8. M. R. Caira, J. M. Haigh and L. R. Nassimbeni, J. Inorg. Nucl. Chem., 34, 3171 (1972).
9. R. A. Bozis and B. J. McCormick, Inorg. Chem., 9, 1541 (1970); B. J. McCormick and R. A. Bozis, ibid., 10, 2806 (1971).
10. B. J. McCormick, ibid., 7, 1965 (1968).
11. B. J. McCormick, Can. J. Chem., 47, 4283 (1969); B. J. McCormick, Inorg. Chem., 9, 1779 (1970).
12. N. M. Atherton and C. J. Winscom, ibid., 12, 383 (1973).
13. E. D. Day, Ph.D. Thesis, University of Alberta, 1972.
14. R. G. Cavell, E. D. Day, W. Byers and P. W. Watkins, Inorg. Chem., 11, 1591 (1972).
15. A. Müller, V. V. K. Rao and E. Deimann, Chem. Ber.,





- 104, 461 (1971); H. Hertel and W. Kuchen, Chem. Ber., 104, 1740 (1971).
16. I. V. Ovchinnikov, I. F. Gainulin, N. S. Garif'yanov and B. M. Kozyrev, Dokl. Akad. Nauk. SSSR., 191, 395 (1970).
17. N. S. Garif'yanov and B. M. Kozyrev, Theor. Eksp. Khim. 1, 525 (1965).
18. J. R. Wasson, Inorg. Chem., 10, 1531 (1971).
19. R. H. Sumner, Ph.D. Thesis, University of Alberta, (1971).
20. G. W. Pake, Paramagnetic Resonance, W. A. Benjamin, New York, 1972.
21. I. Bernal and P. H. Rieger, Inorg. Chem., 2, 256 (1963).
22. C. M. Guzy, J. B. Raynor and M. C. R. Symons, J. Chem. Soc. A, 2791 (1969).
23. K. Wüthrich, Helvetica Chimica Acta, 48, 779 (1965); K. Wüthrich, ibid., 48, 1012 (1965).
24. B. McGarvey, Transition Metal Chem., 3, 89 (1966).
25. D. Kivelson and S. K. Lee, J. Chem. Phys., 41, 1896 (1964).
26. M. A. Hitchman, C. D. Olson and R. L. Belford, ibid., 50, 1195 (1969).
27. M. A. Hitchman and R. L. Belford, Inorg. Chem., 8, 958 (1969).
28. R. Wilson and D. Kivelson, J. Chem. Phys., 44, 154 (1966).



29. C. K. Jorgensen, Acta Chem. Scand., 11, 73 (1957); C. Furlani, Ricerca Sci., 27, 1141 (1957).
30. M. B. Palma-Vittorelli, M. V. Palma, D. Palumbo and F. Sgarlata, Nuovo Cimento, 3, 718 (1956).
31. C. J. Ballhausen and H. B. Gray, Inorg. Chem., 1, 111 (1962).
32. L. G. Vanquickenborne and S. P. McGlynn, Theor. Chim. Acta (Berl.), 9, 390 (1968).
33. C. J. Ballhausen, B. F. Djurinskij and K. I. Watson, J. Amer. Chem. Soc., 90, 3305 (1968).
34. M. H. Valek, W. A. Yeranov, G. Basu, P. K. Hon and R. L. Belford, J. Mol. Spectrosc., 37, 228 (1971).
35. K. Nakamoto, Y. Morimoto and A. E. Martell, J. Amer. Chem. Soc., 83, 4533 (1961).
36. J. J. R. Fraústo da Silva and R. Wootton, Chem. Commun., 421 (1969).
37. W. E. Bull, S. K. Madan and J. E. Willis, Inorg. Chem., 2, 303 (1963).
38. R. S. Drago, D. W. Meek, M. D. Joesten and L. LaRoche, ibid., 2, 124 (1963).
39. F. A. Walker, R. L. Carlin and P. H. Rieger, J. Chem. Phys., 45, 4181 (1966).
40. J. A. Pople, W. G. Schneider and H. J. Bernstein, High Resolution Nuclear Magnetic Resonance, McGraw-Hill, New York, 1959, Chap. 10.



41. A. Carrington and A. McLachlan, Introduction to Magnetic Resonance, Harper and Row, New York, 1967.
42. J. Reuben and D. Fiat, Inorg. Chem., 6, 579 (1967).
43. K. Wüthrich and R. E. Connick, ibid., 6, 583 (1967).
44. N. S. Angerman, Ph. D. Thesis, University of Alberta (1968).
45. R. B. Jordan and N. S. Angerman, J. Chem. Phys., 48, 3983 (1968).
46. N. S. Angerman and R. B. Jordan, Inorg. Chem., 8, 65 (1969).
47. K. Wüthrich and R. E. Connick, ibid., 7, 1377 (1968).
48. R. B. Jordan and N. S. Angerman, ibid., 8, 1824 (1969).
49. Handbook of Chemistry and Physics, edited by R. C. Weast, Chemical Rubber Co., Cleveland, Ohio, 50th Ed., pp. C-429 (1969).
50. J. Selbin and L. H. Holmes Jr., J. Inorg. Nucl. Chem., 24, 1111 (1962).
51. S. H. Glarum and J. H. Marshall, J. Chem. Phys., 41, 2182 (1964).
52. Publication No. 87-100-110, Varian Associates, Palo Alto, Calif., pp.29,32.
53. M. Bersohn and J. C. Baird, An Introduction to Electron Paramagnetic Resonance, W. A. Benjamin, New York, 1966, pp.8.
54. R. Rogers and G. Pake, J. Chem. Phys., 33, 1107 (1960).



55. B. Bleany, Phil. Mag., 42, 441 (1951).
56. A. Abragam, J. Horowitz and M. H. L. Pryce, Proc. Roy. Soc. (London), A230, 169 (1955).
57. P. W. Atkins and D. Kivelson, J. Chem. Phys., 44, 169 (1966).
58. N. Bloembergen, E. M. Purcell and R. V. Pound, Phys. Rev., 73, 679 (1948).
59. R. J. Fort and W. R. Moore, Trans. Faraday Soc., 62 112 (1966).
60. J. Selbin and T. R. Ortolano, J. Inorg. Nucl. Chem., 26, 37 (1964).
61. J. Selbin, H. R. Manning and G. Cessac, ibid., 25, 1253 (1963).
62. E. B. Millard, Physical Chemistry for Colleges, McGraw-Hill, New York, 1953, Chap. 8.
63. M. Szwarc, Accounts Chem. Research, 2, 87 (1969).
64. Handbook of Chemistry and Physics, edited by R. C. Weast, Chemical Rubber Co., Cleveland, Ohio, 50th Ed., pp.E61-65 (1969).
65. V. Gutmann, Record of Chemical Progress, 30, 169 (1969).
66. B. R. McGarvey, Transition Metal Chem., 3, 89 (1966).
67. N. D. Yordanov and D. Shopov, Inorg. Nucl. Chem. Letters, 9, 19 (1973).
68. P. B. Ayscough, Electron Spin Resonance in Chemistry, Methuen and Co. Ltd., London, 1967, pp.438-439.





69. R. A. Chittenden and L. S. Thomas, Spectrochim. Acta, 20, 1679 (1964).
70. P. Porta, A. Scamellotti and N. Vinciguerra, Inorg. Chem., 7, 2625 (1968).
71. T. J. Swift and R. E. Connick, J. Chem. Phys., 37, 307 (1962).
72. R. K. Wangsness and F. Bloch, Phys. Rev., 89, 728 (1953); F. Bloch, Phys. Rev., 102, 104 (1956).
73. H. M. McConnell, J. Chem. Phys., 28, 430 (1958).
74. T. R. Stengle and C. H. Langford, Coord. Chem. Rev., 2, 349 (1967).
75. S. Glasstone, K. J. Laidler and H. Eyring, The Theory of Rate Processes, McGraw-Hill Book Co., New York, 1941.
76. I. Solomon, Phys. Rev., 99, 559 (1955).
77. I. Solomon and N. Bloembergen, J. Chem. Phys., 25, 261 (1956); N. Bloembergen, ibid., 27, 572 (1957).
78. N. S. Angerman and R. B. Jordan, ibid., 54, 837 (1970).
79. N. Bloembergen, J. Chem. Phys., 27, 595 (1957).
80. R. S. Drago, Physical Methods in Inorganic Chemistry, Reinhold Publishing Corp., New York, 1965, Chapter 7.
81. G. Durgaprasad and D. N. Sathyanarayana and C. C. Patel, Bull. Chem. Soc. Japan, 44, 316 (1971).
82. Dupont Product Information Bulletin (DMF), E. I. Dupont de Nemours and Co. Inc., Wilmington, Del. (1967).
83. M. Frucht and A. Lewin, Tet. Lett., 42, 3707 (1970).
84. D. W. Marquardt, J. Soc. Indust. Appl. Math., 11, 431



(1963).

85. L. Luz and S. Meiboom, J. Chem. Phys., 40, 2686 (1964).
86. J. V. Hatton and R. E. Richards, Mol. Phys., 3, 253 (1960).
87. M. Alei, Inorg. Chem., 3, 44 (1964).
88. N. Matwiyoff, ibid., 5, 788 (1966).
89. M. A. Robb and I. G. Csizmadia, Theor. Chim. Acta  
(Berl.), 10, 269 (1968).
90. F. N. Tebbe and E. L. Muetterties, Inorg. Chem., 9,  
629 (1970).



A P P E N D I X      A

The Tables in Appendix A give the observed proton magnetic resonance linewidths at half height and the calculated values of  $1/T_{2P}$  for the systems described in Chapter IV.



TABLE A-1

Proton Line Broadening of DMA Solutions Containing Various Concentrations

of VO(DMA)<sub>5</sub>(ClO<sub>4</sub>)<sub>2</sub>

$10^3/T$ (K <sup>-1</sup> )	C-methyl		trans-N-methyl		cis-N-methyl	
	$\Delta\nu_{\text{obs}}$ (Hz)	$1/T_{2P}$ (10 <sup>3</sup> sec <sup>-1</sup> )	$\Delta\nu_{\text{obs}}$ (Hz)	$1/T_{2P}$ (10 <sup>3</sup> sec <sup>-1</sup> )	$\Delta\nu_{\text{obs}}$ (Hz)	$1/T_{2P}$ (10 <sup>3</sup> sec <sup>-1</sup> )
<u>0.0414 molal</u>						
3.89	6.1	3.9	4.3	2.8	5.4	3.3
3.83	6.2	4.0	4.7	3.2	5.9	3.8
3.79			5.0 <sup>†</sup>	3.4 <sup>†</sup>	6.7	4.4 <sup>†</sup>
3.75	6.6	4.4	4.9	3.3	6.5	4.3
3.68	7.7	5.3	6.7	4.8	8.0	6.3
3.61	9.3	6.7	8.2	6.2	11.0	8.0
3.54	11.6	8.6				
3.47	13.8	10.4				
3.41	16.6	12.8				
3.41			17.4 <sup>†</sup>	14.0 <sup>†</sup>	15.3 <sup>†</sup>	11.6 <sup>†</sup>

0.0196 molal

2.54 <sup>††</sup>	10.7	17.6	45.0	80.2
2.54 <sup>††</sup>	11.7 <sup>†</sup>	19.4 <sup>†</sup>	49.0 <sup>†</sup>	85.1 <sup>†</sup>
2.48 <sup>††</sup>	10.7 <sup>†</sup>	17.6 <sup>†</sup>	44.4 <sup>†</sup>	78.9 <sup>†</sup>
2.47 <sup>††</sup>	9.2	14.8	41.0	72.9

(continued.....)





$10^3/T$ ( $K^{-1}$ )	C-methyl $\Delta\nu_{obs}$ (Hz)	$1/T$ $10^3 sec^{-1}$	trans-N-methyl $\Delta\nu_{obs}$ (Hz)	$1/T$ $10^3 sec^{-1}$	cis-N-methyl $\Delta\nu_{obs}$ (Hz)	$1/T$ $10^3 sec^{-1}$
<u>0.0196 molal (continued)</u>						
2.42 <sup>††</sup>	8.4	13.4	37.3	66.1		
2.42 <sup>††</sup>	9.3	14.8 <sup>†</sup>	42.1	76.3 <sup>†</sup>		
<u>0.0295 molal</u>						
3.61			3.3	4.7	3.9	4.6
3.54			4.7	7.3	4.9	6.4
3.48			5.7	9.2	6.1	8.6
3.42	7.1	10.6	7.8	13.0	8.3	12.6
3.37	8.8	13.9				
3.31	10.7	17.3				
3.26	12.9	21.3				
3.20	14.4	24.1				
3.14	15.3	25.8				
<u>0.0134 molal</u>						
3.15	10.6	25.2				
3.10	11.4	27.4				
3.05	11.8	28.5				
3.00	12.0	29.0				
2.91	11.5	27.7				
2.83	10.5	22.0				

(continued.....)



$10^3/T \text{ (K}^{-1}\text{)}$	C-methyl		trans-N-methyl		cis-N-methyl	
	$\Delta\nu_{\text{obs}}$ (Hz)	$1/T_{2P}$ ( $10^3 \text{ sec}^{-1}$ )	$\Delta\nu_{\text{obs}}$ (Hz)	$1/T_{2P}$ ( $10^3 \text{ sec}^{-1}$ )	$\Delta\nu_{\text{obs}}$ (Hz)	$1/T_{2P}$ ( $10^3 \text{ sec}^{-1}$ )
<u>0.0134 molal (continued)</u>						
2.75	9.7	20.0				
2.67 <sup>††</sup>	9.0	21.5	39.2	100		
2.61 <sup>††</sup>	8.1	19.0	33.6	87		
2.54 <sup>††</sup>	7.6	17.4	30.8	80		
2.48 <sup>††</sup>	6.7	15.0	28.3	73		
2.42 <sup>††</sup>	6.1	13.4	25.1	64		
2.36 <sup>††</sup>	5.4	11.5	21.1	53		
<u>0.00494 molal</u>						
3.49			3.0	16.8	2.7	9.9
3.42			3.8	22.7	3.3	13.9
3.35			4.6	28.6	4.0	19.0
3.29			5.7	35.1	4.8	24.9
3.23			6.6	48.3	5.9	33.0
3.16			8.5	52.0	6.9	37.4
3.15			7.5	49.1	6.2	36.6
3.10			11.0	66.0	8.5	46.2
2.79 <sup>††</sup>			17.1	102		
2.71 <sup>††</sup>			15.1	99		
2.64 <sup>††</sup>			13.7	91		

(continued.....)



$10^3/T \text{ (K}^{-1}\text{)}$	C-methyl		trans-N-methyl		cis-N-methyl	
	$\Delta\nu_{\text{obs}}$ (Hz)	$\frac{1}{T}_{2P}$ ( $10^3 \text{ sec}^{-1}$ )	$\Delta\nu_{\text{obs}}$ (Hz)	$\frac{1}{T}_{2P}$ ( $10^3 \text{ sec}^{-1}$ )	$\Delta\nu_{\text{obs}}$ (Hz)	$\frac{1}{T}_{2P}$ ( $10^3 \text{ sec}^{-1}$ )
<u>0.00494 molal (continued)</u>						
2.57 <sup>††</sup>			12.3	81		
2.51 <sup>††</sup>			11.0	72		
2.45 <sup>††</sup>			9.8	63		
2.39 <sup>††</sup>			9.3	59		

<sup>†</sup> Spectra recorded at 100 MHz. All other data from spectra recorded at 60 MHz.

<sup>††</sup> N-methyl resonances are collapsed to a single line.



TABLE A-2

Proton Line Broadening of DMF Solutions Containing Various Concentrations

of VO(DMF)<sub>5</sub>(ClO<sub>4</sub>)<sub>2</sub>

$10^3/T$ (K <sup>-1</sup> )	Formyl		trans-N-methyl		cis-N-methyl	
	$\Delta\nu_{\text{obs}}$ (Hz)	$1/T_{2P-1}$ (10 <sup>3</sup> sec <sup>-1</sup> )	$\Delta\nu_{\text{obs}}$ (Hz)	$1/T_{2P-1}$ (10 <sup>3</sup> sec <sup>-1</sup> )	$\Delta\nu_{\text{obs}}$ (Hz)	$1/T_{2P-1}$ (10 <sup>3</sup> sec <sup>-1</sup> )
<i>0.0573 molal</i>						
4.54	16.5	10.3				
4.44	13.8	8.4				
4.33	12.6	7.4		4.2	10.4	6.5
4.23	10.1	5.6	7.0	4.3	10.3	6.5
4.15	9.2	4.9	6.4	3.7	7.3	4.3
4.06	8.6	4.4	5.6	3.2	6.7	3.9
3.98	8.4	4.2	5.1	2.8	6.0	3.3
3.89	8.3	4.1	4.8	2.6	5.7	3.1
3.80	8.4	4.2	4.3	2.1	5.1	2.6
3.72	9.1	4.6	3.9	1.8	4.7	2.3
3.68	10.0	5.2	4.1	1.9	4.8	2.3
3.64	10.0	5.2	3.7	1.6	4.4	2.0
3.56	11.1	6.0	3.5	1.5	4.3	1.9
3.48	12.1	6.7	4.0	1.9	4.3	1.9
3.41	13.2	7.4	3.8	1.7	4.4	2.1
3.40	13.1	7.3	4.3	2.2	4.8	2.5
3.35	13.2	7.3	4.2	2.1	4.7	2.4

(continued.....)





$10^3/T$ ( $K^{-1}$ )	Formyl		trans-N-Methyl		cis-N-Methyl	
	$\Delta\nu_{obs}$ (Hz)	$\frac{1/T}{10^3 sec^{-1}}$	$\Delta\nu_{obs}$ (Hz)	$\frac{1/T}{10^3 sec^{-1}}$	$\Delta\nu_{obs}$ (Hz)	$\frac{1/T}{10^3 sec^{-1}}$
<u>0.0573 (continued)</u>						
3.34	13.2	7.3	4.8	2.6	5.2	2.7
3.27	13.6	7.6	5.0	2.7	5.3	2.8
3.22	14.5	8.1	5.7	3.2	6.2	3.4
3.15	15.7	8.9	6.9	4.2	7.6	4.4
3.10	16.5	9.3	9.8	6.2	9.8	6.0
3.04	17.8	10.1				
3.00	18.9	10.8				
2.91	22.4	13.1				
2.83	26.6	16.0				
2.75	30.8	18.9				
2.67	32.3	19.7				
2.61	35.0	21.5				
2.54	39.0	24.3				
2.48 <sup>††</sup>	36.8	22.2	77.0	53.6		
2.42 <sup>††</sup>	37.8	22.8	74.5	52.8		
<u>0.0246 molal</u>						
4.54	7.8	9.5	5.7	7.5	6.7	8.7
4.44	6.2	6.6	4.7	5.8	5.5	6.8
4.39 <sup>†</sup>	6.9 <sup>†</sup>	7.9 <sup>†</sup>	5.3 <sup>†</sup>	5.8 <sup>†</sup>	6.2 <sup>†</sup>	6.9 <sup>†</sup>
4.33	5.8	5.8	4.1	4.9	4.7	5.6

(continued.....)



$10^3/T(K^{-1})$	Formyl		<u>trans-N-Methyl</u>		<u>cis-N-Methyl</u>	
	$\Delta\nu_{obs}$ (Hz)	$1/T_{2P}$ ( $10^3 sec^{-1}$ )	$\Delta\nu_{obs}$ (Hz)	$1/T_{2P}$ ( $10^3 sec^{-1}$ )	$\Delta\nu_{obs}$ (Hz)	$1/T_{2P}$ ( $10^3 sec^{-1}$ )
<u>0.0246 molal (continued)</u>						
4.11	5.2 <sup>†</sup>	4.5 <sup>†</sup>	3.7 <sup>†</sup>	3.7 <sup>†</sup>	4.3 <sup>†</sup>	4.4 <sup>†</sup>
3.86	4.8 <sup>†</sup>	3.5 <sup>†</sup>	3.0 <sup>†</sup>	2.5 <sup>†</sup>	3.5 <sup>†</sup>	2.7 <sup>†</sup>
3.66	6.0 <sup>†</sup>	5.3 <sup>†</sup>	2.8 <sup>†</sup>	2.2 <sup>†</sup>	3.1 <sup>†</sup>	2.0 <sup>†</sup>
3.47	7.1 <sup>†</sup>	6.6 <sup>†</sup>	2.5 <sup>†</sup>	1.7 <sup>†</sup>	2.8 <sup>†</sup>	1.7 <sup>†</sup>
3.47	7.5	7.7				
3.41	7.8	8.2				
3.34	8.3	8.8				
3.28	8.3	8.8				
3.10	9.2	9.4	4.0	4.7	4.2	6.0
3.00	10.7	11.3	7.0	9.9	7.2	9.7
2.91	13.0	14.7				
2.83	15.1	17.9				
2.75	16.6	19.3				
2.67	18.6	22.8				
2.61	19.5	24.0				
2.54	20.9	26.0				
2.48 <sup>††</sup>	21.8	26.8	42.6	67.1		
2.42 <sup>††</sup>	22.0	26.6	41.0	66.9		
<u>0.0101 molal</u>						
3.10	6.1	29.6				
3.05	6.2	9.6	2.5	5.2	2.6	4.6



$10^3/T(K^{-1})$	Formyl		trans-N-Methyl		cis-N-Methyl	
	$\Delta\nu_{\text{Obs}}$ (Hz)	$1/T_{2P}$ ( $10^3 \text{ sec}^{-1}$ )	$\Delta\nu_{\text{Obs}}$ (Hz)	$1/T_{2P}$ ( $10^3 \text{ sec}^{-1}$ )	$\Delta\nu_{\text{Obs}}$ (Hz)	$1/T_{2P}$ ( $10^3 \text{ sec}^{-1}$ )
<u>0.0101 molal (continued)</u>						
3.00	6.7	10.8	3.2	8.1	3.4	7.7
2.96	7.2	12.2	4.1	11.3	4.4	11.9
2.91	7.6	13.0	5.1	15.2	5.7	17.2
2.87	8.2	15.1	6.8	22.4	6.9	21.7
2.84	8.8	18.8	8.5	29.2	8.6	28.6
2.83	8.8	16.8	7.9	26.8	7.7	24.9
2.79	9.3	18.5				
2.75	9.6	19.4				
<u>0.00442 molal</u>						
3.00			2.1	7.4	2.3	6.5
2.91			3.3	17	3.3	14
2.83			4.9	31	4.9	29
2.75			6.9	50	6.8	42
2.67			9.2	67	8.6	58
2.61	8.1 <sup>†</sup>	22.8 <sup>†</sup>	10.1 <sup>†</sup>	73 <sup>†</sup>	8.4 <sup>†</sup>	53 <sup>†</sup>
2.48 <sup>††</sup>			10.5	63		
2.42 <sup>††</sup>			9.0	61		

<sup>†</sup> Spectra recorded at 100 MHz. All other data from spectra recorded at 60 MHz.

<sup>††</sup> N-methyl resonances are collapsed to a single line.



TABLE A-3

Proton Line Broadening<sup>†</sup> of DMF Solutions Containing Various Concentrations

of Bis-(o-phenanthroline)-oxo-vanadium(IV) Perchlorate

$10^3/T(K^{-1})$	Formyl		trans-N-Methyl		cis-N-Methyl	
	$\Delta\nu_{\text{Obs}}$ (Hz)	$1/T_{2P}$ ( $10^3 \text{ sec}^{-1}$ )	$\Delta\nu_{\text{Obs}}$ (Hz)	$1/T_{2P}$ ( $10^3 \text{ sec}^{-1}$ )	$\Delta\nu_{\text{Obs}}$ (Hz)	$1/T_{2P}$ ( $10^3 \text{ sec}^{-1}$ )
<u>0.1175 molal</u>						
3.18	6.2	10.0	3.1	6.6	3.5	7.4
3.12	6.5	10.6	3.2	6.9	3.6	7.9
3.02	6.3	8.2	2.7	5.1	3.1	5.5
2.93	6.5	7.7	2.7	4.6	3.1	5.5
2.84	7.0	8.0	3.3	6.4	3.7	6.6
2.76	7.7	9.7	4.5	9.5	4.9	10.2
2.68	9.1	13.7	7.5	19	8.0	20
2.60	11.1	19.4				
<u>0.0538 molal</u>						
4.31	9.9	6.0	7.8	5.2	8.7	5.6
4.13	7.6	4.1	5.5	3.4	6.3	3.9
4.05	6.6	3.2	4.5	2.6	5.2	3.0
3.97	6.2	2.9	4.4	2.5	4.9	2.7
3.89	5.6	2.3	3.6	1.8	4.2	2.1
3.83	5.5	2.3	3.5	1.6	4.0	2.0

(continued....)





$10^3/T (K^{-1})$	Formyl		trans-N-Methyl		cis-N-Methyl	
	$\Delta\nu_{\text{Obs}}$ (Hz)	$1/T_{2P}$ ( $10^3 \text{sec}^{-1}$ )	$\Delta\nu_{\text{Obs}}$ (Hz)	$1/T_{2P}$ ( $10^3 \text{sec}^{-1}$ )	$\Delta\nu_{\text{Obs}}$ (Hz)	$1/T_{2P}$ ( $10^3 \text{sec}^{-1}$ )
<u>0.0538 (continued)</u>						
3.66	4.8	1.6	2.9	1.1	3.4	1.4
3.54	4.7	1.4				
3.41	4.3	1.0				
3.32	4.8	1.3				
3.21	4.6	0.9				
3.11	4.7	0.8				
<u>0.0306 molal</u>						
4.50	8.2	8.1	6.0	6.2	6.9	7.8
4.40	7.0	6.4	5.2	5.5	5.6	5.7
4.22	5.3	3.9	3.7	3.4	4.3	4.0

† Spectra recorded at 60 MHz.



TABLE A-4

Formyl Proton Line Broadening<sup>†</sup> of DMF Solutions Containing  
VO(acac)<sub>2</sub>

<u><math>10^3/T(K^{-1})</math></u>	<u><math>\Delta\nu_{obs}</math> (Hz)</u>	<u>Formyl <math>1/T_{2P} (10^3 sec^{-1})</math></u>
<u>0.0449 molal</u>		
4.69	35.8	34.2
4.57	26.1	25.0
4.47	20.4	19.6
4.40	16.4	15.7
4.32	13.0	12.4
4.24	10.6	10.1
4.14	8.9	8.5
4.07	7.6	7.3
3.99	6.6	6.3
3.91	5.8	5.6
3.84	4.9	4.7
3.79	5.3	5.1
3.71	4.5	4.3
3.54	3.5	3.3
3.39	2.7	2.5
3.26	2.2	2.1
3.16	1.8	1.7

<sup>†</sup> Spectra recorded at 60 MHz.



TABLE A-5

Proton Line Broadening<sup>†</sup> of DMA Solutions Containing Various Concentrations of Bis-(diphenyldithiophosphinato)-oxo-vanadium(IV)

$10^3/T(K^{-1})$	Formyl		trans-N-Methyl		cis-N-Methyl	
	$\Delta\nu_{obs}$ (Hz)	$1/T_{2P}$ ( $10^3 sec^{-1}$ )	$\Delta\nu_{obs}$ (Hz)	$1/T_{2P}$ ( $10^3 sec^{-1}$ )	$\Delta\nu_{obs}$ (Hz)	$1/T_{2P}$ ( $10^3 sec^{-1}$ )
<i>0.0248 molal</i>						
3.91	4.9	5.1	3.2	3.4	4.6	4.6
3.79	4.7	4.8	3.5	3.7	4.6	4.7
3.71	4.9	5.2	4.0	4.3	4.9	5.1
3.62	5.4	6.0	5.3	6.5	5.8	6.5
3.54	6.5	7.5	6.8	8.7	7.2	9.9
3.46	8.1	9.9	9.6	13.0	9.6	10.5
3.39	10.6	13.6				
3.33	13.8	18.2				
3.26	17.5	23.7				
3.20	18	25				
3.14	20	28				
3.09	22	31				
3.04	21	29				
2.94	20.7	28.4				
2.85 <sup>††</sup>	20.2	27.8	70	120		
2.76 <sup>††</sup>	19.3	26.5	67	118		
2.69 <sup>††</sup>	17.2	23.6	57	102		

(continued.....)



$10^3/T(K^{-1})$	Formyl		trans-N-Methyl		cis-N-Methyl	
	$\Delta\nu_{obs}$ (Hz)	$1/T_{2P}$ ( $10^3 sec^{-1}$ )	$\Delta\nu_{obs}$ (Hz)	$1/T_{2P}$ ( $10^3 sec^{-1}$ )	$\Delta\nu_{obs}$ (Hz)	$1/T_{2P}$ ( $10^3 sec^{-1}$ )
<u>0.0248 (continued)</u>						
2.61 <sup>††</sup>	15.2	20.7	52	95		
2.55 <sup>††</sup>	13.5	18.2	43	61		
2.49 <sup>††</sup>	11.5	15.3	36	51		
2.43 <sup>††</sup>	9.4	12.2	29	41		
2.37 <sup>††</sup>	7.5	9.8	24	33		
2.28 <sup>††</sup>	4.9	5.6	19	26		
<u>0.0104 molar</u>						
3.88	2.9	5.2	1.9	3.5	2.6	4.2
3.79	2.7	4.4	1.9	3.6	2.6	4.2
3.71	2.7	4.6	2.1	4.1	2.6	4.3
3.62	2.8	5.0	2.5	5.5	3.0	5.6
3.54	3.0	5.8	3.3	6.5	2.8	7.3
3.46	3.5	7.4	4.0	11.3	4.0	9.0
3.39	4.3	10.6	5.5	16.8	5.5	14.2
3.33	5.2	13.8	7.0	19.5	7.6	23.7
3.26	6.3	17.5				
3.20	7.6	21.9				
3.14	8.3	24.4				
3.09	8.9	26.7				
3.04	9.0	26.9				

(continued.....)





$10^3/T(K^{-1})$	Formyl		trans-N-Methyl		cis-N-Methyl	
	$\Delta\nu_{\text{obs}}$	$1/T_{2P}$ ( $10^3 \text{ sec}^{-1}$ )	$\Delta\nu_{\text{obs}}$	$1/T_{2P}$ ( $10^3 \text{ sec}^{-1}$ )	$\Delta\nu_{\text{obs}}$	$1/T_{2P}$ ( $10^3 \text{ sec}^{-1}$ )
	—	—	(Hz)	( $10^3 \text{ sec}^{-1}$ )	(Hz)	( $10^3 \text{ sec}^{-1}$ )
<u>0.0104 (continued)</u>						
3.02	9.0	27.1				
2.99	9.1	27.4				
2.94	9.2	27.7				
2.89	9.2	28.1				
2.85 <sup>††</sup>	8.9	27.1	31.7	92.9		
2.76 <sup>††</sup>	8.5	25.7	31.8	102		
2.69 <sup>††</sup>	7.8	23.6	27.2	89.2		
2.61 <sup>††</sup>	7.0	20.8	23.0	75.7		
2.55 <sup>††</sup>	6.4	18.9	21.0	68.7		
2.49 <sup>††</sup>	6.1	17.8	17.4	56.3		
2.43 <sup>††</sup>	5.4	15.1	14.3	45.5		
2.37 <sup>††</sup>	4.3	11.3	12.1	37.9		
2.32 <sup>††</sup>	3.7	9.2	10.5	32.2		
<u>0.00667 molal</u>						
3.54	2.4	6.1	2.0	6.9	2.6	6.4
3.46	2.8	8.4	3.0	12.6	3.5	11.5
3.39	3.5	12.0	4.3	19.3	4.2	15.2
3.33	4.2	15.7	6.0	28.2	5.8	23.8
3.26	5.0	20.2	9.0	43.9	7.4	32.5
3.20	5.6	23.8	11.2	54.7	10.2	47.1
3.14	6.1	26.5	12.8	59.0		
					(continued....)	



Footnotes to Table A-5

<sup>†</sup> Spectra recorded at 60 MHz

<sup>††</sup> N-methyl resonances are collapsed to a single line.



TABLE A-6

Proton Line Broadening<sup>†</sup> of DMF Solutions Containing Various Concentrations of Bis-(di-phenyldithiophosphinato)-oxo-vanadium(IV)

$10^3/T(K^{-1})$	Formyl		trans-N-Methyl		cis-N-Methyl	
	$\Delta\nu_{\text{obs}}$ (Hz)	$1/T_{2P}$ ( $10^3 \text{ sec}^{-1}$ )	$\Delta\nu_{\text{obs}}$ (Hz)	$1/T_{2P}$ ( $10^3 \text{ sec}^{-1}$ )	$\Delta\nu_{\text{obs}}$ (Hz)	$1/T_{2P}$ ( $10^3 \text{ sec}^{-1}$ )
<u>0.0596 molal</u>						
4.35	13.8	8.2	9.6	5.8	11.7	7.5
4.15	10.8	5.9	7.4	4.3	9.2	5.7
3.97	10.2	5.4	5.6	3.0	6.2	3.5
3.77	10.5	5.6	4.9	2.4	5.2	2.8
3.64	11.2	6.1	4.6	2.2	4.6	2.4
2.75	19.2	10.5				
<u>0.0505 molal</u>						
3.80	8.6	5.0	4.5	2.7	5.0	3.0
3.72	9.6	5.9	9.1	2.3	4.8	2.8
3.56	11.7	7.5	3.9	2.1	4.6	2.6
3.41	13.1	8.5	5.1	2.7	5.5	3.4
3.27	13.9	9.0	7.1	4.9	7.8	5.4
3.15	16.5	11.0				

0.0474 molal

4.40

12.6

9.2

9.4

7.3

11.6

9.2

(continued.....)



$10^3/T(K^{-1})$	Formyl		trans-N-Methyl		cis-N-Methyl	
	$\Delta\nu_{\text{obs}}$ (Hz)	$1/T_{2P}$ ( $10^3 \text{ sec}^{-1}$ )	$\Delta\nu_{\text{obs}}$ (Hz)	$1/T_{2P}$ ( $10^3 \text{ sec}^{-1}$ )	$\Delta\nu_{\text{obs}}$ (Hz)	$1/T_{2P}$ ( $10^3 \text{ sec}^{-1}$ )
<u>0.0474 (continued)</u>						
4.32	11.0	7.7	8.6	6.6	9.6	7.3
4.24	9.3	6.2	7.0	5.2	8.0	5.9
4.14	8.4	5.3	6.2	4.5	7.4	5.4
4.07	8.0	4.9	5.4	3.7	6.8	4.9
3.99	7.6	4.5	5.0	3.4	5.8	4.0
3.91	8.0	4.8	4.9	3.3	5.3	3.5
3.84	8.2	5.0	4.0	2.4	4.5	2.7
<u>0.0204 molal</u>						
3.11	8.3	9.7	5.6	8.6	5.6	9.1
3.05	9.9	12.7	10.9	19.8	10.8	20.0
<u>0.0116 molal</u>						
2.94	8.0	13.7	9.6	29.6	9.0	28.1
<u>0.0088 molal</u>						
2.84			11.4	47	10.0	41

---

† Spectra recorded at 60 MHz





TABLE A-7

Formyl Proton Line Broadening<sup>†</sup> of DEF Solutions Containing  
Bis-(diphenyldithiophosphinato)-oxo-vanadium(IV)

$10^3/T(K^{-1})$	Formyl	
	$\Delta\nu_{\text{obs}} \text{ (Hz)}$	$1/T_{2P} (10^3 \text{ sec}^{-1})$
<u>0.00995 molal</u>		
4.74	25.7	75.2
4.61	17.9	51.1
4.50	12.5	34.2
4.39	9.0	23.6
4.29	7.0	17.4
4.19	6.0	14.3
4.10	5.1	11.0
4.01	4.4	9.0
3.92	4.1	7.8
3.84	3.9	7.2
3.82	3.9	7.2
3.77	3.8	6.7
3.71	3.8	6.5
3.62	3.8	6.3
3.54	4.0	6.9
3.46	4.2	7.5
3.39	4.6	8.4
3.33	5.0	9.5
3.26	5.3	10.1
3.20	6.0	12.0
3.14	6.4	13.2
3.09	6.7	13.9
3.05	7.4	15.5
3.02	7.5	15.9
2.94	8.8	19.4

(continued.....)



$10^3/T(K^{-1})$	Formyl	
	$\Delta\nu_{\text{obs}}(\text{Hz})$	$1/T_{2P}(10^3\text{sec}^{-1})$
<u>0.00995 (continued)</u>		
2.85	9.6	21.3
2.76	9.5	19.1
2.69	8.9	17.9
2.60	7.3	10.7
2.53	6.4	8.7
2.48	6.2	7.9
2.40	5.7	5.1
2.35	5.5	3.7

†

Spectra recorded at 60 MHz.



A P P E N D I X    B

Appendix B gives the conductance measurements of several solvents containing various concentrations of bis-(diphenyldithiophosphinato)-oxo-vanadium(IV). The Tables give the molarity of the phenyl complex,  $M$ , the measured resistance of the conductance cell,  $R$ , and the calculated conductance,  $L$ .



TABLE B-1

Conductance of Several Solvents Containing Various Concentrations of Bis-(diphenyldithiophosphinato)-oxo-vanadium(IV).

<u>Solvent</u>	<u>M(ml<sup>-1</sup>)</u>	<u>R(ohm)</u>	<u>L(ohm<sup>-1</sup>)</u>
1% HMP/toluene	0	1.0 x 10 <sup>6</sup>	1.0 x 10 <sup>-6</sup>
	1.7 x 10 <sup>-4</sup>	1.0 x 10 <sup>6</sup>	1.0 x 10 <sup>-6</sup>
	9.0 x 10 <sup>-4</sup>	1.0 x 10 <sup>6</sup>	1.0 x 10 <sup>-6</sup>
	1.37 x 10 <sup>-3</sup>	1.0 x 10 <sup>6</sup>	1.0 x 10 <sup>-6</sup>
	2.58 x 10 <sup>-3</sup>	1.0 x 10 <sup>6</sup>	1.0 x 10 <sup>-6</sup>
	4.44 x 10 <sup>-3</sup>	1.0 x 10 <sup>6</sup>	1.0 x 10 <sup>-6</sup>
	6.44 x 10 <sup>-3</sup>	1.0 x 10 <sup>6</sup>	1.0 x 10 <sup>-6</sup>
	8.98 x 10 <sup>-3</sup>	1.0 x 10 <sup>6</sup>	1.0 x 10 <sup>-6</sup>
5% pyridine/CS <sub>2</sub>	0	1.0 x 10 <sup>6</sup>	1.0 x 10 <sup>-6</sup>
	4.1 x 10 <sup>-4</sup>	1.0 x 10 <sup>6</sup>	1.0 x 10 <sup>-6</sup>
	8.63 x 10 <sup>-4</sup>	1.0 x 10 <sup>6</sup>	1.0 x 10 <sup>-6</sup>
	1.67 x 10 <sup>-3</sup>	1.0 x 10 <sup>6</sup>	1.0 x 10 <sup>-6</sup>
	2.67 x 10 <sup>-3</sup>	1.0 x 10 <sup>6</sup>	1.0 x 10 <sup>-6</sup>
	4.22 x 10 <sup>-3</sup>	1.0 x 10 <sup>6</sup>	1.0 x 10 <sup>-6</sup>
	7.02 x 10 <sup>-3</sup>	1.0 x 10 <sup>6</sup>	1.0 x 10 <sup>-6</sup>
10% HMP/toluene	0	1.0 x 10 <sup>6</sup>	1.0 x 10 <sup>-6</sup>
	1.6 x 10 <sup>-4</sup>	1.0 x 10 <sup>6</sup>	1.0 x 10 <sup>-6</sup>
	6.4 x 10 <sup>-4</sup>	9.0 x 10 <sup>5</sup>	1.1 x 10 <sup>-6</sup>
	1.54 x 10 <sup>-3</sup>	6.2 x 10 <sup>5</sup>	1.6 x 10 <sup>-6</sup>
	2.26 x 10 <sup>-3</sup>	5.0 x 10 <sup>5</sup>	2.0 x 10 <sup>-6</sup>
	3.60 x 10 <sup>-3</sup>	3.7 x 10 <sup>5</sup>	2.7 x 10 <sup>-6</sup>
	5.58 x 10 <sup>-3</sup>	2.47 x 10 <sup>5</sup>	4.09 x 10 <sup>-6</sup>
	7.88 x 10 <sup>-3</sup>	1.67 x 10 <sup>5</sup>	6.05 x 10 <sup>-6</sup>
	1.06 x 10 <sup>-2</sup>	1.10 x 10 <sup>5</sup>	9.18 x 10 <sup>-6</sup>

(continued.....)





TABLE B-1 (continued)

<u>Solvent</u>	<u>M(ml<sup>-1</sup>)</u>	<u>R(ohm)</u>	<u>L(ohm<sup>-1</sup>)</u>
HMP	0	$2.82 \times 10^3$	$3.58 \times 10^{-4}$
	$2.6 \times 10^{-4}$	$2.64 \times 10^3$	$3.83 \times 10^{-4}$
	$5.6 \times 10^{-4}$	$2.48 \times 10^3$	$4.07 \times 10^{-4}$
	$1.11 \times 10^{-3}$	$2.23 \times 10^3$	$4.53 \times 10^{-4}$
	$2.43 \times 10^{-3}$	$1.83 \times 10^3$	$5.52 \times 10^{-4}$
	$4.64 \times 10^{-3}$	$9.2 \times 10^2$	$1.10 \times 10^{-3}$
	$6.30 \times 10^{-3}$	$7.45 \times 10^2$	$1.36 \times 10^{-3}$
	$8.59 \times 10^{-3}$	$5.90 \times 10^2$	$1.71 \times 10^{-3}$
	$1.22 \times 10^{-2}$	$4.60 \times 10^2$	$2.20 \times 10^{-3}$
pyridine	0	$3.0 \times 10^5$	$3.3 \times 10^{-6}$
	$2.5 \times 10^{-4}$	$6.73 \times 10^3$	$1.49 \times 10^{-4}$
	$5.9 \times 10^{-4}$	$4.18 \times 10^3$	$2.39 \times 10^{-4}$
	$1.24 \times 10^{-3}$	$2.58 \times 10^3$	$3.88 \times 10^{-4}$
	$2.48 \times 10^{-3}$	$1.63 \times 10^3$	$6.13 \times 10^{-4}$
	$3.84 \times 10^{-3}$	$1.21 \times 10^3$	$8.26 \times 10^{-4}$
	$6.63 \times 10^{-3}$	$8.20 \times 10^2$	$1.22 \times 10^{-3}$
	$9.26 \times 10^{-3}$	$6.45 \times 10^2$	$1.55 \times 10^{-3}$
DMF	0	$3.2 \times 10^4$	$3.1 \times 10^{-5}$
	$7.8 \times 10^{-4}$	$1.49 \times 10^3$	$6.83 \times 10^{-4}$
	$3.9 \times 10^{-3}$	$3.30 \times 10^2$	$3.08 \times 10^{-3}$
	$1.95 \times 10^{-2}$	$7.9 \times 10^1$	$1.3 \times 10^{-2}$

---



A P P E N D I X      C

Appendix C gives the FORTRAN computer program which was used to simulate EPR spectra of liquids as discussed in Chapter III.







```

DIMENSION SFT(2000),SFP(2000),NPR(20),A(20),SPOP(2000),SPOT(2000),
X      EINT(2000), TITLE(20), OUT(120), NOW(120), SPIN(20),
X      FLD(20,100), STM(20,100), NLIN(20), W(1000),R(1000),C(1000)
X,FIELD(2000),WIDTH(1000),ISD(20),FEINT(2000),FW(1000)
X,NPR(20),FA(20),FSPIN(20)
EQUIVALENCE (FIELD(1),SPOT(1)),(EINT(1),SFT(1))
COMMON /CCWRIT/ A,TITLE, SPIN, W, SWP, SINT, SMAX, SMIN, NPR, ICC,
XNGP,NLWCC,NFGP,NFPR,FSPIN,FA,FRAC,FFRAC,CM,NSPEC,SHIFT,FSHIFT
LOGICAL LOG

```

## SECTION 1.

```

NDIM = 1000
ICC = 1
1 CONTINUE
ISPEC=0
READ (5,1000,END=2000) (TITLE(I), I = 1, 18)
WRITE(6,1001) (TITLE(I), I = 1, 18)
READ(5,1010)NPT,NSPEC
READ(5,1020)SINT,SWP,CM
WRITE(6,1021)SINT,SWP,CM
100 READ(5,1030)NLW,NRPLW,IWC
READ(5,1020)(W(I),I=1,NLW)
READ(5,1020)SHIFT,FRAC
WRITE(6,1022)FRAC,SHIFT
WRITE(6,1023)(W(I),I=1,NLW)
READ(5,1030)NGP
READ(5,1030)(NPR(I),I=1,NGP)
READ(5,1031)(A(I),SPIN(I),ISD(I),I=1,NGP)
WRITE(6,1032)(NPR(I),SPIN(I),A(I),I=1,NGP)

```

## SECTION 2.

```

NLWCC = NLW
DO 570 I=1,NGP
S=SPIN(I)
AD=A(I)

```





```

ADD = 1.536E-4 * AD * AD * AD
N=NPRI
S1=S*FLOAT(N)
SA = -S1 * AD
LM=2.*S + 1.1
II = 2.0 * S1 + 1.1
DO 510 J=1, II
SFT(J)=C.0
510 SPOT(J) = SA + AD * FLOAT(J - 1)
NL=1
SFP(1)=1.0
DO 550 II=1,N
DO 530 J=1,LM
DO 520 K=1,NL
N1=J+K-1
520 SFT(N1)=SFT(N1) + SFP(K)

530 CONTINUE
NL=N1
DO 540 K=1,NL
SFP(K)=SFT(K)
540 SFT(K)=0.0
550 CONTINUE
IF(ISD(I).LE.0) GO TO 5529
IBTM = 1
FLIP = SFP(1)
FLOP = 0.0
K = 1

551 S2 = S1 * (S1 + 1.0)
ITOPS = NL - IBTM + 1
DO 552 J = IBTM , ITOPS
EMJSQ = (FLOAT(J - IBTM) - S1)**2
SPOP(K) = SPOT(J) - ADD * (S2 - EMJSQ)
SFT(K) = FLIP
552 K = K + 1
S1 = S1 - 1.0
IF(S1.LT.0.0) GO TO 5531
IBTM = IBTM + 1
FLOP = FLOP + FLIP

```



```

FLIP = SFP(IBM) - FLOP
IF(FLIP.LT.1.0E-05) GO TO 5531
GO TO 551
5529 DO 5530 K = 1, NL
      STM(I,K) = SFP(K)
5530 FLD(I,K) = SPOT(K)
      NLIN(I) = NL
GO TO 570
5531 IBM = IBM - 1
553  NL = K - 1
      DO 560 K = 1, NL
        STM(I,K) = SFT(K)
560  FLD(I,K) = SPOP(K)
      NLIN(I)=NL
570  CONTINUE
      SFP(1)=1.0
      SPOP(1)=0.0
      NL=1
      DO 610 I=1,NGP
        N1=1
        N=NLIN(I)
        DO 590 J=1,N
          SA=STM(I,J)
          SB=FLD(I,J)
          DO 580 K=1,NL
            SFT(N1)=SFP(K)*SA
            SPOT(N1)=SPOP(K) +SB
            N1=N1+1
580  CONTINUE
590  CONTINUE
        NL=N1-1
        TEMP = 0.0
        DO 600 K=1,NL
          SFP(K)=SFT(K)
          SPOP(K)=SPOT(K)
          TEMP = TEMP + SFP(K)
600  CONTINUE

```



```

610 CONTINUE
  IF(NSPEC.EQ.1) GO TO 699
  IF(ISPEC.EQ.1) GO TO 699
  NF=NL
  NRPLW=NRPLW
  NFGP=NGP
  FFRAC=FRAC
  FSHIFT=SHIFT
  DO 705 K=1,NGP
    NFR(K)=NPR(K)
    FSPIN(K)=SPIN(K)
705  FA(K)=A(K)
    DO 706 K=1,NLW
706  FW(K)=W(K)
699  DO 650 I=1,NL
    CA=1.0E+14
    DO 640 J=1,NL
      S=SPOT(J)
      IF (CA .LE. S) GO TO 630
      CA=S
      II = J
630 CONTINUE
640 CONTINUE
      SPOP(I)=SPOT(II)
      SFP(I)=SFT(II)
      SPOT(II)=1.0E+15
650 CONTINUE
      DO 660 K=1,NL
        SPOP(K)=SPOP(K)+SHIFT
660  SFP(K)=SFP(K)*FRAC/TEMP
      WRITE(6,1500)NL,(SPOP(K),SFP(K),K=1,NL)
1500 FORMAT(' SPECTRUM CONTAINS ',I4,' LINES',/,
           (2X,2E12.5,4X,2E12.5,
           X4X,2E12.5,4X,2E12.5,/) )

```

C  
C  
C

SECTION 3.



```

      IF(NL.LE.2000) GO TO 829
      WRITE(6,1998) NL
1998 FORMAT('GSTICK SPECTRUM CONTAINS MORE THAN 2000 LINES',
X/,'GIT CONTAINS',15,' LINES')
      GO TO 2000
829 CONTINUE
      IF (NLW .GT. 1) GO TO 340
      CI = (W(1)*0.8660254)**2
      LOG = .FALSE.
      GO TO 871
840 CONTINUE
      LOG = .TRUE.
      K = 1
      DO 998 I = 1 , NLW
      DO 998 J = 1 , NRPLW
      WIDTH(K) = W(I)
998 K = K + 1
      IF(IWC.LT.5) GO TO 999
      DO 997 J=1,5
      L=NRPLW*J
      N=L+1
      WCI=WIDTH(L)
      WIDTH(L)=WIDTH(N)
997 WIDTH(N)=WCI
999 IF((K-1).EQ.NL) GO TO 860
      WRITE(6,1035)
      GO TO 1
860 CONTINUE
861 CONTINUE
      DO 870 I=1,NL
1999 FORMAT(3E18.8)
      WI = WIDTH(I) * 0.8660254
      B(I)=0.6366198*WI
870 C(I)=WI*WI
871 CUTOFF = 10.0*W(I)
      DELTA=SWP/FLOAT(NPT)
      HMIN =-0.5*SWP

```





```

NPT=NPT+1
DO 60 I=1,NPT
H=HMIN+DELTA*FLOAT(I-1)
EIT=0.0
DO 50 J=1,NL
HA=H-SPOP(J)
IF(HA.GT.CUTOFF) GO TO 50
IF(HA.LT.-CUTOFF) GO TO 51
IF(LOG) GO TO 45
TRUMP = HA/(CI + HA*HA)**2
GO TO 46
45 TRUMP = HA*B(J)/(C(J)+HA*HA)**2
46 EIT = EIT - SFP(J) * TRUMP
50 CONTINUE
51 CONTINUE
FINT(I)=EIT
FIELD(I)=H
60 CONTINUE
ISPEC=ISPEC+1
IF(NSPEC.EQ.1) GO TO 200
IF(ISPEC.EQ.2) GO TO 199
DO 61 K=1,NPT
FEINT(K)=EINT(K)
61 FEINT(K)=EINT(K)
GO TO 100
199 DO 62 I=1,NPT
62 EINT(I)=EINT(I)+FEINT(I)
200 SMIN=0.0
SMAX=0.0
DO 63 K=1,NPT
IF(EINT(K).GT.SMAX)SMAX=EINT(K)
63 IF(EINT(K).LT.SMIN)SMIN=EINT(K)
C
C
C
C
CALCOMP PLOT:
IF(ICC.NE.1) GO TO 203
CALL CPLOT1 (FIELD, EINT, NPT)
GO TO 206

```

SECTION 4.



```

203 CALL CPLOT2 (FIELD, EINT, NPT)
C      ICC IS AN INDEX FOR THE COUNTING AND POSITIONING OF THE
C      PLOTS.
206 ICC = ICC + 1
C
C      GO TO 1
C
C      TERMINATE PLOT.
200 CALL CCEND
STOP
C
1000 FORMAT(18A4)
1001 FORMAT(56H1COMPUTER SIMULATION OF ESR SPECTRA IN LIQUID SOLUTIONS.
1/1H0,18A4)
1010 FORMAT(18I4)
1020 FORMAT(6E12.5)
1021 FORMAT(26H0INTENSITIES NORMALIZED TO F10.1/ 7H SWEEP F9.2,7H GAUSS
X, 'SPANNING', F7.2, ' CENTIMETERS. ')
1022 FORMAT(' FRACTION OF THIS SPECIES =', F10.5, '/', ' SHIFT OF THIS SPECI
XES =', F10.5, ' GAUSS')
1023 FORMAT(' SPECTRUM CONSTRUCTED FROM LORENTZIAN LINES OF PEAK TO PEAK
XK WIDTHS IN GAUSS OF :', /, 8(E12.3, 2X))
1030 FORMAT(24I3)
1031 FORMAT(2E12.5, I2)
1032 FORMAT(1H0, I3, 17H NUCLEI WITH SPIN, F4.1, 14H AND SPLITTING, F6.2, 6H
1GAUSS)
1035 FORMAT(29H0ERROR IN WIDTH SPECIFICATION)
END
C
C
C
C
SUBROUTINE CPLOT1 (X, Y, NPT)

```

THIS SUBROUTINE CALCOMP PLOTS DATA OF ESR SPECTRA IN  
LIQUID SOLUTIONS. MULTIPLE ENTRY POINTS ARE USED TO HANDLE



```

C
C      MULTIPLE GRAPHS FOR EACH RUN OF THE MAIN PROGRAM.

      DIMENSION AREA(2048), X(1 ), Y(1 )
      COMMON /CCWRIT/A(20),TITLE(20),SPIN(20),W(1000),SWP,SINT,SMAX,SMIN
      X,NPR(20),ICC,NGP,NLW,NFGP,NFPR(20),FSPIN(20),FA(20),FW(1000)
      X,FRAC,FFRAC,SHIFT,FSHIFT,CM,NSPEC

C
C      INITIALIZE PLOT
C
      CALL PLOTS (AREA, 8192)
      CALL PLOT (0.0, 0.0,-100)
      CALL SYMBOL(0.0,0.0,0.15,'COMPUTER SIMULATION OF ESR SPECTRA IN LI
      XQUID SOLUTIONS.',90.0,55)
      ENTRY CPlot2 (X, Y, NPT)

C
C      WRITE INPUT DATA
C
      CALL SYMBOL(0.3,0.0,0.15,TITLE(1),90.0,72)

      CALL SYMBOL(0.6,0.0,0.15,' FRACTION OF SPECIES ONE =
      XTH SHIFT =          GAUSS',90.0,61)
      CALL NUMBER(0.6,3.5,0.15,FRAC,90.0,3)
      CALL NUMBER(0.6,6.2,0.15,SHIFT,90.0,3)
      DO 20 I=1,NGP
      XSTEP=0.6+0.3*I
      CALL SYMBOL(XSTEP,0.0,0.15,' NUCLEI WITH SPIN      AND SPLITTING
      X          GAUSS',90.0,53)
      CALL NUMBER (XSTEP, 0.0, 0.15, FLOAT(NPR(I)), 90.0, -1)
      CALL NUMBER (XSTEP,2.7,0.15,SPIN(I),90.0,1)
      CALL NUMBER (XSTEP, 5.05, 0.15, A(I), 90.0, 2)
20 CONTINUE
      CALL SYMBOL(XSTEP+0.3,0.0,0.15,'SPECTRUM CONSTRUCTED FROM LORENTZI
      XAN LINES OF PEAK-ID-PEAK WIDTHS IN GAUSS',90.0,75)
      YSTEP=0.0
      XSTEP=XSTEP+0.3
      DO 25 I=1,NLW
      CALL NUMBER(XSTEP,YSTEP,0.15,W(I),90.0,3)

```



```

25 YSTEP=YSTEP+1.25
   IF(NSPEC.EQ.1) GO TO 310
   CALL SYMBOL(XSTEP+0.3,0.0,0.15,' FRACTION OF SPECIES TWO =
X   WITH SHIFT = GAUSS',90.0,63)
   CALL NUMBER(XSTEP+0.3,3.5,0.15,FFRAC,90.0,3)
   CALL NUMBER(XSTEP+0.3,6.2,0.15,FSHIFT,90.0,3)
   XVAL=XSTEP+0.3
   DO 21 I=1,NFGP
   XSTEP=XVAL+0.3*I
   CALL SYMBOL(XSTEP,0.0,0.15,' NUCLEI WITH SPIN AND SPLITTING
X   GAUSS',90.0,53)
   CALL NUMBER(XSTEP,0.0,0.15,FLOAT(NFPR(I)),90.0,-1)
   CALL NUMBER(XSTEP,2.7,0.15,FSPIN(I),90.0,1)
   CALL NUMBER(XSTEP,5.05,0.15,FA(I),90.0,2)
21 CONTINUE
   CALL SYMBOL(XSTEP+0.3,0.0,0.15,'SPECTRUM CNSTRUCTED FROM LORENTZI
XAN LINES OF PEAK-TO-PEAK WIDTHS IN GAUSS',90.0,75)
   YSTEP=0.0
   XSTEP=XSTEP+0.6
   DO 26 I=1,NLW
   CALL NUMBER(XSTEP,YSTEP,0.15,FW(I),90.0,3)
26 YSTEP=YSTEP+1.25
310 CALL SYMBOL(XSTEP+0.3,0.0,0.15,'INTENSITIES NORMALIZED TO ',
1   90.0, 26)
   CALL NUMBER (XSTEP+0.3, 3.5, 0.15, SINT, 90.0, 1)
   CALL SYMBOL (XSTEP+0.6, 0.0, 0.15, 'SWEEP
X   CM',90.0,42)
   CALL NUMBER (XSTEP+0.6, 0.9, 0.15, SWP, 90.0, 2)
   CALL NUMBER(XSTEP+0.6,3.9,0.15,CM,90.0,2)

```

C  
C  
C  
C

OUTLINE OF PAGE FOR CUTTING

```

ORG = XSTEP + 0.5
XMOVE = ORG + 0.75
CALL PLOT (ORG,0.0,-3)
CALL PLOT (0.0,11.0,2)
CALL PLOT (16.5,11.0,2)

```





```

C      CALL PLOT (16.5,0.0,0.2)
C      CALL PLOT (0.0,0.0,0.2)
C
C      MOVE THE X-AXIS TO THE MIDDLE OF THE PAGE
C
C      CALL PLOT(0.75,5.5,-3)
C
C      SET UP SCALING FACTORS FOR X AND Y
C
C      PLOT DATA POINTS
C      CALL OFFSET(X(1),SWP/(CM*0.3937) , 0.0, 25.4*(SMAX-SMIN)/SINT)
C
C      CALL PLOT(X(1),Y(1),13)
C      DO 27 I=2,NPT
C      27 CALL PLOT(X(I),Y(I),12)
C
C      DRAW CENTER LINE
C
C      CALL PLOT(0.0,0.0,0.2)
C
C      MOVE PEN FOR NEXT PLOT
C
C      IF (ICC .GT. 2*(ICC/2)) GO TO 30
C      IF (XMOVE.GT.XMOVE) XMOVE = XMOVE
C      CALL PLOT(16.5 + XMOVE,-19.0,-3)
C      RETURN
C      30 CALL PLOT (-XMOVE, 8.0, -3)
C      XMOVE = XMOVE
C      RETURN
C
C      TERMINATE PLOT
C
C      ENTRY CCEND
C      CALL PLOT (0.0, 0.0, 999)
C      RETURN
C      END

```







**B30076**